THESE DE DOCTORAT

Pour obtenir le grade de

Docteur de l'Université de Lille

Spécialité Chimie

Ecole Doctorale des Sciences de la Matière, du Rayonnement et de l'Environnement

Methodological development for the structural elucidation of natural and synthetic insoluble polymers by chemical depolymerization and ultra-high-resolution mass spectrometry

Développement méthodologique pour l'élucidation structurale des polymères insolubles naturels et synthétiques par dépolymérisation chimique et spectrométrie de masse à ultra-haute résolution

Présentée et soutenue publiquement par

Ziad MAHMOUD

Le 31 Janvier 2022 devant le jury composé de

Mme. Laurence CHARLES	Professeur à l'Université Aix-Marseille, Laboratoire ICR, Marseille	Rapporteur
M. Edwin DE PAUW	Professeur à l'Université de Liège, Laboratoire MolSys, MSLAB, Liège	Rapporteur
Mme. Corinne LOUTELIER-BOURHIS	Maitre de Conférence à l'Université de Rouen Normandie, Laboratoire COBRA, Mont Saint Aignan	Examinateur
M. Philippe ZINCK	Professeur à l'Université de Lille, Laboratoire UCCS, Villeneuve d'Ascq	Président du jury
M. Fabrice BRAY	Ingénieur de recherche à l'Université de Lille, Laboratoire MSAP, Villeneuve d'Ascq	Co-encadrant de thèse
M. Christian ROLANDO	Directeur de recherche CNRS, Université de Lille, Laboratoire MSAP, Villeneuve d'Ascq	Directeur de thèse

Acknowledgements

This thesis was carried out in the Miniaturization for Synthesis, Analysis and Proteomics (MSAP) laboratory at the University of Lille, faculty of science and technology under the supervision of Doctor Christian Rolando within the framework of the EU_FT-ICR European network.

First of all, I would like to thank Laurence Charles and Edwin De Pauw for accepting to be reviewers for this manuscript and for their interest in this work. I also thank Corinne Loutier-Bourhis and Philippe Zinck for kindly examining this thesis work.I would like to express my sincere thanks and express my gratitude to Christian Rolando, my thesis supervisor, for first giving me the chance to carry out my PhD at the MSAP laboratory and second for his great availability during these 3 years, during which he transmitted his scientific and technical knowledge to me. I also thank him for the confidence he had shown in me, in many occasions, and for all the chances he offered me inside and outside the laboratory. Thank you Christian for all the discussions, meetings and advices which will accompany me for the rest of my career.

I warmly thank Fabrice Bray for the time he devoted to me, as well as for all the help he offered me during these three years and with whom I shared very pleasant moments, whether in the laboratory or during summer schools. Thank you for having enough patience to answer all my questions leading to my current knowledge in mass spectrometry.

I would like to thank the members of the MSAP laboratory: The lab director Ahmed Mazzah, Stephanie, Laetitia, Melanie, Elise, Mael, Matthieu, Francoise, Nicolas, Marc, Amandine and especially Marie, Manal, Lamees, Ranine and Wissal for their continuous support and for the good moments we spent together.

I like to thank as well the members of the teams with whom I had the chance to work: Julien Molina from Mader. Marie Hubert-Roux and Carlos Afonso from COBRA,University of Rouen, thank you for welcoming me in your laboratory and giving me the opportunity to work with you. Severine le Gac and Bastien Venzac from AMBER and the University of Twente, thank you for trusting me to conduct you mass *spectrometry analyses. Anais Genty and Michel Menu from the C2RMF and Marie-Amelie Senot from the LaM. Michel Sablier from the CRC and MNHN, Paris.*

Thank you to all the Masters and bachelor students who worked with me during these three years: Anais, Aurelie, Caterina, Elisa, Lucas, Meftah, Moana, Nathan and Thomas.

I would never forget to thank my family (My father, my mother, my sister and my brothers) for always supporting and believing in me during all these years. I will never be able to thank you enough.

Finally, I would like to thank my love and partner in life for her continuous support and help, for her encouragement and for her patience during the past three years. Without you I would never be able to achieve anything.

Table of Contents

Abbreviations

2D	Bidimensional
3D	Tridimensional
ADMET	Acyclic diene metathesis polymerization
APCI	Atmospheric Pressure Chemical Ionization
APPI	Atmospheric Pressure Photo Ionization
ASAP	Atmospheric Solids Analysis Probe
C#	Carbon number
CAD	Collision activated dissociation
CCS	Collision Cross Section
CID	Collision-Induced Dissociation
CM	Cross-metathesis
CTA	Chain Transfer Agent
Da	Dalton
DBE	Double Bond Equivalent
DCM	Dichloromethane
DIP	Direct Insertion Probe
DMAPA	3-(dimethylamino)-1-propylamine
DTIMS	Drift Tube Ion Mobility Spectrometry
ECD	Electron capture dissociation
ER-MS	Energy-resolved mass spectrometry
ESI	Electrospray
ESI-MS	Electrospray-mass spectrometry
ETD	Electron transfer dissociation
FID	Free Induction Decay
FTICR	Fourier Transform Ion Cyclotron Resonance
FTIR	Fourier Transform Infrared Spectroscopy
FTMS	Fourier Transform mass spectrometry
G-I	Grubbs 1st generation catalyst
G-II	Grubbs 2nd generation catalyst
G-III	Grubbs 3rd generation catalyst
HG-I	Hoveyda-Grubbs 1st generation catalyst
HG-II	Hoveyda-Grubbs 2nd generation catalyst
GC	Gas Chromatography
GCxGC	Comprehensive two-dimensional Gas Chromatography
GC-MS	Gas chromatography-mass spectrometry
HCD	Higher energy collisional dissociation
HTPB	Hydroxy-terminated polybutadiene
ICR	Ion Cyclotron Resonance
IE	Ionization energy
IM-MS	Ion Mobility Mass Spectrometry
IMS	Ion Mobility Spectrometry
IR	Infra-rouge
IRMPD	Multiphoton Infrared Dissociation
IUPAC	International Union of Pure and Applied Chemistry
KM	Kendrick Mass

KMD	Kendrick Mass Defect
L	Linoleic acid
LC	Liquid chromatography
LC-MS	Liquid chromatography-mass spectrometry
Ln	Linolenic acid
MALDI	Matrix Assisted Laser Desorption Ionization
MALDI-TOF	Matrix Assisted Laser Desorption Ionization-Time of flight
MS/MS	Tandem Mass spectrometry
MSAP	Miniaturization for the synthesis, analysis and proteomics
m/z	mass to charge ratio
NR	Natural rubber
NMR	Nuclear Magnetic Resonance
O	Oleic acid
P	Palmitic acid
PB	Polybutadiene
PE	Polyethylene
PEG	Poly (ethylene glycol)
PDMS	polydimethylsiloxane
PI	Polyisoprene
PP	Polypropylene
ppb	part per billion
ppm	part per million
Py-GC/MS	Pyrolysis-gas chromatography/mass spectrometry
Py-GC×GC-MS	Pyrolysis-comprehensive two-dimensional gas chromatography/mass spectrometry
Q	Quadrupole
Q-TOF	Tandem Quadrupole-Time of flight
RCM	Ring-closing metathesis
RF	Radio frequency
ROM	Ring-opening metathesis
ROMP	Ring-opening metathesis polymerization
S	Stearic acid
SR	Synthetic rubber
SRIG	Sacked ring ion guide
ssNMR	Solid-state NMR spectroscopy
SWIFT	Stored Waveform Inverse Fourier Transform
TAGs	Triacylglycerides
THF	Tetrahydrofuran
TIMS	Trapped Ion Mobility Spectrometry
TOF	Time of flight
T-Wave	Travelling Wave
TWIMS	Travelling Wave Ion Mobility Spectrometry
UV	Ultra-violet
XRF	X-ray fluorescence

List of Tables

List of Figures

Methodological development for the structural elucidation of natural and synthetic insoluble polymers by chemical depolymerization and ultra-high-resolution mass spectrometry

Abstract: The study of the depolymerization and degradation of polymers of natural or synthetic origin is still a major analytical challenge today, particularly with regard to insoluble polymers. The characterization of polymers and the study of their degradation pathways raise important environmental, economic and scientific issues and by improving our knowledge in these fields we will be able to fully understand the phenomena involved in their ageing, crosslinking (polymerization) as well as their degradation pathways in order to improve industrial processes leading to their manufacturing and recycling. The classical solution for characterizing such polymers is pyrolysis coupled to the gas phase. If this technique provides very characteristic imprints of the analyzed polymers, it hardly allows reliable structural studies due to complex pyrolysis mechanisms. In addition, pyrolysis does not identify the crosslinking units which are key elements for understanding the structure and biosynthesis or the development of a polymer. The work carried out in this thesis aims to find new solutions for the analysis of polymers by developing new methods of chemical cleavage using new generation organometallic catalysts, as well as the development of new instrumental methods capable of providing crucial information on the complex mixtures issued from the chemical cleavage. The interest of these methods is that they can be applied on minimal quantities of environmental and cultural heritage samples. The new catalysts allow the degradation reactions of natural or synthetic polymers to be carried out under milder conditions, further preserving the original structure of the monomers. While, the developed analysis methods, essentially based on the use of high-resolution mass spectrometry, in particular three complementary techniques to afford a comprehensive, rich and detailed description of the molecular structure: pyrolysis-comprehensive two-dimensional gas chromatography/mass spectrometry (Py-GC×GC-MS) and Atmospheric solid analysis probe (ASAP) mass spectrometry to identify the polymer blend, chemical depolymerization of the polymer followed by high resolution infusion using Fourier transform ion cyclotron resonance mass spectrometry (FT-ICR MS) analysis to identify the crosslinking motifs and finally, ion mobility spectrometry (IMS) to access the polymer stereochemistry. These techniques were allowed the characterization of synthetic polymers such as commercial and industrial poly(dienes), polyesters and natural polymers such as amber and dried siccative oils, the structures of which are largely complex.

Développement méthodologique pour l'élucidation structurale de polymères insolubles naturels et synthétiques par dépolymérisation chimique et spectrométrie de masse à ultra-haute résolution

Résumé : L'étude de la dépolymérisation et de la dégradation des polymères d'origine naturelle ou synthétique est encore aujourd'hui un enjeu analytique majeur, notamment en ce qui concerne les polymères insolubles. La caractérisation des polymères et l'étude de leurs voies de dégradation soulèvent d'importants enjeux environnementaux, économiques et scientifiques et en améliorant nos connaissances dans ces domaines nous pourrons bien comprendre les phénomènes impliqués dans leur vieillissement, leur réticulation ainsi que leurs voies de dégradation afin d'améliorer les procédés industriels conduisant à leur fabrication et à leur recyclage. La solution classique pour caractériser de tels polymères est la pyrolyse couplée à la phase gazeuse. Si cette technique fournit des empreintes très caractéristiques des polymères analysés, elle permet difficilement des études structurales fiables en raison de mécanismes de pyrolyse complexes. De plus, la pyrolyse n'identifie pas les unités de réticulation qui sont des éléments clés pour comprendre la structure et la biosynthèse ou l'élaboration d'un polymère. Les travaux menés dans cette thèse visent à trouver de nouvelles solutions pour l'analyse des polymères insolubles en développant de nouvelles méthodes de clivage chimique utilisant des catalyseurs organométalliques de nouvelle génération, ainsi que le développement de nouvelles méthodes instrumentales capables de fournir des informations sur les mélanges complexes émis du clivage chimique. Ces méthodes peuvent aussi être appliquées sur des quantités minimales d'échantillons du patrimoine environnemental et culturel. Les nouveaux catalyseurs permettent d'effectuer les réactions de dégradation des polymères dans des conditions plus douces, préservant davantage la structure d'origine des monomères. Alors que les méthodes d'analyse développées, essentiellement basées sur l'utilisation de la spectrométrie de masse à haute résolution, en particulier trois techniques complémentaires pour permettre une description complète de la structure moléculaire: pyrolyse-chromatographie en phase gazeuse bidimensionnelle/spectrométrie de masse (Py-GC×GC-MS) et spectrométrie de masse à sonde d'analyse des solides atmosphériques (ASAP) pour identifier le mélange de polymères, dépolymérisation chimique suivie d'une infusion à l'aide de l'analyse par la spectrométrie de masse à transformée de Fourier par résonance cyclotronique des ions (FT-ICR MS) pour identifier les motifs de réticulation et enfin, la spectrométrie de mobilité ionique (IMS) pour accéder à la stéréochimie des polymères. Ces techniques ont permis la caractérisation de polymères synthétiques tels que les poly(diènes), les polyesters et les polymères naturels tels que l'ambre et les huiles siccatives séchées, dont les structures sont largement complexes.

Introduction

General Introduction

Polymers, either from synthetic or natural origin, are present nowadays in most of our surroundings. These extremely large molecules are essential to our very existence as they are used in a wide variety of applications, ranging from our food (starch, protein…), our clothes (polyesters, nylons…), our cars (tires, automotive parts…), our houses (wood cellulose, oil and alkyd paints…) and finally our bodies (nucleic acid polymer, proteins…). The first known insoluble polymers were natural polymers including such things as tar and shellac, tortoise shell and horns, ivory, as well as tree exudates that give amber and rubber latex. During the 1800s, these polymers were in many cases chemically treated and modified under heat and pressure to produce many useful materials such as vulcanized rubber and nitrocellulose. As the demand on these versatile molecules started to increase, synthetic polymers begin to appear. The first organic semi-synthetic polymer, called Bakelite was produced in 1909 and then followed in 1911 by the first synthetic fiber known as rayon. However, it was not until the start of the World War II that significant developments in the polymer industry took place as natural polymers were no longer available and the use of synthetic polymers became crucial. For these reasons, synthetics such as synthetic rubber and many more polymers from the polyolefin’s family were largely produced and took the place of natural materials.

The polymer industry using both organic natural and synthetic polymers has continued to grow since then and has evolved into one of the fastest growing industries in the world. In 2007, Europe’s consumption of natural rubber reached 1.3 million tones and 2.6 million tons of synthetic rubber. France and Germany alone were the largest consumers and accounted for approximately 39% of this consumption. It is worth noting that the majority of these polymers are considered as permanent waste and current trends that involve environmental standards require the use of cleaner green polymers.

On the molecular level, the simplest description of a polymer is something made of many units, called monomers. These monomers form macromolecules with a very long chain in which hundreds or thousands of atoms are linked together to form a one-dimensional array. For example, polyolefins are derived from one simple olefin or alkene monomer. Although they may contain one simple structure that repeats itself over and over down the chain, they are considered among the most complicated molecules known. Their complexity results in a great variety of chemical and supramolecular structures offering a wide range of properties. According to their structure and properties, polymers are susceptible to chemical ageing under exposure to various conditions of commonly encountered environments. In fact, ageing in caused by chemical transformations in the chain of these macromolecules leading to their degradation and formation of branched or three-dimensional structures, a phenomenon known as cross-linking. In some cases, ageing can be harmful and manifests itself as a deterioration of the mechanical characteristics of polymers such in the case of natural and synthetic isoprene rubber, and in other cases, for example the natural polymer amber, ageing can help in the formation of the polymer itself. In cultural heritage, especially in the case of oil paintings, ageing plays a major role in allowing oil paint to dry and form a very solid insoluble film able to be fixed on a canvas for hundreds of years. In all pathways, the final product obtained is highly insoluble with very high molecular weight. This kind of polymer is usually very complex due to the chemical modifications and degradations that occurred during the ageing process and may be composed as well from different types of molecules.

Therefore, in order to understand the different phenomena involved in the ageing, degradation and reticulation of polymers, it is essential to develop experimental protocols adapted to elucidate their chemical and structural properties based on their molecular characterization. Due to their complexity, the characterization of such polymers is today a key research subject requiring the use of state-of-the-art analytical tools with a very large separation capacity.

This thesis was carried out in the 'Miniaturization for the Synthesis, Analysis and Proteomics (MSAP)' laboratory created in 2010 and regrouping different research areas such as mass spectrometry, separation techniques and organic and physical chemistry. The MSAP laboratory has an exceptional range of analytical technologies namely the Fourier transform ion cyclotron resonance mass spectrometer (FT-ICR MS) installed in 2018 and equipped with a 9.4 Tesla magnet and different ionization sources.

The thesis work presented here relates to the development and evaluation of innovative depolymerization reactions, ionization techniques and separation by FT-ICR ultra-high-resolution mass spectrometry and ion mobility spectrometry (IMS) for the analysis of different classes of insoluble natural and synthetic polymers. The development of soft chemical depolymerization techniques allowed the solubility of these polymers in organic solvents while preserving their structural composition. Ultra-high-resolution mass spectrometry allowed the separation of detected species according to their *m/z* and assigning each signal a unique raw molecular formula thanks to precise mass measurements. The capabilities of Fourier transform mass spectrometry helps to describe very complex materials, such as those resulting from the depolymerization and analysis of polymers. However, despite the exceptional performance of the FT-ICR mass spectrometry, this technique cannot directly separate isomers. For this reason, it is essential to use ion mobility spectrometry. It is a technique for separating ions in gas phase, depending on their mobility within a drift tube, in a buffer gas and in the presence of an electric field. The Ion mobility spectrometry is increasingly used for analytical applications, via its coupling with mass spectrometry (IMS-MS), then allowing separation at both as a function of the *m/z* ratio and the drift time (t_D).

This manuscript is divided into two major sections.

The first section includes four chapters which deal mainly with commercial, industrial and real-world natural and synthetic polymers, with an in-depth study of polydienes such as polybutadiene and polyisoprene.

The first chapter presents some generalities on polymers with a brief description on their history, origin, formation, chemical composition and their different types and applications. It discusses details on specific classes of polymers, namely natural and synthetic polyolefins and polydienes, their classes, degradation pathways and structural modifications.

The second chapter discusses the different analytical techniques used during this work. It presents mass spectrometry in general, ionization sources and analyzers especially the FT-ICR, tandem mass spectrometry, ion mobility spectrometry and comprehensive two-dimensional gas chromatography. It also presents the different available data treatment and visualization methods used in these types of analyses.

The third chapter presents a bibliographical study of analytical researches based on mass spectrometry and applied for insoluble organic polymers analysis in general. It discusses mainly the studies concerned by the depolymerization and structural and molecular characterization of natural and synthetic polymers with emphasis on polyolefins and polydienes.

The fourth chapter is dedicated to results and discussions obtained from the research work of this thesis. This chapter is itself divided into several parts. The first part deals with the application of the developed analytical methodology on two major polydienes, polybutadiene and polyisoprene, their depolymerization and their analysis either by pyrolysis-based methods such as ASAP-MS and DIP-FTICR-MS or by electrospray ionization-based methods such as ESI-FTICR-MS and IMS-MS. All these different analytical techniques helped uncover their structure and specific finger-print. The second and third parts describe the application of the depolymerization reaction on natural and synthetic real world and industrial polydienes.

The second section represents a thorough study on polymers found in cultural heritage samples such as drying oils and oil paints. It includes chapter 5, 6 and 7.

The fifth chapter is an introduction on drying oils and oil paints. It describes the components of oil paints and the different phenomena that occur during their drying and polymerization.

The sixth chapter describes and discusses the different analytical techniques used for the analysis oil paints.

The seventh and final chapter presents the development of a specific strategy to study drying oils and oil paints in cultural heritage. Oil paints, when dry, tend to harden by forming a very complex insoluble molecular network. This chapter discusses the optimization of the protocol for the structural deciphering of this network together with understanding the degradation of paint films. The protocol consists on the soft depolymerization of present-day and old drying oils as well as oil paints followed by an analysis by ultra-high-resolution mass spectrometry leading to a very detailed identification and characterization.

Natural and synthetic insoluble polymers

Chapter 1:

Introduction to polymers

Chapter 1. Introduction to polymers

I. History of polymers

Since the beginning of life, polymers have existed in natural form. These polymers such as DNA, RNA, proteins and polysaccharides played crucial roles in plant and animal life. In fact, humans have started from the earliest times to exploit the naturally-occurring polymers and used them as materials for essential requirements such as clothing, decoration, shelter, tools, weapons, writing materials and many others. Later on, in the nineteenth century, important discoveries were made concerning the modification of certain natural polymers and these discoveries began to shape today's polymer industry. The first real example of polymer modifications was carried out by Henri Braconnot in the 1830s, as he developed along with Christian Schönbein different derivatives of the natural polymer cellulose, creating new semi-synthetic polymers called cellulose acetate and nitrocellulose. Nitrocellulose also known as gun cotton was at first commercially produced as an explosive. However, it was found that this polymer can be used as a hard-elastic material, soluble and able to be molded into different shapes. Ten years earlier, Thomas Hancock proved that when subjected to a repeated high force, raw natural rubber (polyisoprene) loses its stickiness helping to blend it with various additives. In the 1840s, Charles Goodyear discovered that adding Sulphur to natural rubber and heating it improved its elastic properties and eliminated its tackiness. This discovery went on to be known as vulcanization of rubber and is nowadays one of the most commonly performed modifications to produce hard rubber used as tires for vehicles. All these polymers can be described as semi-synthetic as they are created following the modification of natural polymers. The first synthetic polymer to be produced and commercialized by Leo Baekeland in the 1910s is the polyoxybenzylmethylenglycolanhydride known as 'Bakelite'. It was formed following the condensation reaction of phenol and formaldehyde and became hugely popular as a synthetic plastic material. During World War II, the demand on polymers surged and it was important to preserve the scarce natural resources, that's why the production of alternative polymers was a priority and a large number of synthetic polymers became commercialized for the first time such as polyolefins and silicones.[1]

As the polymer industry became firmly established, the global demand for polymers and their production increased dramatically. Following World War II, the production of different types of synthetic polymers was at about 25 million metric tons between 1950 and 1970. Today, the global polymer production increased to 600 million metric tons for the market is valued at about $533.6 billion. On the other hand, the surge in polymer production created environmental problems as most synthetic polymers are disposable and last forever in the environment. In the twenty first century, advances continue to be achieved in both scientific and industrial fields and as a result there is increasing demand on the understanding of polymers behavior and fate in nature as well as the development of more environmentally friendly, specialized and functionalized polymers.[2]

II. Origin of polymers

Polymers are macromolecules built from units called monomers, linked to each other by covalent bonds which according to their structure and chemical nature can give rise to polymers of various types. These covalent bonds which constitute the macromolecular skeleton can give rise to a variety of polymers according to the nature of atoms: carbon-carbon simple and double bonds are the backbone of polyolefins. The bonding of atoms of carbon with other atoms, in particular oxygen form the polymeric chain of polyesters. Other types of polymers are formed from chains not comprising any carbon atoms such as polysilanes.[3] The types of polymers may vary; however, they belong in general to two major groups: Natural or Synthetic polymers. The group of natural or biological polymers which is related to the essence of life itself, is constituted among other substances by polysaccharides, such as starch and cellulose, proteins and nucleic acids, natural rubber, and amber fossils. Apart from these polymers, a group of synthetic polymers has been developed. The first objective of synthetic polymers is to obtain substitutes for some natural macromolecules such as rubber and silk, however with technological advances, hundreds of substances which do not have natural analogues were produced and they became practically essential of the development of modern life. In the contemporary world, polymers have covered all areas of development and manufacturing of products. The use and applications of these materials grows every day, so it is very important to know these materials as well as possible, not only for the advantages they offer, but also for the inconveniences they cause due to their accumulation when they are no longer usable tools.

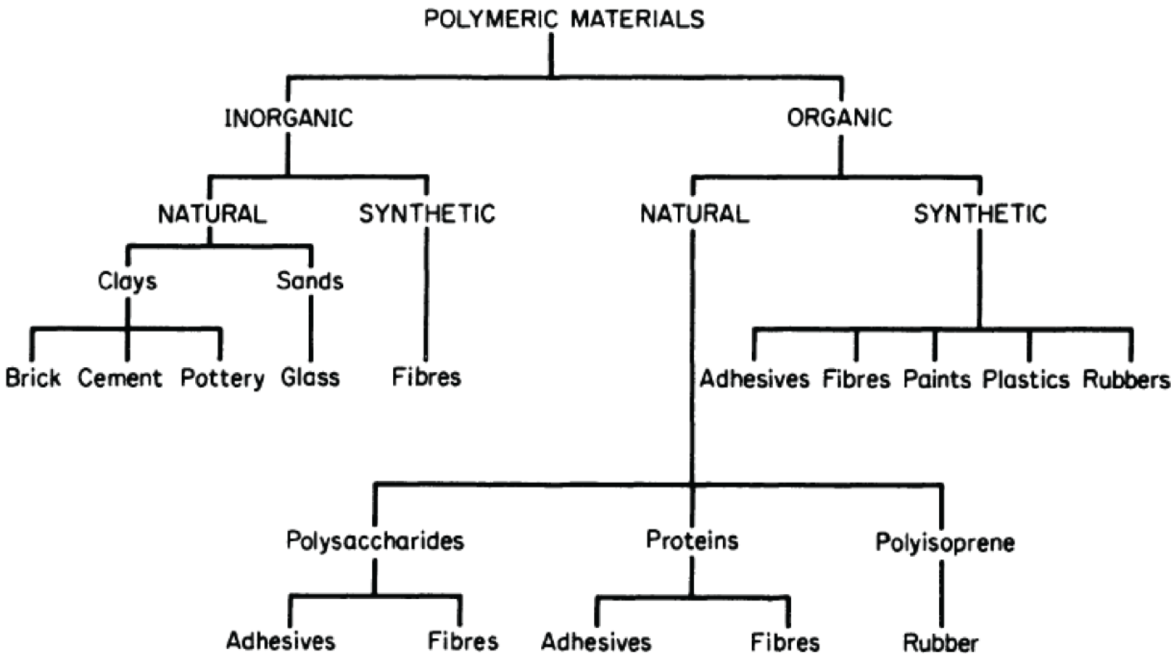

Figure 1. Classification of polymeric materials

Table 1. Comparison between natural and synthetic polymers

Natural Polymers	Synthetic Polymers
Occurs naturally	Artificially produced
Have been in used since thousands of years	Have been made significant since the last 125 years
Natural reaction controls the properties	Highly engineered properties could be determined by controlling the reaction
Usually biodegradable	Some synthetic polymers are biodegradable
Similar chain lengths of molecules	Chain lengths could be significantly varied based on the reaction conditions
Backbone could be of carbon, oxygen, and nitrogen	Backbone is mostly carbon, oxygen, sulfur, nitrogen and silicon
Environmentally friendly	Environmental friendliness is of concern
Limited recyclability	Some of the synthetic polymers could be recycled multiple times

II.1. Natural polymers

Nature has always been a very powerful source of designing and engineering of novel polymeric materials. In general, natural polymers are polymers which are present in, or created by, living organisms. They can widely occur in nature or are extracted from plants or animals. There exist two major types of natural polymers: The first type includes polymers that are produced or found in living organisms such as carbohydrates and proteins and the second type consists on polymers that need to be polymerized in order to give the final polymeric product. Their main source is usually renewable resources such as tree resins that polymerize into amber fossils, triglycerides found in vegetable oils like linseed oil, walnut oil and soybean oil and natural rubber. Some of the examples of natural polymers are proteins and nucleic acid which occur in human body, cellulose, lignin, silk, wool, natural rubber and amber.[4] The last two polymers will be depolymerized to study their structure and finger print by chemical characterization and mass spectrometry and the results will be presented in the manuscript.

Natural polymers are naturally built mainly by condensation polymerization. In fact, most of these polymers can be used as reference for remarkable performances such as strength and adhesion. They are currently gaining interest among the research community as they exhibit high biocompatibility, biodegradability, accessibility, stability, lack of toxicity and low cost. They tend to undergo reactions that create bonds between their polymeric chains known as cross-linking and forming very complex structures. These properties as well as many others are the result of billions of years of optimization and ageing. Nowadays, the strategy to produce valuable synthetic materials is based on mimicking the extremely efficient production processes carried out in nature. As a consequence, it is crucial to understand the structures and functions which give these exceptional properties of natural polymers.[5]

II.2. Synthetic polymers

The increasing demand on polymeric materials and the decreasing availability of natural polymers during the past decades led to the need of developing synthetic polymers. Synthetic polymers can be defined in general as artificially produced or man-made polymers. They are commercially produced in large quantities and can be used in most day-to-day life applications. The most famous and used synthetic polymers are polyethylene, polystyrene, polyamides (nylon), poly(vinyl chloride), synthetic rubber, Teflon, epoxy resin and many others.[6] They can be classified into four different categories: thermoplastics, thermosets, elastomers and synthetic fibers. The first category can be moldable when specific temperatures are applied and solidify when cooled. Thermosets are usually used in adhesives as they become solid one they have set. On the other hand, elastomers such as rubber are very flexible and can be easily shaped. Finally, synthetic fibers are produced by modifying natural plant and animal fibers. The main polymeric chain of synthetic polymers can vary widely according to their atomic composition.

For example, polyethylene, polystyrene and polyacrylate contain a backbone made up of carbon-carbon bonds. Polyamides, polyesters and polysulfides contain other heteroatoms such as oxygen, sulfur or nitrogen and are usually called heteropolymers. There exist also synthetic polymers with no carbon atoms in their backbone such as silicone-based polymers.[7]

Synthetic polymers are very versatile and have a variety of applications. They are often used in multiple fields of life such as electrical devices, sports and musical equipment, food packaging, coatings and adhesives, fabrics and textiles, optical fibers, automotive industry, non-stick pans and many other applications. Their most important features are chemical inertness, insolubility, resistance to various kinds of chemicals and resistance to degradation. As a result, they are often non-biodegradable and last a very long time in nature which is harmful to the environment. Due to the environmental issues created by these polymers, it is crucial to understand their structure and degradation in order to find new ecological alternatives such as bioplastics. [8]

IV. Classes of polymers

Natural and synthetic polymers can both be classified into different classes according to their chemical structure and composition, synthesis or formation and properties. Most of these classes are considered as nondegradable polymers and include polyolefins and polydienes, polyesters, polysiloxanes, polyurethanes, polycarbonates, polyamides, polyethers, polsulphones as well as other types. The following manuscript will outline the structural study of only the first three classes of polymers: polyolefins, polydienes and polyesters.[9]

III.1. Polyolefins

In spite the fact that polyolefins were one of the last types of polymers to be commercialized, they have become the most widely used polymers through-out the world. Polyolefins can be defined as a group of polymers which is based on unsaturated aliphatic hydrocarbons containing one double bond per molecule (olefin). They constitute almost 50% of the annual polymer production worldwide and are typically used in our everyday life. As they have wide range of properties, many applications and low cost, they have gained a lot of attention in recent years. They are most often derived from natural gas or form low-molecular-weight constituents of petroleum. Polyolefins can be distinguished into two groups: lower olefins whose molecules contain only one pair of carbon atoms and higher olefin in which two or more pairs of carbon atoms are present per molecule. Both groups can be made into polymers but the most famous commercial and important are polyethylene and polypropylene. Other more specialized polyolefins are also produced and include polybutene and polyisobutylene. The presence of a double bond in their molecules is the key to a successful polymerization. In fact, by using specific chemical catalysts and under the influence of heat and pressure, the double bond tends to open forming two single bonds which will link one molecule to another. [10]

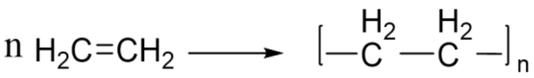

$$n\ H_2C{=}CH_2 \longrightarrow [-\overset{H_2}{C}-\overset{H_2}{C}-]_n$$

Figure 2. Polymerization of ethylene leading to polyethylene

Polyolefins are lightweight, flexible, thermoplastic materials that can be made into clear films and sheets, strong and resilient bottles and containers, water-resistant carpet fibers and many other products. [11]

Polyolefins are produced by the polymerization of olefins units. The most common industrial source of olefins is a process called cracking of crude oil. Cracking is performed to breakdown complex organic molecules into simpler molecules such as light hydrocarbons by breaking the carbon-carbon bonds in the original precursors. It is the principal industrial method to produce ethylene and propylene. There are different classes of polyolefins that are produced depending on the polymerization conditions. For example, producing low-density polyethylene requires severe polymerization conditions such as high pressure and high temperature. However, high-density polyethylene is polymerized in the presence of Ziegler-Natta catalyst systems. This process produces a polymer with increased strength and chemical resistance. Another type of polyolefin can be produced, linear low-density polyethylene, by copolymerizing ethylene and other monomers such as butene or hexene.[12] Despite the importance of polyolefins, they pose special challenges for their analysis due to their semi crystalline nature insolubility in common solvents at ambient temperatures.

III.2. Polydienes

Polydienes constitute an extremely important group of polymers. This group includes natural rubber, synthetic rubber and all the products of polymerization and copolymerization of conjugated dienes. This part of the manuscript will present a bibliographical study on polydienes namely polyisoprene and polybutadiene rubber as well as amber, a natural polymer with a polymeric chain based on isoprenic units. The analytical work carried out in this thesis is mainly focused on this type of polymers.

III.2.1. Natural rubber

Europeans explorers arrived to Central and South America at the end of the 15th century and the discovered that the natives knew how to make certain objects such as bouncing balls from a very flexible material. After observation, they noticed that an emulsion can be extracted from certain trees called *Hevea Brasiliensis* by making a spiral incision on the bark of the tree. This emulsion, known as latex, is formed of almost 60% water and when spread on fabric and allowed to dry, it can be used to produce waterproof and flexible materials. The solid material formed after drying latex is thus named rubber. However, it wasn't until the start of the 19th century that scientists became interested in the structure of rubber. In 1770, rubber was used by Joseph Priestley to rub out pencil marks. In 1820, Hancock noticed that rubber became plastic and able to be manipulated when mechanically masticated. As natural rubber was not yet fully understood, the world consumption was limited to only about 100 tons in 1830.[13] Ten years later, Charles Goodyear makes a discovery that revolutionized the rubber industry worldwide. He realizes that the addition of sulfur followed by heating for a certain time makes the material more elastic and stable to temperature changes. This process would be known as vulcanization. Vulcanization is a form of reticulation and the process of forming sulfur bridges between the chains of the polymer transforming it into a strong and elastic material. As result to this significant advance, the use of rubber developed considerably as well as the research associated with it. [14]

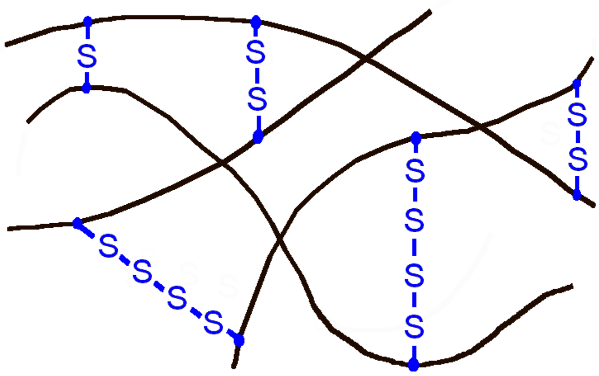

Figure 3. Vulcanized rubber with sulfur

Due to the flexibility of rubber and the improved mechanical properties due to the development of the vulcanization process, John Boyd Dunlop develops the idea of using air-filled bands around the rims to protect them. He deposits the first patent for the manufacture of tires in 1888, while four years later the Michelin brothers develop the first removable tires.

On the molecular level, natural rubber is composed almost entirely of *cis*-1,4-polyisoprene with the molecular formula $(C_5H_8)_n$ and a very wide range of molecular weight (Figure 4). The physicochemical properties of this material are a direct consequence of its structure. The building block of this macromolecule, the polyisoprene, has a reactive carbon-carbon double bond. In fact, the responsiveness of these unsaturation a variety of chemical modifications, but it can also cause the deterioration of its mechanical properties by oxidation.

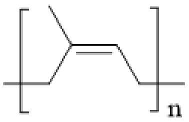

Figure 4. Structure of cis-1,4-polyisoprene

III.2.2. Synthetic rubber

Faced with growing demand and despite the many plantations in Southeast Asia, South-East, the quantity of available natural rubber began falling and its prices increasing. Multiple attempts are then performed from the twentieth century to synthesize polymers with properties equivalent to those of natural rubber. These polymers are known as "synthetic rubber". Fritz Hofmann, a German chemist, synthesizes in 1909 a synthetic rubber by polymerization of 2,3-dimethyl-1,3-butadiene.[15] The demand for vehicles and tires intensified during the First World War and the Russian Revolution in October 1917 made it difficult to have any supply of natural rubber. Therefore, intense research has been developed in Germany and Russia for the development of substitute products for this matter. And this is how the German company Bayer produced, in 1918, 150 tons per month of hard-type methyl rubber for the manufacture of submarine accumulator tanks. For their part, the Russians made a rubber from ethyl alcohol and also from oil whose production ceased permanently in 1926. Research did not stop, which resulted in polybutadiene polymerized with sodium. Then the butadiene-styrene copolymer was discovered in 1929, and its annual output reached 5000 tons in 1938. America's first synthetic rubber, polymerized chloroprene or Neoprene®, was manufactured and marketed by the company Dupont de Nemours. It's an elastomer that costs twenty times more than natural rubber. The end of the second world war allowed the return of the natural rubber trade with South-East Asia. In 1980, synthetic rubber, essentially polybutadiene rubber "BR", once again became the first rubber consumed in the world. [16]

Nowadays, synthetic rubber can be obtained by the polymerization of isoprene or butadiene giving polyisoprene (PI) and polybutadiene (PB) respectively. Unlike natural rubber which is mainly made up of 1,4-cis units, synthetic rubbers depending on the type of polymerization used (radical, coordination, organometallic or even ionic) can have different microstructures. In fact, it is possible to obtain polymers with variable microstructures containing 1,4-cis, 1,4-trans units and vinyl (Figure 5). Depending on the respective fractions of the different units, the thermal and mechanical properties such as resistance to temperature and stress mechanics will be largely affected.

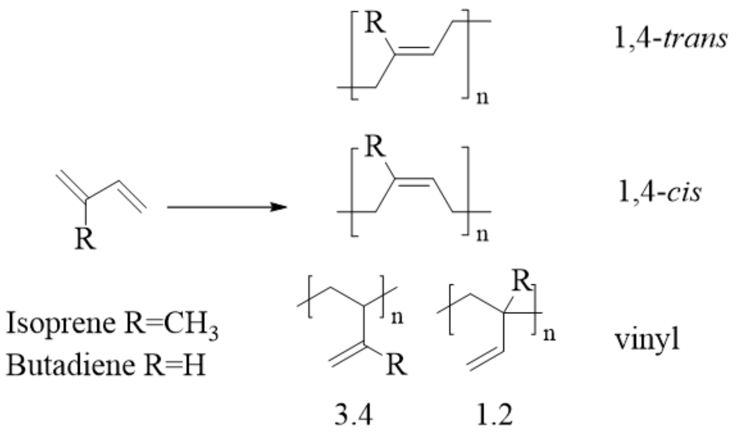

Figure 5. Possible microstructures of isoprene and butadiene units obtained after polymerization

Among the most widely used synthetic rubbers, we can cite a few general-purpose rubbers:[17]

Synthetic polyisoprene is directly comparable to natural rubber, although it contains only 98% *cis* configuration instead of almost 100% for natural rubber. The synthetic polyisoprene withstands tensile stress well, has good abrasion resistance, is resistant to tear, absorbs shock and provides vibration damping. But similar to natural rubber, it has poor resistance to light, ozone and heat. He has no resistance to oils and fuels. This rubber can be synthesized by the process of Ziegler-Natta polymerization, starting from an unsaturated hydrocarbon, isoprene.

Polybutadiene (PB): 1,4-cis-polybutadiene is the main competitor of natural rubber because it is very similar to it, by its high resistance to abrasion, its good absorption of shock and its ability to decrease vibration. In addition, it has excellent resistance to cold, this is the best of general-purpose rubbers. On the other hand, it has a worse resistance to stress than natural rubber. 1,4 *trans*-polybutadiene (PB) is a thermoplastic with a melting point of 140 °C and low resistance to light, ozone and heat. This rubber is used for belts, hoses, seals.

III.2.3. Amber

Humans were fascinated by amber resins since they were first discovered along the shores of the North and Baltic seas. Many efforts and studies were carried out to understand the structure and origin of amber, however, little significant progress has been made in order to characterize amber structurally and chemically. In general, fossil resins such as amber, originate from resinous exudates of resin-rich trees. When fossilized, they polymerize and turn into a complex diene system carried by a terpene structure which is based on the linking together of isoprene units. The fossilization process of amber resins is still not fully understood and some theories suggest a progressive oxidation and polymerization by a free-radical mechanism.

According to their chemical constituents, amber resins can be classified into five different classes. For example, class I is the most abundant and is based on labdatriene carboxylic acids such as communic acid. Communic acid polymerizes to provide a structure with isolated double bonds similar to that of natural and synthetic rubbers. This polymerized structure is highly insoluble and difficult to analyze by the usual methods of elucidating structures of organic compounds. However, as polymerized amber consists on the same back bone as rubbers, it can be considered as part of polydiene polymers affording similar behavior and degradation pathways.

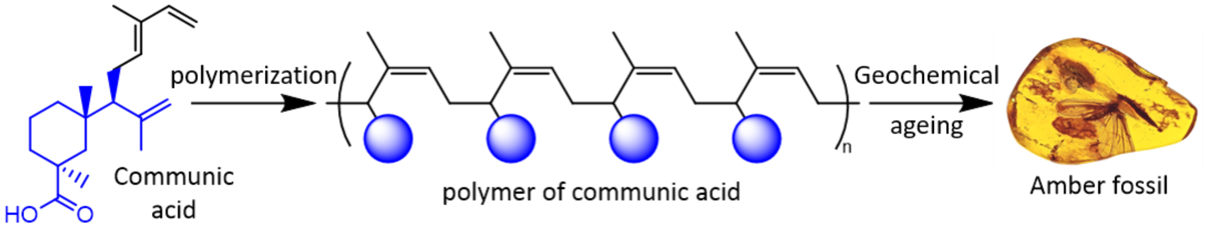

Figure 6. Polymerization of communic acid and ageing of amber

V. Degradation of polydienes

Advances and developments in polydienes chemistry led to an increase in the demand on their products. With the increased demand, it became very essential to find new methods to describe these polymers. An alternative method of transforming and modifying polydienes to obtain soluble and analyzable interesting products is degradation. It allows the formation of molecules with preserved structure and controlled molecular mass. In fact, controlled degradation of long chains polydienes such as polyisoprene and polybutadiene, is an area that has largely been studied in recent years, in particular degradation by photochemical means, by ozonolysis, by biodegradation, by metathesis or even chemically under oxidizing conditions. In all cases, the main objective of these methods is to have good control on the molar mass obtained and chain ends. The work presented in this section of the manuscript will mainly focus on the depolymerization of polydienes using degradation by metathesis. A literature study on the depolymerization of polydienes by olefin metathesis reactions is presented in chapter 3 and the application of this study of polybutadiene and polyisoprene polymers will be discussed in chapter 4.

IV.1. Degradation by redox systems

The degradation of polydienes, especially rubbes by redox systems requires an appropriate mixture of oxidizing and reducing agents in order to be able to cleave the chains.[18] The most used oxidizing/reducing agents are organic peroxides, hydrogen peroxides and atmospheric oxygen together with phenylhydrazine or sulfamic acid. Depending on the couple used, breaking the polydiene chains makes it possible to obtain low molar masses and introduce reactive functions at the end of chains such as carbonyl or hydroxyl groups. A very good example on this type of degradation is the redox couple atmospheric oxygen/phenylhydrazine used for the degradation of natural rubber following the mechanism in Figure 7. It allowed to preserve the initial structure of the polyisoprene polymer and obtain a wide range of molar masses. [19-20]

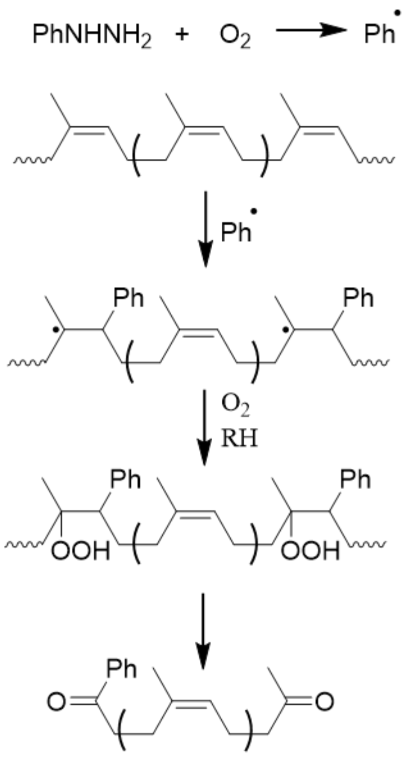

Figure 7. Mechanism of degradation of natural rubber by the redox couple phenylhydrazine/oxygen

IV.2. Degradation by photochemical pathway

The depolymerization under UV irradiation of NR in solution in toluene represents a photochemical degradation. The presence of hydrogen peroxide and methanol or THF made it possible to obtain after irradiation of the chains, liquid polymers with alcohol functions at the ends (Figure 8). The HO• radicals obtained after breaking homolytic hydrogen peroxide by UV radiation will oxidize the α chain of the double bond, causing the chain to break, associated with the formation of ends hydroxyl. This method has the advantage of having a low cost without affecting the stereochemistry of the polymer. However, a small fraction of crosslinked polymer is formed during the reaction.[21]

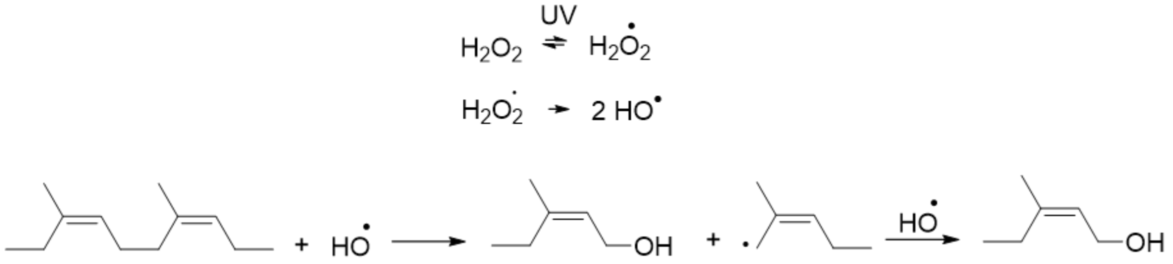

Figure 8.Mechanism of degradation of natural rubber by UV in the presence of hydrogen peroxide

IV.3. Biodegradation

The majority of studies that report degradation of rubbers by microorganisms explain that the first step in cleavage of double bonds is an oxidation reaction.[22-23] A complex mechanism of biodegradation, using β-oxidation to depolymerize chains was proposed by Bode in 2001 (Figure 9).[24] Natural, synthetic or even crosslinked NRs can be degraded with this method, obtaining molar masses between 1000 - 10 000 g.mol^{-1} with aldehyde functions and / or carbonyl groups at the chain ends. In parallel with this degradation, oligomers can also be obtained with carbonyl functions at the chain ends. [25-26]

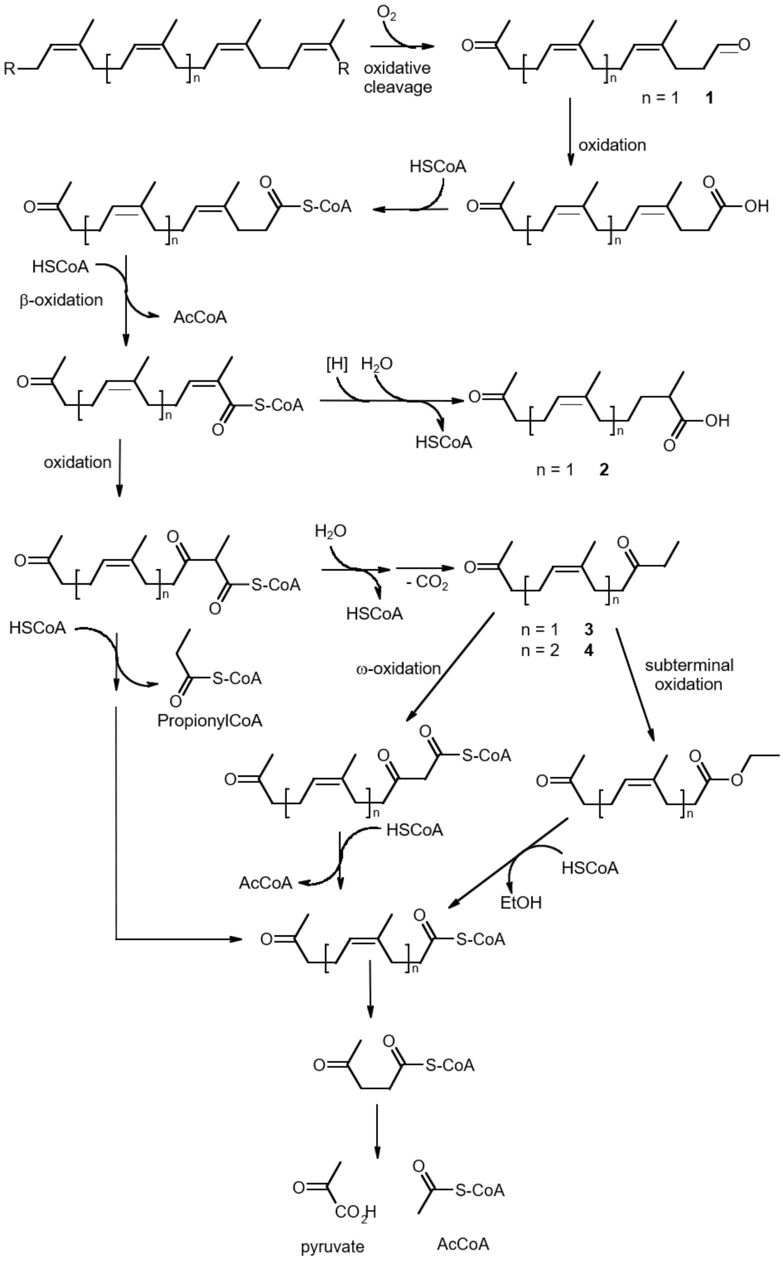

Figure 9. Mechanism of biodegradation of natural rubber

IV.4. Degradation by ozonolysis

Discovered in 1840 by Schönbein during experiments on the electrolysis of water,[27] ozonolysis was first used for the structural determination of organic molecules. The oxidizing cut at the level of alkenes of large molecules into small molecules allowed easier identification. It was from 1903 and thanks to the studies of Harries that ozonolysis has become an important chemical tool, especially for determining the structure of rubbers.[28] Today, many studies of ozonolysis of rubbers have been reported. It can in particular be used for the preparation of rubbers of low molar masses with carbonyl functions at the end of the chain.[29-31] This method has for example allowed to obtain, from 1,4-cis polybutadiene, low molar mass telechelic hydroxyl PB (HTPB).[32-33] The complex mechanism of ozone attack on the double bond carbon-carbon polydienes have been widely described by Criegee and Ebdon (Figure 10).[30, 34] Ozone will initially form an unstable molozonide intermediate, which quickly decomposes into a stable carbonyl compound (aldehyde or ketone) and an oxide of unstable carbonyl (zwitterion). The carbonyl oxide will then be able to rearrange itself into stable compounds leading to a decrease in the molar mass of the polymer, accompanied by an increase in the number of oxygenated functional groups such as aldehyde, ketone, carboxylic acid or even peroxides.

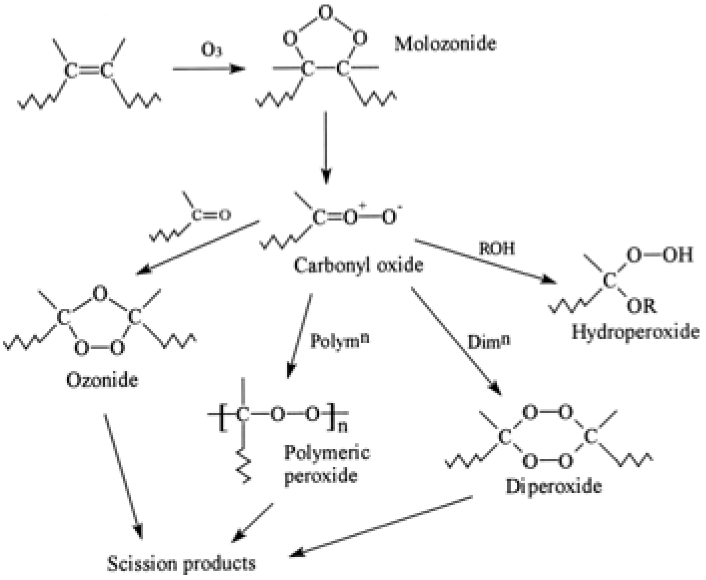

Figure 10. Mechanism of degradation of natural rubber by ozonolysis

IV.5. Degradation by periodic acid

The oxidative degradation of polydienes under the action of periodic acid is currently the method which allows to have the best control of the length of final chains and the best control of the functionalization of chain ends. It was first described in 1977 by Reyx and Campistron for the degradation of NR and PI.[35] This method notably involves periodic acid to cut the doubles bonds of polydienes in order to obtain ketone and aldehyde ends for PI and aldehydes for PB. We can however distinguish two variations of this method according to whether the polymer has been previously epoxidized or not (Figure 11).[36]

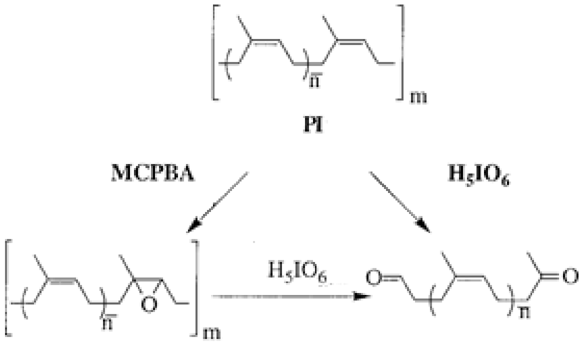

Figure 11. Degradation and functionalization of PI using periodic acid

The degradation of PI by periodic acid is a two-step process involving two molecules of acid per double bond. A slow first step is oxidation of a double bond of the polymer chain by H_5IO_6. Epoxy units and diols will be obtained. The second, faster step involves a second periodic acid molecule to cleave previously modified units to obtain an aldehyde and a ketone. (Figure 12).

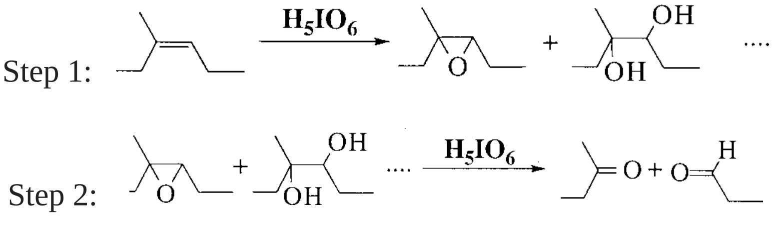

Figure 12. Degradation steps of PI by periodic acid

IV.6. Degradation by metathesis

The recent discovery of olefin metathesis reactions has opened up new avenues for the chemical modification of polydienes. The mechanism of this reaction was described by Hérisson and Chauvin in 1971.[37] It involves an active species formed from the precatalyst by the departure of a ligand from the coordination sphere of the metal. The reaction begins with the coordination of an alkene with the resulting metal-alkylidene to form a metallacyclobutane. The latter leads, by opening the cycle, to a new alkene and a new metal-alkylidene. The metal-alkylidene reacts with a new alkene, giving rise to a catalytic cycle (Figure 13).

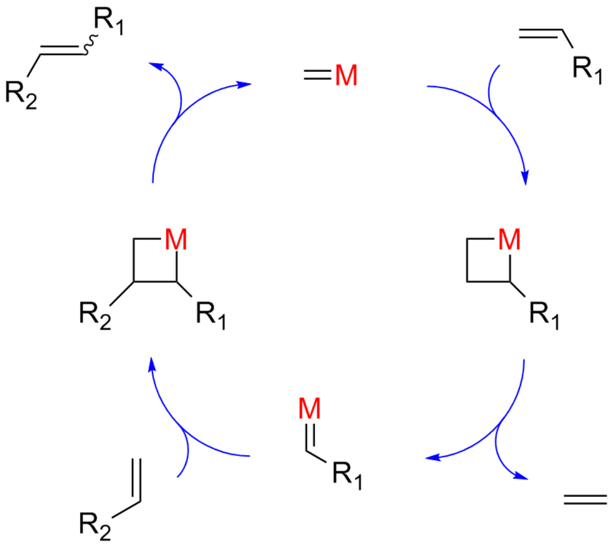

Figure 13. Catalytic cycle in olefin metathesis

The main catalysts originally contained transition metals such as molybdenum or tungsten, in particular following the work of Schrock.[38-39] These catalysts nevertheless have drawbacks. Being sensitive to air and water, they should be handled in a glove box. Moreover, they tend to be disabled by polar functions, thus reducing the choice of substrates for the metathesis reaction. But, from the 1990s, they were gradually replaced by ruthenium complexes, the best known of which are those of Grubbs of 1st (G1), 2nd (G2) and 3rd (G3) generation and Hoveyda 2nd generation (HG2) [40-42] (Figure 14), which do not have the previously mentioned disadvantages.

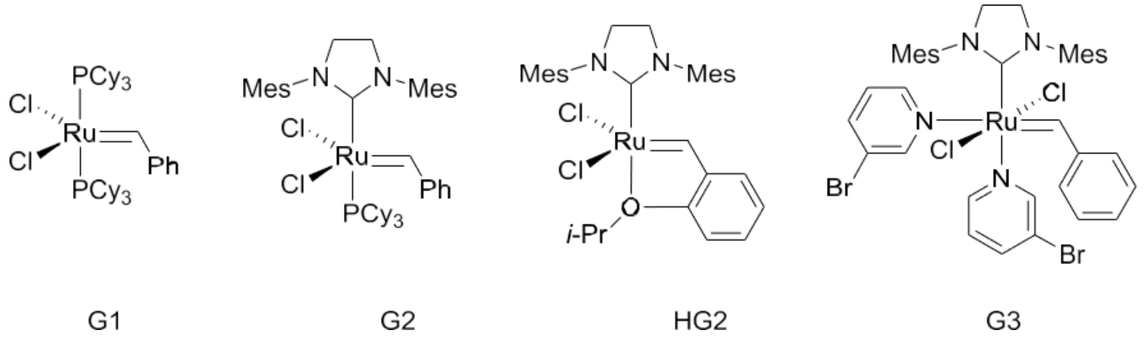

Figure 14. 1st, 2nd and 3rd generation Grubbs catalyst and 2nd generation Hoveyda Grubbs catalyst

Several types of metathesis reaction deriving from the same mechanism are possible depending on the types of reagents involved (Figure 15). The most common are cross metathesis (CM) between two acyclic alkenes, ring-closing metathesis (RCM), ring-closing metathesis (ROM) between a cyclic alkene and another acyclic, ring-opening metathesis polymerization, ROMP) and acyclic diene metathesis (ADMET)

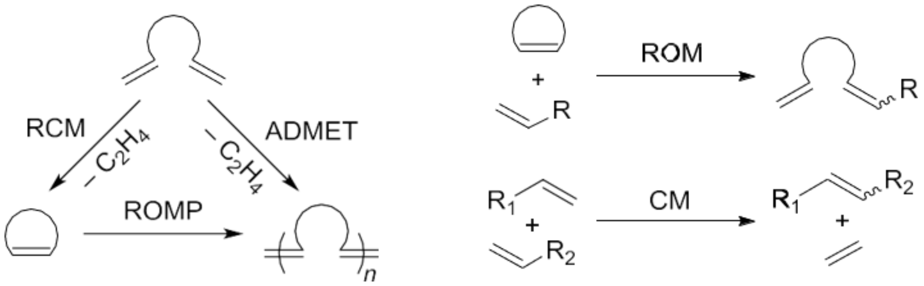

Figure 15. Principal reactions of olefin metathesis

In the case of polyisoprene, the degradation can be carried out by metathesis using second generation Grubbs or Hoveyda Grubbs catalysts. Thus, it is possible to obtain telechelic PI carrying various groups depending on the chain transfer agent.

In conclusion, the metathesis reaction of the alkenes, applied to *cis*-1,4-polyisoprene which constitutes natural rubber, therefore allows, in addition to depolymerization, the modification of the structure of the polymer by the contribution of chemical functions. Furthermore, all these methods of depolymerization of polydienes aim to obtain oligomers with specific functional groups at the end of their chains which will increase their solubility and allow a better understanding of their structure.

References

1. Young, R. J.; Lovell, P. A., *Introduction to polymers*. CRC press: 2011.
2. Polymer Market Research Report: By Type, Base Material, Application - Global Industry Analysis and Growth Forecast to 2030. https://www.reportlinker.com.
3. Barrere, C. Analyse de polymères synthétiques par résonance magnétique nucléaire et spectrométrie de masse. Aix-Marseille 1, 2011.
4. John, M. J.; Thomas, S., *Natural polymers: composites*. Royal society of chemistry: 2012; Vol. 1.
5. Bassas-Galia, M.; Follonier, S.; Pusnik, M.; Zinn, M., Natural polymers: a source of inspiration. In *Bioresorbable polymers for biomedical applications*, Elsevier: 2017; pp 31-64.
6. Shrivastava, A., 1 - Introduction to Plastics Engineering. In *Introduction to Plastics Engineering*, Shrivastava, A., Ed. William Andrew Publishing: 2018; pp 1-16.
7. Peacock, A. J.; Calhoun, A., *Polymer chemistry: Properties and application*. Carl Hanser Verlag GmbH Co KG: 2012.
8. Ouellette, R. J.; Rawn, J. D., 28 - Synthetic Polymers. In *Organic Chemistry Study Guide*, Ouellette, R. J.; Rawn, J. D., Eds. Elsevier: Boston, 2015; pp 587-601.
9. Gunatillake, P.; Adhikari, R., Nondegradable synthetic polymers for medical devices and implants. In *Biosynthetic Polymers for Medical Applications*, Elsevier: 2016; pp 33-62.
10. Vasile, C., *Handbook of polyolefins*. CRC Press: 2000.
11. Britannica, T. E. o. E., polyolefin. *Encyclopedia Britannica* **26 Jul. 2012**.
12. Posch, D. W., Polyolefins. In *Applied Plastics Engineering Handbook*, Elsevier: 2017; pp 27-53.
13. Saunders, K. J., *Organic polymer chemistry: an introduction to the organic chemistry of adhesives, fibres, paints, plastics and rubbers*. Springer Science & Business Media: 2012.
14. Guise-Richardson, C., Redefining Vulcanization: Charles Goodyear, patents, and industrial control, 1834-1865. *Technology and Culture* **2010,** *51* (2), 357-387.
15. Hofman, F. D., Germany, K. 1909.
16. Rouhi, A. M., Olefin metathesis: the early days. *Chem. Eng. News* **2002,** *80* (51), 34-38.
17. Arlie, J.-P., *Caoutchoucs synthétiques: procédés et données économiques*. Éditions Technip: 1980.
18. Bobade, S.; Wang, Y.; Mays, J.; Baskaran, D., Synthesis and Characterization of Ureidopyrimidone Telechelics by CuAAC “Click” Reaction: Effect of T g and Polarity. *Macromolecules* **2014,** *47* (15), 5040-5050.
19. Fang, Y.; Zhan, M.; Wang, Y., The status of recycling of waste rubber. *Materials & Design* **2001,** *22* (2), 123-128.
20. Brosse, J.; Campistron, I.; Derouet, D.; El Hamdaoui, A.; Houdayer, S.; Reyx, D.; Ritoit-Gillier, S., Chemical modifications of polydiene elastomers: A survey and some recent results. *Journal of Applied Polymer Science* **2000,** *78* (8), 1461-1477.
21. Ravindran, T.; Nayar, M. G.; Francis, D. J., Production of hydroxyl-terminated liquid natural rubber—mechanism of photochemical depolymerization and hydroxylation. *Journal of applied polymer science* **1988,** *35* (5), 1227-1239.
22. Tsuchii, A.; Takeda, K., Rubber-degrading enzyme from a bacterial culture. *Applied and Environmental Microbiology* **1990,** *56* (1), 269-274.
23. Linos, A.; Berekaa, M. M.; Reichelt, R.; Keller, U.; Schmitt, J. r.; Flemming, H.-C.; Kroppenstedt, R. M.; Steinbüchel, A., Biodegradation of cis-1, 4-polyisoprene rubbers by distinct actinomycetes: microbial strategies and detailed surface analysis. *Applied and environmental microbiology* **2000,** *66* (4), 1639-1645.
24. Bode, H. B.; Kerkhoff, K.; Jendrossek, D., Bacterial degradation of natural and synthetic rubber. *Biomacromolecules* **2001,** *2* (1), 295-303.
25. Rose, K.; Steinbuchel, A., Biodegradation of natural rubber and related compounds: recent insights into a hardly understood catabolic capability of microorganisms. *Applied and environmental microbiology* **2005,** *71* (6), 2803-2812.
26. Shah, Z.; Hameed, A.; Hasan, F., Effect of pretreatments on enhanced degradation of polyisoprene rubber by newly isolated bacillus sp, strain S10. *Journal of the Chemical Society of Pakistan* **2009,** *31* (4), 638-646.

27. Schönbein, C., On the Odour Accompanying Electricity, and on the Probability of Its Dependence on the Presence of a New Substrate. *Proceedings of the Royal Society of London Series I* **1837,** *4*, 226.

28. Rubin, M. B., The History of Ozone. Part III: CD Harries and the Introduction of Ozone into Organic Chemistry. *Helvetica chimica acta* **2003,** *86* (4), 930-940.

29. Anachkov, M.; Rakovsky, S.; Zaikov, G., Ozonolysis of polybutadienes with different microstructure in solution. *Journal of applied polymer science* **2007,** *104* (1), 427-433.

30. Nor, H. M.; Ebdon, J. R., Ozonolysis of natural rubber in chloroform solutionPart 1. A study by GPC and FTIR spectroscopy. *Polymer* **2000,** *41* (7), 2359-2365.

31. Anachkov, M.; Rakovsky, S.; Shopov, D.; Razumovskii, S.; Kefely, A.; Zaikov, G., Study of the ozone degradation of polybutadiene, polyisoprene and polychloroprene in solution. *Polymer degradation and stability* **1985,** *10* (1), 25-42.

32. Stephens, W. D.; McIntosh, C. R.; Taylor, C. O., Synthesis of low molecular weight hydroxy-terminated cis-1, 4-polybutadiene. *Journal of Polymer Science Part A-1: Polymer Chemistry* **1968,** *6* (4), 1037-1043.

33. Odinokov, V.; Ignatyuk, V.; Tolstikov, G.; Monakov, Y. B.; Berg, A.; Shakirova, A.; Rafikov, S.; Berlin, A., Synthesis of cis-1, 4-oligodien-α, ω-glycols by ozonolis of cis-1, 4-polydienes. *Bulletin of the Academy of Sciences of the USSR, Division of chemical science* **1976,** *25* (7), 1475-1481.

34. Criegee, R., Mechanism of ozonolysis. *Angewandte chemie international edition in english* **1975,** *14* (11), 745-752.

35. Reyx, D.; Campistron, I., Controlled degradation in tailor-made macromolecules elaboration. Controlled chain-cleavages of polydienes by oxidation and by metathesis. *Die Angewandte Makromolekulare Chemie: Applied Macromolecular Chemistry and Physics* **1997,** *247* (1), 197-211.

36. Gillier-Ritoit, S.; Reyx, D.; Campistron, I.; Laguerre, A.; Pal Singh, R., Telechelic cis-1, 4-oligoisoprenes through the selective oxidolysis of epoxidized monomer units and polyisoprenic monomer units in cis-1, 4-polyisoprenes. *Journal of Applied Polymer Science* **2003,** *87* (1), 42-46.

37. Jean-Louis Hérisson, P.; Chauvin, Y., Catalyse de transformation des oléfines par les complexes du tungstène. II. Télomérisation des oléfines cycliques en présence d'oléfines acycliques. *Die Makromolekulare Chemie: Macromolecular Chemistry and Physics* **1971,** *141* (1), 161-176.

38. Murdzek, J. S.; Schrock, R. R., Well-characterized olefin metathesis catalysts that contain molybdenum. *Organometallics* **1987,** *6* (6), 1373-1374.

39. Schrock, R. R.; Hoveyda, A. H., Molybdenum and tungsten imido alkylidene complexes as efficient olefin-metathesis catalysts. *Angewandte Chemie International Edition* **2003,** *42* (38), 4592-4633.

40. Nguyen, S., Grubbs, RH; Ziller, JWJ Am. *J. Am. Chem. Soc* **1993,** *115*, 9858.

41. Scholl, M.; Ding, S.; Lee, C. W.; Grubbs, R. H., Synthesis and activity of a new generation of ruthenium-based olefin metathesis catalysts coordinated with 1, 3-dimesityl-4, 5-dihydroimidazol-2-ylidene ligands. *Organic Letters* **1999,** *1* (6), 953-956.

42. Schwab, P.; France, M. B.; Ziller, J. W.; Grubbs, R. H., A Series of Well-Defined Metathesis Catalysts–Synthesis of [RuCl2 (□ CHR′)(PR3) 2] and Its Reactions. *Angewandte Chemie International Edition in English* **1995,** *34* (18), 2039-2041.

Chapter 2 :

Analytical techniques

Chapter 2. Analytical techniques

I. Mass spectrometry

I.1. Introduction to mass spectrometry

Mass spectrometry (MS) is one of the most widely used analytical techniques, which allows the determination of atomic or molecular masses of individual species present in a sample from the measurement of mass to charge ratios (m / z) of ions in the gas phase. It can provide detailed knowledge of the composition and structure of substances in a complex mixture. Most of the techniques based on mass spectrometry provide exceptional results in terms of specificity, sensitivity, fast response, mass accuracy and resolving power. These characteristics represent the most powerful tools in the field of analytical instruments.

Basically, a mass spectrometer consists of the following: an introduction system of the substance to be analyzed, a source to ionize the compounds, an analyzer to separate the different compounds, a detector, and a processing system for the acquired data thus providing the mass spectrum.

The sample to be analyzed, when introduced in a mass spectrometer, is subjected to a succession of stages:

The first step is the ionization. Many processes can be used for this first step which leads to the formation of ions in the gas phase. The sources can operate under vacuum or atmospheric pressure. According to the ionization method, the sample may be introduced under solid, liquid or gas form. The second step consists on accelerating and focusing the newly formed ions using ionic optics. Next, ions are separated in a third step according to their *m/z* ratio inside the analyzer. After separation, ions finish their journey by striking a detector whose signal is proportional to the charges of the received ions. The detector will send a signal which is finally treated to obtain the mass spectrum.

Moreover, mass spectrometry has remarkably progressed in recent years especially due to advances in informatics and electronics but also due to the arrival of new analyzers. New sources of ionization have been developed to understand many analytical issues ranging from the field of biology to the environment. In addition, the existing analyzers have been perfected to become faster and more resolving while new hybrid instruments have been developed to achieve more versatile applications.[1]

As part of this thesis work, soft ionization techniques were mainly used, associated to ultra-high-resolution analyzers such as Fourier transform mass spectrometry (FT-MS). The sources used were atmospheric pressure ionizations such as electrospray ionization (ESI) adapted to ionize polar compounds with high molecular weight and atmospheric pressure chemical ionization (APCI) used to ionize low polarity compounds. This chapter will discuss the details on these ionization technique as well as principles of used analyzers.

I.2. Ionization sources

I.2.1. Electrospray ionization (ESI)

Electrospray ionization (ESI) is one of the most versatile and used ionization technique as it is applicable to a wide range of samples in solution. Its development and coupling to mass spectrometry are attributed in 1968 to John Fenn who received the Nobel Prize in chemistry in 2002 for his contributions.[2] It all began when Fenn proved that intact multicharged ions could be obtained from proteins, which made it possible to determine their molecular mass. The possibility of analyzing multicharged ions allows the analysis of molecules of large masses on instruments with a modest mass range. Its use also has been extended to other polymers and biopolymers. The electrospray is easy to pair with chromatography or capillary electrophoresis because the sample is introduced in solution and at atmospheric pressure. This source of mild ionization leads most often to intact ions even with non-covalent systems and requires small amounts of sample.

Ionization by electrospray starts by the formation of very fine charged droplets under the influence of a strong electric field. The sample is dissolved in specific compatible solvents and introduced continuously through a capillary tube, the tip of which is maintained at a high potential relative to the counter electrode. The electric field induces an accumulation of charge on the liquid surface located at the end of the capillary, which breeze to form highly charged droplets. These droplets then pass through a curtain of heated inert gas, most often nitrogen. The solution at the end of the capillary forms a ‘Taylor cone’ due to charge accumulation.[3]

Droplets break up when the solvent is evaporated and the coulombic forces increase. In fact, Rayleigh limit is the point at which the coulombic repulsion forces between charges are equal to the surface tension forces of the liquid. Once the coulombic repulsions overcome the surface tension, a jet of smaller electrically charged droplets is released from the end of the capillary.[4]

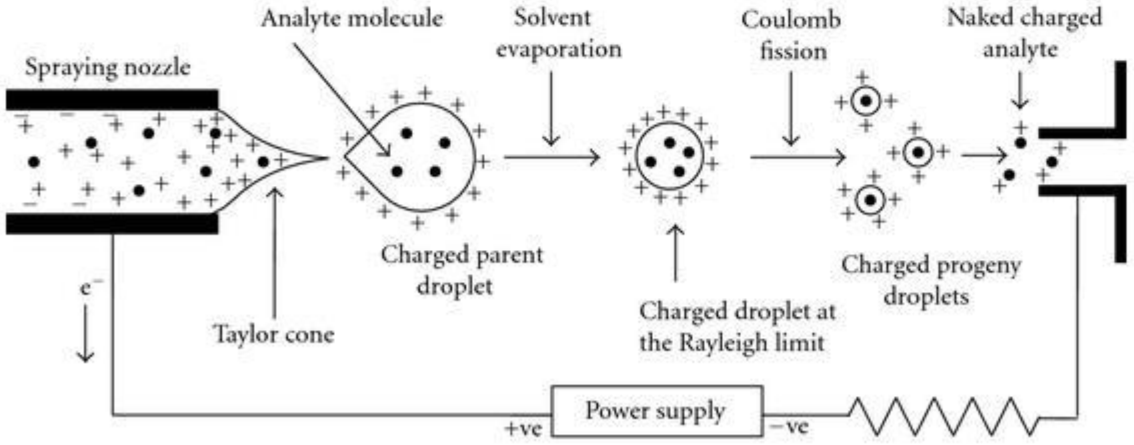

Figure 16. Representation of the principal of electrospray ionization source (ESI)[5]

Analysis using electrospray ionization can be carried out in positive or negative ionization modes. Changing the polarity of the electrodes makes it possible to pass from the positive mode to the negative mode. The ions observed by mass spectrometry can be protonated molecules $[M + H]^{+}$ or deprotonated $[M - H]^{-}$, or adduct ions with a cation such as sodium ion (Na^{+}) or ammonium (NH_4^{+}), or anions like chloride ion $[M + Cl]^{-}$. Multicharged ions $[M + nH]^{n+}$ or $[M - nH]^{n-}$ can also be generated.

I.2.2. Atmospheric Pressure Chemical Ionization (APCI)

Atmospheric pressure chemical ionization called APCI, developed by A. Milne in 1969 [6], is an ionization technique that takes place in the gas phase. This is a method analogous to chemical ionization (CI) in which ions are produced by discharges corona on a sprayed solvent which generates a nitrogen plasma and a cascade of reactions in gas phase. Complementary with the electrospray, the APCI operates at much higher temperatures, and is used in the analysis of polar and nonpolar low molecular weight compounds (<1500 Da). As in the case of electrospray, the

APCI is a gentle ionization method, and it does not produce fragmentation. On the other hand, the APCI leads to monocharged ions.

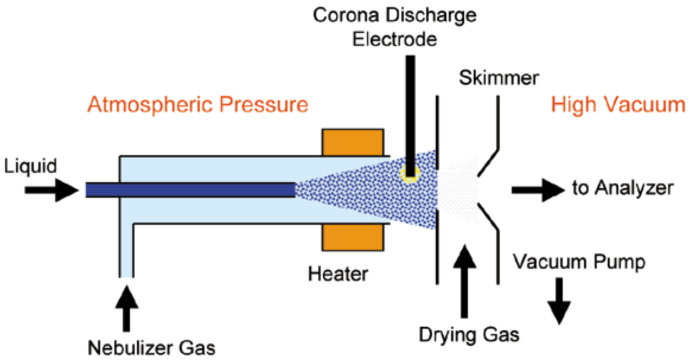

Figure 17. Representation of the principal of APCI source[7]

The analyte in solution is directly introduced into a nebulizer, where it is transformed into fog by a flow of nitrogen (N_2). The droplets are moved through a heated tube. The heat transferred allows the solvent and the sample to vaporize in the gas stream. The temperature of the tube is controlled, depending on the nature of the solvent. At the exit of this tube, an electrode emits electrons in the form of a corona discharge leading to ionization of the gas and then indirectly solvent and analyte. In the positive mode, most often $[M + H]^+$ ions are obtained by a process of proton transfer as a function of the relative proton affinity of reactive ions and molecules of the gaseous analyte. In the negative mode, the ions of the molecular species are generated by loss of a proton to lead to $[M - H]^-$ ions. In the absence of a protic solvent molecular ions $M^{+\bullet}$ or $M^{-\bullet}$ can be obtained.

Corona discharge leads by electronic ionization of primary ions such as $N_2^{+\bullet}$. Those ions collide with vaporized solvent molecules to form gaseous ions secondary reagents. Radical ions ($N_2^{+\bullet}$ and $N_4^{+\bullet}$) in plasma then participate in a cascade of chemical reactions that induce the ionization of the molecules of the sample by a charge exchange or proton transfer process. [1, 8-9]

$$
\begin{aligned}
&N_2 + e^- \longrightarrow N_2^{+\bullet} + 2e^- \\
&N_2^{+\bullet} + 2N_2 \longrightarrow N_4^{+\bullet} + N_2 \\
&N_4^{+\bullet} + H_2O \longrightarrow H_2O^{+\bullet} + 2N_2 \\
&H_2O^{+\bullet} + H_2O \longrightarrow H_3O^{+} + HO^{\bullet} \\
&H_3O^{+} + nH_2O + N_2 \longrightarrow H^{+}\left(H_2O\right)_n + N_2 \\
&H^{+}\left(H_2O\right)_n + A \longrightarrow AH^{+} + nH_2O \\
&N_2^{+\bullet}\left(or\ N_4^{+\bullet}\right) + A \longrightarrow A^{+\bullet} + (2)N_2
\end{aligned}
$$

Figure 18. Mechanism of ionization in APCI

I.2.3. Atmospheric Solids Analysis Probe (ASAP) and Direct Insertion Probe (DIP)

The ASAP (Atmospheric Solids Analysis Probe) or DIP (Direct Insertion Probe) -APCI source was developed by Charles N. McEwen[10-11] in 2005. A glass tube on which is deposited the sample in solid or liquid form is introduced into the atmospheric pressure ionization chamber. A stream of hot nitrogen gas desorbs the analyte from the surface of the tube which is ionized under atmospheric pressure via a corona discharge from an APCI source (Figure 19). The hot gas flow (between 350 °C and 500 °C) can be supplied by the nebulizer APCI or by an ESI nebulizer. No solvent is used in DIP-APCI.

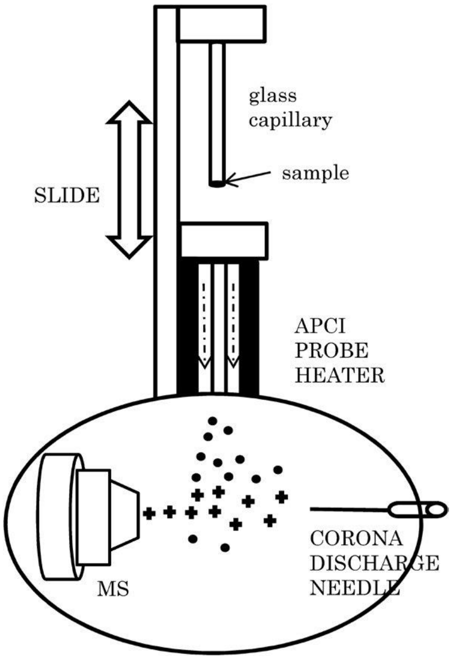

Figure 19. Representation of the principal of ASAP or DIPI source[12]

I.3. Analyzers

I.3.1. Time of flight analyzer (TOF)

The time-of-flight (TOF) analyzer was first described times by Stephens in 1946. Subsequently, Wiley and McLaren published in 1955 the design of a linear TOF mass spectrometer which later became the first instrument commercial.[13]

The principle of a TOF analyzer is to separate the ions after their initial acceleration by an electric field, as a function of their velocity in a field-free vacuum tube. First, the ions are expelled from the source in beams. They are then accelerated under the action of an electric field. Under the effect of this applied voltage potential difference U, the electrostatic potential energy is converted into kinetic energy. Since they all acquire the same kinetic energy, the ions which are characterized by a distribution of their mass have a distribution of their speed. So, when leaving the acceleration zone, they enter an area without a field where they are separated according to their speed, before reaching the detector located at the other end of the flight tube. The *m/z* ratios are determined by measuring the time it takes for the ions to travel in the vacuum area between the source and the detector. Before leaving the source, an ion of mass m and of total charge q is accelerated by a potential U. Its potential energy electrostatic is converted into kinetic energy, shown in equation (1) below:

$$Ec = \frac{1}{2}mv^2 = qU = zeU = Ep \qquad (1)$$

The speed of the ion leaving the source is given by the following relation (2) by rearrangement of the previous equation

$$v = \sqrt{\frac{2qU}{m}} \qquad (2)$$

After the initial acceleration, the ion moves in a straight line at constant speed towards the detector, and can be measured with knowledge of its time and distance of travel. The time t necessary to travel the distance d before reaching the detector is given by the relation (3)

$$t = \frac{d}{v} \qquad (3)$$

Relation 1 can then be converted into relation 4 by rearranging the previous equation 3:

$$qU = \frac{1}{2} m \left(\frac{d}{t}\right)^2 \tag{4}$$

The *m/z* ratios are then determined as a function of the time of flight.

Ions of different *m/z* move at different speeds in the TOF MS analyzer and arrive separately at the ion detector. The time traveled by the ions therefore depends only on the *m/z* ratio. Ions with a low *m/z* ratio have a short time of flight to the detector. Ions with a high *m/z* ratio will have a higher time of flight up to the detector.

The resolution of a TOF analyzer depends on the length of the tube. The longer the tube, the better the resolution. In practice, the resolution is limited by the dispersion of the kinetic energy of ions. One way to improve the resolution is to use an electrostatic mirror also called reflectron (Figure 20). The reflectron was first proposed by Mamyrin in 1973.[14] It consists of electrostatic lenses on which is applied a voltage gradient which acts as an ionic mirror by deflecting the ions and causing them to return in the flight tube. The detector is positioned on the source side of the ion mirror to capture the arrival of the ions after their reflection. It aims to correct the dispersion of the kinetic energy of ions leaving the source with the same *m/z* ratio. Ions with more of kinetic energy, i.e. with a higher speed, will penetrate the reflectron deeper than ions with less kinetic energy. Therefore, the fastest ions will spend more time in the reflectron and will reach the detector at the same time as the slower ions with the same *m/z*. The reflectron therefore increases the flight path without increasing the dimensions of the mass spectrometer. However, reflectron increases the mass resolution but lowers sensitivity and introduces a limitation of the range of mass. TOF analyzers associated with a reflectron are now high-resolution devices, between 8000 and 100000, thanks to the reduction of the dispersion of ions.

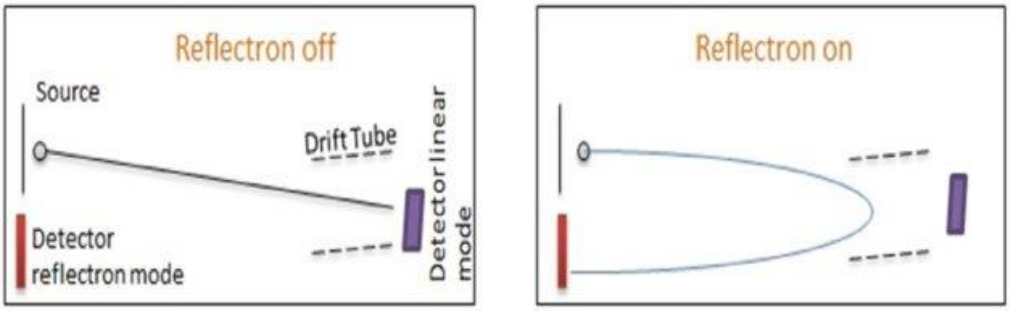

Figure 20. Scheme showing the principle of a TOF analyzer[15]

I.3.2. Quadrupole mass analyzer

The principle of the quadrupole was described in 1953 by Paul and Steinwedel[16] based on their work on ion focusing. These analyzers were then applied to commercial instruments following the work of Shoulders, Finnigan and Story.

The quadrupole is one of the devices that uses the stability of trajectories in an oscillating electric field to separate the ions according to their *m/z* ratio. A quadrupole analyzer is made up of four parallel electrodes of cylindrical or ideally hyperbolic section, positioned in the z direction. The remote electrodes of $2r_0$ opposed and connected to each other are maintained at the same potential. The adjacent electrodes are brought to potentials of values Φ_0, sum of a direct voltage U and an alternating radiofrequency voltage V (ω). An electrostatic field quadrupole is thus created in the region between the four electrodes.

The total potential Φ_0 is represented by equation 5 as a function of the direct voltage U and of a radiofrequency voltage of amplitude V with the angular speed ω.

$$\phi 0 = 2(U - V\cos\omega t) \tag{5}$$

When an ion enters in the z direction of the quadrupole assembly, it is subjected to a force of attraction by one of the electrodes whose charge is opposite to the ionic charge. The voltage applied to the electrodes is periodic; attraction and repulsion in x and y directions will alternate in time, because the sign of the electric force also changes periodically over time.

The potentials applied to each electrode are alternately reversed, allowing successively and vice versa from one polarity to the other.

On entering the quadrupole, the ions are accelerated and maintain a longitudinal velocity along the z axis. These ions progress through the analyzer thanks to the potential difference between the entry and exit of the quadrupole. This potential difference makes it possible to guide the ions in the desired direction.

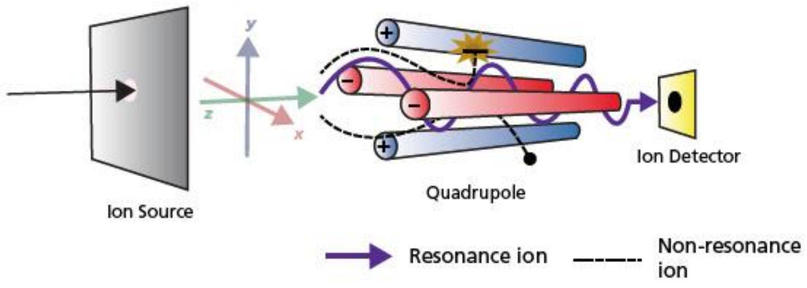

Figure 21. Scheme showing the principle of a Quadrupole analyzer[17]

I.3.3. Q-TOF hybrid analyzer

The hybrid Q-TOF analyzer combining a quadrupole (Q) and time of flight (TOF) separated by a collision cell was first described in 1996 by Morris et al. [18]. This type of analyzer is suitable for analysis by tandem mass spectrometry.

The operating principle of this hybrid analyzer remains the same as the principle of Quadrupole and time-of-flight analyzers taken separately. The quadrupole plays the role of ion guide, and the TOF allows precise mass measurement. In the case of mass spectrometry in tandem, the quadrupole allows the selection of ions, avoiding problems of surcharge in the analyzer. The time of flight has a high mass resolution, and a good mass accuracy when internal calibration is performed.

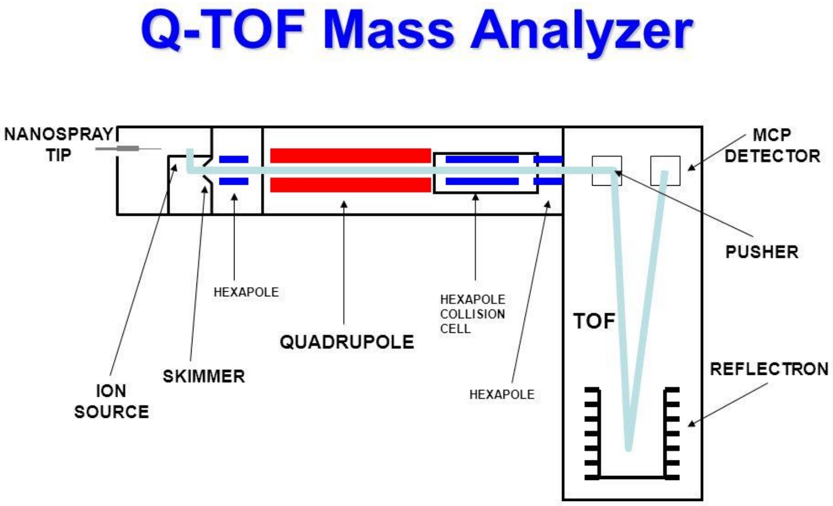

Figure 22. Scheme showing the principle of a hybrid Q-TOF analyzer

I.3.4. Fourier Transform Ion Cyclotron Resonance Mass Spectrometry (FTICR)

Fourier transform ion cyclotron resonance mass spectrometry (FTICR) is today the most resolutive analysis technique, offering the highest mass accuracy in measurement. This technique is a powerful tool, essential in the analysis of complex mixtures and small amounts of samples.

Fourier transform cyclotron resonance mass spectrometry (FTICR) was developed by Alan G. Marshall[19] and Melvin Comisarow[20] in 1974, thanks to advances in computing and analog-to-digital converters, enabling the real-time digitalization of the electrical signal induced by the cyclotronic movement of the ions in the ICR cell.[21-23] In 1989, McLafferty et al.[24] implemented the coupling of electrospray source with FTICR, which opened up new fields of application. From there, other ionization modes were coupled with FTICR mass spectrometry.

Today, FTICR mass spectrometry is an indispensable technique and widely used in various research fields, thanks to its many advantages, such as its high resolving power, its high precision of mass measurement (<0.1 ppm), high sensitivity, large dynamic range and flexibility allowing it to be coupled with different external ion sources (ESI, APCI, APPI, MALDI ...) and modes of fragmentations.

FTICR is a technique based on the trapping and excitation of ions in a Penning (or ICR cell), under the action of a magnetic field and an electric field. The mass spectrum is obtained via the Fourier transform which converts the time signal (FID) in frequency spectrum inversely proportional to the mass. In an ICR cell, the ions are trapped axially by two plates perpendicular to the magnetic field, to which a direct voltage is applied.

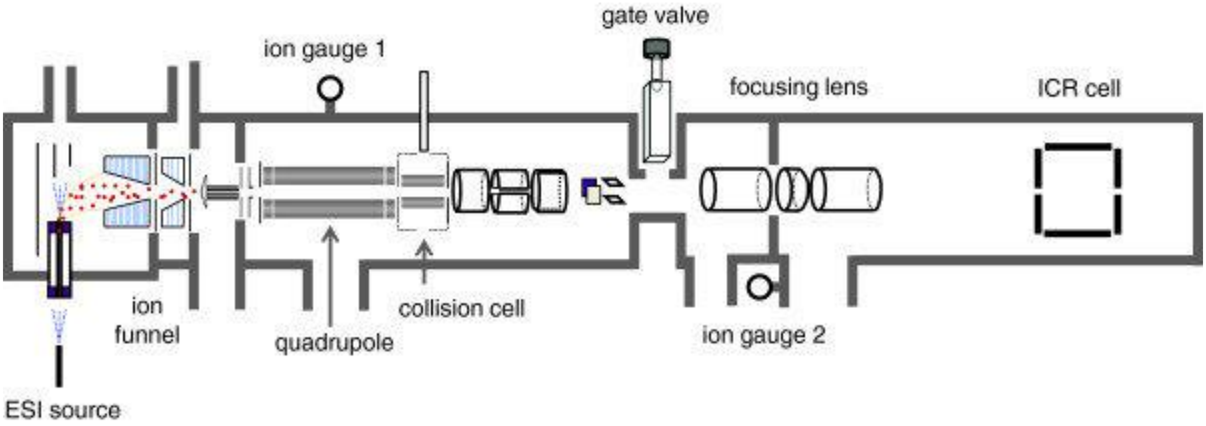

Figure 23. Schematic representation of FT-ICR[25]

I.3.4.1. Ion trapping, excitation in FTICR cell

Ions are generated in the source coupled to the FTICR, and pass through a series of pumping stages, under vacuum until reaching the cell where pressure is between 10^{-10} and 10^{-11} mBar.

The FTICR cell is composed of detection and excitation plates and is placed inside a superconducting magnet able to generate a uniform magnetic field B. The combining effect of magnetic field B and the constant field traps the ions inside the ICR cell radially by the magnetic field and axially by an electric field. In fact, when ions pass in the magnetic field, they are influenced by Lorentz force giving them a circular motion in a perpendicular plan to the magnetic field. This circular motion is known as the cyclotronic movement. The frequency of rotation of the ions or cyclotronic frequency depends on their *m/z* ratio. At this stage no signal is observed, the cyclotron radius is very low and ions are not in phase. The excitation of each individual *m/z* is obtained by a radiofrequency pulse swept through the excitation plates of the cell. Each individual excitation frequency pairs with the cyclotronic motion of the ions, and excites them to a higher orbit with a coherent motion. This movement induces an alternating current between the detection plates. The frequency of this current is the same as the cyclotron frequency of the ions and the intensity is proportional to the number of ions.

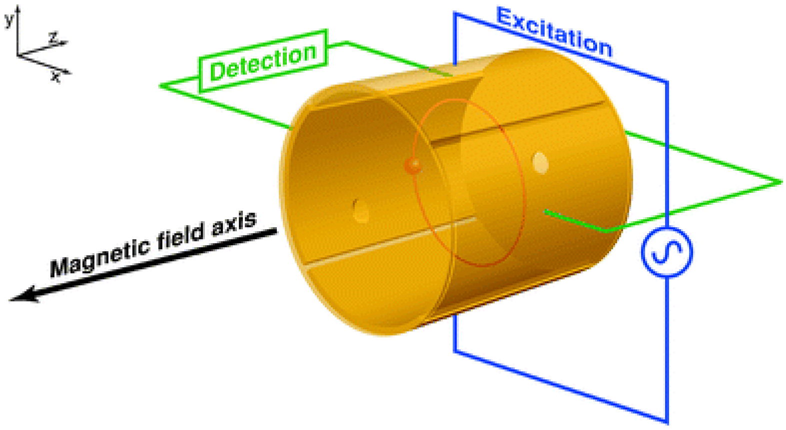

Figure 24. Schematic representation of a cylindrical FT-ICR analyzer cell [26]

Ions in the gas phase form a small cloud with rotational movement in the center of the ICR cell. In order to obtain a detectable signal, the orbit of the ion package must be increased to be close to the receptor plates (Figure 25). this is obtained by the application of a transverse oscillating electric field at the reduced frequency of the cyclotron. This electric field, perpendicular to the magnetic field, brings the ions into resonance, which induces their excitation and acceleration. This electric field of RF radio frequency is delivered by the excitation plates.

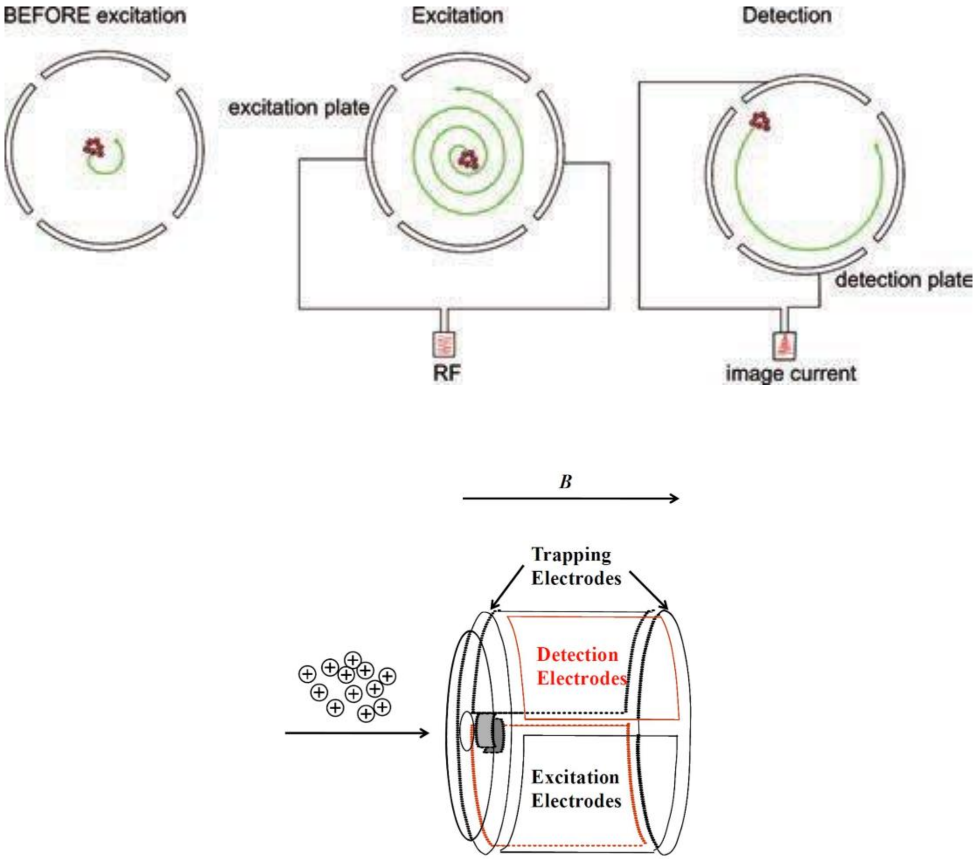

Figure 25. Ion excitation and detection in an ICR cell [27-28]

Irradiation by an electromagnetic wave of the same frequency as that of an ion in a cyclotron allows the absorption of this wave by resonance. The energy thus transferred to the ion causes a corresponding increase in its kinetic energy, leading to an increase in the radius of the trajectory. The first stage of FTICR is simultaneous excitement of all ions present in the cell by rapid scanning of a wide range of frequencies, in a time of the order of ten microseconds. This results that all ions are in phase.

Ions can be excited according to different modes of excitation (Figure 26):

Rectangular pulse excitation based on the application of an excitation frequency corresponding to a population of ions with the same *m/z* ratio.

Broadband excitation based on the excitation of a whole range of frequencies of interest. It contains two approaches:

Chirp method consisting on the use of a single excitation pulse that sweeps the entire frequency range of interest.[29] The limitations of this method are the homogeneity of the amplitude of the frequency over the frequency range and the lack of selectivity at the limits of the frequency range

SWIFT (Stored Waveform Invers Fourier Transform)[30] method: the domain of excitation frequency is defined beforehand, and the excitation wave calculated accordingly by inverse Fourier transform. This method is the most used because it is very precise, allowing to achieve the correct consistency between arousal and response in the cell. Thus, the ions similarly *m/z* will be excited homogeneously thereby improving the resolution.

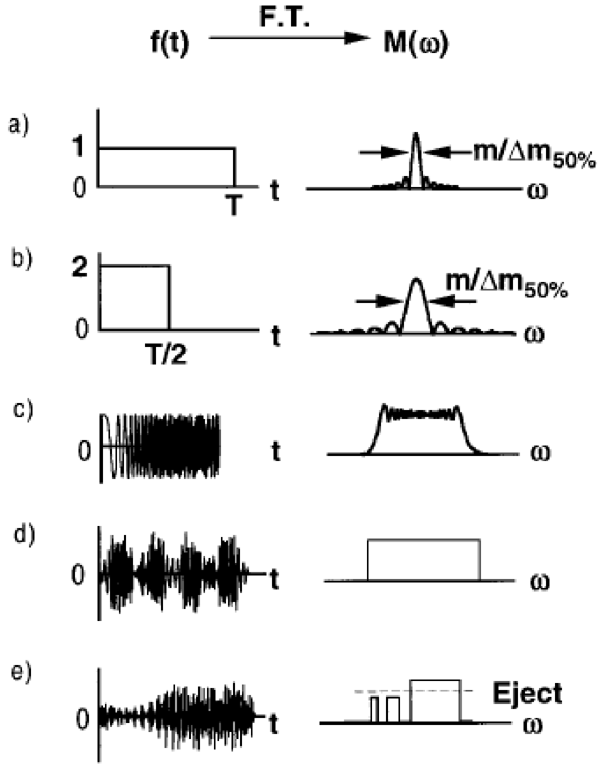

Figure 26. Time-domain (left) and frequency-domain (right) excitation waveforms. (a), (b) Rectangular pulses. (c) Frequency-sweep (''chirp''), (d), (e) Stored waveform inverse Fourier transform (''SWIFT'') wave-forms [31]

I.3.4.2. Cyclotron movement of ions

When ions move in the presence of a uniform magnetic field, they are subjected to a given force following equation 6 in which in which m, q and v represent ion mass, charge and velocity respectively

$$F = qvB \qquad (6)$$

And the vector cross product term means that the direction of the magnetic component of the Lorentz force is perpendicular to the plane determined by v and B (Figure 27). If the ion maintains a constant speed (i.e. no collisions), the magnetic field bends the ion in a circle of radius r.

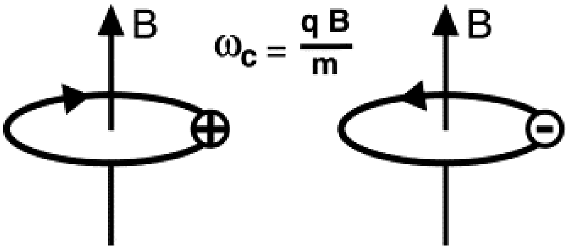

Figure 27. Cyclotronic motion of positive and negative ions in a magnetic field [19]

Thus, the trajectory of ions curves in the magnetic field. If the speed of ions is low and the magnetic field is strong, the radius of curvature of the path becomes small. The ion is trapped in a circular path in the magnetic field.

In the case of the cyclotron, the rotational motion is a cyclotronic motion, meaning that the centrifugal (equations 7) and centripetal forces are equal (equation 8).

$$F' = \frac{mv^2}{r}$$

$$(7)$$

$$qvB = \frac{mv^2}{r}$$

$$qB = \frac{mv}{r} \qquad (8)$$

A measurement of the frequency of this rotational movement allows an *m/z* determination of the species considered (equation 9).

$$\nu = \frac{v}{2\pi r} = \frac{qB}{2\pi m} \qquad (9)$$

The angular velocity, ω_c (in rad / s), around the z axis is defined by equation 10.

$$\omega_c = 2\pi\upsilon = \frac{v}{r} = \frac{qB}{m} \qquad (10)$$

I.3.4.3. Detection of ions

Excited ions have a higher cyclotron radius with coherent movement, which makes them detectable by the opposite detection plates. When an ion packet of the same *m/z*, at a cyclotronic frequency ω_c passes several times in front of the detection plates, an image current is induced.

The signal acquisition time is limited by the collisions of the ions with each other and with the residual neutral gas in the ICR cell, reducing the homogeneity of the ion packet. It is essential to work at very low pressure (around 10^{-10} mbar). The stream induced by the ions decreases to zero. The signal recorded by the detection plates decay according to an exponential law to generate a decrease called free induction decay (FID). The resolving power represented in the following relation (11) is directly proportional to the measurement of the acquisition time in the ICR cell.

$$R = \frac{\omega T}{2\pi} \qquad (11)$$

After acquisition of the signal, it will be processed by the Fourier transform, which consists of the conversion of the time signal into a frequency signal. But before that, a first treatment called apodization should be applied. Apodization is a signal processing method applied with the aim of reducing spectral leakage and smoothing the shape of the spectral line. The cutoff at the start and end of the time signal is responsible for auxiliary movements of the two sides of the main peaks. These peaks are annoying because they can hide smaller peaks close to the big ones. To reduce these peaks, the apodization function is applied, forcing the start and end of the signal to tend towards zero. From there, the temporal sinusoidal signal FID is converted into a frequency signal via the Fourier transform and then into a mass spectrum.

Various methods of treatment of the signal are accessible to improve its quality. By adding several successive detections, it is possible to improve the signal-to-noise ratio of the transformed spectrum. To increase the sampling rate of the mass spectrum it is possible before the Fourier transform to perform a zero-filling by adding points of zero values to the FID.

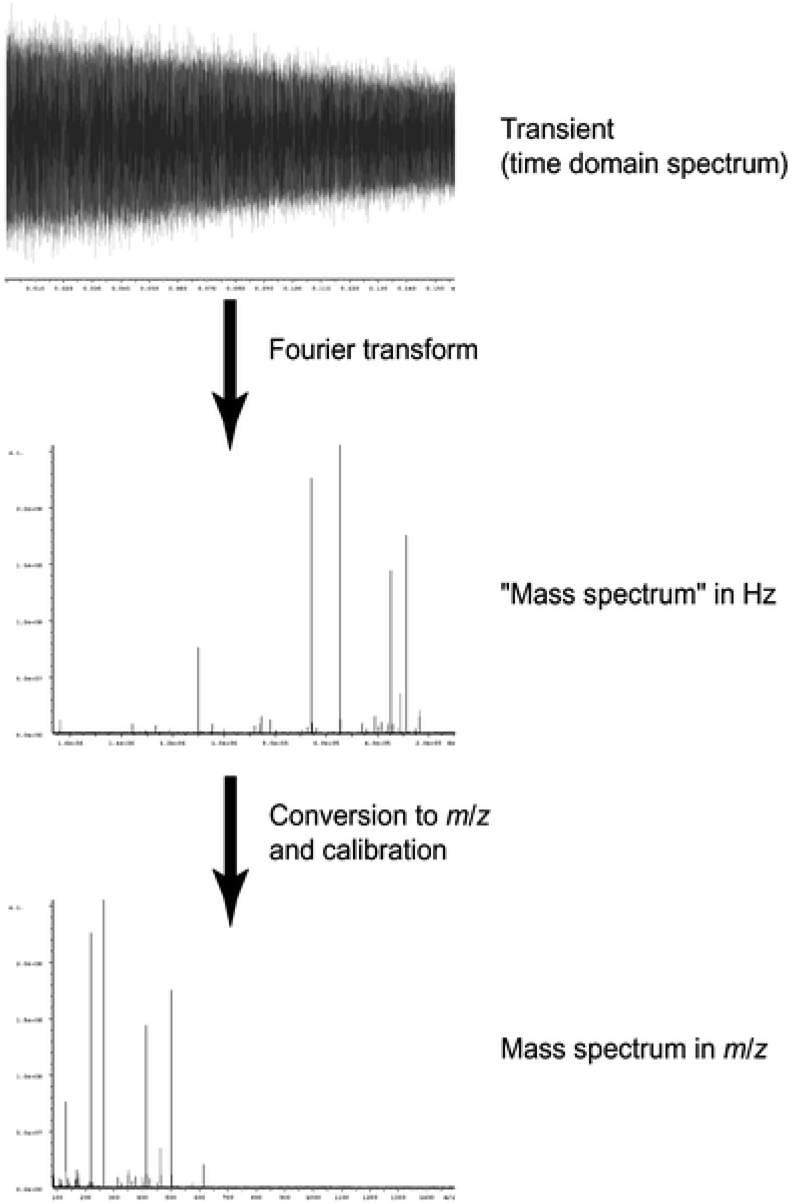

Figure 28. Illustration of the processing of raw data. A Fourier transform is performed on the time-domain data to convert it to the frequency domain, and this resulting spectrum is then calibrated in terms of *m/z*

III. Tandem mass spectrometry or MS/MS

Tandem mass spectrometry (MS/MS) allows the determination of the structure of an ion based on its fragmentation profiles. The objective of this technique is to break down specific ions called precursor ions into smaller fragments called product ions. The obtained fragments reveal different aspects of the chemical structure of the precursor ion.[32-33]

First, samples are ionized in the ionization source (ESI, APCI, MALDI…) to generate a mixture of ions. Next, precursor ions with a specific *m/z* ratio are selected in the MS1 step in order to be fragmented in MS2 step leading to the production of detectable smaller ions. This sequence can be also applied on the generated MS2 ions which can be further fragmented to produce an additional group of MS3 product ions. [34]

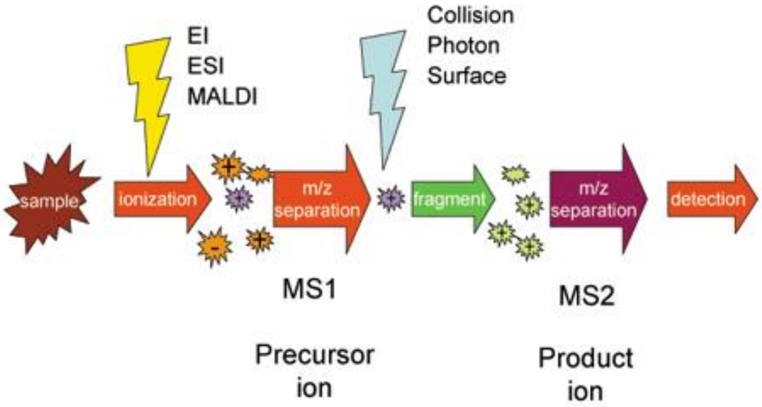

Figure 29. Principle of tandem mass spectrometry (MS/MS)

II.1. Instruments used for MS/MS

Tandem MS involves three different steps consisting on selection-fragmentation-detection. These three steps can be separated either in space or in time.

I1.1.1. Spatial MS/MS

The most classical spatial MS/MS instrument include Q-q-Q, Q-TOF as well as hybrid ion trap/FTMS.

In the case of Q-q-Q (triple quadrupole), three quadrupoles are lined up in a row. Precursor ion are first selected in the first quadrupole then sent to the second where they are fragmented. The generated ions are finally sent to the third quadrupole for mass scanning.

In the Q-TOF, the first step is similar to that of Q-q-Q. The selected ions are dissociated in a collision cell before being detected by a time-of-flight (TOF) mass spectrometer.

For the hybrid ion trap/FTMS which include FT-ICR and Orbitrap instruments, precursor ions are selected and fragmented in an external ion trap. The generated ions are then detected by FTMS providing high mass accuracy and high resolution.

II.1.2 Temporal MS/MS

Consists on a single mass analyzer and typically ion traps and FT-ICR instruments are used.

II.2. Fragmentation methods

There exist many different ways to increase the internal energy of precursors leading to their fragmentation. Collision-induced dissociation (CID)[35] and infrared multiphoton dissociation (IRMPD)[36] are the most common and robust fragmentation techniques. They are very efficient for small chemical compounds. Other methods include electron capture dissociation (ECD)[37], electron transfer dissociation (ETD)[38] and higher energy collisional dissociation (HCD).[39]

Collision induced dissociation (CID) or collision activated dissociation (CAD) is a common mass spectrometry fragmentation technique. It aims to study the fragmentation of ions through the impact with an inert buffer gas. The collisional translational energy of the ion is converted into internal energy which can induce its dissociation. Ions are accumulated in the first octopole and the precursor ion is selected with a quadrupole. Next the precursor is transferred to the second octopole where it starts to collide with a collision gas. The generated product ions are held in the second octupole for cooling then transferred to the ICR cell for isolation and detection.[40]

Multiphoton Infrared Dissociation (IRMPD) is a technique used in mass spectrometry to break up molecules in the gas phase. An infrared laser is directed through a window into the vacuum of the mass spectrometer, where the ions are present. The fragmentation mechanism comprises the absorption by an ion of several infrared photons given by the laser beam. The parent ion becomes excited in more vigorous vibratory states until one or more bonds are fragmented into the gas phase. In the case of powerful laser pulses, dissociation takes place by the inner valence of electron ionization. IRMPD fragmentation is most commonly used in FT-ICR mass spectrometer. [36, 41]

IV. Ion mobility spectrometry

Ion mobility spectrometry (IMS) is a rapid analysis technique, of the order of millisecond, allowing the separation of ions according to their size, charge and shape in gas phase.[42-43] This technique has existed for a large number of years and has been shown to be particularly effective as a stand-alone portable detection device for explosives and drugs.[44-45] In classical IMS experiments, the clusters of analyte ions pass through a drift tube filled with buffer gas (usually He or N_2) at sufficient low pressure (between 1 and 20 mbar), under the influence of a uniform electric field. Their arrival is then recorded by a detector. Under the effect of the electric field applied to the tube, the ions are accelerated, but also slowed down by collisions with the buffer gas. Although the IMS has a number of uses, coupling of ion mobility with mass spectrometry (IM-MS) creates a much more powerful analytical tool, improving the analysis of complex mixtures and facilitating structural determination of ions. The use of IM-MS is particularly useful in the analysis of isomeric ions with different structural arrangements. In addition, the IMS offers deadlines of separation significantly shorter than liquid chromatography (LC) or chromatography in gas phase (GC), so that these techniques can be combined with IMMS measurements, thus offering three-dimensional separations. One of the advantages of introducing the separation of ion mobility is that it reduces the need for long separations of LC or GC before MS analysis, reducing overall analysis time and increases processing efficiency.

III.1. Principle of ion mobility mass spectrometry

Ion mobility was introduced by Paul Langevin[46] in 1903 by the study of the influence and interaction of gases on the mobility of ions. He showed that ions can be separated by their characteristic velocity in a gas-filled tube under the application of an electric field. Following Langevin's theories, other scientists such as McDaniel and Mason designed ion mobility spectrometers. During the 1990s and early 2000s, the groups of Bowers, Jarrold, Clemmer and Hill have built IM-MS instruments and applied them to structural, biomolecular and complex mixtures. Consequently, IM-MS has become particularly interesting for solving many analytical challenges.

Ions are accelerated via the electric field at a specific speed, dependent on their interaction with buffer gas. The ion mobility factor K is influenced by the operating parameters of the instrument, which are the gas temperature and pressure, but more importantly for the separation, the physicochemical properties of the ion and the gas, charge, molecular masses of ions and gas and the average collision cross section (CCS) of ion rotation in gas. Thus, the larger the ion, the more its collisions with the gas will be significant, inducing a drop in its speed in the drift tube.

When a uniform electric field is applied to the drift tube, the average speed of an ion or drift rate (ν_d) is proportional to the strength of the electric field E, according to equations 12 and 13:

$$v_d = K \times E \qquad (12)$$

$$t_d = L/(K \times E) \qquad (13)$$

Drift times (t_d) of ions correspond to the required time in order to pass through the ion mobility cell. They can be measured and depend on the length of the mobility tube (L) and the speed of the ion (ν_d), according to equation 14:

$$t_d = \frac{L}{v_d} \qquad (14)$$

For the same charge, a compact ion will reach the detector faster than an unfolded ion. For the same value of CCS, an ion with a high state of charge will arrive more quickly to the detector than an ion with a lower state of charge. The principle of separation of ions in ion mobility in a drift tube is shown in Figure 30.

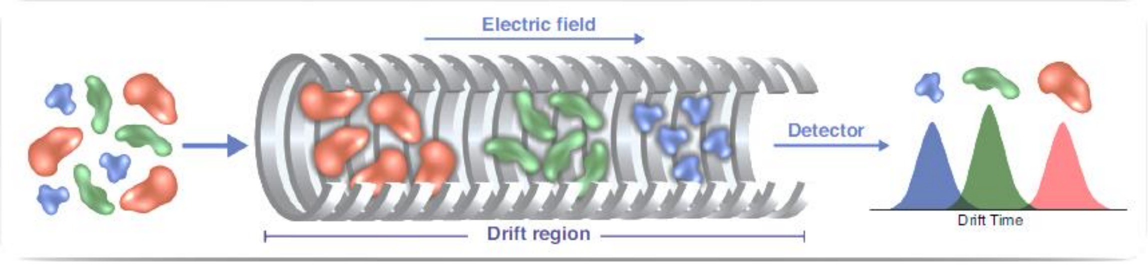

Figure 30. Principle of ion separation in ion mobility [47]

III.2. Ion mobility cells

There are many ion mobility cells that are available in the purpose of separating the ions in the gas phase. These cells are classified into two main categories, according to the nature of the electric field (uniform, high asymmetric or oscillating field), and according to the nature of the separation (as a function of time or electric field). In this manuscript, we will discuss two different types of cells and techniques: Drift Tube Ion Mobility Spectrometry (DTIMS) and Traveling Wave Ion Mobility Spectrometry (TWIMS)

III.2.1. Drift Tube Ion Mobility Spectrometry (DTIMS)[48-51]

Drift Tube Ion Mobility Spectrometry (DTIMS) is the most traditional IMS analysis technique. It consists on injecting ions into a drift tube made up of ring electrodes, with the aim of migrate under the effect of a uniform electric field, and in the presence of a neutral gas (usually N_2 or He). The ions are injected in packets into the drift tube, at time intervals which can be between 50 and 200 µs. Buffer gas is generally maintained at a constant pressure of the order of 1 to 15 mbar although some instruments operate at atmospheric pressure. At the level of the electrodes, a voltage between 2 and 20 $V.cm^{-1}$ is applied in order to maintain a uniform electric field along the drift tube. The ions are then both entrained by the electric field and slowed down by the collisions with buffer gas. The ions thus pass through the drift tube at constant speed.

This approach is the only one which allows the direct determination of the value of the effective section. experimental collision (CCS) from the measurement of the drift time without the need of a calibration. Following their passage and measurement of their mobility in the drift tube, ions are directed towards the detector.

However, DTIMS technology does not only have advantages. its main problem is its lack of sensitivity due to the phenomenon of diffusion. It is also limited in resolution which depends essentially on the length of the drift tube.

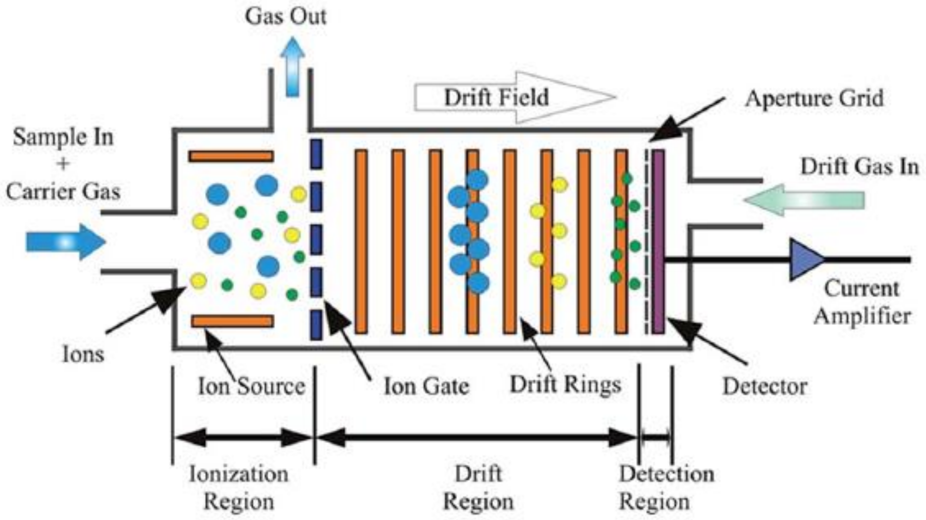

Figure 31. Separation of ions in DTIMS [51]

III.2.2. Travelling Wave Ion Mobility Spectrometry (TWIMS)[52-54]

Traveling Wave Ion Mobility Spectrometry (TWIMS) is an analytical technique using a non-uniform electrical field. The mobility cell, filled with a buffer gas (usually helium or nitrogen) consists of a series of ring electrodes subjected to radio frequency (RF) forming an ion guide called a stacked ring ion guide (SRIG). The electrodes are alternately charged positively and negatively, creating a potential well allowing radial confinement of the ions at the center of the rings. This technique allows the increase in ion transmission efficiency, thus avoiding radial diffusion phenomena and limit the loss of sensitivity. The principle of SRIG is illustrated in Figure 32.

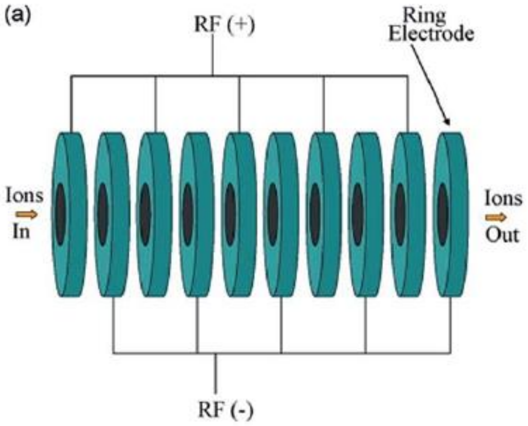

Figure 32. A schematic diagram of a stacked-ring ion guide (SRIG)

Unlike the drift tube, TWIMS uses a non-uniform electric field which creates a pulsed voltage, represented as waves, moving successively from one electrode to the other alternating positive and negative charge, throughout the tube. The ions are therefore accelerated by the impulse wave called the traveling wave or T-Wave, and slowed down by the collisions with buffer gas. They follow the pressurized ion guide of the buffer gas at constant speed via the mobile electric field propagated along the mobility cell. As in the case of the drift tube, the ions are separated according to their state of charge, their size and of their shape. Successive waves of potentials associated with friction with the buffer gas induce a rolling phenomenon called roll-over. For the same state of charge, the larger size ions will experience more collisions with the buffer gas, thus a greater number of rollovers. This results in a longer residence time in the ion mobility cell, therefore a longer drift time. As for the more compact ions, they will undergo a lower number of collisions and therefore lower roll-over, resulting in a shorter duration within the mobility cell. The principle of functioning and transport of ions in the TWIMS cell is shown in Figure 33.

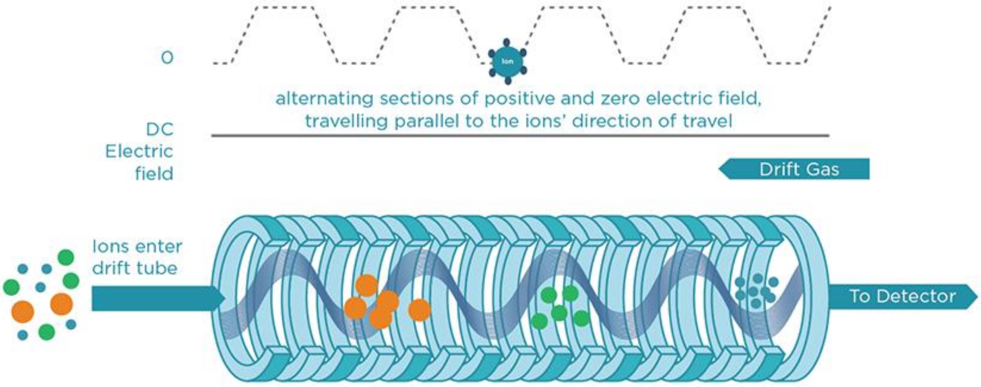

Figure 33. The principle of functioning and transport of ions in a TWIMS cell

V. Comprehensive two-dimensional gas chromatography [55]

GCxGC is a gas phase separation technique in which a sample is subjected to two orthogonal separation processes. The two columns are connected in series via a modulator. The compounds eluted from the first column are trapped by the modulator, refocused and injected continuously into the second, shorter column. The second separation is carried out in a period corresponding to a modulation period. The separation in this second column is extremely fast and lasts only 1 to 10 s whereas the separation in the first column lasts 45 to 120 min. Figure 34 illustrates the principle of GCxGC

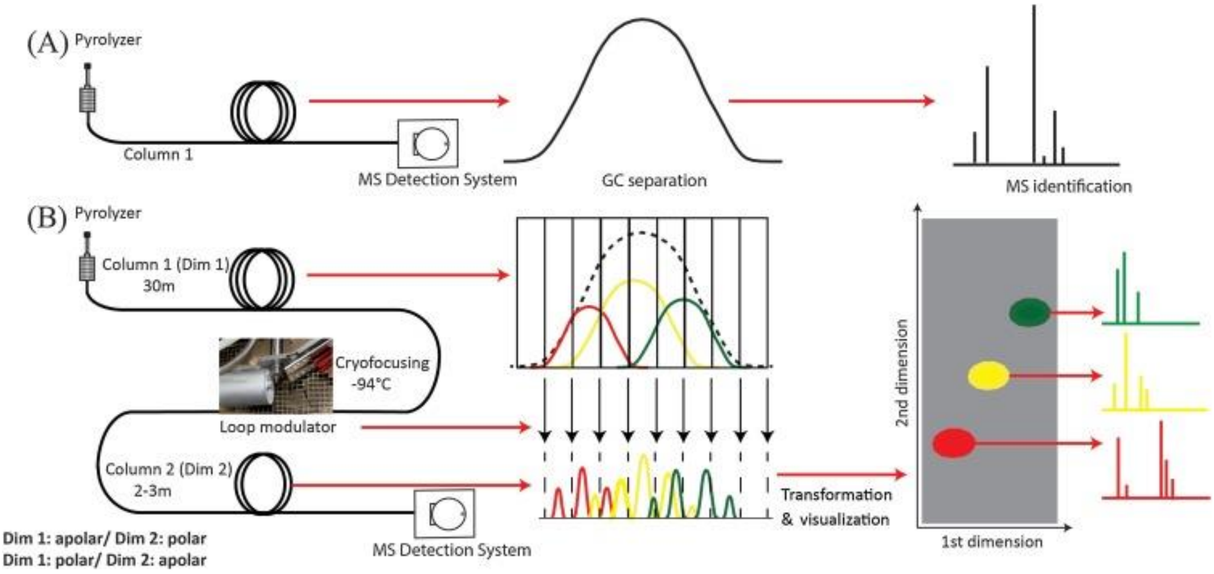

Figure 34. Principle of comprehensive two-dimensional gas chromatography

IV.1. Orthogonality and column selection

In order to have a so-called orthogonal separation in a GCxGC systems, the retention mechanisms in the first and second dimension should be independent. For a separation in temperature programming, this orthogonality condition is fulfilled by the use of columns whose stationary phases have different chemical nature. Generally, GCxGC systems combine a first column (15-30 m x 0.25 mm x 0.25 µm) of non-polar stationary phase (100% dimethylpolysiloxane, 5% phenylene-95% dimethylpolysiloxane) and a second column (1-2 m x 0.1 mm x 0.1 µm) polar stationary phase. The most commonly used polar stationary phases are: 35 to 50% phenylene-65 to 50% dimethylpolysiloxane, polyethylene glycol (Carbowax), carborane (HT-8) and cyanopropyl-phenyl-dimethylpolysiloxane. [55]

IV.2. Modulator

The modulator is considered to be the "heart" of a GCxGC system because it is the element mainly responsible for a good orthogonal separation of the analytes of the sample. The modulator fulfills three main functions, it allows: (1) to accumulate in continuous or to retain the effluent from the first column while the first separation occurs; (2) to focus the effluent collected on a very narrow strip; (3) injecting bands sequentially onto the second column, resulting in additional separation for each injected strip.

There are different types of modulators. They can be classified into five major groups according to the chronology of technological advances: (1) mechanical heating modulators; (2) the valve modulators; (3) mechanical cryogenic modulators; (4) cryogenic jets modulators; (5) flow modulation microfluidic systems

IV.3. Detector

The "fast GC" conditions imposed by the second-dimension column and the width of the peaks resulting from modulation of the order of 100 to 200 ms require the use of a high acquisition frequency detector to obtain a correct reconstruction of the chromatogram. The most commonly used detectors in comprehensive two-dimensional gas chromatography are the flame ionization detector (FID) and quadrupoles or time-of-flight mass spectrometers. The FID has the advantage of being efficient in terms of acquisition speed because it can reach, depending on the manufacturer, frequencies of the order of of 250-300 Hz. It also allows to obtain a more realistic analysis in terms of quantification relative analytes compared to a mass spectrometer, but its downside is that it does not provide any information as to the structure of the analytes. Using a spectrometer, in particular a quadrupole or time-of-flight mass spectrometer is therefore essential to allow the identification of many separate analytes. Many GCxGC systems are equipped with a quadrupole mass analyzer because they are more affordable than the time-of-flight spectrometer. However, one of the disadvantages is that its acquisition speed is moderate. For GCxGC, the time-of-flight mass spectrometer detection system is arguably the most powerful detection system.[56] The advantage of the time-of-flight spectrometer is that its acquisition speed is higher and therefore its sensitivity is increased. On the other hand, its drawback is that it provides significantly different mass spectra, which makes it difficult to identify structures when using commercial databases.

VI. Data Treatment

FTICR mass spectrometry offers ultra-high resolution and remarkable mass accuracy. As a result, mass spectra generated on the FTICR instrument are very complex and contains thousands or tens of thousands of different signals. Due to the very important quantity of information, interpretation and comparison can be very challenging to carry out. Therefore, it was crucial to use powerful tools to manage and visualize the generated results. *i*-van Krevelen also known as FTMSVisualization, a specific script based on a python code was chosen for the interpretation and data treatment. It allows access to different graphical representations such as Kendrick and Van Krevelen diagrams. The purpose of these representations is to present one-dimensional data from the mass spectrometers in multidimensional graphs from precisely determined masses and formulas of the allocated species.

V.1. *i*-van Krevelen [57]

The *i*-van Krevelen script are composed of three different parts:

1- Formula generator: this script will generate lists of possible ion formulas according to strict rules and predefined elemental limits. The list is generated between a well-defined *m/z* region (for example 100 and 1000 *m/z*) which can be adjusted according to the user's needs. Elements present in the analyzed compounds can be chosen such as C, H, O, N and many others as well as adducts such as K, Na or Li. The list generated by this script represents the maximum number of each element present in the molecules in the defined *m/z* range.

2- Formula assignment: this script will automatically assign input peak lists to molecular formulas. It is based on the Kendrick mass defect (KMD) and z* approach.
3- Static plotter: This tool generates a number of van Krevelen, DBE vs C# and other plots to simplify data visualization and interpretation.

V.2. Kendrick Diagram [58-60]

In 1962, Edward Kendrick proposed a scale of mass with CH_2 as reference. The goal of the mass scale of Kendrick is to reduce the data so that homologous compounds can be recognized by their identical Kendrick mass defect (KMD). On complex mixtures, compounds of the same family will involve different lengths of alkyl groups. With the Kendrick mass scale, these compounds will have the same KMD.

Kendrick's mass analysis identifies different types of compounds. Each atom has a different mass defect, so each ion of elemental composition has a different mass. In fact, the usual IUPAC mass scale is converted to the mass scale of Kendrick:

$$\text{Kendrick mass} = \text{IUPAC mass} \times (14/14.01565)$$

Thus, the Kendrick scale converts the mass of CH_2 from 14.01565 Da to exactly 14.00000 Da and homologous series (compounds having the same constitution in heteroatom and the same number of unsaturation, but a different number of CH_2 units) will have an identical mass defect.

$$\text{Kendrick mass defect} = \text{nominal Kendrick mass} - \text{exact Kendrick mass}$$

Compounds of the same class and type but with a different number of CH_2 units therefore fall on a single horizontal line, with peaks separated by 14 Da in nominal mass

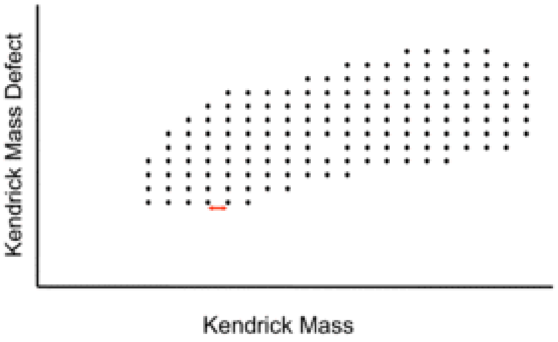

Figure 35. Kendrick diagram

V.3. Van Krevelen Diagram [61-62]

As in the case of Kendrick diagrams, the van Krevelen diagram is an approach for examining ultra-high-resolution mass spectra. It was proposed by Diek Willem van Krevelen to highlight the maturity of Kerogen. This diagram is constructed using the atomic ratios of hydrogen / carbon (H / C) and oxygen /carbon (O / C). Other ratios, including nitrogen / carbon, can be used. Thus, a component having its own gross formula can be represented by a point whose x and y coordinates are O / C and H / C ratios, respectively.

This diagram was originally based on information of elementary analysis and was later extended by Kim et al. [62] to view spectrometry datamass at high resolution.

Ultra-high-resolution mass spectrum data can indeed be easily transposed in the van Krevelen diagram. The diagram obtained makes it possible to highlight evidence the main biochemical classes of compounds characterized by their own H / C and O / C (N / C or S / C) ratios. Each family of compounds corresponds to a specific location on the diagram. Thus, lipids, proteins, lignin, hydrocarbons, carbohydrates and cellulose can be highlighted. This type of diagram is useful to assess the response of different ionization sources and different detection modes.

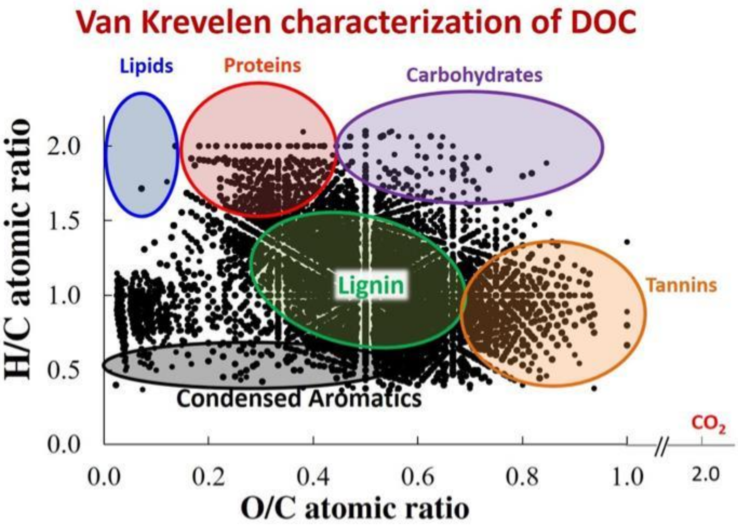

Figure 36. Different zones based on the classification of compounds in organic matter studies

V.4. DBE vs Carbon number plots [63]

Among the different types of characterization diagrams, DBE plots (double bond equivalents) as a function of the number of carbons for a given class of atoms are particularly used. Starting from the molecular formulas determined from precise mass measurements, we can calculate the number of equivalent double bonds (DBE) using this equation:

$$DBE = 1 + 1/2(2C – H + N)$$

Where c: carbon number; h: number of hydrogen and n: nitrogen number for a molecular formula $C_cH_hN_nO_oS_s$.

This type of map allows us to identify the most abundant compounds according to their number of carbon and their number of unsaturation for a given class. It provides information on the structural composition and can determine the fingerprint of a sample.

References

1. Dass, C., *Fundamentals of contemporary mass spectrometry*. John Wiley & Sons: 2007; Vol. 16.
2. Fenn, J. B.; Mann, M.; Meng, C. K.; Wong, S. F.; Whitehouse, C. M., Electrospray ionization for mass spectrometry of large biomolecules. *Science* **1989,** *246* (4926), 64-71.
3. Aebersold, R.; Mann, M., Mass spectrometry-based proteomics. *Nature* **2003,** *422* (6928), 198-207.
4. Bruins, A. P., Mechanistic aspects of electrospray ionization. *Journal of Chromatography A* **1998,** *794* (1-2), 345-357.
5. Banerjee, S.; Mazumdar, S., Electrospray ionization mass spectrometry: a technique to access the information beyond the molecular weight of the analyte. *International journal of analytical chemistry* **2012,** *2012*.
6. Axenrod, T.; Pregosin, P., M. J. Wieder. *J. Am. Chem. SOC* **1969,** *91*, 3682.
7. Farenc, M. Apports de la mobilité ionique couplée à la spectrométrie de masse pour l’analyse des matrices complexes. Normandie, 2017.
8. Menet, M.-C., Principes de la spectrométrie de masse. *Revue francophone des laboratoires* **2011,** *2011* (437), 41-53.
9. Gross, J. H., *Mass spectrometry: a textbook*. Springer Science & Business Media: 2006.
10. McEwen, C. N.; McKay, R. G.; Larsen, B. S., Analysis of solids, liquids, and biological tissues using solids probe introduction at atmospheric pressure on commercial LC/MS instruments. *Analytical Chemistry* **2005,** *77* (23), 7826-7831.
11. Maire, F.; Neeson, K.; Denny, R.; McCullagh, M.; Lange, C.; Afonso, C.; Giusti, P., Identification of ion series using ion mobility mass spectrometry: the example of alkyl-benzothiophene and alkyl-dibenzothiophene ions in Diesel fuels. *Analytical chemistry* **2013,** *85* (11), 5530-5534.
12. Ito, S.; Chikasou, M.; Inohana, S.; Fujita, K., Analysis of Processed Foods Containing Oils and Fats by Time of Flight Mass Spectrometry with an APCI Direct Probe. *Shokuhin eiseigaku zasshi. Journal of the Food Hygienic Society of Japan* **2016,** *57* (5), 160-165.
13. Wiley, W.; McLaren, I. H., Time-of-flight mass spectrometer with improved resolution. *Review of scientific instruments* **1955,** *26* (12), 1150-1157.
14. Mamyrin, B.; Karataev, V.; Shmikk, D.; Zagulin, V., The mass-reflectron. A new nonmagnetic time-of-flight high resolution mass-spectrometer. *Zhurnal Ehksperimental'noj i Teoreticheskoj Fiziki* **1973,** *64* (1), 82-89.
15. Kumar, K. J.; Vijayan, V., An overview of liquid chromatography-mass spectroscopy instrumentation. **2014**.
16. Paul, W.; Steinwedel, H., Ein neues massenspektrometer ohne magnetfeld. *Zeitschrift für Naturforschung A* **1953,** *8* (7), 448-450.
17. Argoti, D., *Liquid chromatography-mass spectrometry for detection and characterization of DNA biomarkers and reactive metabolites*. Northeastern University: 2008.
18. Morris, H. R.; Paxton, T.; Panico, M.; McDowell, R.; Dell, A., A novel geometry mass spectrometer, the Q-TOF, for low-femtomole/attomole-range biopolymer sequencing. *Journal of protein chemistry* **1997,** *16* (5), 469-479.
19. Marshall, A. G.; Hendrickson, C. L., Fourier transform ion cyclotron resonance detection: principles and experimental configurations. *International Journal of Mass Spectrometry* **2002,** *215* (1-3), 59-75.
20. Comisarow, M. B.; Marshall, A. G., Frequency-sweep Fourier transform ion cyclotron resonance spectroscopy. *Chemical Physics Letters* **1974,** *26* (4), 489-490.
21. Bharti, A.; Ma, P. C.; Salgia, R., Biomarker discovery in lung cancer—promises and challenges of clinical proteomics. *Mass spectrometry reviews* **2007,** *26* (3), 451-466.
22. Marshall, A. G.; Chen, T., 40 years of Fourier transform ion cyclotron resonance mass spectrometry. *International Journal of Mass Spectrometry* **2015,** *377*, 410-420.
23. Boldin, I. A.; Nikolaev, E. N., Fourier transform ion cyclotron resonance cell with dynamic harmonization of the electric field in the whole volume by shaping of the excitation and detection electrode assembly. *Rapid Communications in Mass Spectrometry* **2011,** *25* (1), 122-126.

24. Henry, K. D.; Williams, E. R.; Wang, B. H.; McLafferty, F. W.; Shabanowitz, J.; Hunt, D. F., Fourier-transform mass spectrometry of large molecules by electrospray ionization. *Proceedings of the National Academy of Sciences* **1989,** *86* (23), 9075-9078.

25. Park, K. H.; Kim, M. S.; Baek, S. J.; Bae, I. H.; Seo, S.-W.; Kim, J.; Shin, Y. K.; Lee, Y.-M.; Kim, H. S., Simultaneous molecular formula determinations of natural compounds in a plant extract using 15 T Fourier transform ion cyclotron resonance mass spectrometry. *Plant methods* **2013,** *9* (1), 1-13.

26. Barrow, M. P.; Burkitt, W. I.; Derrick, P. J., Principles of Fourier transform ion cyclotron resonance mass spectrometry and its application in structural biology. *Analyst* **2005,** *130* (1), 18-28.

27. Thangaraj, S. K. Applications of high-resolution mass spectrometry to structure-function studies of proteins. Itä-Suomen yliopisto, 2019.

28. Wang, N. Negative Ion Electron Capture Dissociation (niECD): A Novel Tandem Mass Spectrometric Technique. 2014.

29. Marshall, A. G.; Roe, D. C., Theory of Fourier transform ion cyclotron resonance mass spectroscopy: Response to frequency-sweep excitation. *The Journal of Chemical Physics* **1980,** *73* (4), 1581-1590.

30. Popov, I. A.; Nagornov, K.; N. Vladimirov, G.; Kostyukevich, Y. I.; Nikolaev, E. N., Twelve million resolving power on 4.7 T Fourier transform ion cyclotron resonance instrument with dynamically harmonized cell—observation of fine structure in peptide mass spectra. *Journal of The American Society for Mass Spectrometry* **2014,** *25* (5), 790-799.

31. Marshall, A. G.; Hendrickson, C. L.; Jackson, G. S., Fourier transform ion cyclotron resonance mass spectrometry: a primer. *Mass spectrometry reviews* **1998,** *17* (1), 1-35.

32. McLafferty, F. W., Tandem mass spectrometry. *Science* **1981,** *214* (4518), 280-287.

33. McLafferty, F. W., Mass spectrometry across the sciences. *Proceedings of the National Academy of Sciences* **2008,** *105* (47), 18088-18089.

34. Bythell, B. J.; Hendrickson, C. L.; Marshall, A. G., Relative stability of peptide sequence ions generated by tandem mass spectrometry. *Journal of The American Society for Mass Spectrometry* **2012,** *23* (4), 644-654.

35. Solouki, T.; Paša-Tolić, L.; Jackson, G. S.; Guan, S.; Marshall, A. G., High-resolution multistage MS, MS2, and MS3 matrix-assisted laser desorption/ionization FT-ICR mass spectra of peptides from a single laser shot. *Analytical chemistry* **1996,** *68* (21), 3718-3725.

36. Little, D. P.; Speir, J. P.; Senko, M. W.; O'Connor, P. B.; McLafferty, F. W., Infrared multiphoton dissociation of large multiply charged ions for biomolecule sequencing. *Analytical Chemistry* **1994,** *66* (18), 2809-2815.

37. Cooper, H. J.; Håkansson, K.; Marshall, A. G., The role of electron capture dissociation in biomolecular analysis. *Mass spectrometry reviews* **2005,** *24* (2), 201-222.

38. Kaplan, D. A.; Hartmer, R.; Speir, J. P.; Stoermer, C.; Gumerov, D.; Easterling, M. L.; Brekenfeld, A.; Kim, T.; Laukien, F.; Park, M. A., Electron transfer dissociation in the hexapole collision cell of a hybrid quadrupole-hexapole Fourier transform ion cyclotron resonance mass spectrometer. *Rapid Communications in Mass Spectrometry: An International Journal Devoted to the Rapid Dissemination of Up-to-the-Minute Research in Mass Spectrometry* **2008,** *22* (3), 271-278.

39. Olsen, J. V.; Macek, B.; Lange, O.; Makarov, A.; Horning, S.; Mann, M., Higher-energy C-trap dissociation for peptide modification analysis. *Nature methods* **2007,** *4* (9), 709-712.

40. Yinon, J., Tandem Mass Spectrometry (MS/MS) and Collision Induced Dissociation (CID)—an Introduction. In *Chemistry and Physics of Energetic Materials*, Springer: 1990; pp 685-693.

41. Laskin, J.; Futrell, J. H., Activation of large lons in FT-ICR mass spectrometry. *Mass spectrometry reviews* **2005,** *24* (2), 135-167.

42. Kanu, A.; Dwivedi, P.; Tam, M.; Matz Jr, L., HHH. Ion mobility–mass spectrometry. *J Mass Spectrom* **2007**.

43. Gabelica, V.; Marklund, E., Fundamentals of ion mobility spectrometry. *Current opinion in chemical biology* **2018,** *42*, 51-59.

44. Campuzano, I.; Bush, M. F.; Robinson, C. V.; Beaumont, C.; Richardson, K.; Kim, H.; Kim, H. I., Structural characterization of drug-like compounds by ion mobility mass spectrometry: comparison of theoretical and experimentally derived nitrogen collision cross sections. *Analytical chemistry* **2012,** *84* (2), 1026-1033.

45. Webb, I. K.; Garimella, S. V.; Tolmachev, A. V.; Chen, T.-C.; Zhang, X.; Norheim, R. V.; Prost, S. A.; LaMarche, B.; Anderson, G. A.; Ibrahim, Y. M., Experimental evaluation and optimization of structures for lossless ion manipulations for ion mobility spectrometry with time-of-flight mass spectrometry. *Analytical chemistry* **2014,** *86* (18), 9169-9176.

46. Lapthorn, C.; Pullen, F.; Chowdhry, B. Z., Ion mobility spectrometry-mass spectrometry (IMS-MS) of small molecules: Separating and assigning structures to ions. *Mass spectrometry reviews* **2013,** *32* (1), 43-71.

47. Ben-Nissan, G.; Sharon, M., The application of ion-mobility mass spectrometry for structure/function investigation of protein complexes. *Current opinion in chemical biology* **2018,** *42*, 25-33.

48. Hupin, S.; Lavanant, H.; Renaudineau, S.; Proust, A.; Izzet, G.; Groessl, M.; Afonso, C., A calibration framework for the determination of accurate collision cross sections of polyanions using polyoxometalate standards. *Rapid Communications in Mass Spectrometry* **2018,** *32* (19), 1703-1710.

49. Ridgeway, M. E.; Lubeck, M.; Jordens, J.; Mann, M.; Park, M. A., Trapped ion mobility spectrometry: A short review. *International Journal of Mass Spectrometry* **2018,** *425*, 22-35.

50. Fernandez-Lima, F.; Kaplan, D. A.; Suetering, J.; Park, M. A., Gas-phase separation using a trapped ion mobility spectrometer. *International Journal for Ion Mobility Spectrometry* **2011,** *14* (2), 93-98.

51. Cumeras, R.; Figueras, E.; Davis, C. E.; Baumbach, J. I.; Gracia, I., Review on ion mobility spectrometry. Part 1: current instrumentation. *Analyst* **2015,** *140* (5), 1376-1390.

52. Shvartsburg, A. A.; Smith, R. D., Fundamentals of traveling wave ion mobility spectrometry. *Analytical chemistry* **2008,** *80* (24), 9689-9699.

53. Giles, K.; Wildgoose, J. L.; Pringle, S.; Langridge, D.; Nixon, P.; Garside, J.; Carney, P., Characterising a T-wave enabled multi-pass cyclic ion mobility separator. *Proceedings of the American Society for Mass Spectrometry and Allied Topics* **2015**.

54. Mortensen, D. N.; Susa, A. C.; Williams, E. R., Collisional cross-sections with T-wave ion mobility spectrometry without experimental calibration. *Journal of The American Society for Mass Spectrometry* **2017,** *28* (7), 1282-1292.

55. Dallüge, J.; Beens, J.; Udo, A., Comprehensive two-dimensional gas chromatography: a powerful and versatile analytical tool. *Journal of Chromatography A* **2003,** *1000* (1-2), 69-108.

56. Dallüge, J.; van Rijn, M.; Beens, J.; Vreuls, R. J.; Udo, A., Comprehensive two-dimensional gas chromatography with time-of-flight mass spectrometric detection applied to the determination of pesticides in food extracts. *Journal of Chromatography A* **2002,** *965* (1-2), 207-217.

57. Kew, W.; Blackburn, J. W.; Clarke, D. J.; Uhrín, D., Interactive van Krevelen diagrams–Advanced visualisation of mass spectrometry data of complex mixtures. *Rapid Communications in Mass Spectrometry* **2017,** *31* (7), 658.

58. Hughey, C. A.; Hendrickson, C. L.; Rodgers, R. P.; Marshall, A. G.; Qian, K., Kendrick mass defect spectrum: a compact visual analysis for ultrahigh-resolution broadband mass spectra. *Analytical chemistry* **2001,** *73* (19), 4676-4681.

59. Wu, Z.; Rodgers, R. P.; Marshall, A. G., Two-and three-dimensional van Krevelen diagrams: A graphical analysis complementary to the Kendrick mass plot for sorting elemental compositions of complex organic mixtures based on ultrahigh-resolution broadband Fourier transform ion cyclotron resonance mass measurements. *Analytical chemistry* **2004,** *76* (9), 2511-2516.

60. Hughey, C., a.; Hendrickson, CL; Rodgers, RP; Marshall, AG; Qian, K. Kendrick Mass Defect Spectrum: A Compact Visual Analysis for Ultrahigh-Resolution Broadband Mass Spectra. *Anal. Chem* **2001,** *73* (19), 4676-81.

61. Van Krevelen, D., Graphical-statistical method for the study of structure and reaction processes of coal. *Fuel* **1950,** *29*, 269-284.

62. Kim, S.; Kramer, R. W.; Hatcher, P. G., Graphical method for analysis of ultrahigh-resolution broadband mass spectra of natural organic matter, the van Krevelen diagram. *Analytical chemistry* **2003,** *75* (20), 5336-5344.

63. Lobodin, V. V.; Marshall, A. G.; Hsu, C. S., Compositional space boundaries for organic compounds. *Analytical chemistry* **2012,** *84* (7), 3410-3416.

Chapter 3:

Characterization of insoluble organic polymers

Chapter 3: Characterization of insoluble polymers

The characterization of insoluble organic polymers is an analytical discipline concerned with the characterization of different polymeric materials on a variety of levels. It typically aims to improve our knowledge on this type of polymers by better understanding the phenomena involved in their manufacturing, polymerization, reticulation, chemical stability and resistance, ageing and degradation under natural conditions and eventually recycling. It also involves molecular characterization in order to acquire information on their general structure and details about their microstructure. This can be achieved by the determination of the mass of chemical compounds present in the polymers with high accuracy and classification according to their elemental composition and their structural properties such as degree of unsaturation and number of carbon atoms. In this chapter, we will discuss the various approaches based on common and innovative mass spectrometry methods for the structural and chemical characterization of insoluble natural and synthetic polymers, in particular polyolefin and polydienes

I. General introduction

Organic molecules can be analyzed using a wide range of analytical methods such as NMR, mass spectrometry, X-Ray diffraction, UV-Visible, Infra-Red, Raman spectroscopies and many other techniques,[1] the majority of which can be hyphenated with chromatography, allowing the analysis of complex mixtures. However, these methods become scarce in the case of insoluble organic polymers. Their insolubilities may be either due to their molar mass, to their cross-linked structures or both. Insoluble organic polymers are present nowadays in most of our surroundings and they have a key importance in most of the aspects of our life. On the other hand, synthetic polymers present an environmental threat due to their long lifetimes and fragmentation in microplastics. As these polymers are considered as complex mixtures, it is important to use ultra-high-resolution mass spectrometers for a better separation. Fourier transform ion cyclotron resonance (FT-ICR) has emerged as a reference technique for the analysis of such polymers.[2] In fact, it offers a very high resolution as well as a remarkable mass accuracy with error lower than 0.1 ppm. This instrument is therefore capable of separating the majority of species present in a polymeric sample and attribute a molecular formula for each detected *m/z* value.[3-4] This allows an easier identification and classification of chemical compounds and families.

II. Chemical depolymerization

Proteins can be easily broken down to smaller peptides by means of specific enzymes such as trypsin which facilitate their characterization. Furthermore, cellulose can be depolymerized by cellulase and starch debranched using amylase. These two polysaccharides are relatively easy to depolymerize in their native forms, however, when chemically modified, they become very resistant to digestion. As effective as enzymes are, not all polymers have specific cleavage enzymes. Natural polymers containing monomer units linked together by C-C bonds such as natural rubber or C-O bonds such as lignin cannot be cleaved by enzymes and are very insoluble. The same is valid for most of insoluble synthetic polymers like polybutadiene, polyethylene and polyacrylates. As a result, the analysis of these polymers by mass spectrometry technique affording structural information requires a depolymerization step in order to solubilize and analyze these classes of polymers.

II.1. Olefin metathesis [5-10]

Olefin metathesis has emerged over the last few years as a very powerful tool in organic and polymer chemistry. It has radically changed the way chemists imagine and synthesize molecules. Thanks to the metathesis reaction, it is possible to access small cycles, medium cycles, macromolecules, polymers and / or complex natural molecules from relatively simple fragments and possessing unsaturation. Developed by the scientists Chauvin, Grubbs and Schrock who were awarded the Nobel prize in 2005 for their contribution in the development of the metathesis method in organic chemistry. It is based on well-defined organometallic catalysts which can induce both cleavage and formation of carbon-carbon double bonds and show tolerance toward different functional groups. Since its discovery, olefin metathesis has been involved in a variety of applications such as petrochemistry, drug synthesis, polymer chemistry and natural products. Olefin metathesis is a set of several different types of reactions:

Cross-metathesis (CM) [11]: It is an intermolecular process which allows the coupling of two linear olefins to form a new olefin

Ring-closing metathesis (RCM)[12]: It is an intramolecular process, it consists on the formation of rings from diene compounds. The RCM allows to form cycles of very variable size (5 to 30 bonds) and tolerates a large number of functional groups.

Ring-opening metathesis (ROM)[13]: It is simply the inverse of RCM. It consists on the opening of an unsaturated cycle by reaction with a simple olefin.

Ring-opening metathesis polymerization (ROMP)[14]: it is a process that consists on the formation of polymers or block copolymers from unsaturated cyclic monomers. This method makes it possible to obtain a polymer of controlled molar mass with a low polydispersity and unique properties.

Acyclic diene metathesis polymerization (ADMET)[15] : this process is considered to be a step polymerization. A polycondensation-type polymerization reaction makes it possible to obtain strictly linear chains from unconjugated dienes. This polymerization allows the formation of linear unsaturated polymers of high molar masses and copolymers

This versatile method can be used as an effective way for the depolymerization of insoluble polymers preserving the main features of the polymer such as the exact geometry of the double bonds if present, the relative stereochemistry of chiral centers, the cross-linkers which are a signature of the polymer manufacturing and of its ageing and the chemical modifications of the polymer during its use or degradation. Several other applications for olefin metathesis include polymer recycling. The olefin metathesis reaction used in this work in the cross-metathesis which requires the presence of carbon double bonds in the polymeric chain of the studied polymers.

II.2. Organometallic catalysts

From the discovery of the metathesis reaction until the 1980s, catalysts used were mixtures of metal salts and alkylating agents used in homogeneous medium or transition metal salts deposited on a solid support.[16] The rise in olefin metathesis in organic synthesis has mainly taken place thanks to the introduction of new stable metal-alkylidene complexes. The first catalysts used were alkylidenes of molybdenum and of tungsten.[17-18] Improving the performance of catalysts requires development of structures which react preferentially with olefins rather than with the heteroatomic functions or solvent. The two most used metals for making catalysts are molybdenum and especially ruthenium, because these two metals are the least sensitive to heteroatomic functions. The most significant progress has been made with the synthesis of the molybdenum catalysts studied by Schrock [19-20] and those with ruthenium developed by Grubbs et al. [21]

In this work, we are more particularly interested in ruthenium catalysts because they show good tolerance to functional groups.

Grubbs and his group synthesized in 1992 the first active ruthenium carbene in metathesis reactions. This catalyst presented a very important activity in metathesis, however, it remained inefficient at the initiation of the reaction. For this reason, Grubbs improved this catalyst [22] to obtain the benzylidene-bis(tricyclohexylphosphine)dichlororuthenium commonly known at Grubbs 1st generation catalyst (Figure 37) which proved to be a very stable, very reactive and very tolerant catalyst.[23]

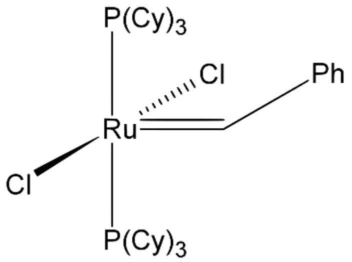

Figure 37. Grubbs 1st generation catalyst

This catalyst paved the way for a very wide range of metathesis reactions including reactions on functionalized olefins [6] and there exist a very important number of studies carried out using this catalyst. [24]

However, olefin metathesis using Grubbs 1st generation catalyst can cause side reactions. The main side reactions that can appear are reactions of cyclization, isomerization (especially double-bond shifting and solvent alkylation when it is aromatic.[25]

Furthermore, the stability to air and humidity in particular, and the compatibility with a large number of functional groups, have made these ruthenium catalysts very popular and have spawned the emergence of a collection of multi-generational metathesis catalysts.

Substitution of a phosphine by an N-heterocyclic carbene ligand allowed to develop second generation Grubbs catalysts (Figure 38).

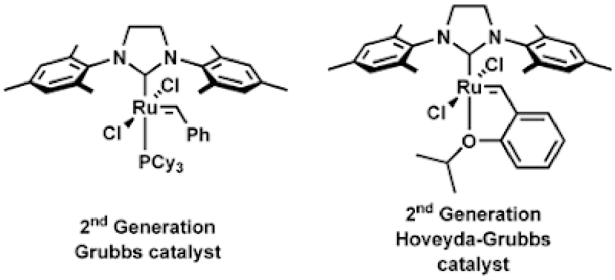

Figure 38. Grubbs and Hoveyda-Grubbs 2nd generation catalysts

These catalysts, stable in air and at high temperature, have been shown to be extremely reactive to substrates which do not react with the usual ruthenium catalysts due to the much more labile alkylidene ligand. They are very easy to handle and show an exceptional tolerance towards numerous polar groups such as esters, amides, ketones, aldehydes and even acids and water. [26] They are more active than Schrock catalysts. They allow in particular the formation of tetra substituted double bonds, inaccessible with first generation catalysts.[27]

II.3. Application on polyolefins

The majority of polyolefins consist on long chain linear polymers with no carbon double bonds. To apply cross-metathesis depolymerization to polyolefins, a dehydrogenation step is required. Polyethylene (PE) is the most produced synthetic polyolefin and its chemical inertness makes its degradation a challenging process. However, in the presence of a short-chain alkane, the depolymerization of polyethylene can occur through three consecutive steps of dehydrogenation, metathesis and hydrogenation. The overall result of these three reactions is known as cross alkane metathesis. Several studies have been carried out in order to find new recycling ways of polyolefins.

In a first study, dehydrogenation using an Iridium-based catalyst has been proposed by Goldman and his team.[28-29] They described systems for alkane metathesis based on the tandem operation of catalyst for alkane dehydrogenation and olefin metathesis. They used a pincer-ligated Iridium complexes as dehydrogenation catalyst followed by Molybdenum and Tungsten Schrock type catalysts for olefin metathesis. They were able to achieve great progress, however, they faced major challenges such as the decomposition of the olefin metathesis catalysts as they used high temperatures compatible with the dehydrogenation catalysts.

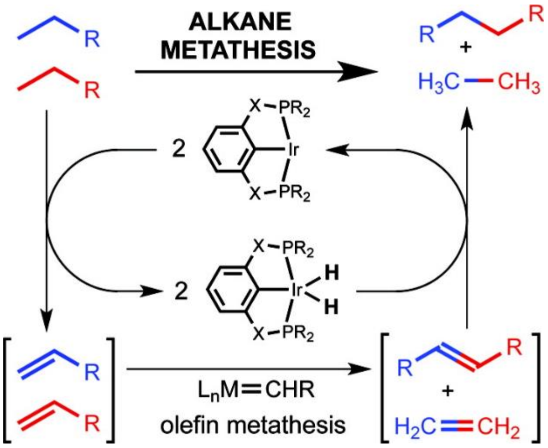

Figure 39. The proposed system by Goldman and his team for alkane metathesis

Additional studies were also conducted for the recycling of PE based on cross-alkane metathesis. In 2016, Huang applied the same methodology on polyethylene.[30] He discussed that PE has created serious environmental problems due to its widespread around the world. It is very inert is caused by that all atoms in the polymer chain are connected by strong simple carbon-carbon and carbon-hydrogen bonds. To overcome this problem, he proposed alkane metathesis with a lighter and smaller alkane (n-hexane) as a recycling method for PE. They used the same dual catalyst system containing a supported "pincer"-ligated iridium complex and obtained a product distribution in a range of C_2-C_{21}.

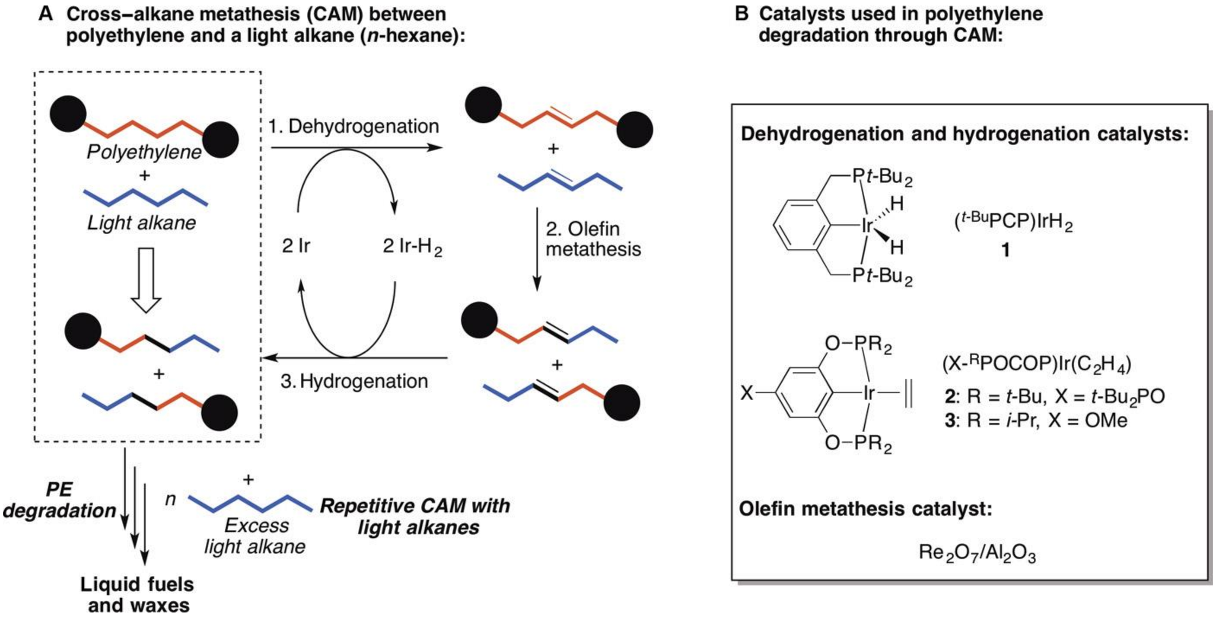

Figure 40. Degradation of PE through alkane metathesis with light alkanes as proposed by Huang

Finally, Roman-Leshkov and his team also worked on the depolymerization of PE in a recent study (2021). However, they developed a fully heterogenous catalyst system and proved that by using this system, they were able to produce a distribution of linear alkane products from a linear PE substrate in am n-pentane solvent.[31]

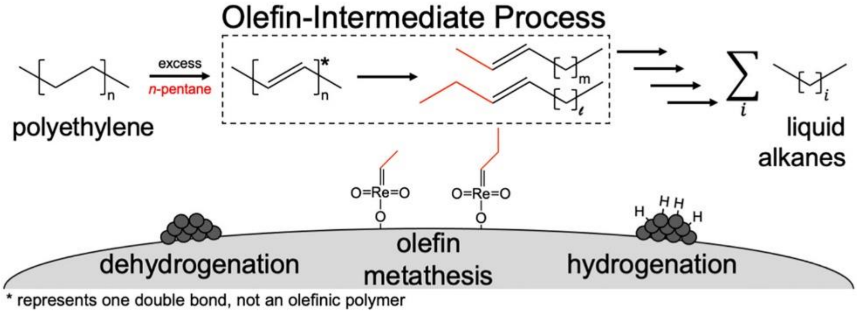

Figure 41. Degradation of PE through alkane metathesis with light alkanes as proposed by Roman-Leshkov

II.4. Application on polydienes

Olefin metathesis chemistry can be applied on a wide range of polymers. However, the most well-known example is the cross-metathesis depolymerization and functionalization of unsaturated polymers or polydienes such as polybutadiene (PB) and polyisoprene (PI). These types of polymeric materials tend to form linear and cross-linked networks that lead to tremendous environmental impact. Therefore, it became very important to develop novel and improved depolymerization methods to overcome this problem.

The first cross-metathesis degradation reaction of polybutadiene with linear olefins was carried out by Ast et al in the presence of a catalytic system based on tungsten and hex-2-ene as a transfer agent. The products have been analyzed, one or two butadiene units were detected with identical or different chain ends (ethylene or butylene).[32]

Abendroth et al.[33], Canji et al.[34] performed studies on the degradation of 1,4- polybutadiene (cis and trans), using $WC1_6$ / Et_4Sn / Et_2O as a catalyst, and hex-3-ene as a transfer agent. In these studies, hex-3-ene is used in large excess compared to the ethylenic macromolecular structures in order to lead the degradation to its ultimate stage. Then in 1986 Campistron et al.[35] studied the catalyzed degradation of polybutadiene by WCl_6 / Sn (Me) $_4$ by co-metathesis with dimethyl hexy-3-enedioate. Molar mass of the obtained products can be controlled by the relative proportions of the ester in relation to the units of polybutadiene.

In the case of metathesis of polyisoprene, limited work has been done. The first attempts at degradation of cis-1,4-polyisoprene carried out by Ast et al.[32] and Pampus et al.[36] in 1970 by metathesis failed, probably due to the short lifespan of the WCl_6 / $Et_3Al_2Cl_3$ catalyst.

The development of new ruthenium-based catalysts, especially 2nd generation Grubbs catalysts, more active and more efficient allowed new possibilities of olefin metathesis reaction and their application to achieve a controlled synthesis or degradation of polymers that were not easily achievable.

Pilard et al.[37] have shown the possibility of degradation of cis-1,4-polyisoprene of Mn = 330 000 g/mol in solvent organic using Grubbs II as catalyst and cis-2-ene-1,4-diacetate as transfer agent in dichloromethane at room temperature.

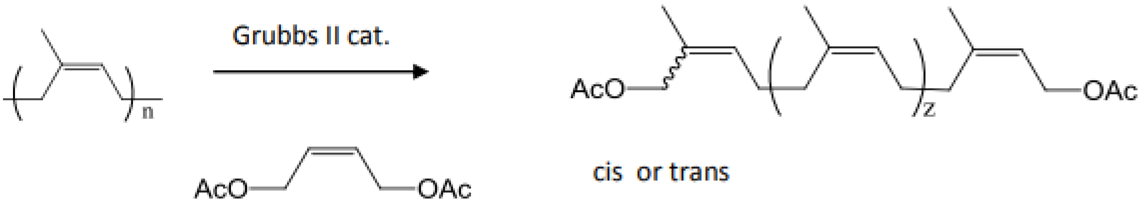

Figure 42. Structure of the product obtained by metathesis degradation of polyisoprene

In another study, they optimized the metathetic degradation of polyisoprene by precisely selecting the different reaction conditions such as the catalyst concentration, the solvent and the polymer concentration. They later applied the depolymerization reaction under optimized conditions on synthetic cis-1,4-polyisoprene using the cis-1,4-diacetoxy-2-butene as chain transfer agent and Grubbs II catalyst. They were able to produce well-defined acetoxy telechelic polyisoprene structures with high selectivity.[38]

Peruch et al [39] performed the degradation of trans-1,4-polyisoprene using 1st and 2nd generation Grubbs and Hoveyda-Grubbs catalysts with ethylene or octene as transfer agents in toluene as solvent at 60 °C. They proved that 1st and 2nd generation Hoveyda-Grubbs catalysts were effective for the controlled and regioselective degradation of high molar mass trans-1,4-PI.

These studies as well as others are very important and crucial, nevertheless, very few works are described in the literature on the metathesis degradation of unsaturated insoluble polydienes.

III. Electrospray based analysis

Polymers with large molecular weight are difficult to analyze using electrospray ionization coupled to mass spectrometry (ESI-MS) due to their high insolubility in compatible solvents and difficulty to ionize. Electrospray ionization (ESI) has several advantages such as minimal fragmentation and high ionization efficiency.

Very few studies are found in the literature describing the analysis of polyolefins and polydienes using electrospray as ionization source for mass spectrometry. We present in this manuscript one of the first studies applied for the analysis of these classes of polymers by ESI-MS. It is based on a depolymerization step using cross-metathesis reaction described previously to transform these very insoluble polymers into soluble products in organic solvents compatible with ESI.

IV. Pyrolysis based analysis

Pyrolysis consists on the degradation, or cracking, of polymers subjected to a high temperature (between 300 and 900 °C) to obtain smaller molecules and volatile fragments called pyrolysate. The process takes place in the absence of oxygen, and does not produce CO_2 or other toxic or polluting gases. Pyrolysis of polymers can provide valuable information on these macromolecules by identifying the products issued from the thermal degradation, however, structural information is often lost due to the complexity of the pyrolysis mechanisms.

This process makes it possible to obtain three different phases, the composition of each of which depends on the temperature of the heat treatment[40-41]:

The gas phase contains a mixture of hydrocarbons of mono- and di- carbon oxide and hydrogen. This gas mixture is used to provide energy necessary for the pyrolysis process.

The liquid phase is a mixture of hydrocarbons and water.

The solid phase constitutes 40% by mass of the initial sample. It is made up of carbon black and minerals.

The classical method for analysis of polymers from different classes is pyrolysis coupled to gas chromatography. In fact, pyrolysis coupled to mass spectrometry is an extremely versatile analytical tool which can be applied to study the structures of polymers both natural and synthetic as well as their thermal degradation profiles. The combination of pyrolysis and high-resolution mass spectrometry can provide an extra specificity required for the analysis of complex mixtures.

IV.1. Application on polyolefins

The increased usage of polyolefinic polymers such as PE and PP resulted in the increase of waste plastics which leads to an important environmental problem. These plastics are not biodegradable and they stay in nature for a long time. Pyrolysis of plastic waste is often used as a thermochemical recycling path, in which the plastic waste materials are treated in inert atmosphere. They can be thus converted into low molecular weight chemicals used later on as raw materials in industry.

Numerous studies have contributed to the theory and practice of the thermal degradation of polymers.[42] Polyolefins in general, and PE and PP are usually the target for such studies as their degradation results in products having desirable properties for further applications.

In a study carried out by Afonso et al,[43] they presented for the first time a detailed description of the structure of PP and PE using pyrolysis coupled to ultrahigh resolution mass spectrometry and ion mobility. Identical species were identified in the three polymers and significant differences concerning the number of oxygen atoms and DBE were recorded by the mean of FTICR mass spectrometry. Ion mobility allowed the detection of several isomeric distribution as PP ions were found to be more compact than those of PE.

In a second study aimed for the characterization of polyalphaolefin, Racaud et al,[44] used atmospheric solid analysis probe (ASAP) coupled to ion mobility spectrometry. They studied different polyalphaolefins grades with different viscosity index and were able to obtain several series of fragment ions which helped to identify the alpha olefin used to synthetize polyalphaolefins. They also acquired information on isomeric species using ion mobility.

IV.2. Application on polydienes

Pyrolysis coupled to mass spectrometry have been used for decades to elucidate the structures of polydienes. Most of studies in literature focused on the pyrolysis of polyisoprene rubber followed by analysis by mass spectrometry.[45-47]

Sarkissian[48] presented in his research the analysis of tire rubber traces after braking from 12 different sources. He used pyrolysis gas chromatography/mass spectrometry to analyze 12 tires from different manufacturers. He used this technique in order to pyrolyze all the samples and perform quantitative and qualitative analysis. He was able to distinguish each sample from the other and identify its original source.

References

1. Marković, G.; Marinović-Cincović, M.; Jovanović, V.; Samaržija-Jovanović, S.; Budinski-Simendic, J., Polymer characterization (II). 2016; pp 397-403.
2. Heeren, R.; Kleinnijenhuis, A.; McDonnell, L.; Mize, T., A mini-review of mass spectrometry using high-performance FTICR-MS methods. *Analytical and bioanalytical chemistry* **2004,** *378* (4), 1048-1058.
3. Baykut, G.; Eyler, J., Fourier transform ion cyclotron resonance mass spectrometry. *TRAC: Trends in Analytical Chemistry: Volume 5* **2013,** *5* (2), 44.
4. Marshall, A. G.; Hendrickson, C. L., Fourier transform ion cyclotron resonance detection: principles and experimental configurations. *International Journal of Mass Spectrometry* **2002,** *215* (1-3), 59-75.
5. Grubbs, R. H., Olefin metathesis. *Tetrahedron* **2004,** *60* (34), 7117-7140.
6. Fürstner, A., Olefin metathesis and beyond. *Angewandte Chemie International Edition* **2000,** *39* (17), 3012-3043.
7. Schuster, M.; Blechert, S., Olefin metathesis in organic chemistry. *Angewandte Chemie International Edition in English* **1997,** *36* (19), 2036-2056.
8. Grubbs, R. H.; Chang, S., Recent advances in olefin metathesis and its application in organic synthesis. *Tetrahedron* **1998,** *54* (18), 4413-4450.
9. Hoveyda, A. H.; Zhugralin, A. R., The remarkable metal-catalysed olefin metathesis reaction. *Nature* **2007,** *450* (7167), 243-251.
10. Katz, T. J.; McGinnis, J., Mechanism of the olefin metathesis reaction. *Journal of the American Chemical Society* **1975,** *97* (6), 1592-1594.
11. Connon, S. J.; Blechert, S., Recent developments in olefin cross-metathesis. *Angewandte Chemie International Edition* **2003,** *42* (17), 1900-1923.
12. Yu, M.; Lou, S.; Gonzalez-Bobes, F., Ring-Closing Metathesis in Pharmaceutical Development: Fundamentals, Applications, and Future Directions. *Organic Process Research & Development* **2018,** *22* (8), 918-946.
13. Bielawski, C. W.; Grubbs, R. H., Living ring-opening metathesis polymerization. *Progress in Polymer Science* **2007,** *32* (1), 1-29.
14. Singh, R.; Czekelius, C.; Schrock, R. R., Living ring-opening metathesis polymerization of cyclopropenes. *Macromolecules* **2006,** *39* (4), 1316-1317.
15. Mathers, R. T., Ring-Opening Metathesis Polymerizations and Acyclic Diene Metathesis Polymerizations with Homogeneous Ruthenium and Molybdenum Catalysts and Initiators. *Handbook of Transition Metal Polymerization Catalysts* **2010**, 513-536.
16. Hoff, R.; Mathers, R. T., *Handbook of transition metal polymerization catalysts*. John Wiley & Sons: 2010.
17. Schrock, R. R.; Murdzek, J. S.; Bazan, G. C.; Robbins, J.; DiMare, M.; O'Regan, M., Synthesis of molybdenum imido alkylidene complexes and some reactions involving acyclic olefins. *Journal of the American Chemical Society* **1990,** *112* (10), 3875-3886.
18. Schrock, R. R.; DePue, R.; Feldman, J.; Schaverien, C.; Dewan, J.; Liu, A., Preparation and reactivity of several alkylidene complexes of the type W (CHR')(N-2, 6-C6H3-iso-Pr2)(OR) 2 and related tungstacyclobutane complexes. Controlling metathesis activity through the choice of alkoxide ligand. *Journal of the American Chemical Society* **1988,** *110* (5), 1423-1435.
19. Bazan, G. C.; Oskam, J. H.; Cho, H. N.; Park, L. Y.; Schrock, R. R., Living ring-opening metathesis polymerization of 2, 3-difunctionalized 7-oxanorbornenes and 7-oxanorbornadienes by Mo (CHCMe2R)(NC6H3-iso-Pr2-2, 6)(O-tert-Bu) 2 and Mo (CHCMe2R)(NC6H3-iso-Pr2-2, 6)(OCMe2CF3) 2. *Journal of the American Chemical Society* **1991,** *113* (18), 6899-6907.
20. Schrock, R., Alkene metathesis in organic synthesis. *Top. Organomet. Chem* **1998,** *1*, 1-36.
21. Nguyen, S. T.; Johnson, L. K.; Grubbs, R. H.; Ziller, J. W., Ring-opening metathesis polymerization (ROMP) of norbornene by a group VIII carbene complex in protic media. *Journal of the American Chemical Society* **1992,** *114* (10), 3974-3975.

22. Schwab, P.; Grubbs, R. H.; Ziller, J. W., Synthesis and applications of RuCl2 (CHR ‘)(PR3) 2: the influence of the alkylidene moiety on metathesis activity. *Journal of the American Chemical Society* **1996,** *118* (1), 100-110.

23. Schwab, P.; France, M. B.; Ziller, J. W.; Grubbs, R. H., A Series of Well-Defined Metathesis Catalysts–Synthesis of [RuCl2 (□ CHR′)(PR3) 2] and Its Reactions. *Angewandte Chemie International Edition in English* **1995,** *34* (18), 2039-2041.

24. Nicolaou, K.; Bulger, P. G.; Sarlah, D., Metathesis reactions in total synthesis. *Angewandte Chemie International Edition* **2005,** *44* (29), 4490-4527.

25. Ivin, K. J.; Mol, J. C., *Olefin metathesis and metathesis polymerization*. Elsevier: 1997.

26. Chao, W.; Weinreb, S. M., The first examples of ring-closing olefin metathesis of vinyl chlorides. *Organic letters* **2003,** *5* (14), 2505-2507.

27. Hoveyda, A. H.; Gillingham, D. G.; Van Veldhuizen, J. J.; Kataoka, O.; Garber, S. B.; Kingsbury, J. S.; Harrity, J. P., Ru complexes bearing bidentate carbenes: from innocent curiosity to uniquely effective catalysts for olefin metathesis. *Organic & biomolecular chemistry* **2004,** *2* (1), 8-23.

28. Haibach, M. C.; Kundu, S.; Brookhart, M.; Goldman, A. S., Alkane Metathesis by Tandem Alkane-Dehydrogenation–Olefin-Metathesis Catalysis and Related Chemistry. *Accounts of Chemical Research* **2012,** *45* (6), 947-958.

29. Kumar, A.; Bhatti, T. M.; Goldman, A. S., Dehydrogenation of Alkanes and Aliphatic Groups by Pincer-Ligated Metal Complexes. *Chemical Reviews* **2017,** *117* (19), 12357-12384.

30. Jia, X.; Qin, C.; Friedberger, T.; Guan, Z.; Huang, Z., Efficient and selective degradation of polyethylenes into liquid fuels and waxes under mild conditions. *Science Advances* **2016,** *2* (6), e1501591.

31. Ellis, L. D.; Orski, S. V.; Kenlaw, G. A.; Norman, A. G.; Beers, K. L.; Román-Leshkov, Y.; Beckham, G. T., Tandem Heterogeneous Catalysis for Polyethylene Depolymerization via an Olefin-Intermediate Process. *ACS Sustainable Chemistry & Engineering* **2021,** *9* (2), 623-628.

32. Ast, W.; Hummel, K., Gaschromatographische Polymer-Analyse nach Abbau durch Metathese. *Naturwissenschaften* **1970,** *57* (11), 545-545.

33. Abendroth, H.; Čanji, E., Anwendung der Metathese-Reaktion auf die Mikrostrukturbestimmung von Polybutadienen. *Die Makromolekulare Chemie: Macromolecular Chemistry and Physics* **1975,** *176* (3), 775-779.

34. Čanji, E.; Perner, H., Das umalkylidenierungsverhalten von polybutadienen mit erhöhtem anteil an 1, 2-Einheiten. *Die Makromolekulare Chemie: Macromolecular Chemistry and Physics* **1978,** *179* (3), 567-570.

35. Reyx, D.; Campistron, I., Controlled degradation in tailor-made macromolecules elaboration. Controlled chain-cleavages of polydienes by oxidation and by metathesis. *Die Angewandte Makromolekulare Chemie: Applied Macromolecular Chemistry and Physics* **1997,** *247* (1), 197-211.

36. Pampus, G.; Witte, J.; Hoffman, M., Rev Gen Caout Plast 47: 1343, 1970.(b) BA Dolgoplosk et al. *Recl Trav Chim Pays-Bas* **1977,** *96*, M35.

37. Solanky, S. S.; Campistron, I.; Laguerre, A.; Pilard, J. F., Metathetic selective degradation of polyisoprene: low-molecular-weight telechelic oligomer obtained from both synthetic and natural rubber. *Macromolecular Chemistry and Physics* **2005,** *206* (10), 1057-1063.

38. Sadaka, F.; Campistron, I.; Laguerre, A.; Pilard, J.-F., Telechelic oligomers obtained by metathetic degradation of both polyisoprene and styrene–butadiene rubbers. Applications for recycling waste tyre rubber. *Polymer Degradation and Stability* **2013,** *98* (3), 736-742.

39. Ouardad, S.; Peruch, F., Metathetic degradation of trans-1,4-polyisoprene with ruthenium catalysts. *Polymer Degradation and Stability* **2014,** *99*, 249-253.

40. Murillo, R.; Aylón, E.; Navarro, M.; Callén, M.; Aranda, A.; Mastral, A., The application of thermal processes to valorise waste tyre. *Fuel processing technology* **2006,** *87* (2), 143-147.

41. Berrueco, C.; Esperanza, E.; Mastral, F.; Ceamanos, J.; García-Bacaicoa, P., Pyrolysis of waste tyres in an atmospheric static-bed batch reactor: Analysis of the gases obtained. *Journal of Analytical and Applied Pyrolysis* **2005,** *74* (1-2), 245-253.

42. Hermabessiere, L.; Himber, C.; Boricaud, B.; Kazour, M.; Amara, R.; Cassone, A.-L.; Laurentie, M.; Paul-Pont, I.; Soudant, P.; Dehaut, A., Optimization, performance, and application of a pyrolysis-GC/MS method for the identification of microplastics. *Analytical and bioanalytical chemistry* **2018,** *410* (25), 6663-6676.

43. Farenc, M.; Witt, M.; Craven, K.; Barrère-Mangote, C.; Afonso, C.; Giusti, P., Characterization of polyolefin pyrolysis species produced under ambient conditions by Fourier transform ion cyclotron resonance mass spectrometry and ion mobility-mass spectrometry. *Journal of The American Society for Mass Spectrometry* **2017,** *28* (3), 507-514.
44. Mendes Siqueira, A. L.; Beaumesnil, M.; Hubert-Roux, M.; Loutelier-Bourhis, C.; Afonso, C.; Bai, Y.; Courtiade, M.; Racaud, A., Atmospheric Solid Analysis Probe Coupled to Ion Mobility Spectrometry-Mass Spectrometry, a Fast and Simple Method for Polyalphaolefin Characterization. *Journal of the American Society for Mass Spectrometry* **2018,** *29* (8), 1678-1687.
45. Hackathorn, M. J.; Brock, M. J., The Determination of “Head-Head” and “Tail-Tail” Structures in Poly(Isoprene)S. *Rubber Chemistry and Technology* **1972,** *45* (5), 1295-1302.
46. Lattimer, R. P.; Harris, R. E.; Rhee, C. K.; Schulten, H.-R., Identification of Organic Components in Uncured Rubber Compounds Using Mass Spectrometry. *Rubber Chemistry and Technology* **1988,** *61* (4), 639-657.
47. Schulten, H.-R.; Plage, B.; Lattimer, R. P., Pyrolysis-Field Ionization Mass Spectrometry of Rubber Vulcanizates. *Rubber Chemistry and Technology* **1989,** *62* (4), 698-708.
48. Sarkissian, G., The Analysis of Tire Rubber Traces Collected After Braking Incidents Using Pyrolysis-Gas Chromatography/Mass Spectrometry. *Journal of Forensic Sciences* **2007,** *52* (5), 1050-1056.

Chapter 4:

Results and Discussion

Chapter 4: Results and discussion

In this chapter, we will discuss the development of a new strategy based on the cross-metathesis reaction of PB and PI using the Hoveyda‒Grubbs organometallic catalyst, which allows us to solubilize the polymers and to generate end-functionalized acetoxy oligomers ionizable by ESI coupled to Fourier transform ion cyclotron resonance (FTICR) for the characterization of PB and PI in both *E*- and *Z*-configurations. Ion mobility spectrometry-mass spectrometry (IMS-MS) showed that, under classical cross-metathesis conditions, the oligomers were isomerized. We successfully suppressed this isomerization during olefin metathesis by adding a hydride scavenger, as shown in IMS-MS and energy-resolved mass spectrometry (ER-MS). Finally, for comparison, we performed classical pyrolysis techniques such as Comprehensive Two-Dimensional Gas Chromatography/Mass Spectrometry (Py/GC × GC‒MS) and atmospheric ionization sources such as Atmospheric Solid Analysis Probe (ASAP) and Direct Inlet Probe-Atmospheric Pressure Chemical Ionization (DIP-APCI) coupled to ion mobility spectrometry-mass spectrometry and Fourier transform ion cyclotron resonance high-resolution mass spectrometry (FTICR MS). High-resolution MS allowed us to attribute the elemental composition of the obtained pyrolysis products and distributions. These results are compared with those from the cross-metathesis reaction and ESI analysis.

Publication: Regio- and Stereo-Specific Chemical Depolymerization of High Molecular Weight Polybutadiene and Polyisoprene for Their Analysis by High-Resolution Fourier Transform Ion Cyclotron Resonance Mass Spectrometry: Comparison with Pyrolysis- Comprehensive Two-Dimensional Gas Chromatography/Mass Spectrometry, Atmospheric Solid Analysis Probe, Direct Inlet Probe- Atmospheric Pressure Chemical Ionization Mass Spectrometry, and Ion Mobility Spectrometry-Mass Spectrometry (Annex 1)

I. Cross metathesis reaction of PB and PI

First, high molecular weight commercial (*E*- and *Z*-) PB and PI (Figure 43) were analyzed by ^{1}H NMR to confirm their microstructures.

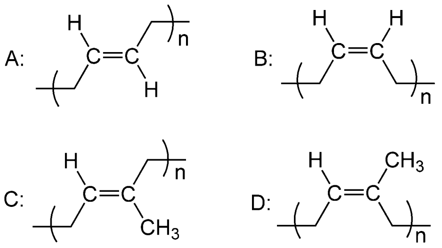

Figure 43. A: *E*-PB, B: *Z*-PB, C: *E*-PI, D: *Z*-PI

E-PB revealed a mixture of both configurations, signals at 1.96, 2.0, 5.3 and 5.4 ppm correspond to *E*-1,4-aliphatic (H4), *Z*-1,4-aliphatic (H3), *E*-1,4-olefinic (H2) and *Z*-1,4-olefinic (H1) protons respectively. The ratio of relative intensities of olefinic protons is comparable to that of aliphatic protons (1.2 vs 1.5). The signal for terminal 1,2-vinyl protons is at 4.9 ppm. For *Z*-PB, two signals were recorded at 5.3 ppm for *Z*-olefinic protons (H1) and 2 ppm for *Z*-aliphatic protons (H2). *E*-olefinic and aliphatic protons signals were not detected (Figure 44).

For polyisoprene, *E*-PI presented 4 different signals. The signal for *E*-olefinic protons (H1) appears at 5.04 ppm and that of aliphatic protons (H2, H3) at 1.98 and 1.93 ppm, while the signal at 1.52 ppm corresponds to *E*-methyl proton (H4). Finally, for *Z*-PI, *Z*-olefinic protons (H1) appear at 5.05 ppm, *Z*-aliphatic protons (H2) at 1.96 ppm and *Z*-methyl proton at 1.6 ppm (H3) (Figure 45).

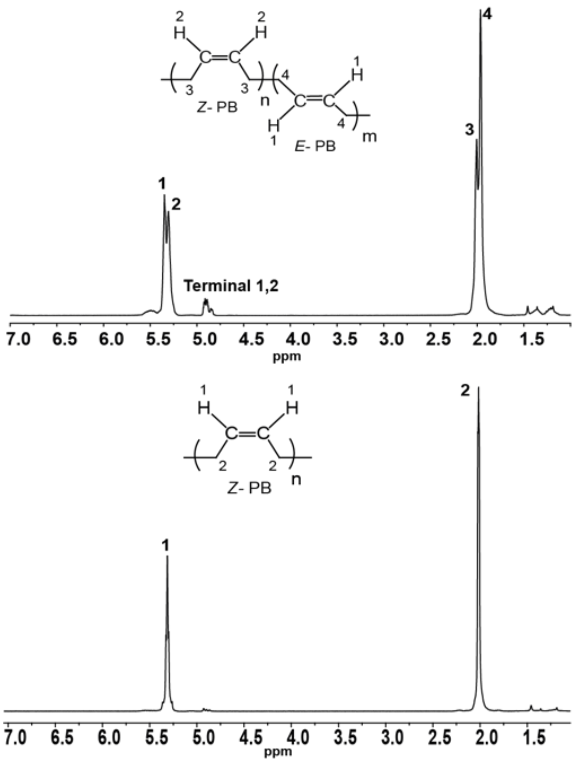

Figure 44. ^{1}H NMR of *E*-PB (55% *E*-1,4/36% *Z*-1,4) (Upper panel) and *Z*-PB (99% *Z*-1,4) (Lower panel)

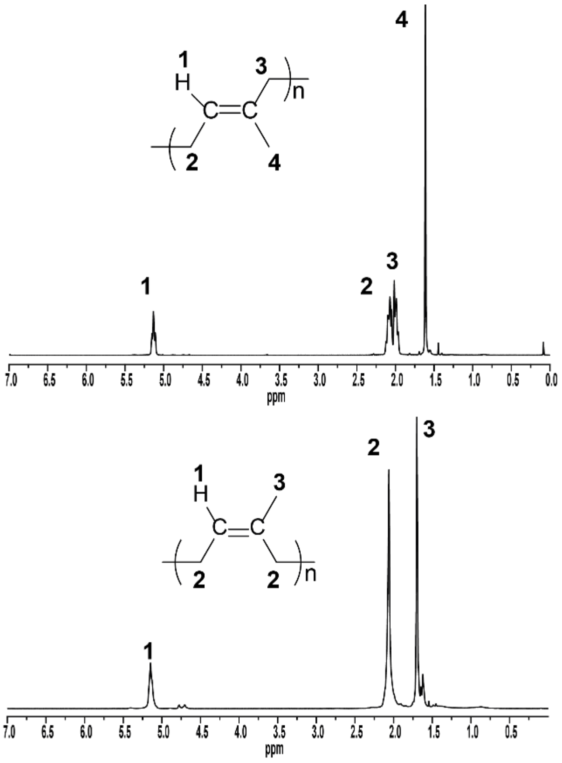

Figure 45. ^{1}H NMR of *E*-PI (99% *E*-1,4) (Upper panel) and *Z*-PI (98% *Z*-1,4) (Lower panel)

(*E*- and *Z*-) PB and PI were then subjected to the cross-metathesis reaction using the second-generation Hoveyda-Grubbs catalyst and *Z*-1,4-acetoxy-2-butene as chain transfer agent and dichloromethane as solvent. The reaction was carried out in less than 1h for a fixed catalyst concentration of 1% (w/w of the polymer) and 5 equiv of CTA (Figure 46).

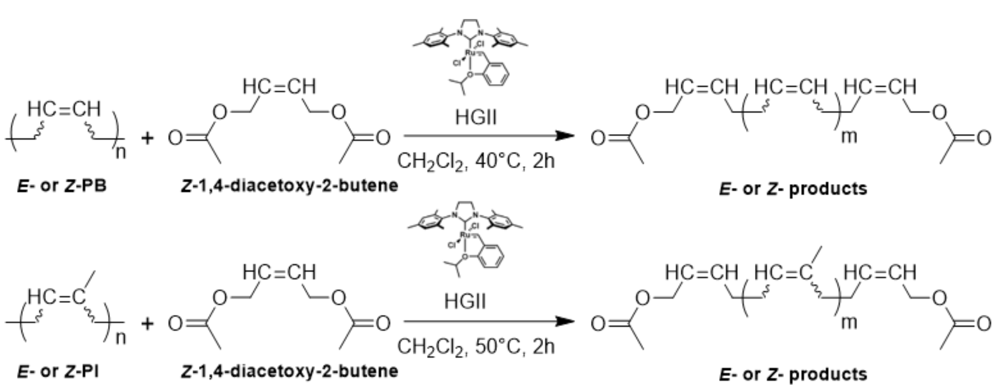

Figure 46. Cross-metathesis reaction of *E*- and *Z*-PB in the presence of *Z*-1,4-diacetoxy-2-butene as chain transfer agent and the Hoveyda-Grubbs second generation catalyst (HGII)

I.1. Analysis of products issued from the cross-metathesis reaction of PB and PI

The microstructure of the obtained products was first characterized by ^{1}H NMR. For PB, enlargement of the signal at 2 ppm revealed 4 different signals of aliphatic protons (Figure 47). The first one at 1.97 ppm corresponds to aliphatic protons (H5) of oligomers with E configuration. The second signal at 1.98 ppm corresponds to those of oligomers with Z configurations (H6). The two last signals at 1.99 and 2 ppm correspond to protons of the methyl groups (H7, H8) of the chain transfer agent in Z and E configurations respectively. Concerning olefinic protons, 4 different signals were identified between 5 and 6 ppm. Peaks at 5.78 and 5.53 ppm correspond to Z-olefinic protons (H1, H3) of the acetoxy oligomers while the E-olefinic protons (H2) appear at 5.66 ppm. The last signal at 5.34 ppm is for the Z-1,4-olefinic protons (H4) of polybutadiene units.

The same analysis can be applied on ^{1}H NMR spectra of depolymerized PI (Figure 47) with additional aliphatic protons (H13) at 1.93 ppm, *E*-PI methyl proton (H15) at 1.52 ppm and *Z*-PI methyl proton (H14) at 1.7 ppm.

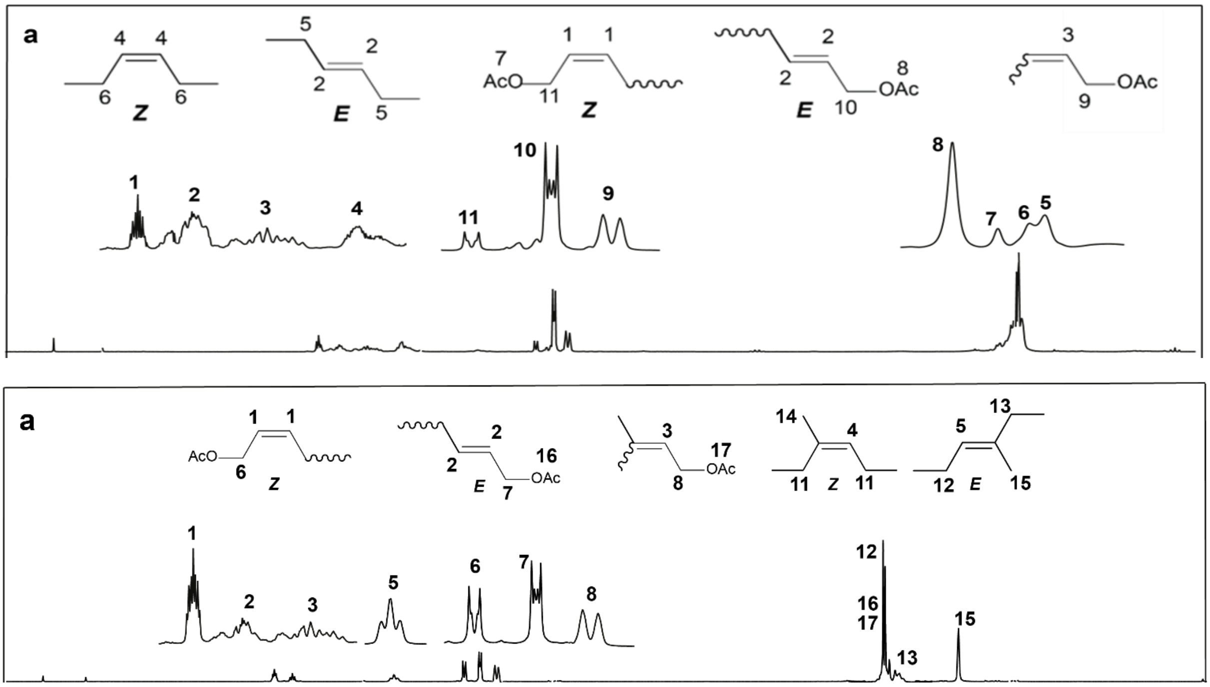

Figure 47. ^{1}**H NMR spectra of depolymerized PB (Upper panel) and depolymerized PI (Lower panel)**

^{1}H NMR analysis helped confirm a successful depolymerization, however, did not provide additional structural and chemical information.

As the reaction yielded a mixture of products formed by acetoxy telechelic oligomers soluble in organic solvents, ESI-MS was used to determine their *m/z* ratios to give a precise structure and fingerprint of each polymer. Unfortunately, the depolymerization of these high molar mass polymers gives very complex mixtures and by consequence very complex mass spectra. However, this problem can be overcome by using high-resolution FT-ICR with a resolving power of 1,000,000 to efficiently separate very close peaks.

High-resolution mass spectra were recorded for both polymers and are shown in Figure 48. In the case of both (*E* or *Z*) PB and PI, the major family of depolymerized products can be easily identified with a low *m/z* error in the range of 10 ppb. For PB, signals separated by 54.0464 Da in average corresponding to the repeating unit C_4H_6 present the highest intensity, while in PI, they are separated by 68.0620 Da corresponding to C_5H_8. However, much more signals appeared when narrowing the mass range of the spectrum. Molecular assignment of the large number of signals was realized using the Fourier transform mass spectrometry (FTMS) visualization (i-van Krevelen) open source program written in Python. This software scans the mass spectrum and attributes molecular formulas considering the number of CH_2, oxygen, and unsaturation. More than 2000 signals for each polymer were assigned to molecular formulas from which more than nine different families of molecules were identified.

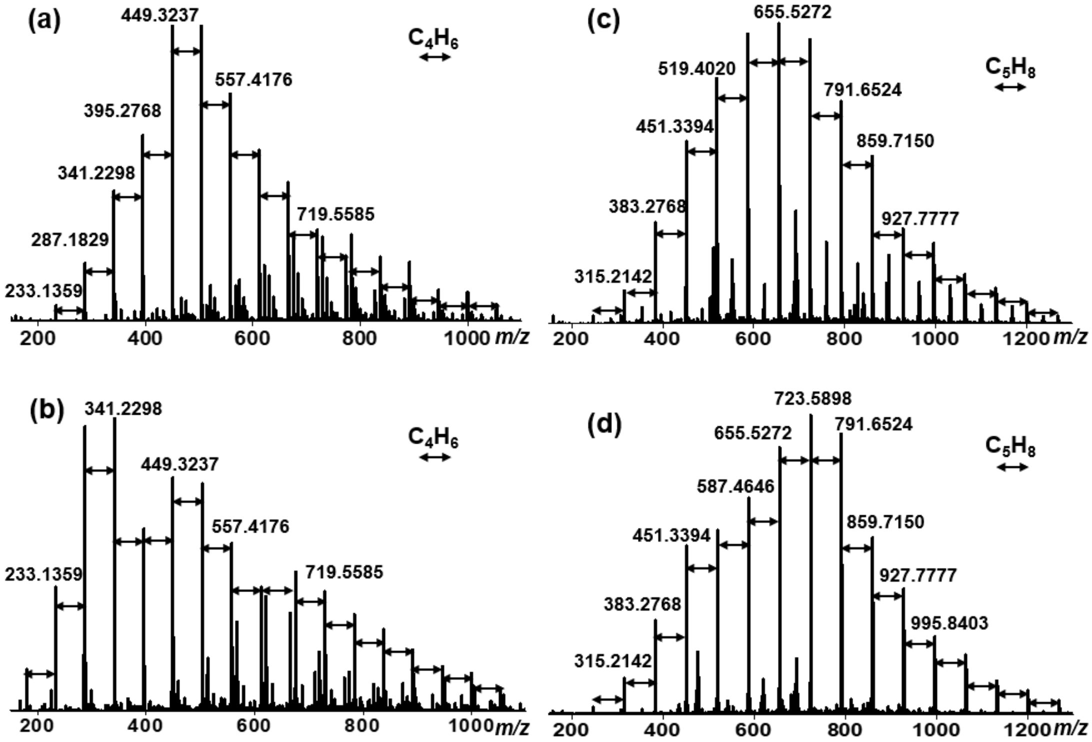

Figure 48. FT-ICR ESI (+) mass spectra of depolymerized (a) *E*-PB, (b) *Z*-PB, (c) *E*-PI, and (d) *Z*-PI in the presence of *Z*-1,4-diacetoxy-2-butene and the Hoveyda−Grubbs second-generation catalyst.

I.2. Identification of the cross-metathesis reaction products

I.2.1. CH_2 variation

In the case of PB, the highest intensity signals correspond to the major family of oligomers $[(C_8H_{12})\,O_4 + (C_4H_6)_n + {}^7Li^+]$ expanding from one monomer of PB at *m/z* 233.1359 ($C_{12}H_{18}O_4 + {}^7Li^+$) up to 19 monomers at *m/z* 1205.9812 ($C_{84}H_{126}O_4 + {}^7Li^+$) (Figure 49). The difference between two consecutive peaks is C_4H_6 which corresponds to one unit of butadiene or three CH_2 molecules and one additional carbon atom. Table 2 presents the identified *m/z* with their formula attribution and number of monomers in the polymeric chain and figure 51 presents the assignment of identified peaks directly on the mass spectrum.

Table 2: Identified peaks from the MS spectrum of depolymerized PB

Theoretical *m/z* [M+Li]$^+$	**Experimental *m/z* [M+Li]$^+$**	**Intensity**	**Error (ppm)**	**Monomers (n)**	**Formula**	**DBE**
179.089014	179.089010	560987200	-0.02	0	$C_8H_{12}O_4$	3
233.135964	233.135960	1071678336	-0.02	1	$C_{12}H_{18}O_4$	4
287.182914	287.182910	2115061760	-0.01	2	$C_{16}H_{24}O_4$	5
341.229864	341.229860	1968276992	-0.01	3	$C_{20}H_{30}O_4$	6
395.276814	395.276810	1167176192	-0.01	4	$C_{24}H_{36}O_4$	7
449.323764	449.323770	1720846208	0.01	5	$C_{28}H_{42}O_4$	8
503.370714	503.370720	1523733504	0.01	6	$C_{32}H_{48}O_4$	9
557.417664	557.417660	1238540544	-0.008	7	$C_{36}H_{54}O_4$	10
611.464614	611.464620	903022848	0.009	8	$C_{40}H_{60}O_4$	11
665.511564	665.511560	689144000	-0.006	9	$C_{44}H_{66}O_4$	12
719.558514	719.558510	424935040	-0.006	10	$C_{48}H_{72}O_4$	13
773.605464	773.605460	287604640	-0.005	11	$C_{52}H_{78}O_4$	14
827.652414	827.652420	177534768	0.006	12	$C_{56}H_{84}O_4$	15
881.699364	881.699370	112552480	0.006	13	$C_{60}H_{90}O_4$	16
935.746314	935.746280	68034032	-0.03	14	$C_{64}H_{96}O_4$	17
989.793264	989.793200	56556148	-0.06	15	$C_{68}H_{102}O_4$	18
1043.840214	1043.840320	30899460	0.1	16	$C_{72}H_{108}O_4$	19
1097.887164	1097.887170	17814042	0.005	17	$C_{76}H_{114}O_4$	20
1151.934114	1151.934080	9066750	-0.03	18	$C_{80}H_{120}O_4$	21
1205.981245	1205.981160	5206249	-0.07	19	$C_{84}H_{126}O_4$	22

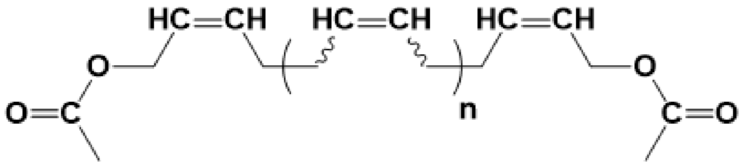

Figure 49. Structure of the major family obtained from the depolymerization of PB

Similarly, for PI, the major family of oligomers with the highest intensity [$(C_8H_{12})\ O_4 + (C_5H_8)_n + {}^7Li^+$] expands from one monomer of PI at *m/z* 247.1516 ($C_{13}H_{20}O_4 + {}^7Li^+$) up to 20 monomers at *m/z* 1540.3410 ($C_{108}H_{172}O_4 + {}^7Li^+$) (Figure 50). The difference between two consecutive peaks is C_5H_8 which corresponds to one unit of isoprene or four CH_2 molecules and one additional carbon atom. Table 3 presents the identified *m/z* with their formula attribution and number of monomers in the polymeric chain and figure 52 presents the assignment of identified peaks directly of the mass spectrum.

Table 3: Identified peaks from the MS spectrum of depolymerized PI

Theoretical *m/z* [M+Li]$^+$	**Experimental *m/z* [M+Li]$^+$**	**Intensity**	**Error (ppm)**	**Monomers (m)**	**Formula**	**DBE**
247.151614	247.151610	45545212	-0.01	1	$C_{13}H_{20}O_4$	4
315.214214	315.214210	500632960	-0.01	2	$C_{18}H_{28}O_4$	5
383.276814	383.276810	751780992	-0.03	3	$C_{23}H_{36}O_4$	6
451.339414	451.339420	739730496	0.01	4	$C_{28}H_{44}O_4$	7
519.402014	519.402000	747082944	-0.02	5	$C_{33}H_{52}O_4$	8
587.464614	587.464610	653774528	-0.007	6	$C_{38}H_{60}O_4$	9
655.527214	655.527240	542638976	0.04	7	$C_{43}H_{68}O_4$	10
723.589814	723.589820	403715776	0.007	8	$C_{48}H_{76}O_4$	11
791.652414	791.652420	303591008	0.007	9	$C_{53}H_{84}O_4$	12
859.715014	859.715010	241741792	-0.005	10	$C_{58}H_{92}O_4$	13
927.777614	927.777640	162331616	0.02	11	$C_{63}H_{100}O_4$	14
995.840214	995.840250	145575344	0.03	12	$C_{68}H_{108}O_4$	15
1063.902814	1063.902760	106535064	-0.05	13	$C_{73}H_{116}O_4$	16
1131.965414	1131.965450	92524968	0.03	14	$C_{78}H_{124}O_4$	17
1200.028014	1200.028110	84415240	0.07	15	$C_{83}H_{132}O_4$	18
1268.090614	1268.090660	53047872	0.03	16	$C_{88}H_{140}O_4$	19

1336.153214	1336.153050	62572972	-0.1	17	$C_{93}H_{148}O_4$	20
1404.215814	1404.215820	41616856	0.004	18	$C_{98}H_{156}O_4$	21
1472.278414	1472.278740	23777010	0.2	19	$C_{103}H_{164}O_4$	22
1540.344423	1540.344440	2613327	-0.01	20	$C_{108}H_{172}O_4$	23

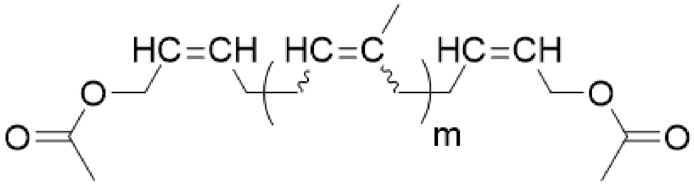

Figure 50. Structure of the major family obtained from the depolymerization of PB

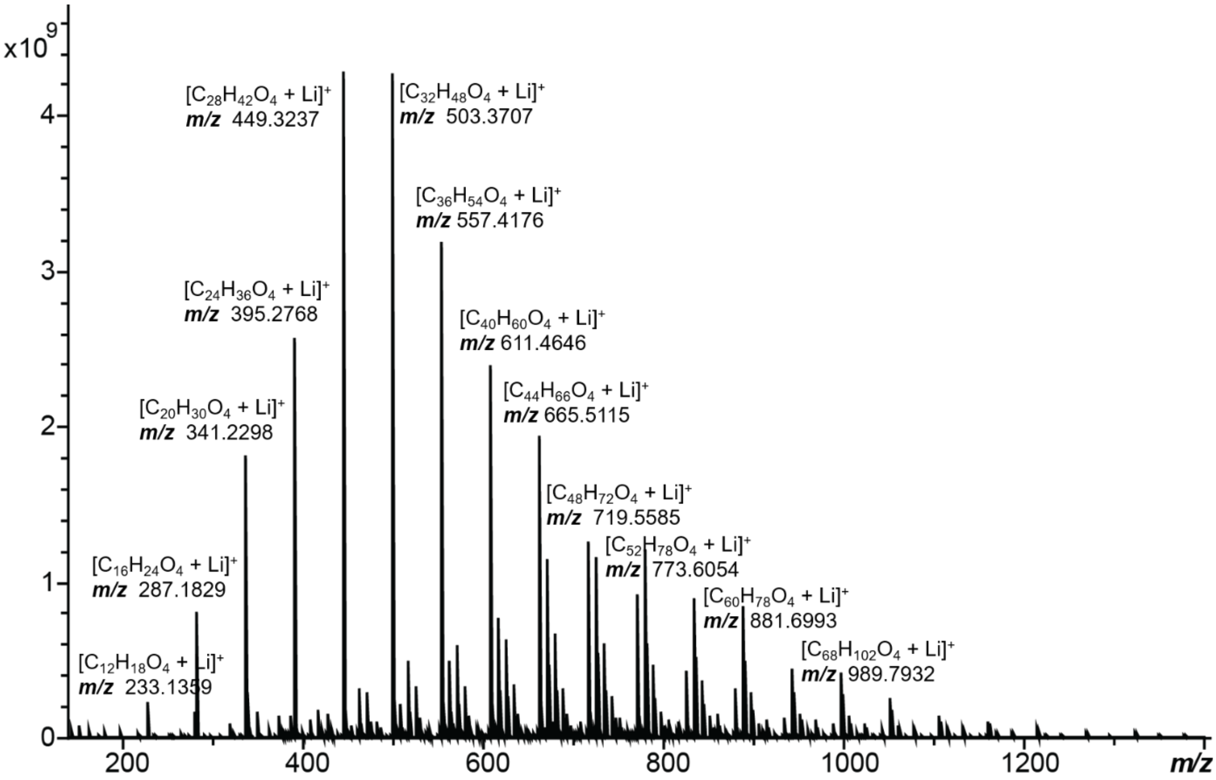

Figure 51. Assignment of signals in the mass spectrum obtained from the depolymerization of PB

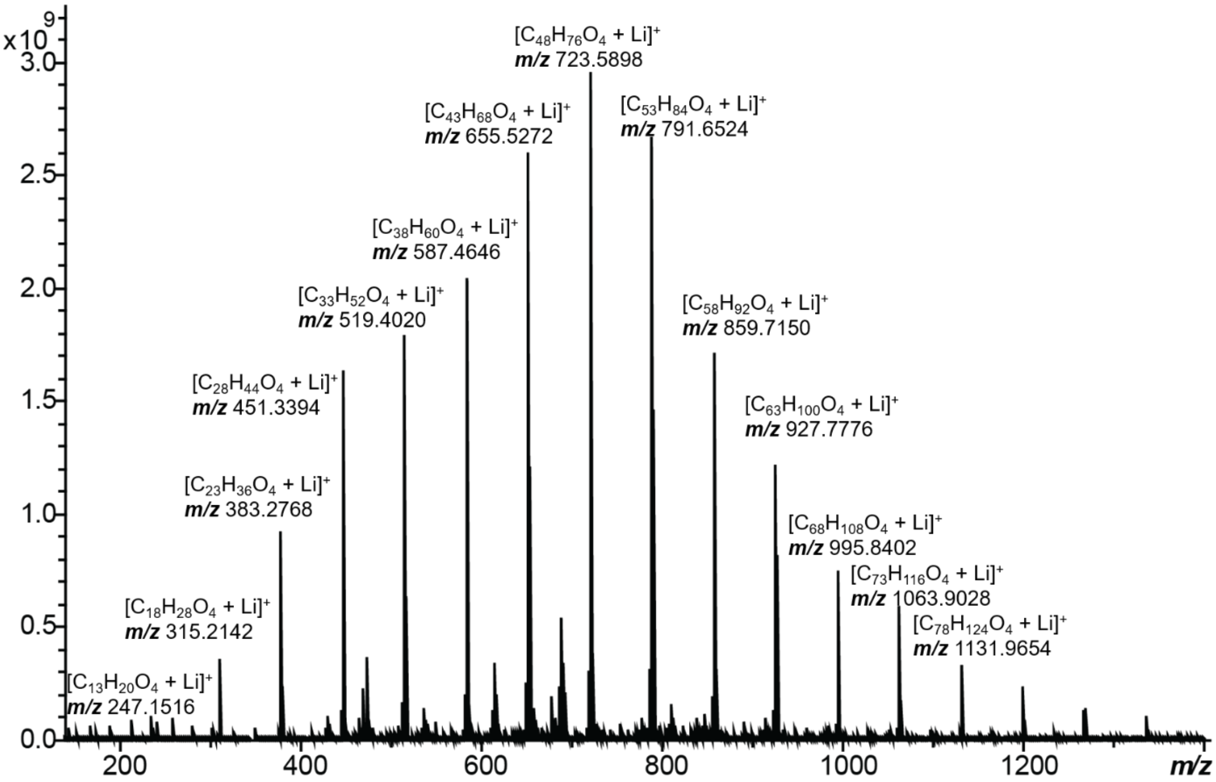

Figure 52. Assignment of signals in the mass spectrum obtained from the depolymerization of PI

I.2.2. Oxygen number variation

Among the products minor families of depolymerized PB, one is characterized by the presence of up to 4 additional oxygen atoms $[(C_8H_{12})O_4 + (C_4H_6)_n + O_m + {}^7Li^+]$ (Figure 53). The difference between two consecutive peaks of this family is C_4H_6 and one or more oxygen atoms. Table 4 presents some examples of identified *m/z* with their formula attribution and number of monomers in the polymeric chain.

Table 4: Identified peaks from the MS spectrum of depolymerized PB

Theoretical *m/z* **$[M+Li]^+$**	**Experimental** *m/z* **$[M+Li]^+$**	**Error (ppm)**	**Monomers (m)**	**O_n**	**Formula**
287.182914	287.182910	-0.01	2	0	$C_{16}H_{24}O_4$
303.177829	303.177820	-0.03	2	1	$C_{16}H_{24}O_5$
319.172743	319.172740	-0.01	2	2	$C_{16}H_{24}O_6$

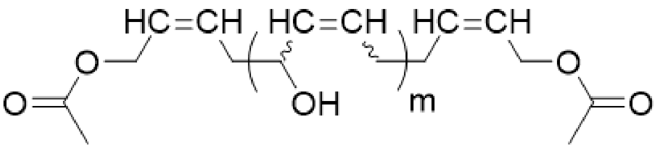

Figure 53. Structure of the oxidized family obtained from the depolymerization of PB

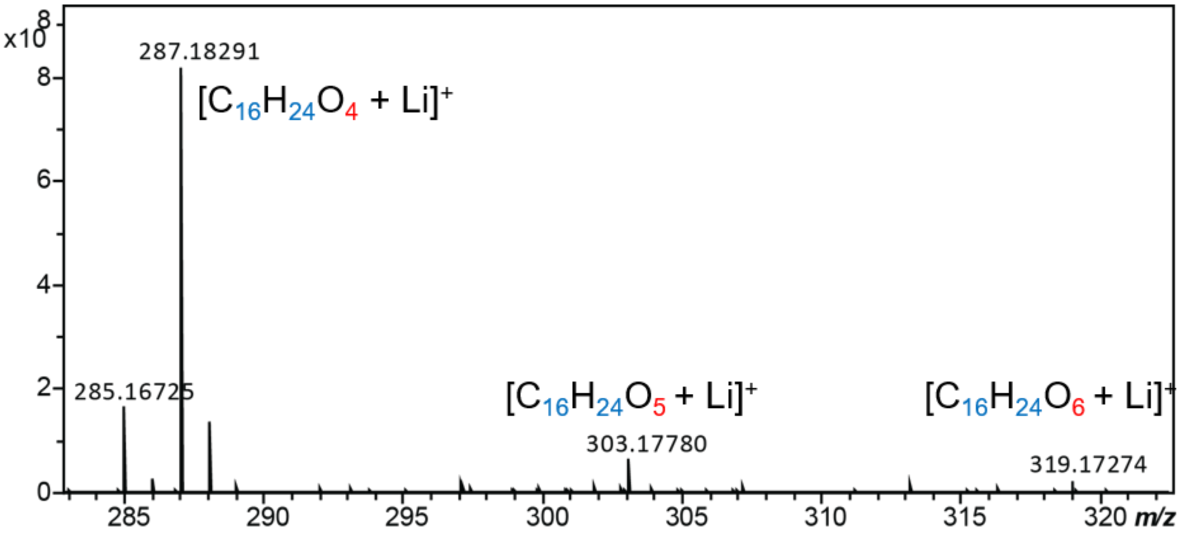

Figure 54. Zoom in on the ESI (+) FTICR mass spectrum of PB showing peaks of the oxidized family

Oxidized low intensity families are also found in depolymerized PI and characterized by the presence of up to 6 additional oxygen atoms $[(C_8H_{12})O_4 + (C_5H_8)_n + O_m + {}^7Li^+]$ (Figure 55).

The difference between two consecutive peaks of this family is C_5H_8 and one or more oxygen atoms. Table 5 presents some examples of identified *m/z* with their formula attribution and number of monomers in the polymeric chain.

Table 5: Identified peaks from the MS spectrum of depolymerized PI

Theoretical *m/z* [M+Li]$^+$	**Experimental *m/z* [M+Li]$^+$**	**Error (ppm)**	**Monomers** (m)	**O_n**	**Formula**
383.276814	383.276810	-0.03	3	0	$C_{23}H_{36}O_4$
399.271729	399.271720	-0.02	3	1	$C_{23}H_{36}O_5$
415.266644	415.266840	0.4	3	2	$C_{23}H_{36}O_6$

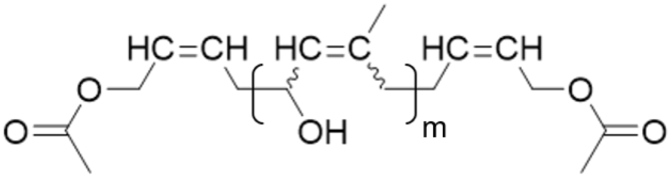

Figure 55. Structure of the oxidized family obtained from the depolymerization of PI

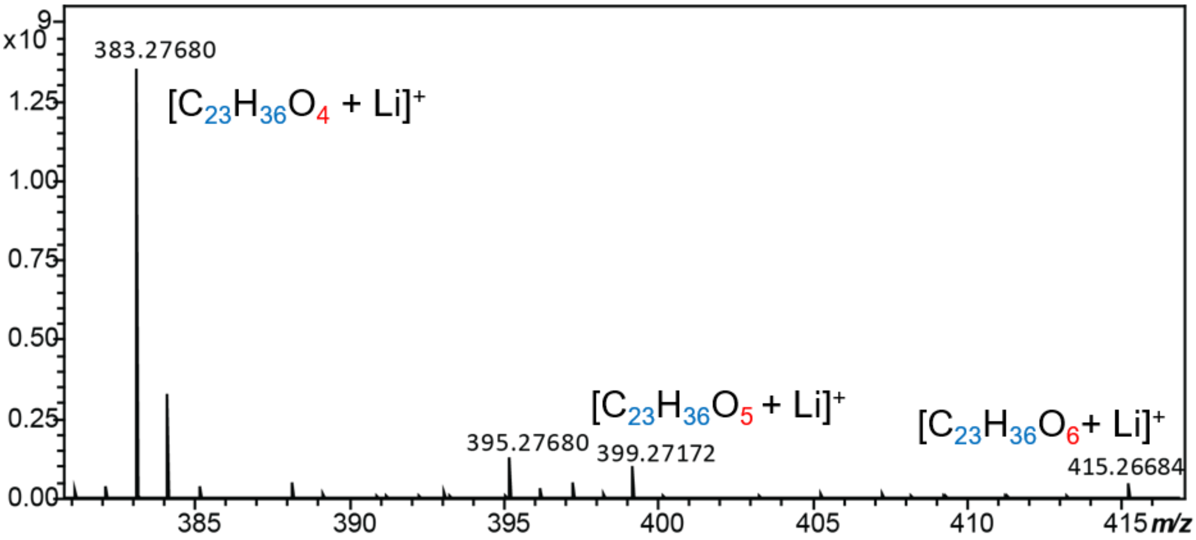

Figure 56. Zoom in on the ESI (+) FTICR mass spectrum of PI showing peaks of the oxidized family

I.2.3. DBE variation

Another family found in the mass spectrum of the depolymerized PB is characterized by the increase in the number of double bonds or unsaturation $[(C_8H_{12})O_4 + (C_4H_6)_n - (H_2)_p + {}^7Li^+]$ (Figure 57). This family consists on compounds with the same number of carbon and oxygen atoms but a variable number of hydrogen atoms.

Table 6: Identified peaks from the MS spectrum of depolymerized PB

Theoretical *m/z* [M+Li]$^+$	**Experimental *m/z* [M+Li]$^+$**	**Error (ppm)**	**DBE**	**Monomers (m)**	**$(H_2)_p$**	**Formula**
395.276814	395.276810	-0.01	7	4	0	$C_{24}H_{36}O_4$
393.261164	393.261140	-0.06	8	4	1	$C_{24}H_{34}O_4$
449.323764	449.323770	0.01	8	5	0	$C_{28}H_{42}O_4$
447.308115	447.308110	-0.01	9	5	1	$C_{28}H_{40}O_4$

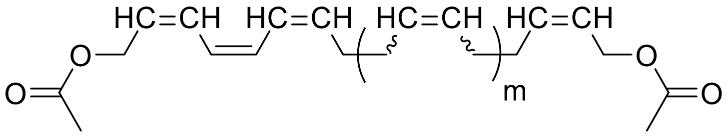

Figure 57. Structure of the unsaturated family obtained from the depolymerization of PB

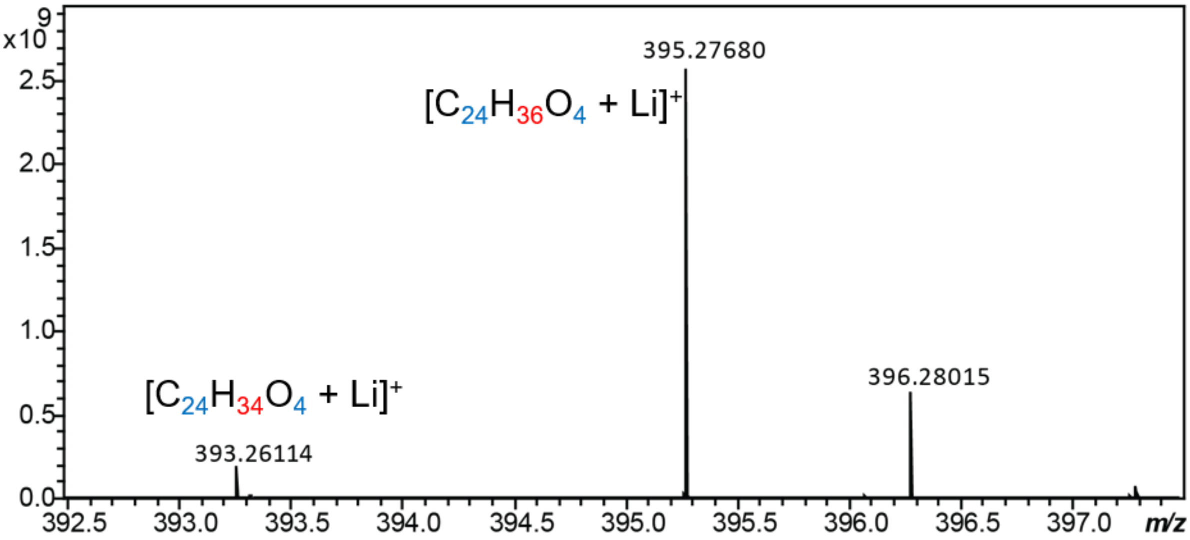

Figure 58. Zoom in on the ESI (+) FTICR mass spectrum of PB showing peaks of the unsaturated family

A similar family can also be found in the case of depolymerized PI with an increase in the number of double bonds [$(C_8H_{12})O_4 + (C_5H_8)_n - (H_2)_p + {}^7Li^+$] (Figure 59).

Table 7: Identified peaks from the MS spectrum of depolymerized PI

Theoretical *m/z* [M+Li]⁺	**Experimental *m/z* [M+Li]⁺**	**Error (ppm)**	**DBE**	**Monomers (m)**	**$(H_2)_p$**	**Formula**
383.276814	383.276810	-0.03	6	3	0	$C_{23}H_{36}O_4$
381.261164	381.261140	-0.06	7	3	1	$C_{23}H_{34}O_4$
379.245514	379.245450	-0.1	8	3	2	$C_{23}H_{32}O_4$

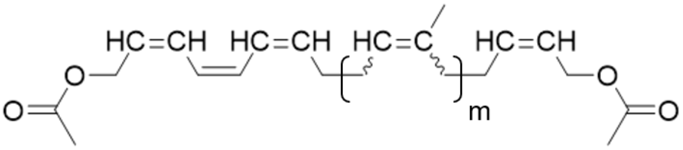

Figure 59. Structure of the unsaturated family obtained from the depolymerization of PI

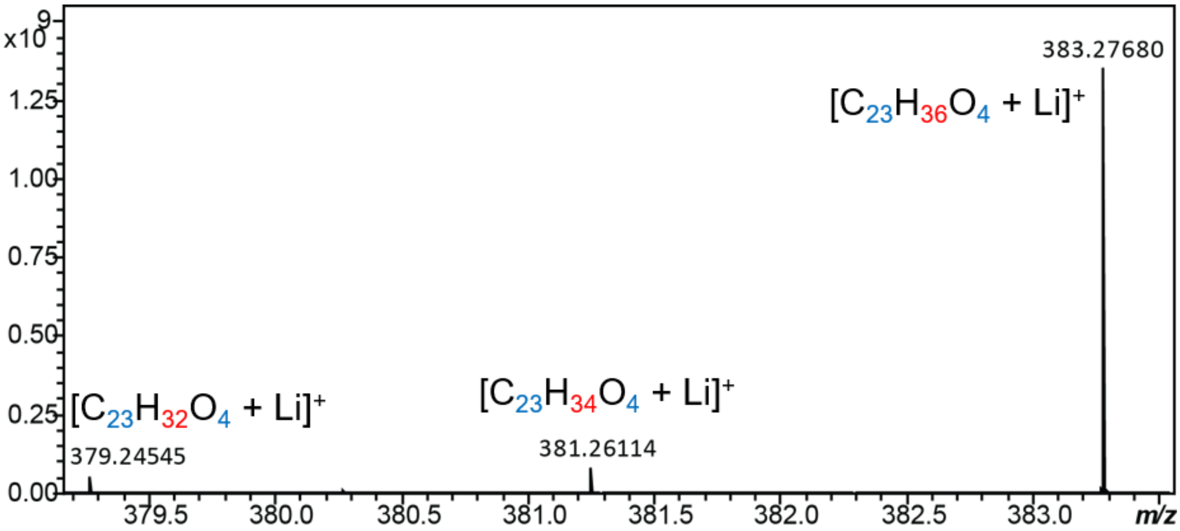

Figure 60. Zoom in on the ESI (+) FTICR mass spectrum of PI showing peaks of the unsaturated family

I.2.4. Effect of reticulation

The last identified family, which can contain up to 10 monomers in total (Table 8), consists of 3 PB chains reticulated by a CH group (Figure 61). These reticulated chains are a signature of the PB manufacturing process

Table 8: Identified peaks from the MS spectrum of depolymerized PB

Theoretical *m/z* **[M+Li]$^+$**	**Experimental** *m/z* **[M+Li]$^+$**	**Error (ppm)**	**Monomers (m,n,p)**	**Formula**
359.204044	359.204090	0.12	3	$C_{19}H_{28}O_6$
413.250994	431.250970	-0.05	4	$C_{23}H_{34}O_6$
467.297944	467.297950	0.01	5	$C_{27}H_{40}O_6$
521.344894	521.344900	0.01	6	$C_{31}H_{46}O_6$
575.391844	575.3918700	0.04	7	$C_{35}H_{52}O_6$
629.438794	629.438810	0.02	8	$C_{39}H_{58}O_6$
683.485744	683.485760	0.02	9	$C_{43}H_{64}O_6$
737.532694	737.532700	0.007	10	$C_{47}H_{70}O_6$

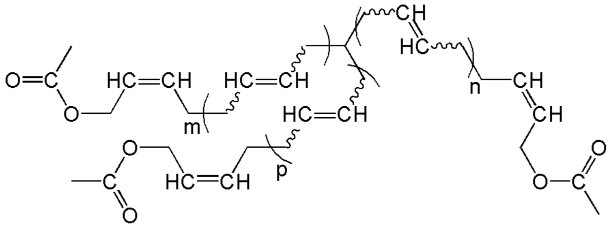

Figure 61. Identified family consisting of 3 PB chains reticulated by a CH group

Finally, a family with 4 reticulated chains of PI connected by one carbon atom was identified and can contain up to 8 monomers in total (Figure 62)

Table 9: Identified peaks from the MS spectrum of depolymerized PB

Theoretical *m/z* **[M+Li]$^+$**	**Experimental** *m/z* **[M+Li]$^+$**	**Error (ppm)**	**Monomers (m,n,p)**	**Formula**
527.319073	527.319070	-0.005	4	$C_{29}H_{44}O_8$
595.381674	595.381670	-0.007	5	$C_{34}H_{52}O_8$
663.444274	663.444310	0.05	6	$C_{39}H_{60}O_8$
731.506874	731.507170	0.4	7	$C_{44}H_{68}O_8$
799.569474	799.569560	0.1	8	$C_{49}H_{76}O_8$

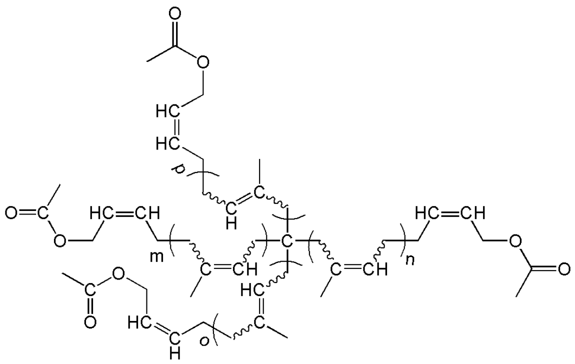

Figure 62. Identified family consisting of 4 PI chains reticulated by one carbon atom

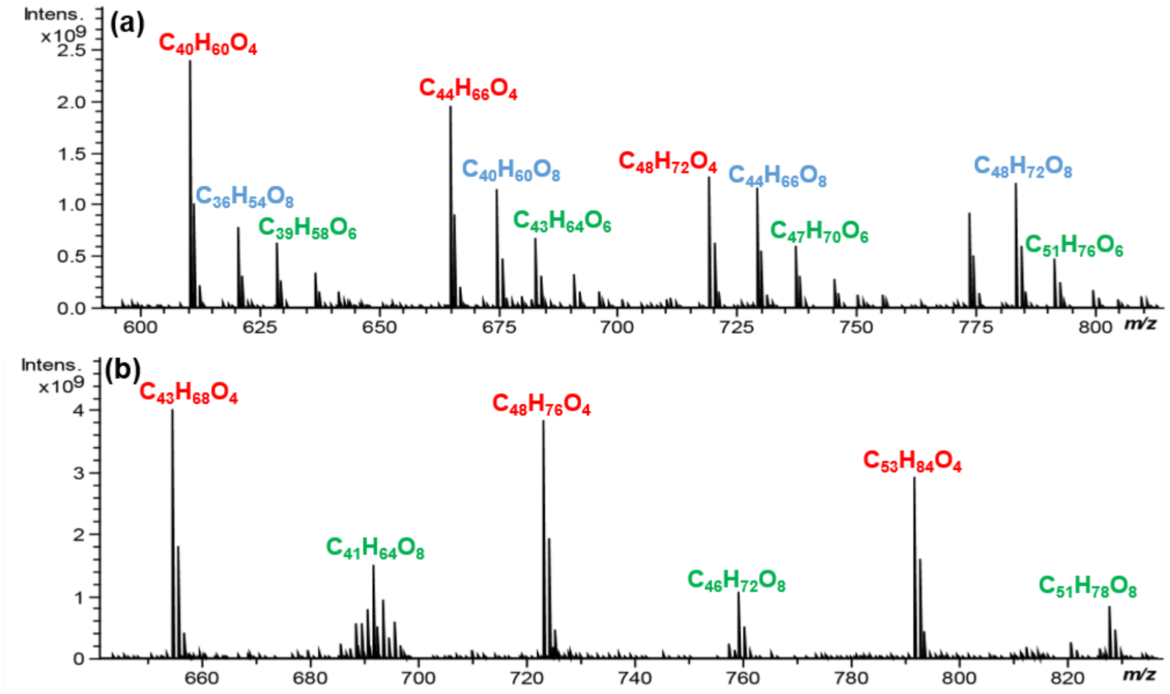

Figure 63. Enlargement of FTICR MS spectra of (a) depolymerized PB showing identifies families: [$(C_8H_{12})O_4$ + $(C_4H_6)n$ + $^7Li+$] (red), [$(C_8H_{12})O_4$ + $(C_4H_6)n$ + Om + $^7Li+$] (blue), reticulated family (green) and (b) depolymerized PI showing identifies familied: [(C_8H_{12}) + $(C_5H_8)_n$ + $^7Li^+$] (red) and reticulated family (green).

I.3. Visual interpretation

Following the identification of an important number of *m/z* signals and the attribution of molecular formulas, the obtained data from the depolymerization of all the samples were graphically represented as Van Krevelen and DBE vs Carbon number plots for easier interpretation.

I.3.1. Van Krevelen diagrams

Based on the assigned formulas, Van Krevelen diagram was first used to highlight the identified species and families. This is achieved by plotting their hydrogen/carbon ratio (H/C) versus oxygen/carbon ratio (O/C) as a function of the mass (Figure 64) and the intensity of the signals obtained from the mass spectrum (Figure 65). These values are reflected by the size of the spheres represented on the plots. Van Krevelen plots are also drawn to have a clearer view on the abundance of the produced species in each sample. It is illustrated by plotting the hydrogen/carbon ratio (H/C) versus oxygen/carbon ratio (O/C) as a function of signals intensity.

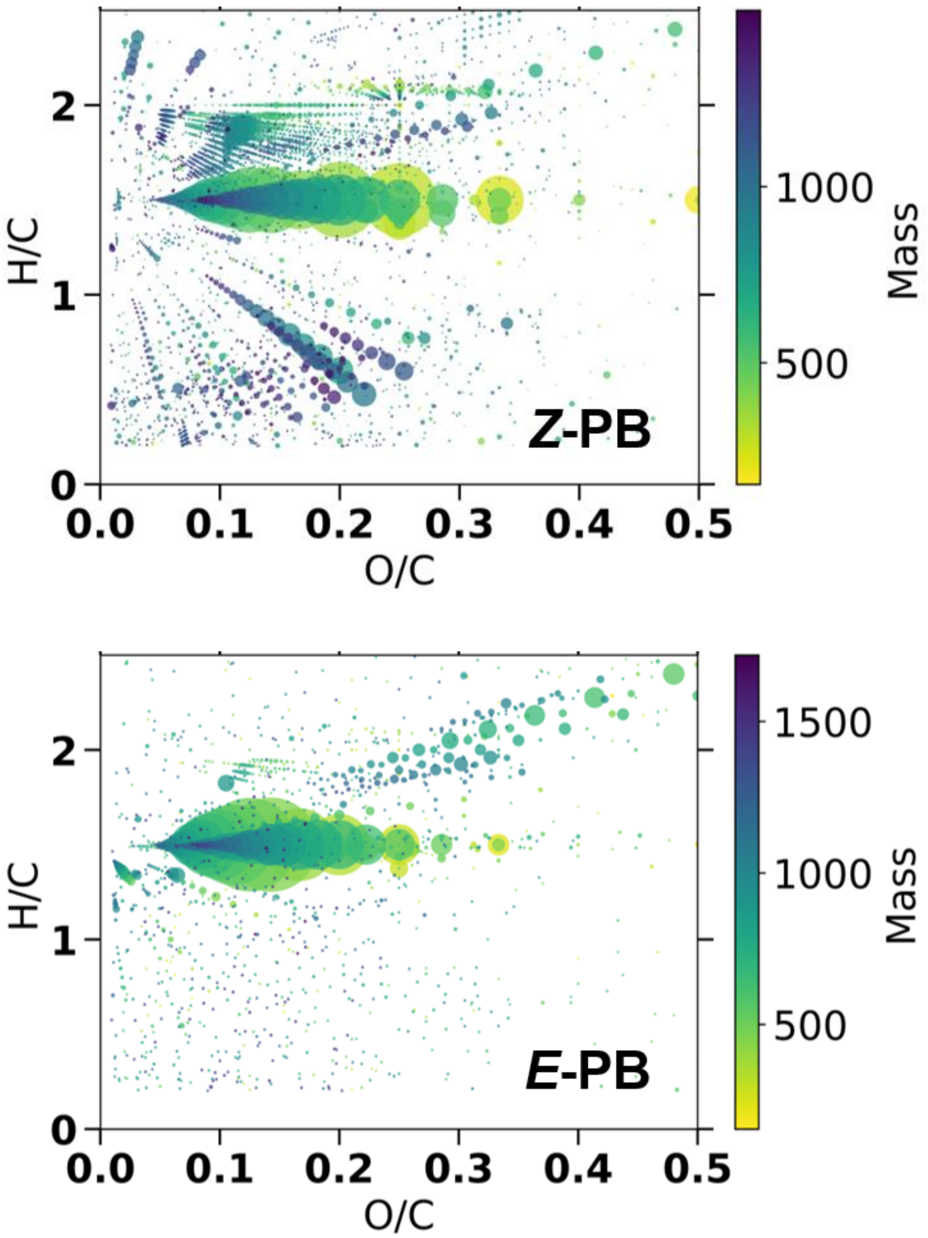

Figure 64. Van Krevelen diagram highlighting the identified species based on the hydrogen to carbon (H/C) versus the oxygen-to-carbon ratios (O/C) in function of the mass for *Z*-PB and *E*-PB

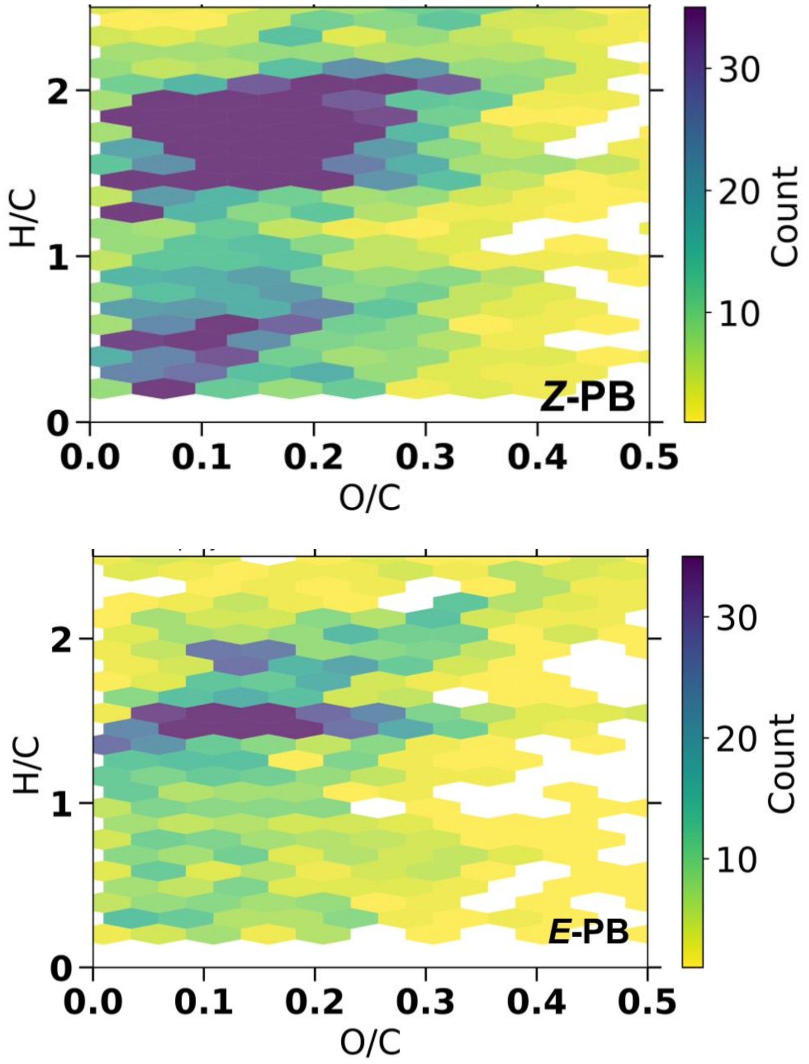

Figure 65. Van Krevelen diagram highlight the identified species based on the hydrogen to carbon (H/C) versus the oxygen-to-carbon ratios (O/C) in function of the intensity for *Z*-PB (left) and *E*-PB (right)

In the case of PB, following the comparison between Van Krevelen plots of *Z*-PB and *E*-PB, we observed the following:

- The majority of the masses are concentrated in the high intensity region (>800 Da) in the case of *E*-PB compared to *Z*-PB where some masses are shifted to the lower intensity region (300-400 Da)
- The oxygen to carbon ratio is higher in the case of *Z*-PB (> 0.5) compared to *E*-PB (< 0.5).
- The hydrogen to carbon ratio is more dispersed in the case of *Z*-PB going from 0 to 2 and more concentrated around 1.7 while in *E*-PB it is more intense in one specific region (1.5).

We can conclude from these observations that the products generated by the depolymerization of *Z*-PB are lighter than those of *E*-PB. They are also more oxidized and have shorter carbon chains or less unsaturation.

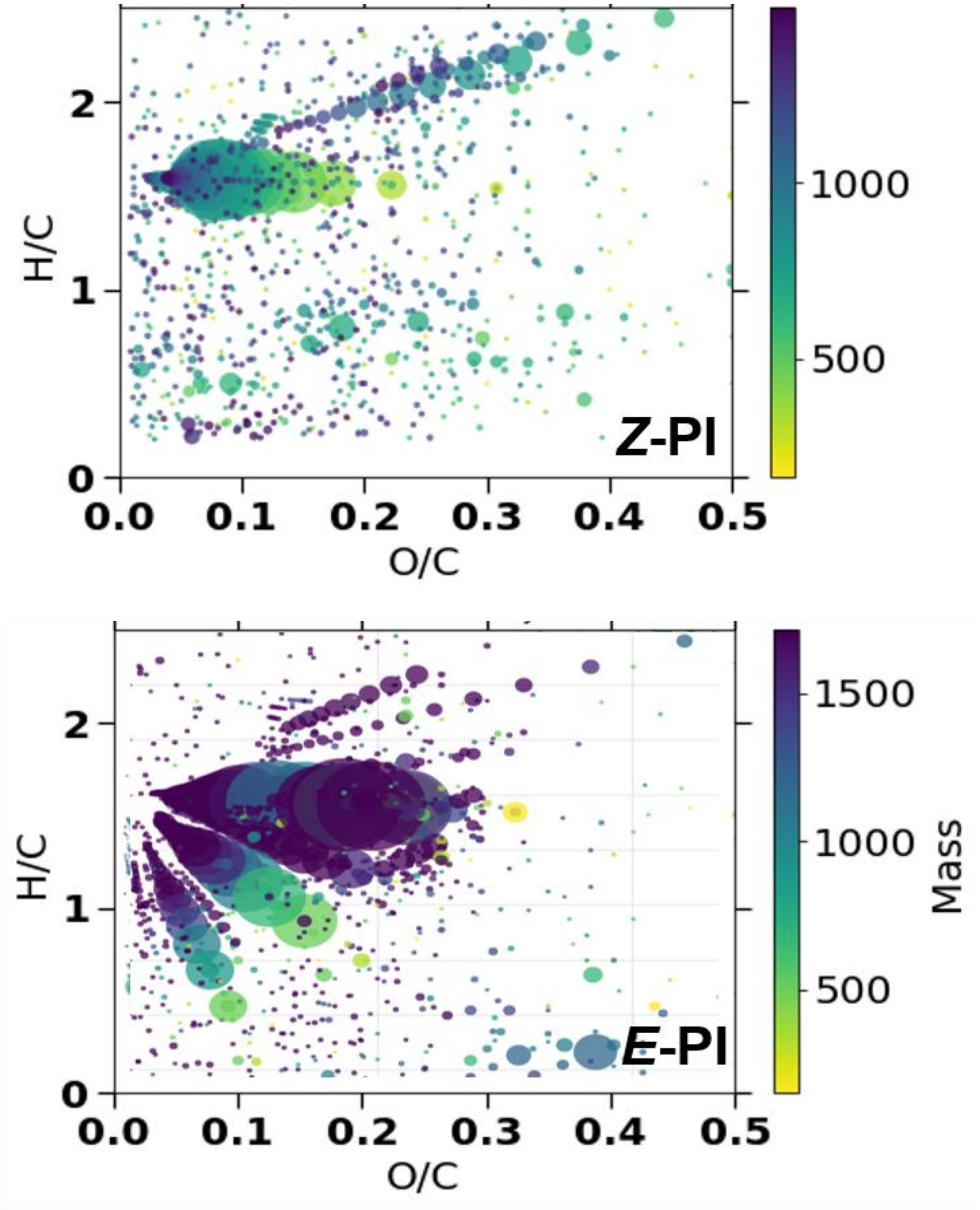

Figure 66. Van Krevelen diagram highlighting the identified species based on the hydrogen to carbon (H/C) versus the oxygen-to-carbon ratios (O/C) in function of the mass for *Z*-PI (left) and *E*-PI (right)

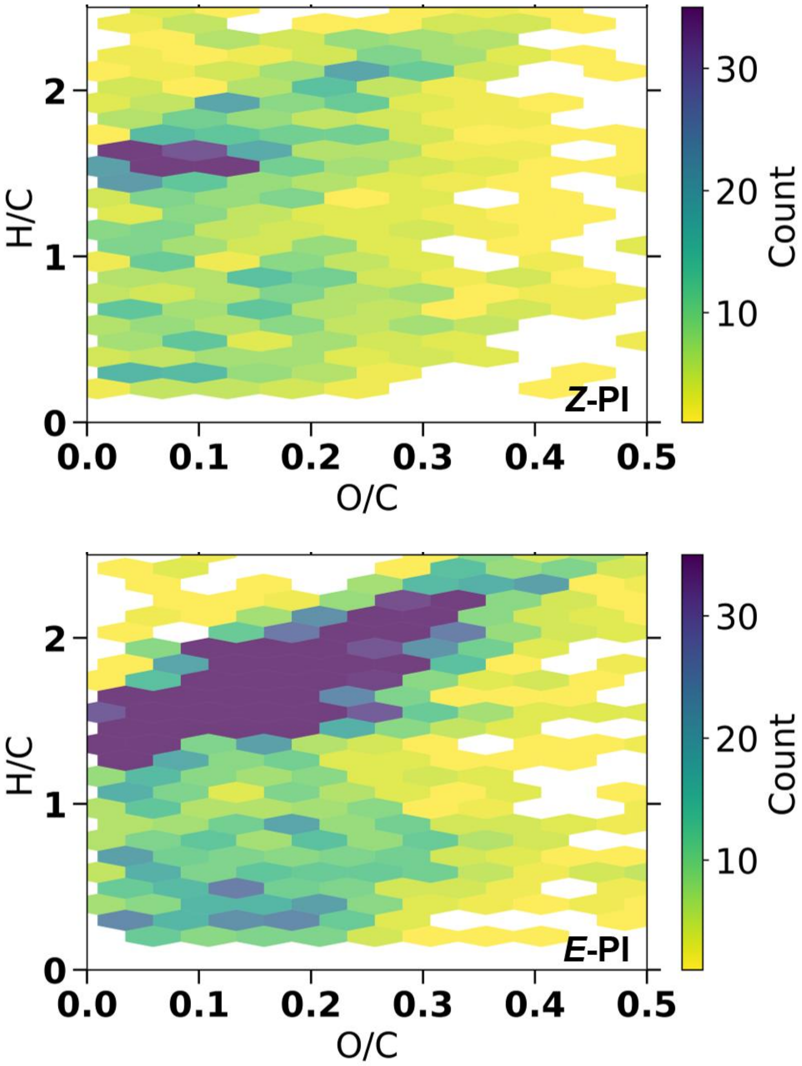

Figure 67. Van Krevelen diagram highlight the identified species based on the hydrogen to carbon (H/C) versus the oxygen-to-carbon ratios (O/C) in function of the intensity for *Z*-PI (left) and *E*-PI (right)

In the case of PI, following the comparison between Van Krevelen plots of *Z*-PI and *E*-PI, we observed the following:

- The majority of the masses are concentrated in the high intensity region (>800 Da) in the case of *Z*-PI compared to *E*-PI where more masses are shifted to the lower intensity region (300-400 Da)
- The oxygen to carbon ratio is higher in the case *E*-PI.
- The hydrogen to carbon ratio is more dispersed in the case of *Z*-PI going from 0 to 2 and more concentrated around 0.5 and 1.7 while in *E*-PI it is most intense in one specific region (1.5).

We can conclude from these observations that the products generated by the depolymerization of *E*-PI are a little bit lighter than those of *Z*-PI. They also have longer carbon chains or more unsaturation.

I.3.2. DBE vs C number plots

The plot DBE versus carbon number in function of oxygen number illustrate the distribution of oxygen atoms, carbon atoms and unsaturation in each compound.

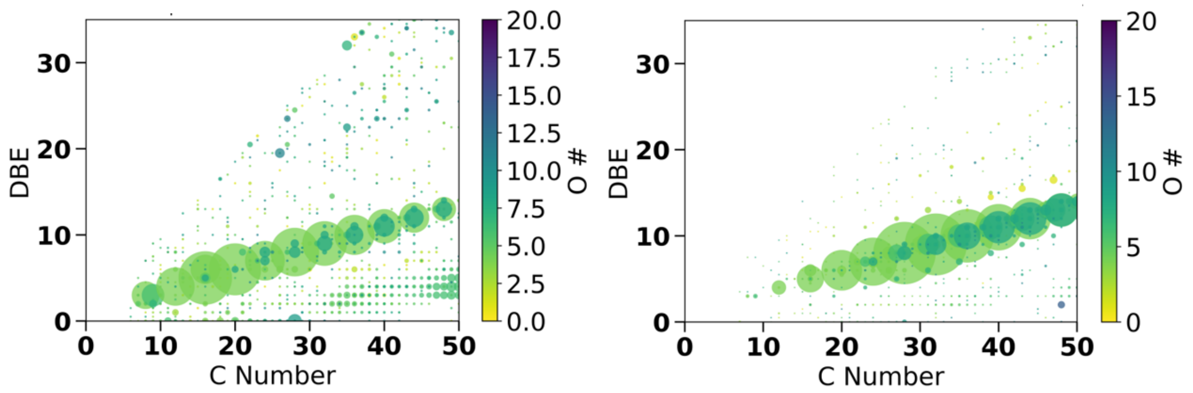

Figure 68. Plot DBE versus carbon number in function of oxygen number for *Z*-PB (left) and *E*-PB (right)

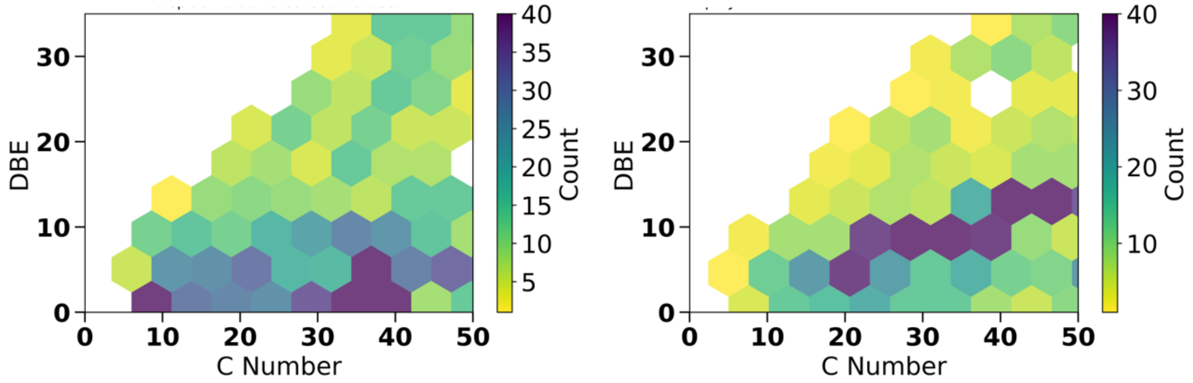

Figure 69. Plot DBE versus carbon number in function of intensity for *Z*-PB (left) and *E*-PB (right)

In the case of PB, we can observe the following:

- Chains of *E*-PB have around 30 carbon atoms while those of *Z*-PB have around 20 carbon atoms.
- *E*-PB products are more concentrated at higher DBE value compared to *Z*-PB.
- Higher mass compounds in *E*-PB have more oxygen atoms than those in *Z*-PB, however, *Z*-PB has more dispersed oxidized compounds

We can conclude from these observations that the products generated by the depolymerization of *Z*-PB are lighter than those of *E*-PB. They are also more oxidized in general and have shorter carbon chains or less unsaturation.

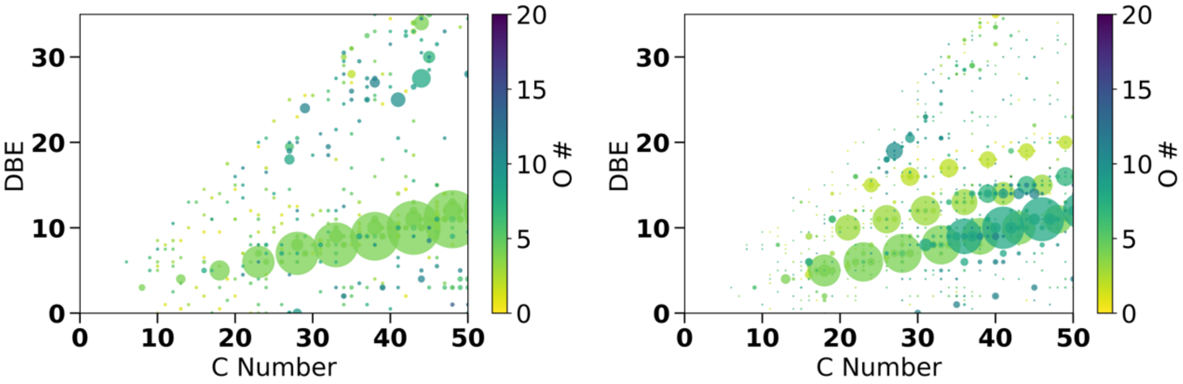

Figure 70. Plot DBE versus carbon number in function of oxygen number for Z-PI (left) and E-PI (right)

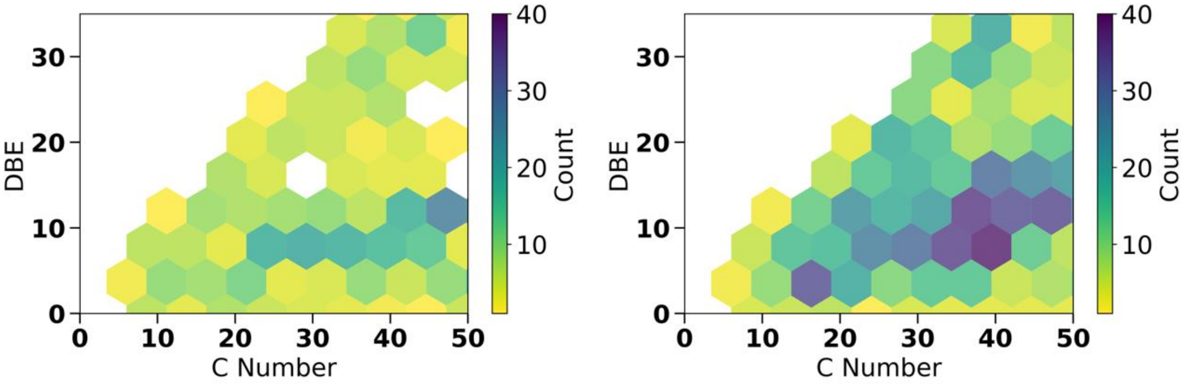

Figure 71. Plot DBE versus carbon number in function of intensity for *Z*-PI (left) and *E*-PI (right)

By comparing the DBE vs C number of *Z*-PI and *E*-PI, we observed the following:

- Chains of *Z*-PI have more carbon atoms than those of *E*-PI
- *E*-PI products are more concentrated at higher DBE value compared to *Z*-PI. They also have multiple distributions.
- Compounds in *E*-PI have more oxygen atoms than those in *Z*-PI.

We can conclude from these observations that the products generated by the depolymerization of *E*-PI are lighter than those of *Z*-PI. They are more oxidized and have more unsaturation.

I.3.2. Kendrick plots

Different depolymerized family were identified, however, the resulting mass spectra are rather complex and the assignment of all the compouds families is very challenging. Kendrick plots can significantly reduce the complexity of the spectra making data processing and products identification more simple. As most of the families separated by C_4H_6 were already identified, Kendrick plots were generated using CH_2 as Kendrick reference in order to aling all compouds having CH_2 as repeationg unit in their chain. Additional, low intensity families are then easily detected. In the case of PB, three different examples of compounds families were identified (Figure 72). The first group in green, separated by a CH_2, contained the *m/z* values: 701.6265, 715.6422, 729.6578, 743.6735, 757.6891 and 771.7048 belonging to a family of reticulated chains. In fact, three completely hydrogenated chains are attached together by a CH group. A similar family with three chains of polybutadiene was previoulsy found containing butadiene unsaturated repeating units. The following identified families consisted on more unsaturated families containing an increasing number of unsaturation. Other families were also identified and contained the *m/z* values: 1036.0593, 1050.0749, 1064.0906 and 1078.1062. This group consits on one completely hydrogenetad long polymeric chain which was depolmerized and having the chain transfer agent on both sides. By comparing both families, we notice that a hydrogenation phenoma took place during the depolymerization reaction. The third group of compounds, represents the original family of depolymerized polybutadiene separated by C_4H_6 repeating units. It contains the *m/z* values: 233.1360, 287.1823, 341.2299, 449.3239, 503.3708, 557.4178 and 675.4446. We noticed that compounds in this family are correlated on the same diagonal line however, they are not aligned on the same horizontal line which means that they don’t have the same mass defect and they are not separated by one or more CH_2 molecule. They are separated by C_4H_6 which consists on two CH_2 molecules and one carbon atom.

Similar interpretation can be used in the case of polyisoprene (figure 73). Three new compound families were identified after plotting the Kendrick mass defect as a function of the Kendrick mas. All three groups were aligned on the same horizontal line and separated by one CH_2 unit. The first group highlighted in green contained the *m/z* values: 561.5064, 575.5221, 589.5377, 603.5534, 617.5690 and 631.5847. This family consists on a saturated isoprene polymeric chain which was oxidized. The next identified families contains increasing unsaturation. Another family can also be identified and is composed of the major family of depolymerized polyisoprene with additional CH_2 molecules. Other families were also identified and contained the *m/z* values: 701.6265, 715.6422, 729.6578, 743.6735, 757.6891 and 771.7048. This family is the same family found following the depolymerization of polybutadiene and consists on three completely hydrogenated chains attached together by a CH group. The presence of this family proves that the depolymerization of both natural (polyisoprene) and synthetic (polybutadiene) rubbers can produce the same degradation products. The second group contains the *m/z* values: 561.5064, 575.5221, 603.5534 and 589.5377. This group is the result of a depolymerized hydorgenated polymeric chain that was oxidized during the reaction. The presence of this family indicates that oxidation phenomena can happen during this reaction. Finally, the last group of compounds found in the depolymerization products of polyisoprene contains the *m/z* value: 799.5694, 813.5851, 827.6007, 841.6164 and 855.6320. The first *m/z* value of this group was previously found in a family of four chains of PI reticulated together by a carbon atom. This reticulated family can then rearang itself to add more butadiene monomers or CH_2 units .

Kendirck mass defect is a very powerful visualization tool that helps combine the chemically related compounds in complex mass spectra. In the case of the depolymerization reactions of PB and PI, taking advantage of Kendrick's mass defect resulted in the identification of additional families and gave us more indications on the phenomena that could occur during the degradation reaction. These findings can push us one step closer to the full understanding of the microstructure of natural and synthetic rubbers.

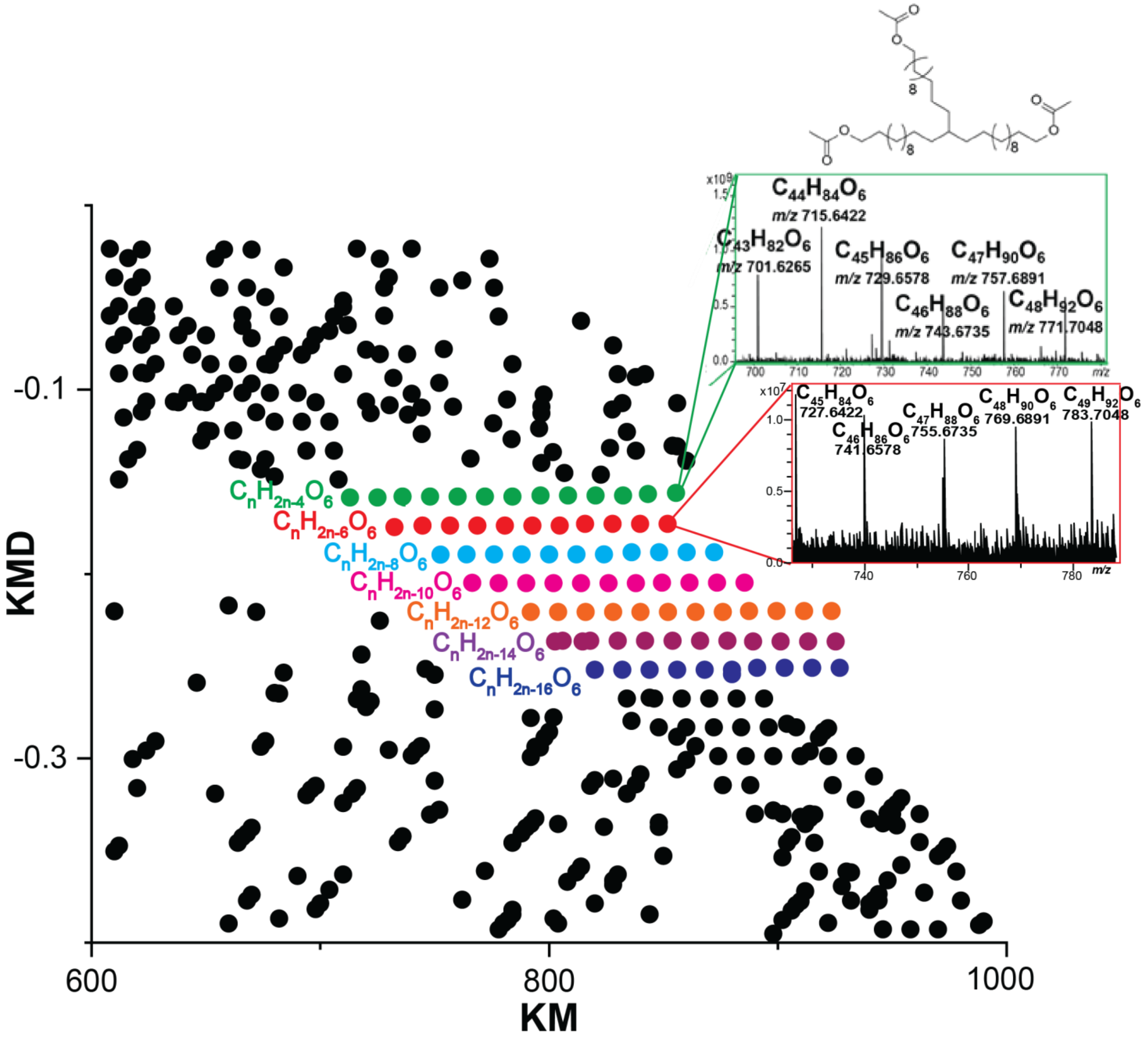

Figure 72. Kendrick mass defect plot of depolymerized PB

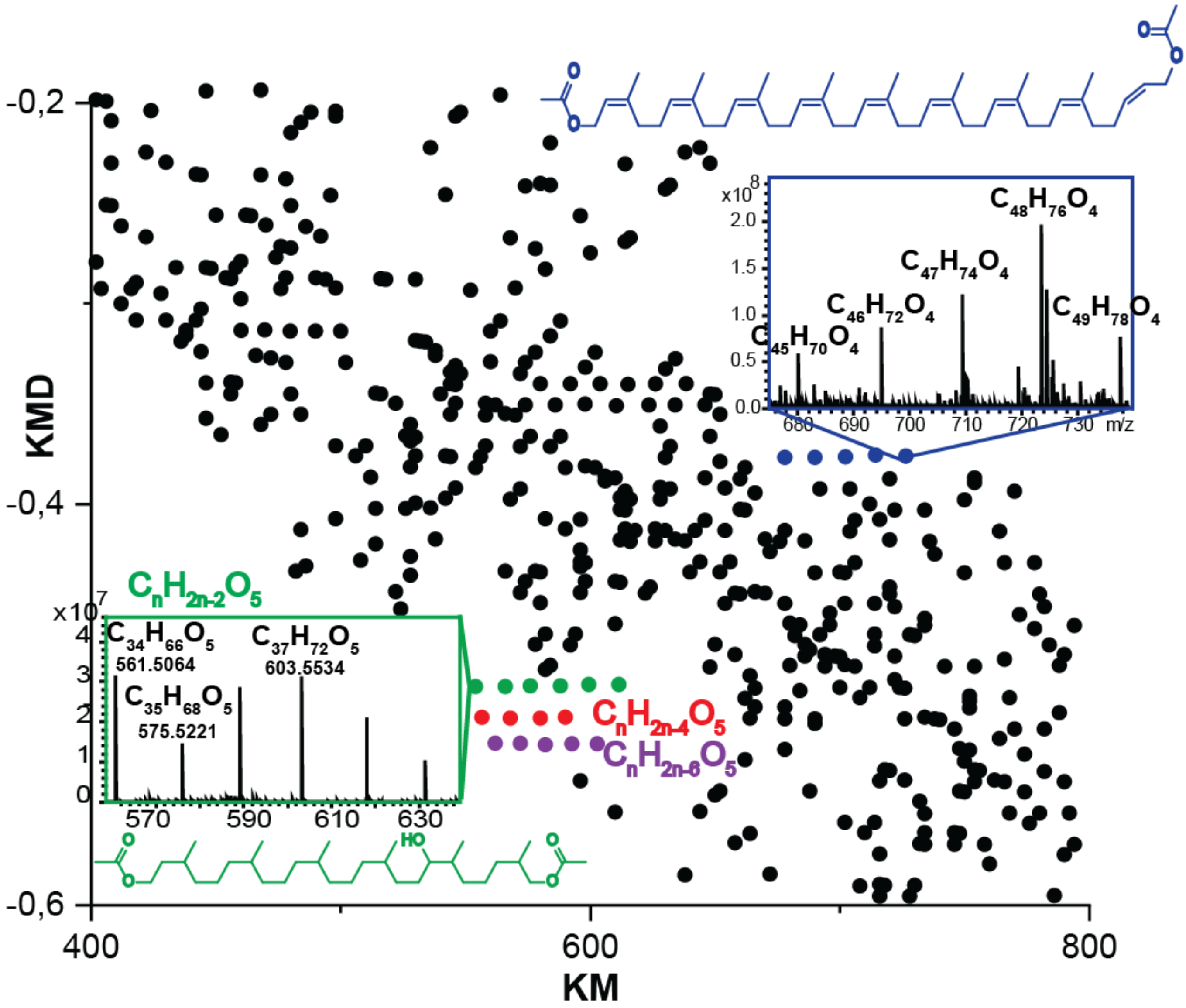

Figure 73. Kendrick mass defect plot of depolymerized PI

II. Optimization of the depolymerization of PB and PI

After the identification of the products of the depolymerization reaction by cross- metathesis of PB and PI, the optimization of this reaction requires the study of the influence of different factors: the type and amount of catalyst used in the reaction, the initial mass of the polymer, the reaction time and finally the solvent.

II.1. Influence of the type of catalyst

Multiple ruthenium-based catalysts are currently commercially available for olefin metathesis (Figure 74). The development and improvement of these catalysts by Grubbs and other offered tolerance towards defined substrates and functional groups which significantly broadened the scope of olefin metathesis.

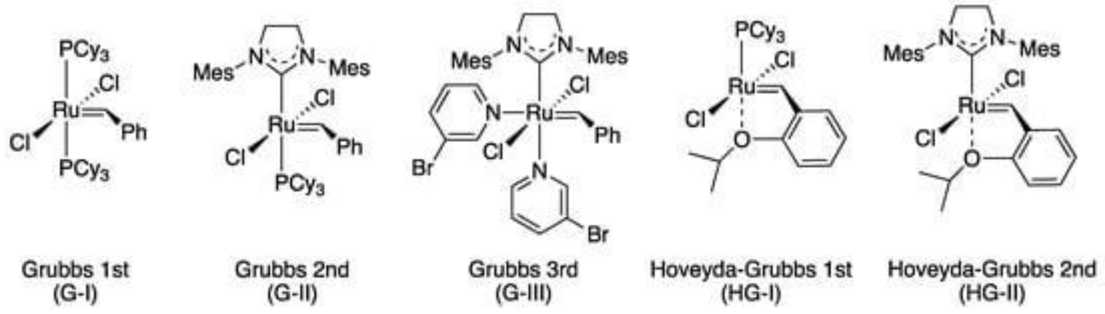

Figure 74. Grubbs catalysts used for olefin metathesis

In the case of the depolymerization of PB and PI, five different Grubbs catalysts were tested: Grubbs 1st, 2nd and 3rd generation catalysts as well as Hoveyda-Grubbs 1st and 2nd generation catalysts. The reaction was performed in dichloromethane for 2 hours with a fixed [polymer]/[CTA] ratio.

The final choice of catalyst fell on the second generation Hoveyda-Grubbs as it proved to have higher reactivity, effectiveness, compatibility with organic solvents and better tolerance to water, oxygen and functional groups.

The evaluation of the influence of the catalyst on the metathesis reaction was a pure analytical comparison based on the lowest and highest number of monomers found in the depolymerization products polymeric chains. In the case of the G-I, PB and PI were successfully depolymerized, however, only oligomers with low numbers of monomers were produced. On the other hand, the depolymerization was not successful when using G-III as the polymers remained intact in the solution even when the reaction time was increased to 48 hours to stress the catalyst. G-II and HG-I were both similarly effective and were able to depolymerize PB and PI for a reaction time of 4 hours. Finally, HG-II was the most reactive catalyst as the reaction time was decreased to 2 hours and the produced oligomers have polymeric chains distributed between low and high numbers of monomers.

II.2. Influence of the amount of catalyst

In order to assess the control of PB and PI depolymerization reaction by metathesis, we varied the amount of used catalyst. The results of the tests carried out are presented in Table 10. Five different entries were made for each polymer with [PB]/[Catalyst] ratios of 20, 30, 50, 75 and 100 and [PI]/[Catalyst] ratios of 5, 10, 20, 30 and 50. The initial quantity of polymer introduced was 0.125 µmol of PB and 0.657 µmol of PI (corresponding to 25 mg each). The reaction was carried out in dichloromethane for a duration of 2 hours and a fixed [Polymer/CTA] ratio of 500 for PB and 100 for PI (10 µl of CTA).

Results show that with higher [Polymer]/[Catalyst] ratios, i.e. with lower amounts of catalyst (Entry 5 and 10), the depolymerization reaction is slower and less effective as the initial polymer is not completely depolymerized and the *m/z* distribution of the obtained products in the mass spectrum is limited to the first low mass oligomers. However, the depolymerization improved remarkably by adding a higher amount of catalyst (Entry 1 and 6) as the polymer is completely depolymerized at the end of the reaction giving a very well-balanced distribution of *m/z* in the mass spectra. Adding even more catalyst to the reaction did not have any significant effect than that observed in entries 1 and 6.

Table 10: Influence of the amount of catalyst added in the depolymerization reaction of PB and PI

Entry	Polymer	Solvent	Time (h)	[Polymer]/[Catalyst]	Lowest number of monomers	Highest number of monomers
1	**PB**	**DCM**	**2**	**20**	**1**	**19**
2	PB	DCM	2	30	1	15
3	PB	DCM	2	50	1	10
4	PB	DCM	2	75	1	10
5	**PB**	**DCM**	**2**	**100**	**1**	**4**

6	**PI**	**DCM**	**2**	**5**	**1**	**20**
7	PI	DCM	2	10	1	18
8	PI	DCM	2	20	1	13
9	PI	DCM	2	30	1	9
10	**PI**	**DCM**	**2**	**50**	**1**	**3**

II.3. Influence of the initial mass of polymers

After the optimization of the amount of catalyst needed in the reaction, entries 1 and 6 (Table 9) were carried out again with the same [Polymer]/[Catalyst] ratio, same solvent and reaction time, however, the initial mass of the polymer was varied. Two different masses were tested for each polymer: 10 and 25 mg corresponding to 0.05 and 0.125 µmol for PB and 0.268 and 0.657 µmol for PI respectively. Analysis by FTICR mass spectrometry revealed that entries 1 and 6 with a higher mass of polymers generated a more balanced distribution and a better depolymerization.

Table 11: Influence of the initial amount of polymer used in the depolymerization reaction of PB and PI

Entry	Polymer	Solvent	Time (h)	[Polymer]/[Catalyst]	Mass of polymer (mg)	Lowest number of monomers	Highest number of monomers
1	**PB**	**DCM**	**2**	**20**	**25**	**1**	**19**
11	PB	DCM	2	20	10	1	7
6	**PI**	**DCM**	**2**	**5**	**25**	**1**	**20**
12	PI	DCM	2	5	10	1	6

We can therefore conclude that the increase in the initial mass of the polymer in the medium reaction medium leads to a better degradation profile.

II.4. Influence of reaction time

In order to verify the effect of reaction time, we performed three studies on entries 1 and 6 (Table 10) varying the reaction time in each case and retaining the same reaction operating conditions (Table 12).

The study of the effect of reaction time on the depolymerization of PB and PI dichloromethane was carried out for the same [Polymer]/[Catalyst] ratio, at the same temperature and for 25 mg of each polymer.

The first reactions were performed during 2 hours. The degradation was successful and generated an ideal mass spectrum following analysis by FTICR MS. The reaction time was progressively increased to 4 hours and then to 24 hours. This increase in time led to a more effective depolymerization meaning that the majority of the long chain of the polymers was broken down to very small fragments. On the analytical level, the generated mass spectrum presented only some low mass depolymerization products with the loss of those with higher mass. We can conclude that increasing the reaction time leads to a very effective degradation and the generation of only low mass oligomers. In our case, the most suitable reaction time for mass spectrometry analysis is 2 hours.

Table 12: Influence of reaction time on the depolymerization reaction of PB and PI

Entry	Polymer	Solvent	Time (h)	[Polymer]/[Catalyst]	Mass of polymer (mg)	Lowest number of monomers	Highest number of monomers
1	PB	DCM	**2**	**20**	**25**	**1**	**19**
			4	20	25	1	10
			24	20	25	1	3
6	PI	DCM	**2**	**5**	**25**	**1**	**20**
			4	5	25	1	8
			24	5	25	1	3

II.5. Influence of the solvent

Using three different solvents allows us to compare their influence on the depolymerization reaction of PB and PI. Examples of the carried-out reactions in THF, dioxane and dichloromethane for a reaction time of 2 hours are presented in Table 13. All other reaction conditions were fixed on their optimized values (Polymer mass = 25 mg, [Polymer]/[Catalyst] = 20 for PB and 5 for PI).

Table 13: Influence of solvents on the depolymerization reaction of PB and PI

Entry	Polymer	Solvent	Time (h)	[Polymer]/[Catalyst]	Mass of polymer (mg)	Lowest number of monomers	Highest number of monomers
1	PB	THF	2	20	25	1	6
		Dioxane	2	20	25	-	-
		DCM	**2**	**20**	**25**	**1**	**19**
6	PI	THF	2	5	25	1	4
		Dioxane	2	5	25	-	-
		DCM	**2**	**5**	**25**	**1**	**20**

For reactions carried out in THF for both PB and PI (Table 13), the depolymerization reaction was successful, however, did not provide a satisfying result. In the case of dioxane, the reaction did not work and the polymers were not depolymerized. In DCM, the reaction was very successful and generated the desired depolymerization profile in mass spectrometry analysis (Figure 75). Dichloromethane prove to be a better solvent for the metathesis reaction of PB and PI but it is worth to mention that this solvent presents risks for the environment.

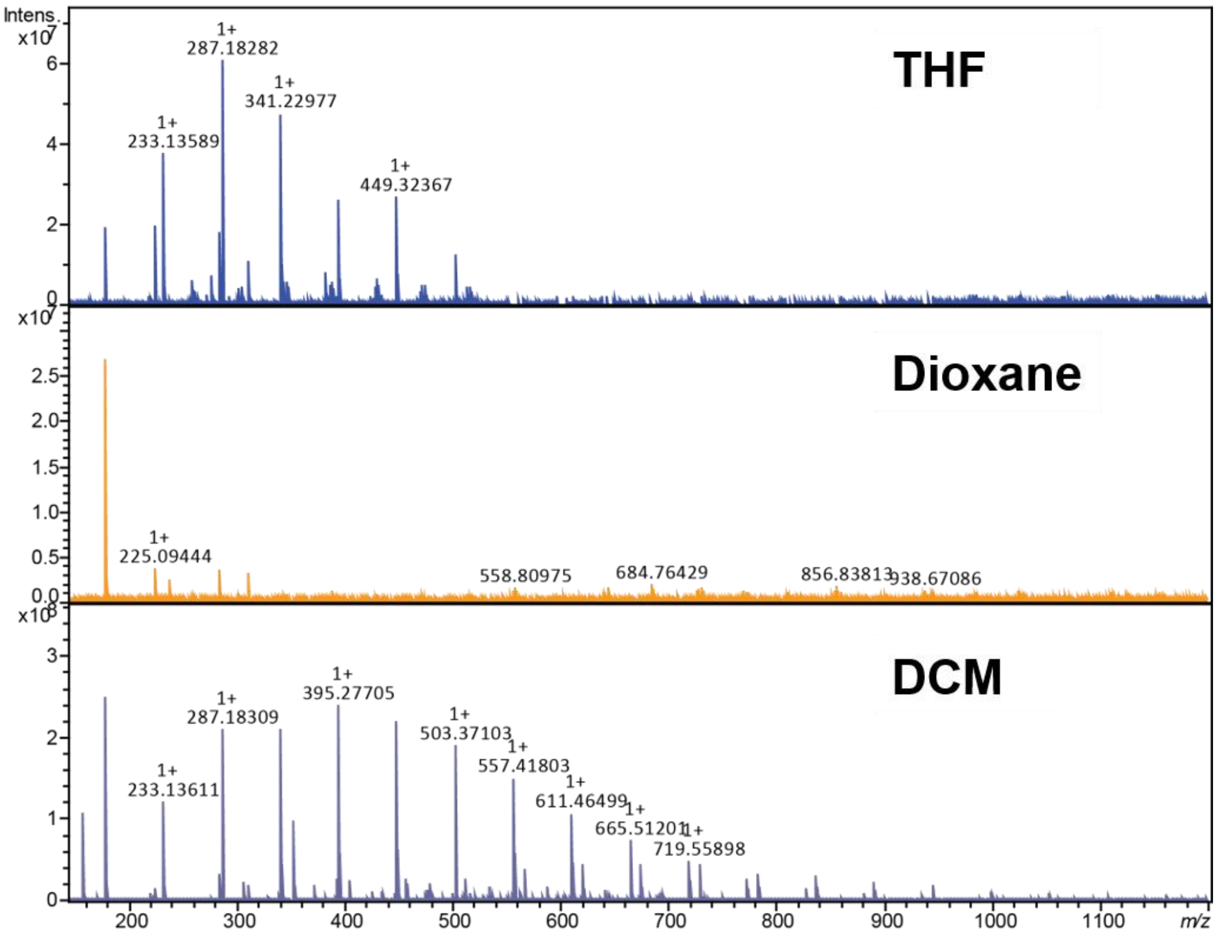

Figure 75. ESI (+) FTICR mass spectra of depolymerized PB showing the effect of solvents on the depolymerization reaction

The study of the degradation reaction by metathesis of PB and PI has shown the efficiency and selectivity of this reaction in an organic medium. The operating conditions have been optimized (reaction time, mass of polymer, molar ratio [Polymer]/[Catalyst], solvent) to have good yields and good analytical distributions. The microstructure of the product obtained is controlled, its average molar mass is controlled by the amount of catalyst used and the reaction time (Figure 76).

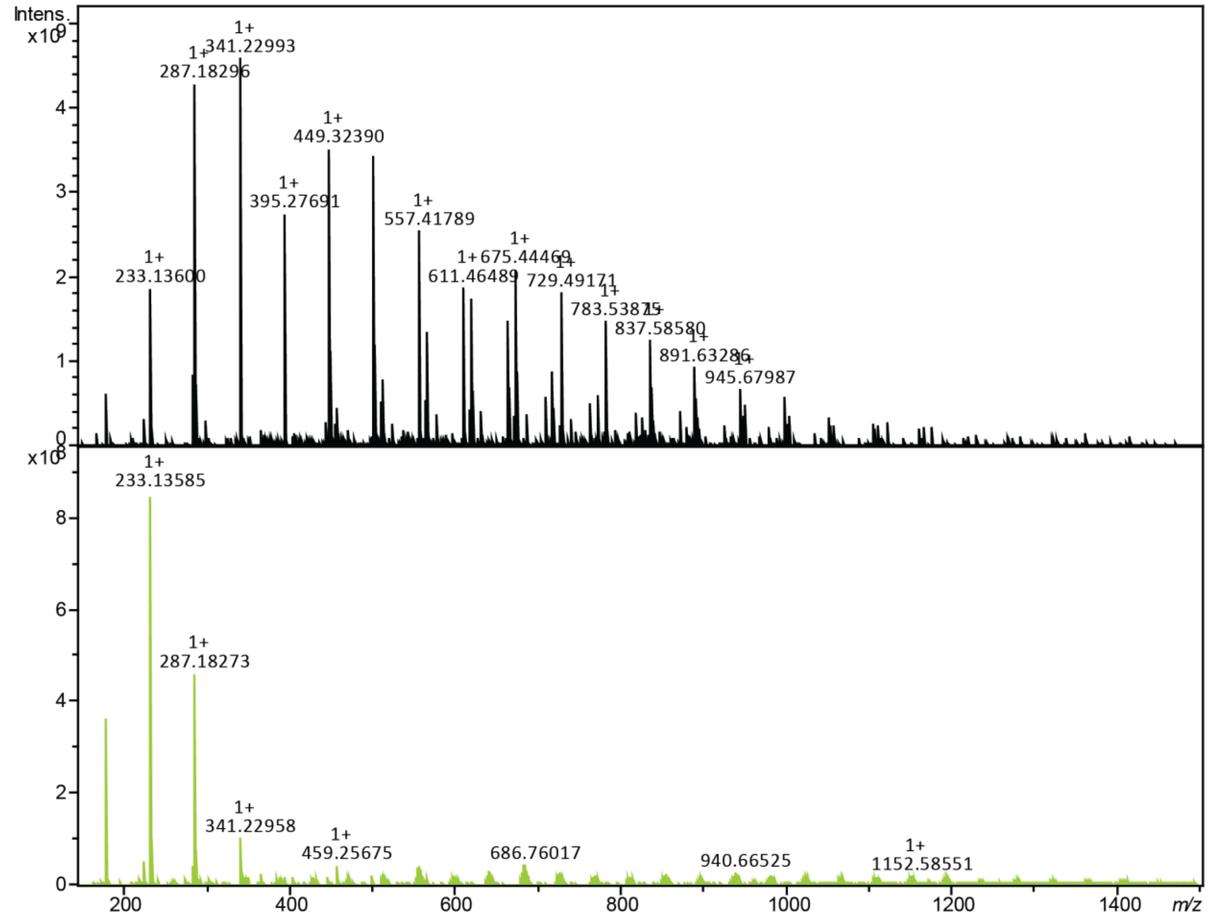

Figure 76. ESI (+) FTICR mass spectra of depolymerized PB with optimized conditions (Upper panel) and without optimization (Lower panel)

III. Stereochemical study of cross-metathesis reaction products

Using electrospray coupled to FT-ICR MS allowed the detailed identification of products issued from the depolymerization of PB and PI in both *E* and *Z* configurations, however, it did not provide information on their stereochemistry.

In order to have a clearer idea on the stereochemistry of the products, ^{1}H NMR spectra were first recorded of the depolymerized (*E* and *Z*) PB and PI polymers. These spectra showed a successful depolymerization in both cases. Further investigations of the spectra obtained after depolymerization of PB and PI provided additional information and proved an inversion of the stereochemistry of the obtained products after the depolymerization reaction. In fact, with the increased popularity of organometallic catalysts used in cross-metathesis, it was found that they can catalyze additional non-metathetic side reactions such as hydrogenation[1-2], dehydrogenation or isomerization[3], as well as transform themselves into new catalytically active species.[4-5] One of the most common non-metathetic reactions catalyzed by ruthenium complexes is isomerization. olefin isomerization can be explained by the intermolecular or intramolecular migration of the protons around the double bond. Various possible mechanistic pathways were proposed in literature for such migrations and these pathways are mainly classified as two major mechanisms: the metal-hydride insertion-elimination mechanism (1) and the π-allyl mechanism (2). The first mechanism, considered as an intermolecular reaction, starts by a metal-hydride bond insertion across the olefinic double bond which is followed by b-hydride elimination from the allylic carbon, giving the final isomerized product. In the case of π-allyl mechanism, it can be summarized in three steps: coordination of the olefin to the metal in the catalyst, C-H addition from the allylic carbon and reductive elimination of the terminal C-H to give the isomerized olefin. As direct hydrogen shift results in the double-bond migration, it is an intramolecular process. [6]

Several studies were carried out to identify the major pathway. A first study by Grubbs supported the metal-hydride insertion-elimination mechanism as he explained that the decomposition of the ruthenium metathesis catalysts facilitates the migration of double bonds in olefins under metathesis conditions. This decomposition is dependent on the thermal stability of catalyst and triggered by elevated temperatures, extended reactions times and the nature of organic solvents usually required for metathesis. He was also able to isolate the hydride complex **4** and used it to catalyze the isomerization in the metathesis reaction of phenylpropene.[7] In another study, Fürstner and his team studied the effect of the N-heterocyclic carbene ligands (NHC-ligands) present in **2** and **3** on the activity of the ruthenium complexes.

They noticed that by increasing the steric bulk of the N-substituents, the metathesis reaction produces by-products. They were able to identify a ruthenium hydride complex $(PCy_3)_2Ru(H)_2Cl_2$ and argued that the presence of this complex can be responsible for an undesirable isomerization side reaction.[8] Wagener and his coworkers also investigated isomerization in olefin metathesis. They studied the extent of this side reaction when using Grubbs ruthenium catalysts and they found that NHC ligands can promote extensive isomerization in the case of both internal and terminal olefin especially at temperatures of 50 to 60 °C in solvent-free or THF and toluene solutions. This isomerization can be suppressed by decreasing the temperature to 30 °C.[9] On the other hand, Fogg presented the role of the two complexes **4** and **5** two of the most common isomerization agents in literature. He proved that these species are not completely involved in the double-bond isomerization by monitoring their catalytic effect in the metathesis reaction. He concluded that isomerization is promoted by further decomposition of the catalyst by losing the PCy3 group and/or NHC ligands and proposed that this reaction can possibly undergo via a π-allyl mechanism.[10]

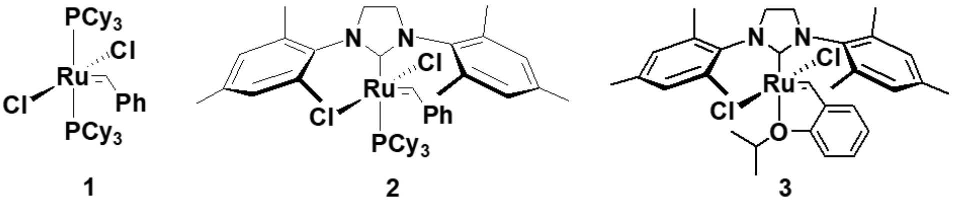

Figure 77. 1st generation Grubbs (1), 2nd generation Grubbs (2), 2nd generation Hoveyda-Grubbs (3) catalysts

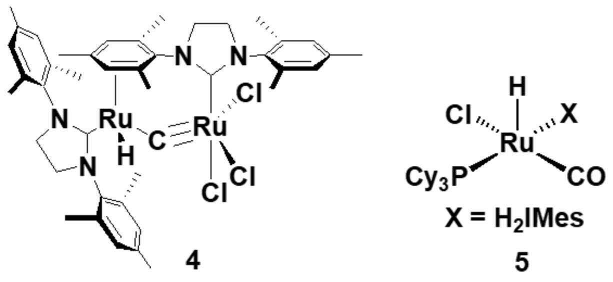

Figure 78. Hydride complexes proposed to account for isomerization side reaction in olefin metathesis

Due to inconveniences that olefin isomerization can pose, various studies have been carried out to find effective ways to prevent it. In the case of simple olefins, product selectivity, regioselectivity and chemo selectivity can be achieved by controlling different aspects of the reaction such as olefin homodimerization, olefin steric and electronic properties and the choice of metathesis catalyst. [11-12] Other studies suggested using additives that act as hydride scavengers to suppress the isomerization reaction. For example, Grubbs compared the impact of different additives on suppressing the unwanted olefin isomerization reactions and the variation of product distributions. He reported that electron-deficient species such as 2,6-dichloro-1,4-benzoquinone and tetrafluoro-1,4-benzoquinone are the most effective additives to prevent double bond migration in various olefins.[10] Gimeno and Vilar investigated the use of phenylphosphoric acid as isomerization inhibitor. They explained that phenylphosphoric acid can react with any potential ruthenium hydride species formed during the metathesis reaction. By using this additive, the reaction favored the formation of the metathesis products and completely suppressed any isomerization process.[11] Acetic acid was also used by Timmer and Ramström in the olefin metathesis of unprotected carbohydrates in which adding small quantities of acetic acid to the solution helped inhibiting alkene isomerization and increase the formation of the metathesis products.[12]

These results prompted us to extend the scope of these additives on complex polyolefin substrates such as polybutadiene and polyisoprene.

The first olefin cross-metathesis reaction of (*E*- or *Z*-) PB and PI was performed without additives and used as control. Further investigations of the spectra obtained after depolymerization of PB and PI provided additional information and proved an isomerization side reaction. In the case of PB, the reaction yielded the same *E/Z* ratio for the obtained product (Figure 80) independently of the polymers starting configuration. Starting with either *E*- or *Z*-PB, produced oligomers had the same percentage of *E* and *Z* units (60% *E* and 40% *Z*) after cross-metathesis in both cases. Enlargement of the signal at 2 ppm revealed 4 different signals of aliphatic protons (Figure 80a). The first one at 1.97 ppm corresponds to aliphatic protons (H5) of oligomers with *E* configuration. The second signal at 1.98 ppm corresponds to those of oligomers with *Z* configurations (H6). The two last signals at 1.99 and 2 ppm correspond to protons of the methyl groups (H7, H8) of the chain transfer agent in *Z* and *E* configurations respectively. Concerning olefinic protons, 4 different signals were identified between 5 and 6 ppm. Peaks at 5.78 and 5.53 ppm correspond to *Z*-olefinic protons (H1, H3) of the acetoxy oligomers while the *E*-olefinic protons (H2) appear at 5.66 ppm. The last signal at 5.34 ppm is for the *Z*-1,4-olefinic protons (H4) of polybutadiene units. An inversion in stereochemistry of the functionalized extremities was also detected. In fact, the acetoxy functions originating from the *Z*-1,4-diacetoxy-2-butene CTA mostly have an *E*-configuration after cross-metathesis. We can conclude that an internal and terminal olefin isomerization occurred in the depolymerization reaction (Figure 80a).

In the case of PI, depolymerization of 99% *E*-PI gave products composed in majority of *Z*-1,4 units (70% *Z*) while starting with a 98% *Z*-PI decreased the stereochemistry of the *Z*-products to 65% with the formation of 35% of *E* units, also proving an isomerization reaction. ^{1}H NMR spectra of depolymerized *E*-PI (Figure 81a) revealed a decrease in the intensity of both *E*-PI aliphatic protons (H13) at 1.93 ppm and *E*-PI methyl proton (H15) at 1.52 ppm together with a large increase in the intensity of the *Z*-PI olefinic protons (H1) at 5.78 ppm and a decrease of the *E*-PI olefinic protons (H2) at 5.54 ppm. For *Z*-PI, we noticed a large decrease in the *Z*-PI methyl proton (H14) at 1.7 ppm and a slight increase in the intensity of *E*-PI olefinic protons at 5.7 ppm (Figure 81b).

To overcome this problem, we studied the cross-metathesis of PB and PI under the same conditions but with the presence of one of the additives mentioned above (Figure 79) .[13-15] The choice of these additives was based on their reactivity towards hydride species and their effect on suppressing the isomerization reaction. They can all be reduced by reacting with the hydride complexes formed during cross-metathesis and therefore limit their formation and revert the decomposition of the catalyst. It is important to mention that these additives did not affect the catalyst activity as the depolymerization was completed within 2 hours. We also investigated if the amount of additive would have an effect on the product distribution. We repeated the cross-metathesis reaction several times while varying the percentage of additives relative to the polymer. It had very little effect on the distribution of products and the isomerization was inhibited with only 10% of additive.

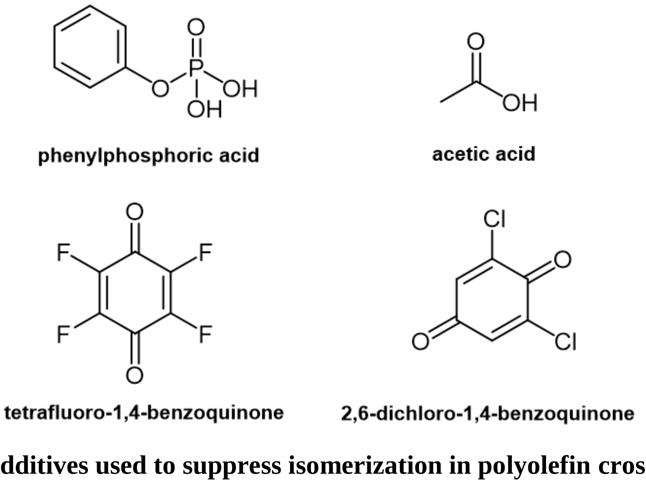

Figure 79. Additives used to suppress isomerization in polyolefin cross-metathesis

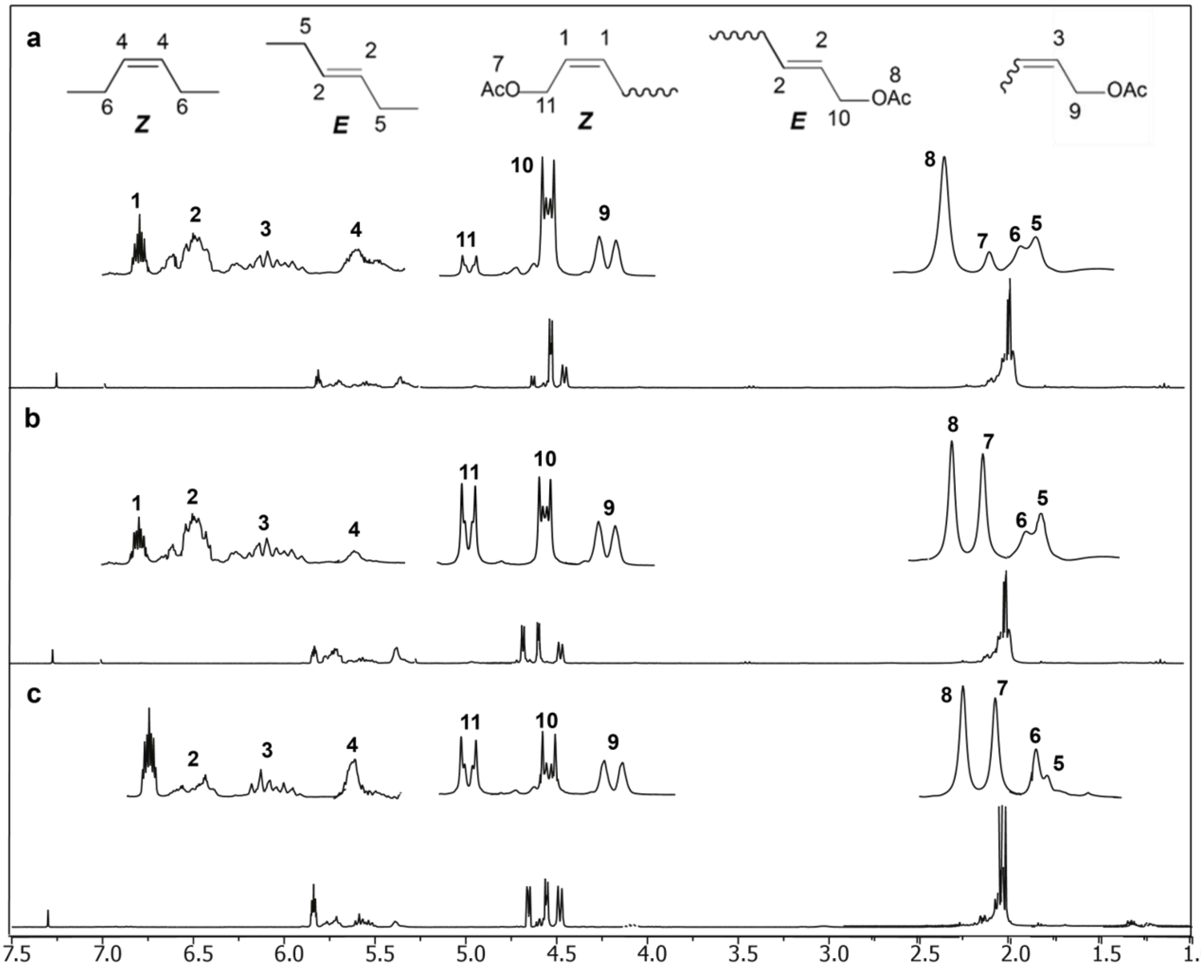

Figure 80. ^{1}H NMR spectra of a) depolymerized *E*-and *Z*-PB without additive, b) depolymerized *E*-PB with additives and c) depolymerized *Z*-PB with additives.

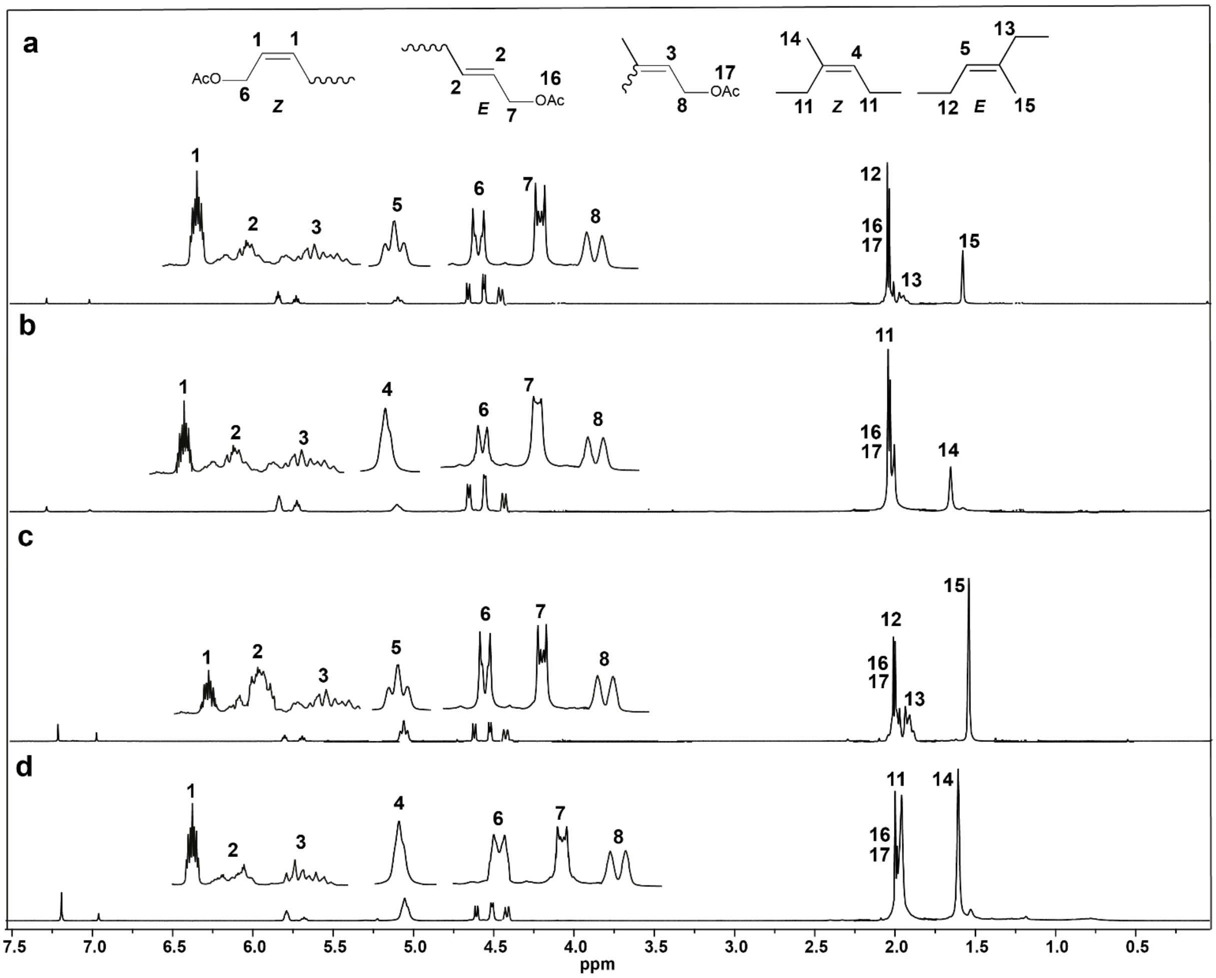

Figure 81. ^{1}**H NMR spectra of a) depolymerized *E*-PI b) depolymerized *Z*-PI c) depolymerized *E*-PI with additives and d) depolymerized *Z*-PI with additives**

We first studied the impact of additives in the cross-metathesis reaction of polybutadiene. Upon addition of phenylphosphoric acid, depolymerization of *E*-PB produced oligomers with slightly higher *E*-units (61%) and less *Z*-units (39%). The same product distribution was also obtained with acetic acid. Both additives were effective to prevent isomerization of *E*-PB as the desired product configurations were obtained with reasonable percentages while majorly preserving the initial polymer stereochemistry. Tetrafluoro-1,4-benzoquinone was more effective as the percentage of *E*-units increased to 64% with a decrease to 36% in *Z*-units. The most effective additive was 2,6-dichloro-1,4-benzoquinone. Following its addition, isomerization was suppressed and the *E*-1,4 metathesis product **6** (Figure 82) was majorly formed (75% vs 25% *Z*). In the NMR spectrum of depolymerized *E*-PB after addition of 2,6-dichloro-1,4-benzoquinone (Figure 80b), the signal at 1.97 ppm corresponding to aliphatic protons (H5) and that at 5.66 ppm corresponding to olefinic protons (H2) of oligomers with *E* configuration significantly increased in comparison to the same signals in Figure 80a. Concerning *Z*-PB, phenyl phosphoric and acetic acids were more effective than with *E*-PB. Distribution of *Z*-units in product 6 increased from 40% up to 55% and 59% respectively. Tetrafluoro-1,4-benzoquinone slightly gave higher distribution of *Z*-units (60%). As expected, 2,6-dichloro-1,4-benzoquinone had the highest effectiveness as the depolymerization yielded 73% of *Z*-1,4 metathesis product **6**. NMR analysis revealed a major increase in the intensity of signals at 1.98 and 5.78 ppm corresponding to *Z*-aliphatic (H6) and olefinic (H1) protons respectively. At the same time, signals of *E*-aliphatic (H5) and olefinic (H2) protons decreased.

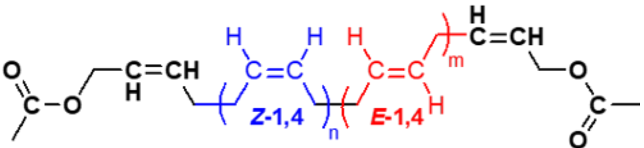

6

Figure 82. Structure of the products obtained from the depolymerization of *E*- or *Z*-PB

As for suppression isomerization in the cross-metathesis of *E*-PI, the addition of phenyl phosphoric acid yielded product **7** with 48% *E*-1,4 units and 52% *Z*-PI units marking a significant change in the product distribution. While with acetic acid, the formation of *E*-units doubled together with a decrease in Z-units. Benzoquinones were more effective in suppression isomerization. In fact, tetrafluoro-1,4-benzoquinone and 2,6-dichloro-1,4-benzoquinone yielded product **13** (Figure 83) with 65% and 79% *E*-1,4 units respectively. Enlargements in the NMR spectrum of depolymerized *E*-PI after addition of 2,6-dichloro-1,4-benzoquinone showed a large increase in the intensity of both *E*- aliphatic protons (H13) at 1.93 ppm and *E*-methyl proton (H15) at 1.52 ppm, as well as an increase in the *E*-PI olefinic protons (H2) at 5.54 ppm together with a decrease in the intensity of the *Z*-PI olefinic protons (H1) at 5.78 ppm (Figure 81c). The same interpretation can be applied on *Z*-PI. In fact, phenyl phosphoric acid increased the percentage of *Z*-1,4 units to 68%. Acetic acid and tetrafluoro-1,4-benzoquinone were much more efficient giving product **13** with a major *Z*-1,4 configuration up to 73% and 75% respectively. Finally, 2,6-dichloro-1,4-benzoquinone afforded 81% of *Z*-units and only 19% of *E*-units. The intensity of *Z*-PI methyl proton (H14) at 1.7 ppm as well as that of *Z*-PI olefinic protons (H1) at 5.78 ppm increased largely. The signal at 5.54 ppm of the *E*-PI olefinic protons (H2) decreased dramatically (Figure 81d).

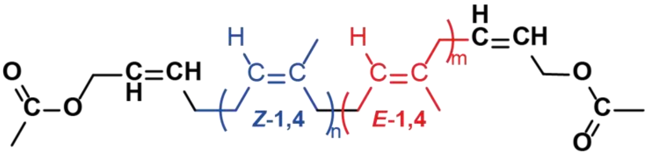

13

Figure 83. Structure of the products obtained from the depolymerization of *E*- or *Z*-PI

Surprisingly, 2,6-dichloro-1,4-benzoquinone was distinctly more efficient in suppressing the isomerization reaction of PB and PI than the more electron-deficient tetrafluro-1,4-benzoquinone. Furthermore, some studies showed that benzoquinone are reduced to their corresponding hydroquinones when reacting with the ruthenium hydride species. [16] Indeed, recorded ^{1}H NMR spectra of the depolymerization products presented two signals at 4.9 at 6.9 ppm which can be attributed to the alcohol group and aromatic protons of hydroquinones respectively (Figure 81). These encouraging results can be used to approve the theory of formation of ruthenium hydride species during olefin metathesis.

In a second step, the stereochemistry of the cross-metathesis products was studied by ion mobility spectrometry mass spectrometry (IMS-MS).

The ion mobility spectra of different ions belonging to products from the depolymerized PB and PI in both *E* and *Z* configurations before and after suppression of isomerization are presented in figure 84 and 85. In both cases, a significant change in the ion mobility peak profile is observed. The *E* configuration of PB and PI has lower drift times than the *Z* configuration. This is due to the fact that the *Z* configuration is less compact having steric effect in its structure and requires more time to travel in the drift tube of the ion mobility spectrometer. In fact, small and compact ions will have smaller collision cross sections and will drift more quickly than large and extended ions with large collision cross sections.

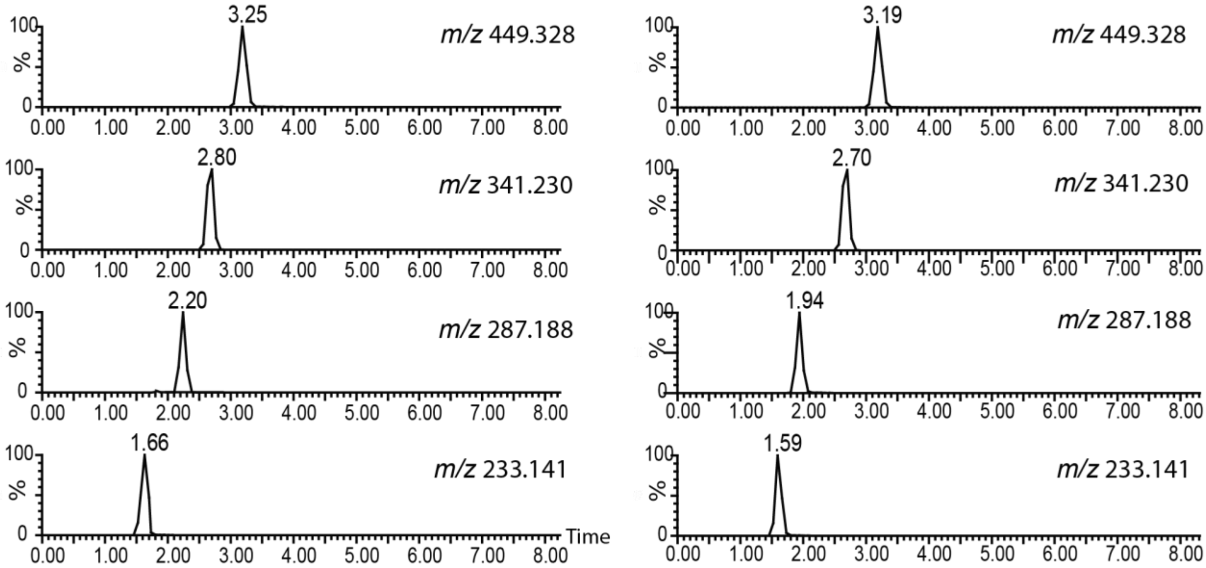

Figure 84. Ion mobility profiles of specific m/z from the depolymerized *E*- and *Z*-PB

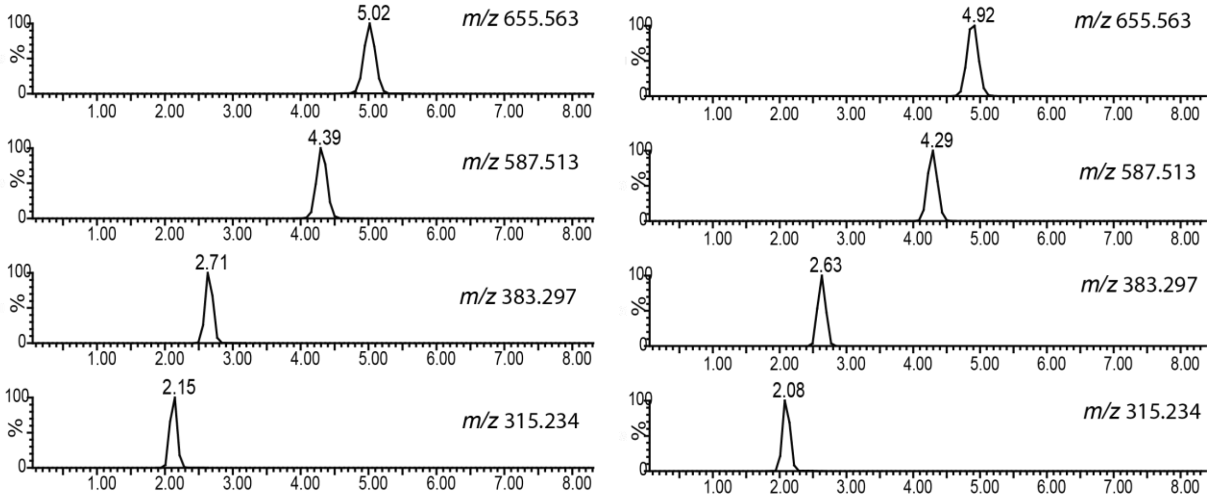

Figure 85. Ion mobility profiles of specific m/z from the depolymerized *E*- and *Z*-PI

In order to go further, we focused on one specific *m/z* belonging to PB. Corresponding ions were extracted and ion mobility profiles replotted using OriginPro 2019 (OriginLab). In Figure 86a and 86c, drift times of *E*- and *Z*-PB oligomer ($C_{24}H_{36}O_4 + {}^7Li^+$) at *m/z* 395.2768 show two peaks at 2.85 and 3.14 ms, but unfortunately with the same *E*/*Z* ratio (60/40).

After optimization, analysis by IMS-MS of *E*- and *Z*-PB oligomer at *m/z* 395.2768 confirmed the formation of only one major isomer by adding 10% (w/w of the polymer) of 2,6-dichloro-1,4-benzoquinone to the metathesis reaction. The major isomer has the same configuration as the starting polymer as shown in the *E*/*Z* ratio in Figure 86b and 86d. By comparing the drift times, *E*- and *Z*-PB showed completely different times. In the case of *Z*-PB as starting polymer, two peaks were recorded at 3.02 ms (*E*-isomer) and 3.22 ms (*Z*-isomer), while for *E*-PB these two peaks were recorded at 2.93 ms (*E*-isomer) and 3.20 ms (*Z*-isomer). The same results were found in the case of *E*- and *Z*-PI.

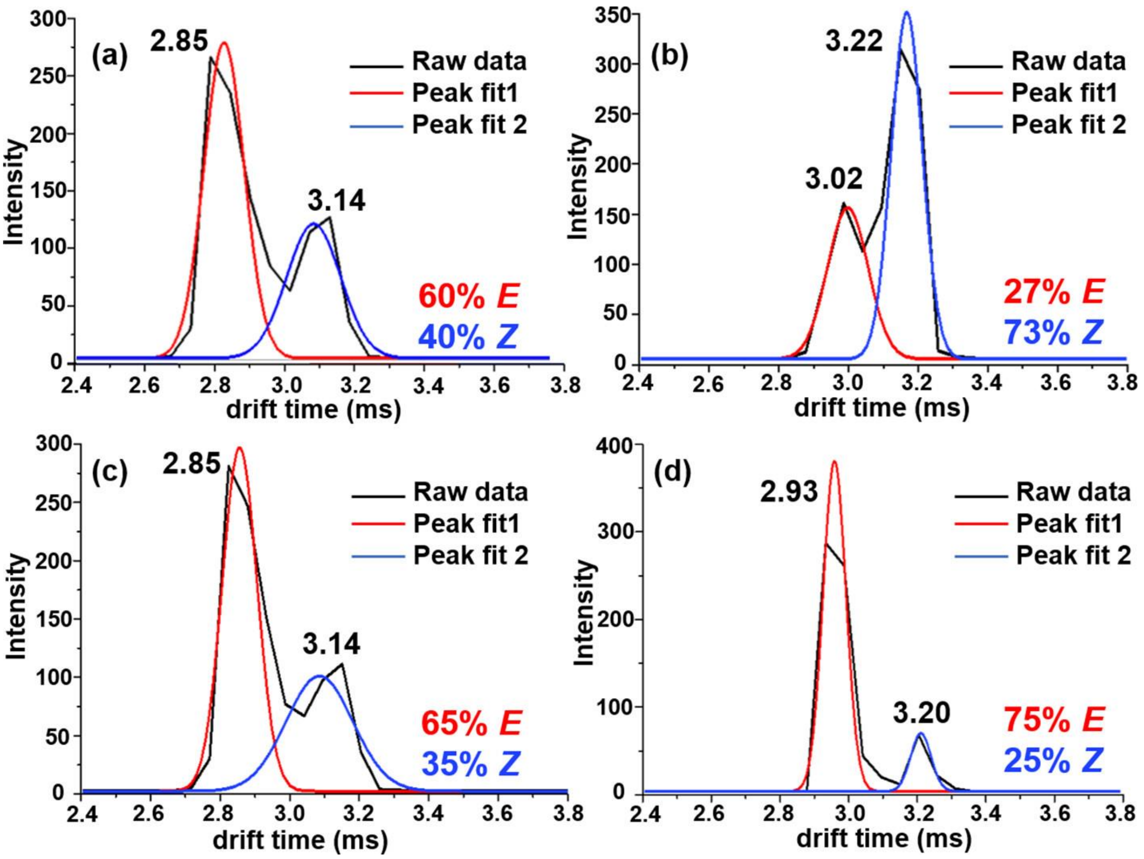

Figure 86. Ion mobility spectra of *m/z* 395.2768 ion extracted from the ESI-IMS-MS data obtained from (a) depolymerized *Z*-PB, (b) depolymerized *Z*-PB after isomerization suppression, (c) depolymerized *E*-PB and (d) depolymerized *E*-PB after isomerization suppression. The black lines are experimental spectra extracted with a *m/z* width of 0.01 Da. The red and blue signals were obtained from the deconvolution of the experimental profile with a Gaussian function.

Then, *E* and *Z* isomers were characterized by energy resolved MS/MS experiments (ERMS).[17-18] The MS/MS spectrum of ion at *m/z* 665.5147 which corresponds to 9 monomers of PB shows two fragment at *m/z* 605.4867 corresponding to the loss of one acetyl group and at *m/z* 545.4679 corresponding the loss of two acetyl groups (Figure 87).

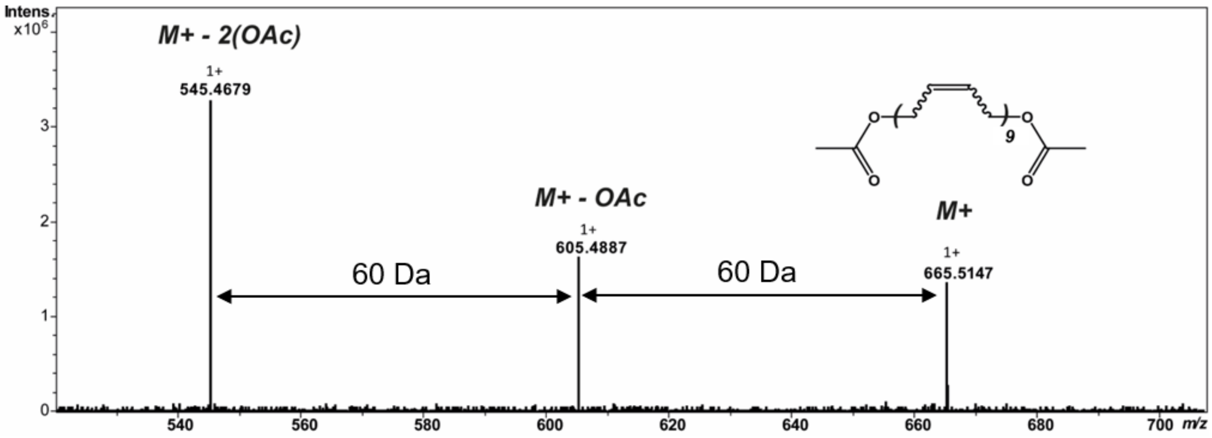

Figure 87. MS/MS spectrum of ion at *m/z* 665.5147

Breakdown curves (Fig. 88) show that the product ion at *m/z* 665.5147 is fragmented in different patterns according to its configurations. The *Z*-isomer, is fragmented directly at low energy giving rise to its first product ion at *m/z* 605 which reaches its highest abundance around 12 eV and starts to fragment at its turn giving the product ion at *m/z* 545 which starts to form at about 14 eV. In the case of the *E*-isomer, the M^+ is stable in the range between 0 to 8 eV and starts to fragment at 10 eV forming its first product ion at *m/z* 605. This ion increases in intensity reaching its highest at 15 eV where it also starts to dissociate and decrease giving rise to the smallest ion at *m/z* 545. Although less quantitative than IMS-MS, ERMS also proves the suppression of the isomerization during the cross-metathesis reaction was successful.

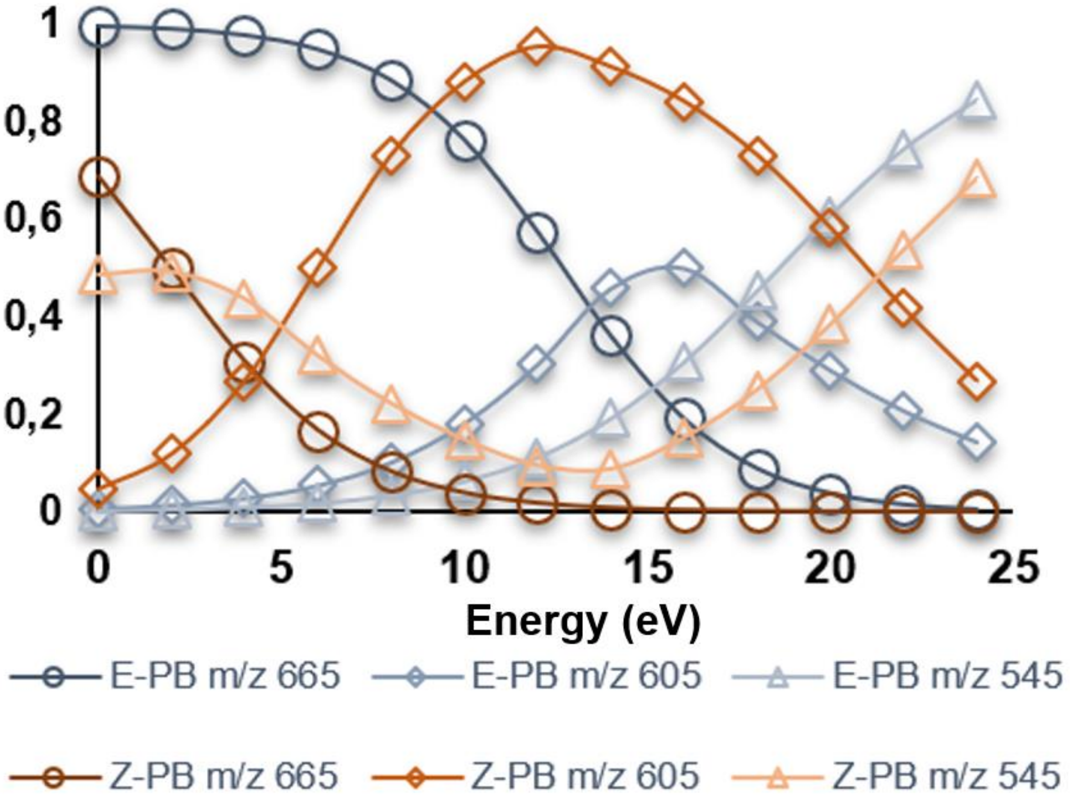

Figure 88. Breakdown curves obtained from the dissociation of $[M+^7Li]^+$ 665.5147 of *E*-PB and *Z*-PB

IV. Comparison with pyrolysis-based mass spectrometry methods

In order to demonstrate the potentialities of the depolymerization reaction and FT-ICR MS and IMS for the analysis of polydienes, we compared it to classical MS methods based on pyrolysis of polymers. Previous studies showed that Py-GC/MS permitted to characterize the pyrolysis pattern of PB using polymers with various content ratio of *Z*-1,4, *E*-1,4 and 1,2-units and identified 13 gaseous products proving that *E*-butadiene oligomers are majorly produced.[16] For all configurations the major pyrolysis products are C_4H_6 (butadiene), C_5H_8 (cyclopentene), C_6H_{10} (cyclohexene), C_7H_{10} (1,4-cycloheptadiene), and C_8H_{12} (4-vinylcyclohexene).[19-21] Py-GC×GC/MS affords more information. (Figure 89).

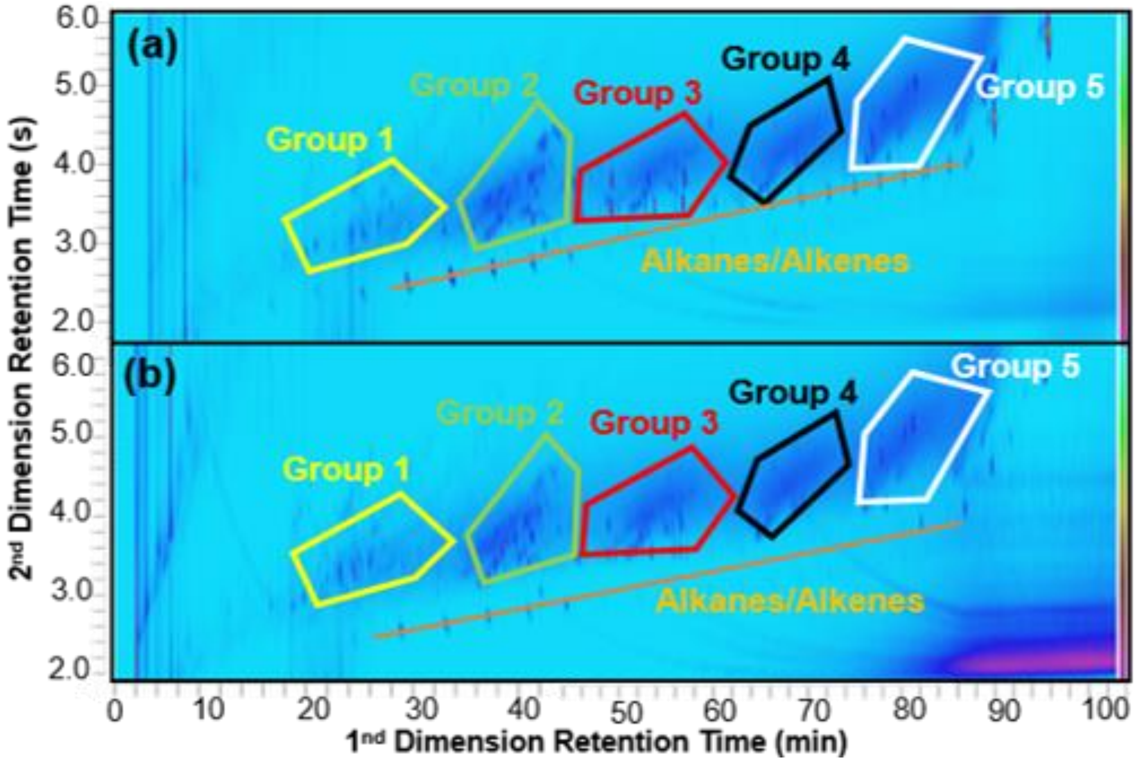

Figure 89. Py-GCxGC/MS chromatograms obtained from the pyrolysis of (a) *E*-PB and (b) *Z*-PB samples. The class of products ob-served are framed in different colors with the series of al-kanes/alkenes in orange.

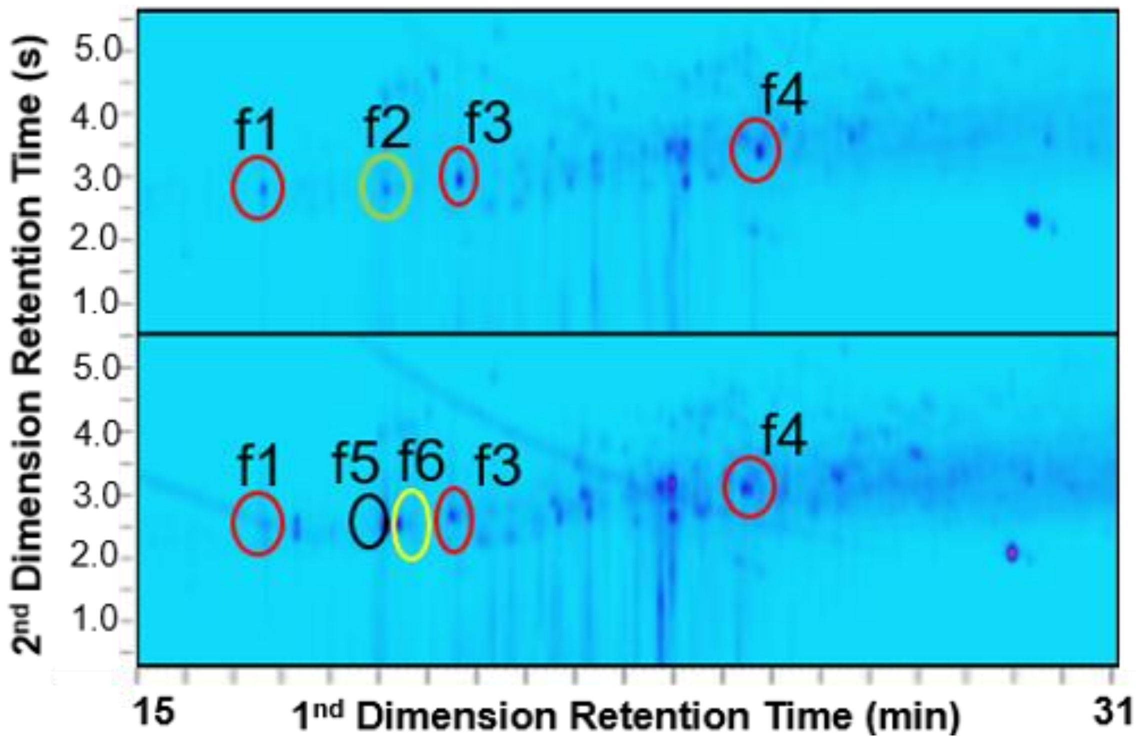

Figure 90. Expanded view of Py-GC×GC/MS of *Z*-PB (Up) and *E*-PB (Down) at the region of retention times in the first dimen-sion: 15-31 minute

For isomer identification the first region afforded the clearest pattern. Pyrolysis products f1, f3 and f4 exist in both configurations and correspond mostly to cyclic hydrocarbons (Figure 90). Product f2 is unique to *Z*-PB while products f5 and f6 are present only in the *E* configuration of the polymer. In the second region extended between 31 and 48 minutes (Figure 91), both PB configurations present a similar product f8 while f7 is only found in *E*-PB. We can also notice that there are different parts of the chromatogram where the intensity of the pyrolysis products varies between *Z*- and *E*-PB. For example, the red framed parts observed in both chromatograms contain the same products but with different intensities.

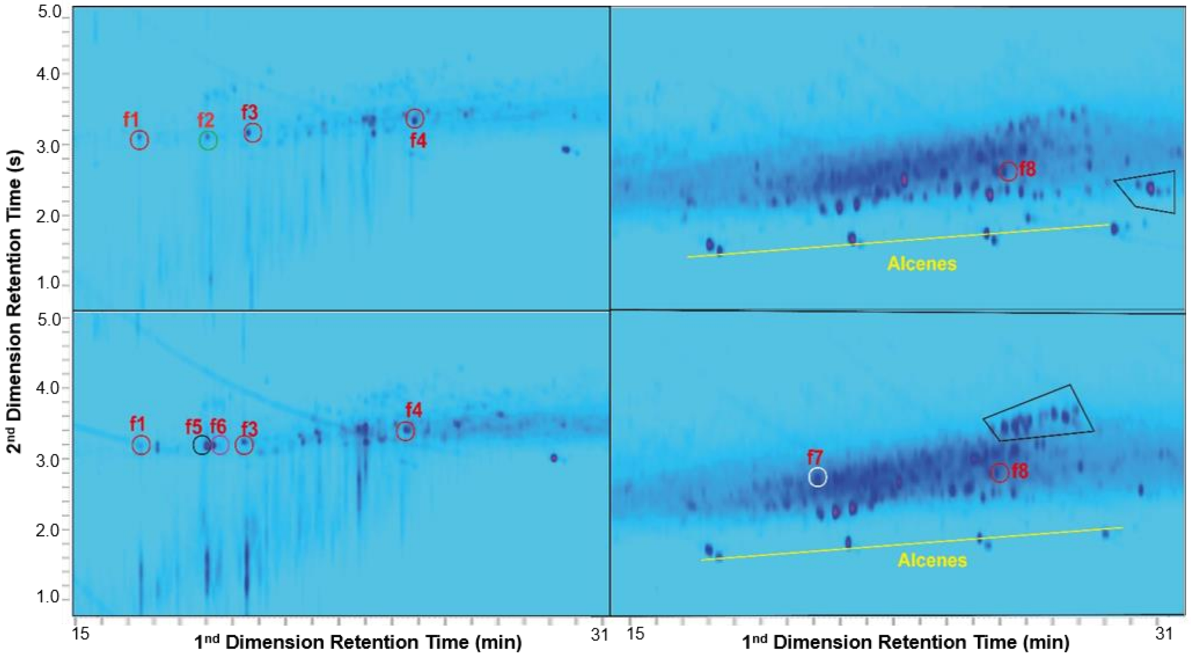

Figure 91. Expanded view of Py-GCxGC/MS of *Z*-PB (Up) and *E*-PB (Down) at two different regions of retention times in the first dimension: 15-31 minutes (Left) and 31-48 minutes (Right).

For the analyzed *E* and *Z*-PI, the same pattern found after the pyrolysis of PB can be observed (Figure 92). Chromatograms can be as well divided into five major groups with the presence of additional products in the early region of retention time in the 1st dimension. We can notice that products issued from the pyrolysis of PI started to appear at around 20 minutes of 1st dimension retention time while in the case of PB, first products appeared at 15 minutes. In the first group, low molecular weight molecules can be identified and consisted mostly on polymerized short chains of isoprene such as dimers and trimers. We also noticed the presence on a series of alkenes similar to that found in PB. In the second group, longer polymerized chains of isoprene could be observed up to five isoprene units. In the higher retention time region, molecules became more difficult to assign however in the last three groups, differences between the *E* and *Z* configurations of PI were visible.

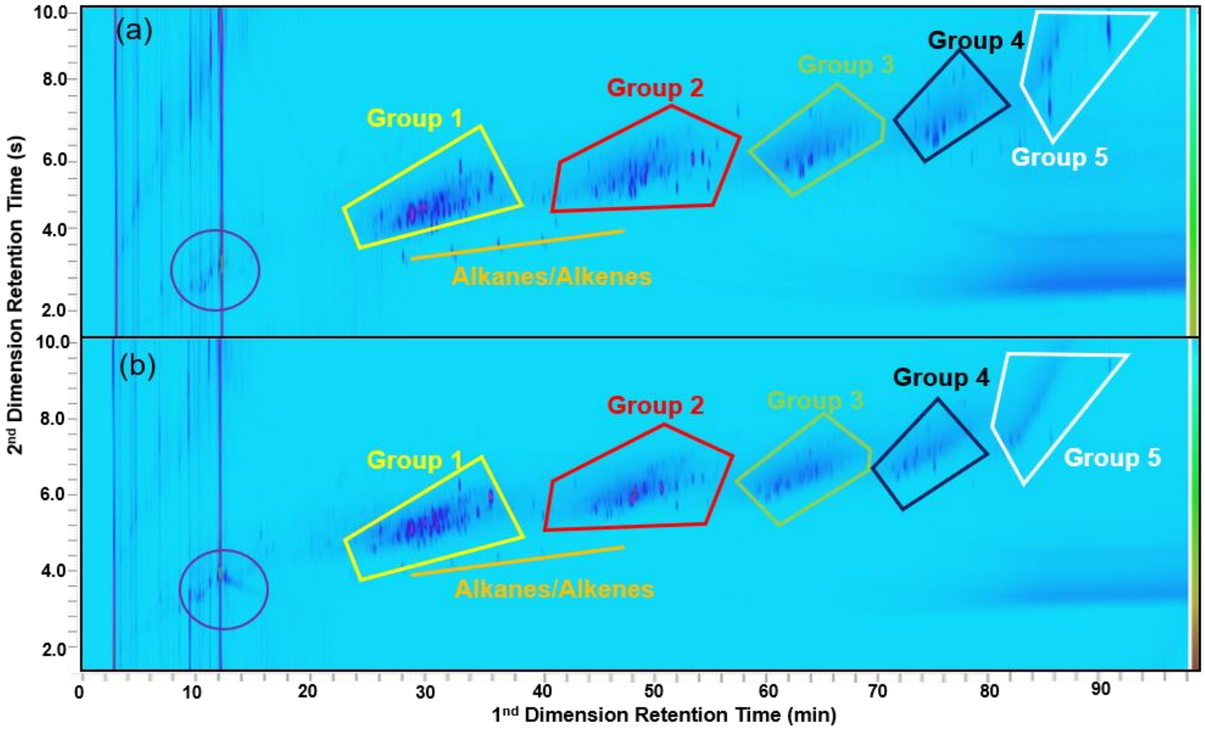

Figure 92. Py-GCxGC/MS chromatograms obtained from the pyrolysis of (a) *E*-PI and (b) *Z*-PI samples. The class of products observed are framed in different colors with the series of alkanes/alkenes in orange

The expansion of each region on the chromatogram allowed to observe that the products obtained after pyrolysis of these two polymers were very different. In the first part of the spectrum, extended between 20 and 41 minutes (Figure 93), we can notice that both configurations have unique products at different retention times. For example, g4 exists only in *Z*-PI and may correspond to a low molecular weight molecule. We can also observe some similarities especially close to 40 minutes. The same series of alkenes in also present in both cases. In the second part which starts at 41 minutes and ends around 62 minutes, the same pattern can be observed. A high number of differences in addition to one clear similarity (g9) with variable intensity. Variations in the pyrolysis products according to the content of each polymer can be highly noted in the third and fourth region. In the third part of the chromatogram, we can see that almost every product present in *E*-PI is completely absent in *Z*-PI and the same is applied to the fourth part between 72 and 99 minutes. This analysis definitely proves that *E* and *Z*-PI rearrange in different patterns after pyrolysis depending on their microstructures. Analysis of inert PB and PI using pyrolysis uncovered valuable information and helped elucidate their structure

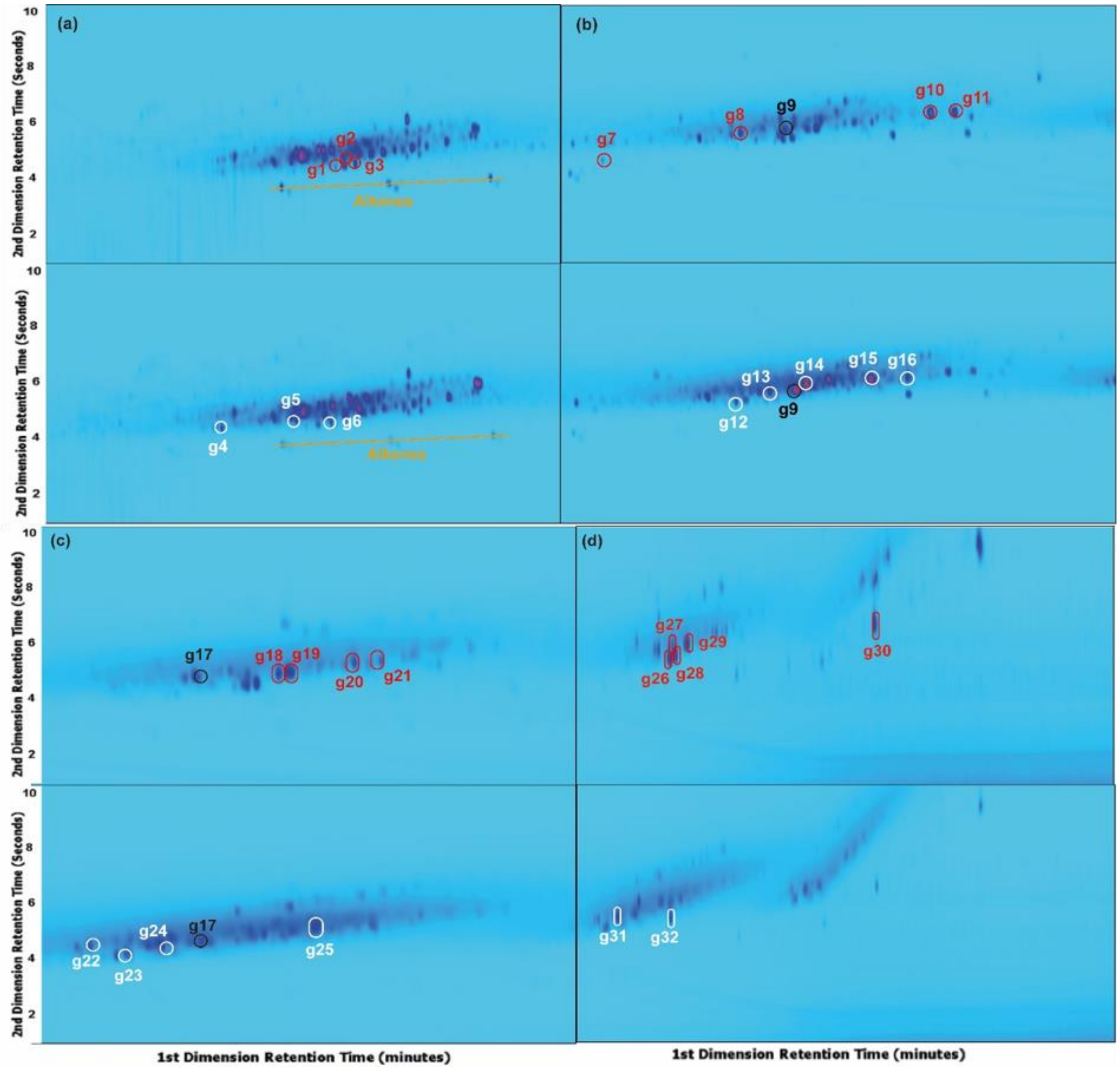

Figure 93. Expanded view of Py-GCxGC/MS of *E*-PI (Up) and *Z*-PI (Down) at four different regions of retention times in the first dimension: (a) 20-41 minutes, (b) 41-62 minutes, (c) 62-72 minutes and (d) 72-99 minutes

Finally PB and PI in both *E* and *Z* configurations were then analyzed by atmospheric solid analysis probe coupled to ion mobility-mass spectrometry on a Q-TOF instrument (ASAP-MS) (Figure 94 and 95).[22-23] The initial analysis showed radical cation series separated by 54.04 Da for *E*- and *Z*-PB and 68.06 Da for *E*- and *Z*-PI, which correspond to C_4H_6 and C_5H_8 repeating units, respectively. Both *E*- and *Z*-polymers yielded similar mass spectra.

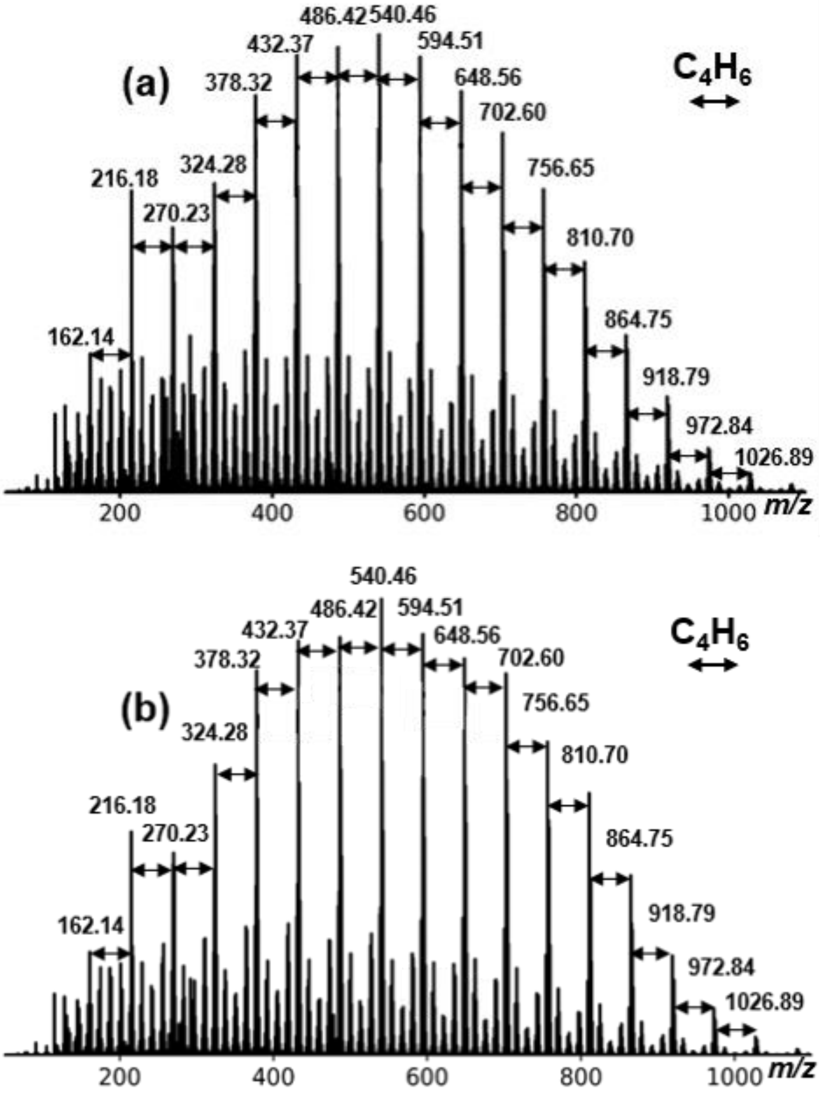

Figure 94. ASAP-MS results of PB samples. The extracted mass spectra obtained for: (a) *E*-PB, (b) *Z*-PB showing ion series separated by 54.0464 Da (C_4H_6)

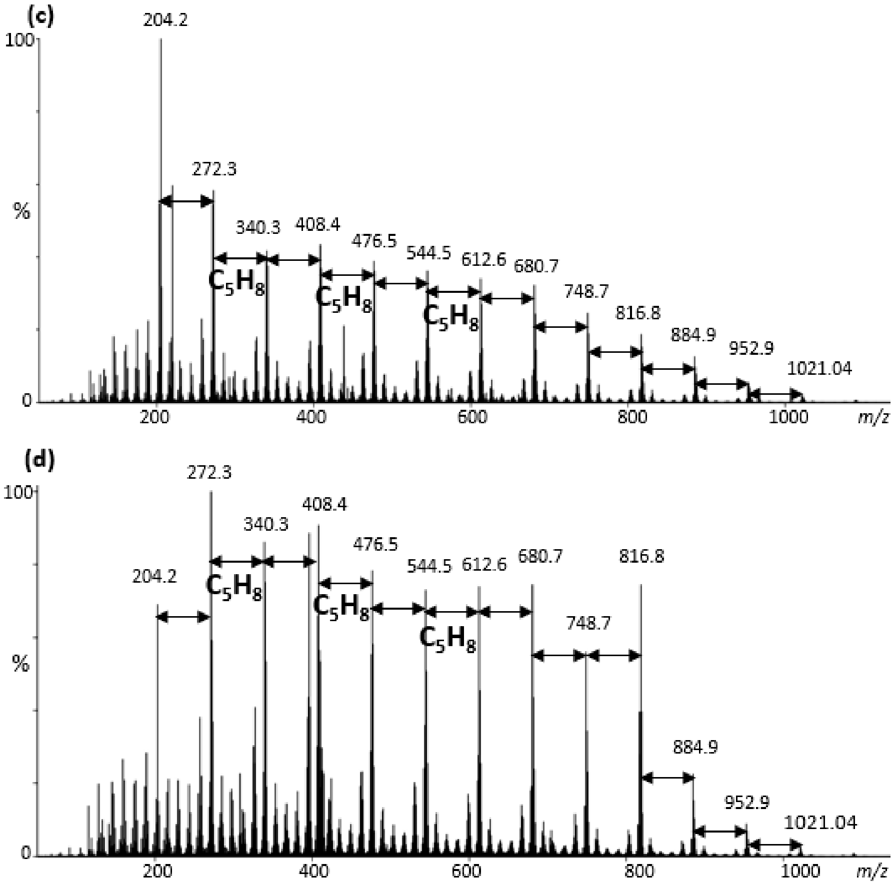

Figure 95. ASAP-MS results of PI samples. The extracted mass spectra obtained for: (c) *E*-PI, (d) *Z*-PI showing ion series separated by 68.0620 Da (C_5H_8).

An expanded view for *E*-PB and *Z*-PB (Figure 96a and 96b) allowed the identification of different ion distributions: I: $M_w = 54.046n$; II: $M_w = 54.046n + 12.000$ (C); III: $M_w = 54.046n + 14.015$ (CH_2); IV: $M_w = 54.046n + 28.031$ (C_2H_4); V: $M_w = 54.046n + 40.031$ (C_3H_4); VI: $M_w = 54.046n + 42.046$ (C_3H_6); VII: $M_w = 54.046n + 15.994$ (O). Distribution I was detected as the most intense (90-95%) and extended on the whole mass range. Distributions II, IV and VI are less intense with approximately similar relative intensities (30-35%) followed by distribution III and V with the lowest intensity.

In the case of *E*-PI (Figure 96c) and *Z*-PI (Figure 96d), the expanded view allowed the identification of the following distributions: I: $M_w = 68.062n$; II: $M_w = 68.062n + 12.000$ (C); III: $M_w = 68.062n + 14.015$ (CH_2); IV: $M_w = 68.062n + 28.031$ (C_2H_4); V: $M_w = 68.062n + 40.031$ (C_3H_4); VI: $M_w = 68.062n + 42.046$ (C_3H_6); VII: $M_w = 68.062n + 56.062$ (C_4H_8); VIII: $M_w = 68.062n + 15.994$ (O). Distribution I was detected with the highest intensity at 90% and extended on the entire mass range. Distributions II and V followed with lower intensity (10-30%) and finally distributions III and IV had the lowest intensity. It should be noted that distribution I in both PB and PI contains cyclic species and radical cations are majorly formed in all distributions. Several additional distributions with low intensities may be explained by in source fragmentation originating from the main distributions. ASAP is an energetic ionization source which is known to induce this type of fragmentations.[24] ASAP coupled to ion mobility spectrometry-mass spectrometry data did not show any differences between the two configurations of each polymer. This is presumably due to the formation of cyclic compounds from the low temperature pyrolysis.[25-27]

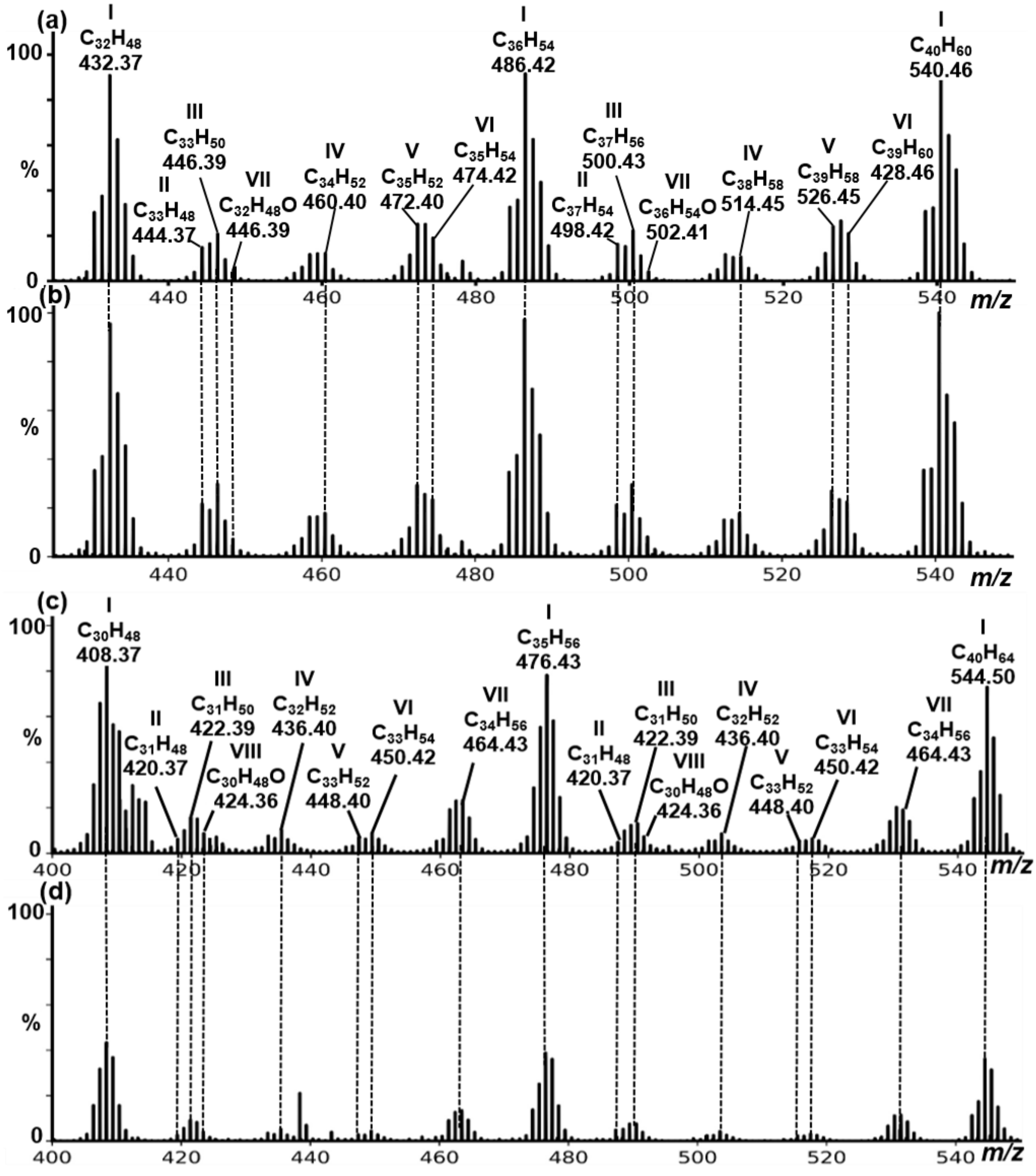

Figure 96. Enlargement of ASAP-MS spectra obtained for the different polymer samples in the mass range *m/z* 400-700 (a) *E*-PB, (b) *Z*-PB, (c) *E*-PI and (d) *Z*-PI showing the different ion distributions.

For *E*- and *Z*-PB (Fig. 97a and 97b), both plots present one diagonal with the same ion distributions. We can also notice the presence of the different distributions mentioned above and especially distributions I, II, III and IV. In the case of PI, *E*-PI presents two diagonals (Fig. 97c). The diagonal with the higher slope corresponds to ions having the highest drift times and these are attributed to the distributions mentioned above with distribution I having the highest intensity. The diagonal with the lower slope corresponds to a family of poly (ethylene glycol) (PEG). In fact, *E*-PI is commercially available as pellets and PEG is used as a plasticizer.[28] However, for *Z*-PI only one diagonal is present and corresponds to the same ion distributions found in *E*-PI (distributions I, II, II, IV and V) (Fig. 97d).

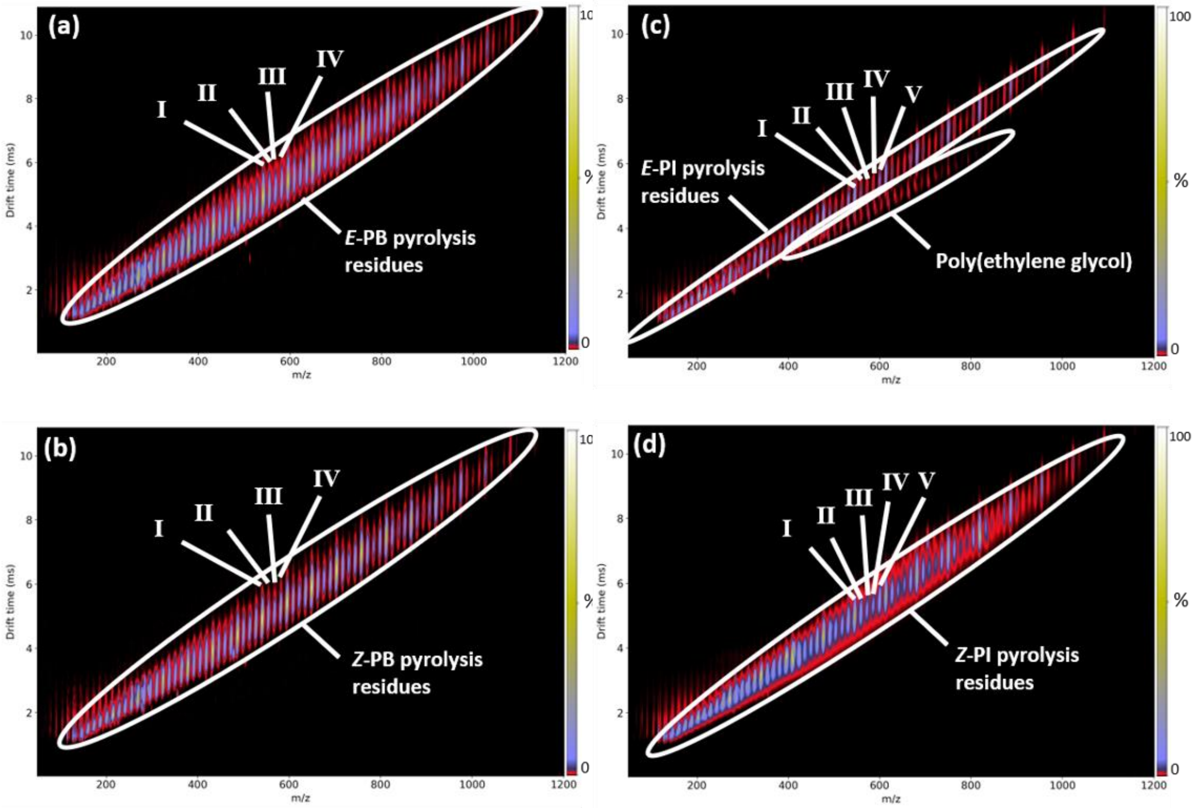

Figure 97. ASAP-IMS-MS results of PB and PI: *m/z*-drift time plot respectively for (a) *E*-PB, (b) *Z*-PB, (c) *E*-PI and (d) *Z*-PI

ASAP-MS helped uncover most of the species issued from pyrolysis of both PB and PI, however, analysis of complex mixtures requires higher-resolution. As expected, the ASAP spectra on a Q-TOF instrument and the DIP-APCI spectra on the FTICR are similar at a first glance showing ion series issued from the pyrolysis of *E*-and *Z*- PB separated by 54.0464 Da corresponding to one C_4H_6 monomer (Figure 98a and 98b) while ion series of *E*- and *Z*- PI were separated by 68.0620 Da corresponds to the monomer C_6H_8 (Figure 98c and 98d).

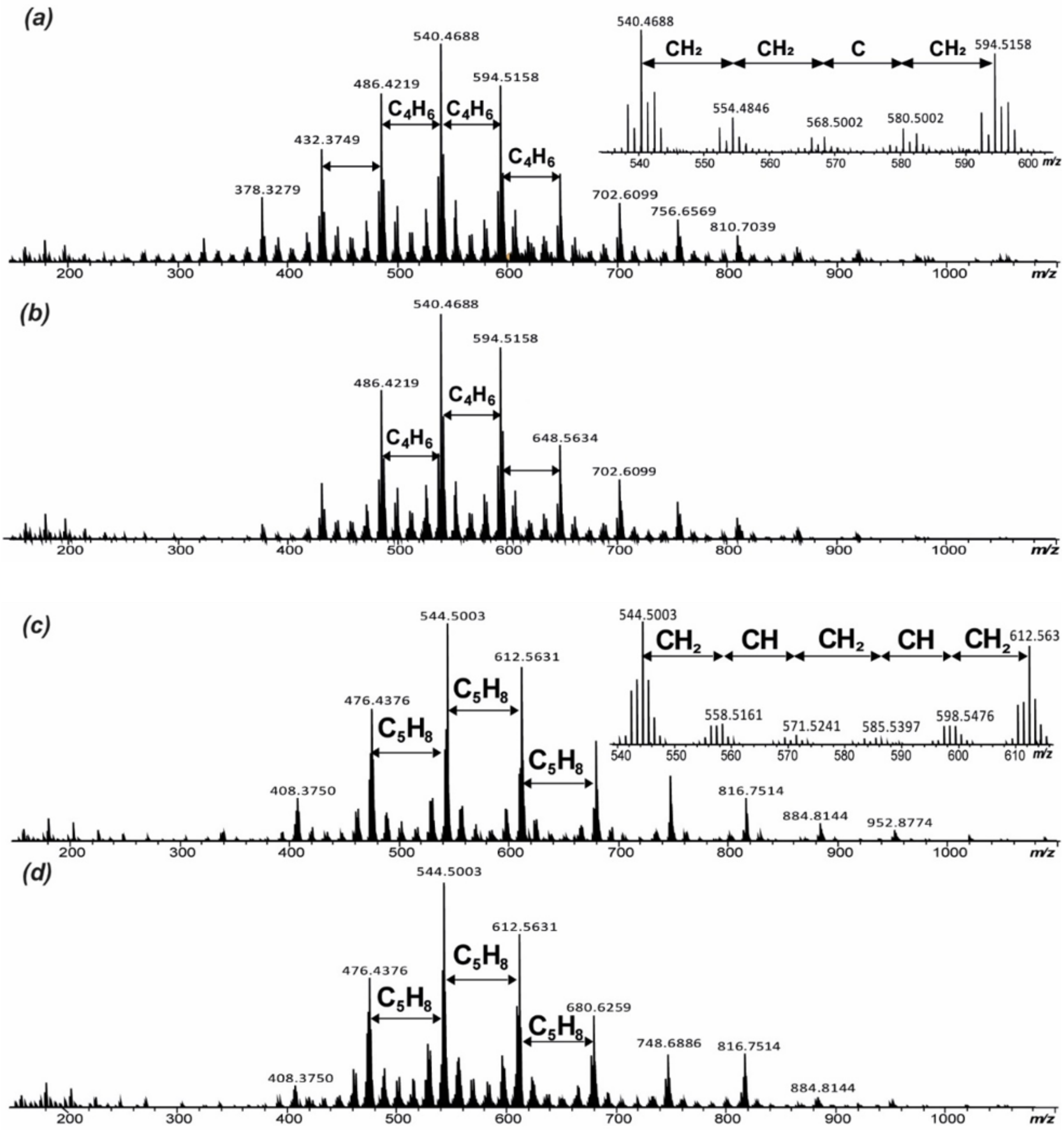

Figure 98. DIP-APCI-FTICR spectra of (a) *E*-PB and (b) *Z*-PB showing ion series separated by 54.0464 Da (C_4H_6) and (c) *E*-PI and (d) *Z*-PI showing ion series separated by 68.0620 Da (C_5H_8).

In the case of PB, an intense peak appeared first at *m/z* 530.4693 and can be attributed to the molecular ion of an antioxidant, *Irganox 1076* ($C_{35}H_{62}O_3$).[28] When mass spectra were analyzed in details, they showed an overlap between different peaks with the same nominal mass (Fig. 99a). ^{13}C isotope of radical cation $M^{+\bullet}$ may be clearly identified from the protonated molecule $[M+H]^+$. For example, the peak at *m/z* 540.4689 corresponds to the $C_{40}H_{60}$ cation radical. The signal at +1 Da can be separated into two peaks: the first one at *m/z* 541.4723 corresponds to radical cation $M^{+\cdot}$ with one ^{13}C isotope ($^{13}C_1{}^{12}C_{39}H_{60}$) while the second peak at *m/z* 541.4767 corresponds to the protonated species with $C_{40}H_{61}$ $[M+H^+]$ (Fig. 99b). So, DIP-APCI and presumably also ASAP affords a mixture of radical cations, which dominates, and protonated molecules.

The DIP-APCI source produces also slightly more products than the ASAP source. For example, for *E*- and *Z*-PB, the species $C_{40}H_{60}$ *m/z* 540.4689 is also present with the addition from one to four oxygen atoms at *m/z* 556.4638 $C_{40}H_{60}O$ up to *m/z* 604.4486 $C_{40}H_{60}O_4$ with four additional oxygen atoms. In addition, the peak at *m/z* 556.4638 is accompanied by a peak *m/z* 556.5002 corresponding to $C_{40}H_{60}$ *m/z* 540.4689 plus CH_4 or *m/z* 542.4846 ($C_{40}H_{62}$) plus one CH_2, giving $C_{41}H_{64}$ as molecular formula (Fig. 99c). The same kind of attribution can be made for *E*- and *Z*-PI (Fig. 100). The peak at *m/z* 544.5002 corresponds to $C_{40}H_{64}$ radical ion. The signal at +1 Da includes two signals: one at *m/z* 545.5036 corresponding to $^{13}C_1{}^{12}C_{39}H_{64}$ radical cation and the other at *m/z* 545.5080 which can be attributed to the protonated species $C_{40}H_{65}$. Also, the nominal mass *m/z* 560 can be separated into different species. The first peak at *m/z* 560.4951 corresponds to *m/z* 544.5002 ($C_{40}H_{64}$) plus one atom of oxygen ($C_{40}H_{64}O$). The second peak with *m/z* 560.5226 corresponds to $C_{41}H_{66}$ with two ^{13}C isotopes giving $^{13}C_2{}^{12}C_{39}H_{66}$ radical cation. The third peak at *m/z* 560.5270 is attributed to $C_{41}H_{67}$ radical cation with one ^{13}C isotope ($^{13}C_1C_{40}H_{67}$). The last peak with *m/z* 560.5315 corresponds to *m/z* 546.5159 ($C_{40}H_{66}$) plus one CH_2 molecule ($C_{41}H_{68}$). It should be pointed out that this behavior is displayed as a continuous distribution at each nominal *m/z* value.

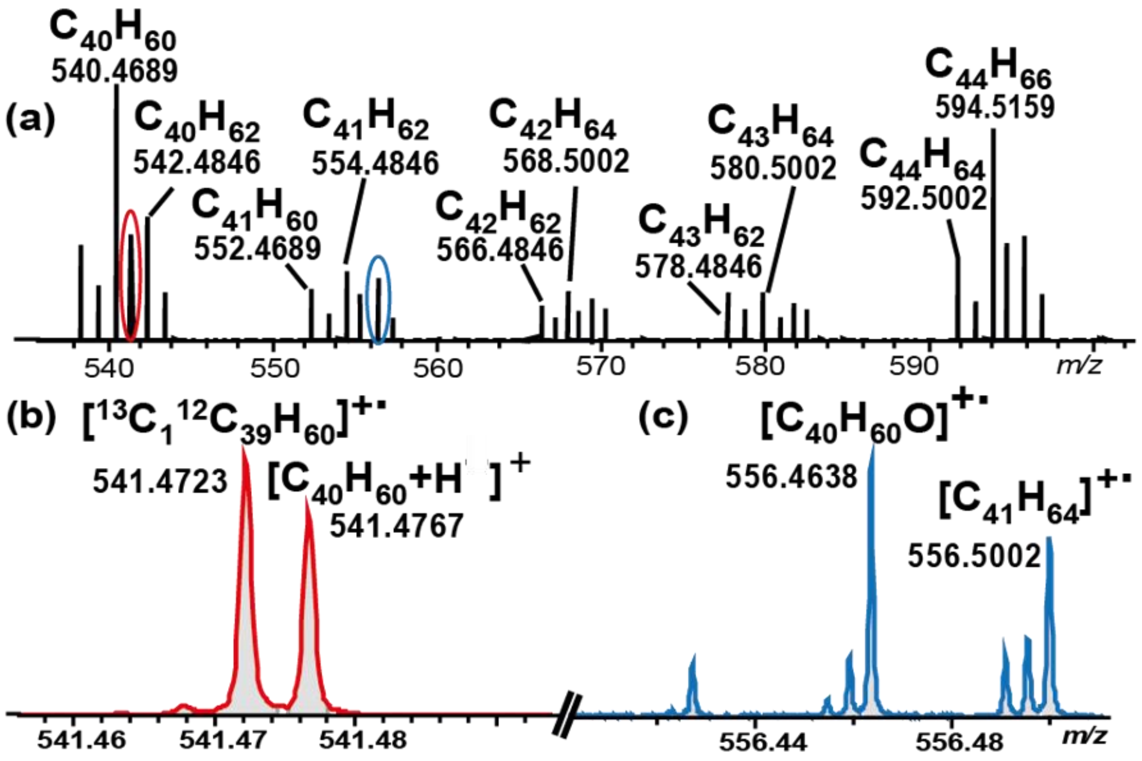

Figure 99. (a) Distribution of ions between *m/z* 540 and 600 ob-tained from DIP-APCI-FTICR analysis of PB and enlarge-ment of the DIP-APCI-FTICR spectrum of PB at the nomi-nal mass (b) *m/z* 541 and (c) *m/z* 556 showing different identified species.

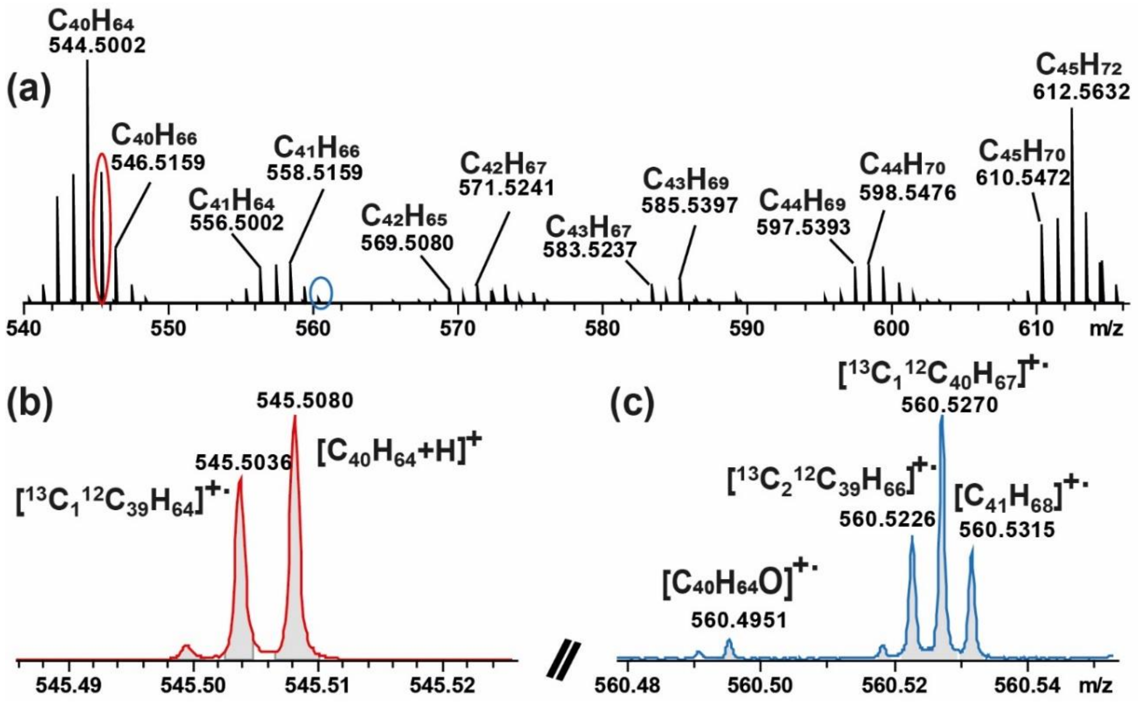

Figure 100. (a) Distribution of ions between *m/z* 540 and 615 obtained from DIP-APCI-FTICR analysis of PI and enlargement of the DIP-APCI-FTICR spectrum of PI at the nominal mass (b) *m/z* 545 and (c) *m/z* 560 showing different identified species.

V. Application on UV irradiated PB and PI

Polymers are ultimately susceptible to chemical degradation under exposure to various conditions of commonly encountered environments. Other than being subjected to high energy or aggressive conditions, a large number of polymers will eventually experience slow chemical degradation. The chemical changes which occur during such degradation require further investigations as these polymers are involved in many aspects of human life. An understanding of the basic chemical mechanisms involved in the degradation process is therefore significant. Usually, polymers in the state of their end-use are not pure materials. Some substances are added which can alter the chemical properties of the polymer. The polymer also may contain small amounts of monomer, entrapped during the polymerization process. These added substances and impurities participate in the slow chemical degradation of the polymer and add to its complexity.

Degradation may be initiated in several ways. In the case of rubber, deterioration is caused by exposure to light, oxygen and heat resulting in cracking, charring and color fading. In fact, absorption of ultraviolet radiation or thermal energy can lead to rupture of weak bonds. This is often followed by formation of new bonds to give an alteration of the original polymer structure. The presence of oxygen, water and atmospheric pollutants can alter these processes and lead to the formation of new types of chemical groups. Bond-breaking processes may occur in polymer backbone bonds to lower the average length of the polymer chains and/or in pendant group bonds leading to the emission of small molecules. Bond-making processes between chains give crosslinked material of increased molecular weight and rigidity.

It is important to realize that the basic processes involved in degradation of common polymers are reasonably well determined, however, the present understanding, in general, is insufficiently advanced in order that predictions can be made of the extent of degradation and the levels of products under typical environmental exposures.

The previous polymers, PB and PI, in *E* and *Z* configurations were irradiated as thin films by UV at 365 nm in conditions of microplastic ageing. Following irradiation, the optimized cross-metathesis reaction was applied and the obtained products were analyzed by FT-ICRS MS, ASAP-MS and IMS-MS

V.1. Irradiation procedure

The previous polymers, PB and PI, in *E* and *Z* configurations were irradiated as thin films by UV at 365 nm overnight using a UV LED floodlight 50W in conditions of microplastic ageing. Following irradiation, the optimized cross-metathesis reaction was applied and the obtained products were analyzed by FT-ICRS MS, ASAP-MS and IMS-MS

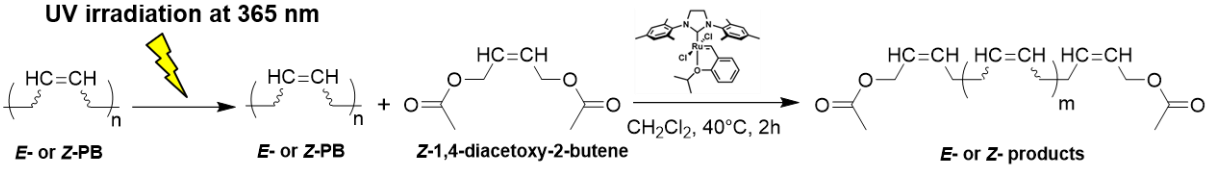

Figure 101. Cross-metathesis reaction of PB and PI after UV irradiation

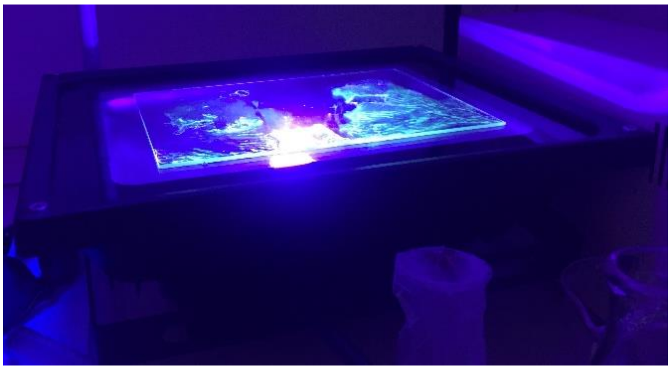

Figure 102. UV LED floodlight 50 W

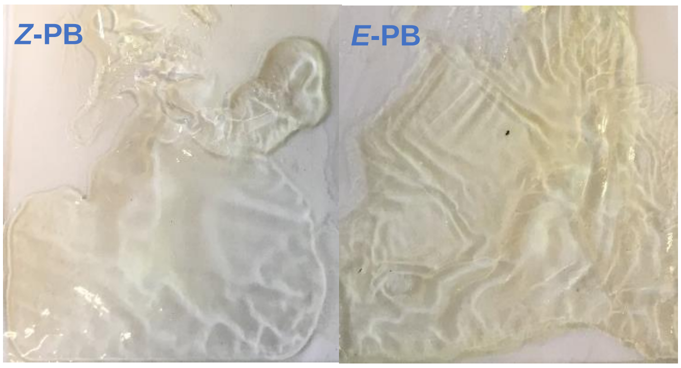

Figure 103. *Z*- and *E*-PB films after UV irradiation

V.2. Case of irradiated commercial polybutadiene

After UV irradiation, (*E*- and *Z*-) PB were subjected to the cross-metathesis reaction using the second-generation Hoveyda-Grubbs catalyst and Z-1,4-acetoxy-2-butene as chain transfer agent and dichloromethane as solvent.

FT-ICR ultra-high-resolution mass spectra were first recorded for both polymers and are shown in Figure 104. For both (*E* or *Z*) PB, the major family of depolymerized products previously identified has almost disappeared and the masses in the spectrum shifted towards the cross-linked species. In the case of *Z*-PB, the five first signals of the previous family can be seen on the spectrum, while for *E*-PB, only the first three signals appear. We should note that signals of newly appeared cross-linked products are also separated by 54.0464 Da in average corresponding to the repeating unit C_4H_6.

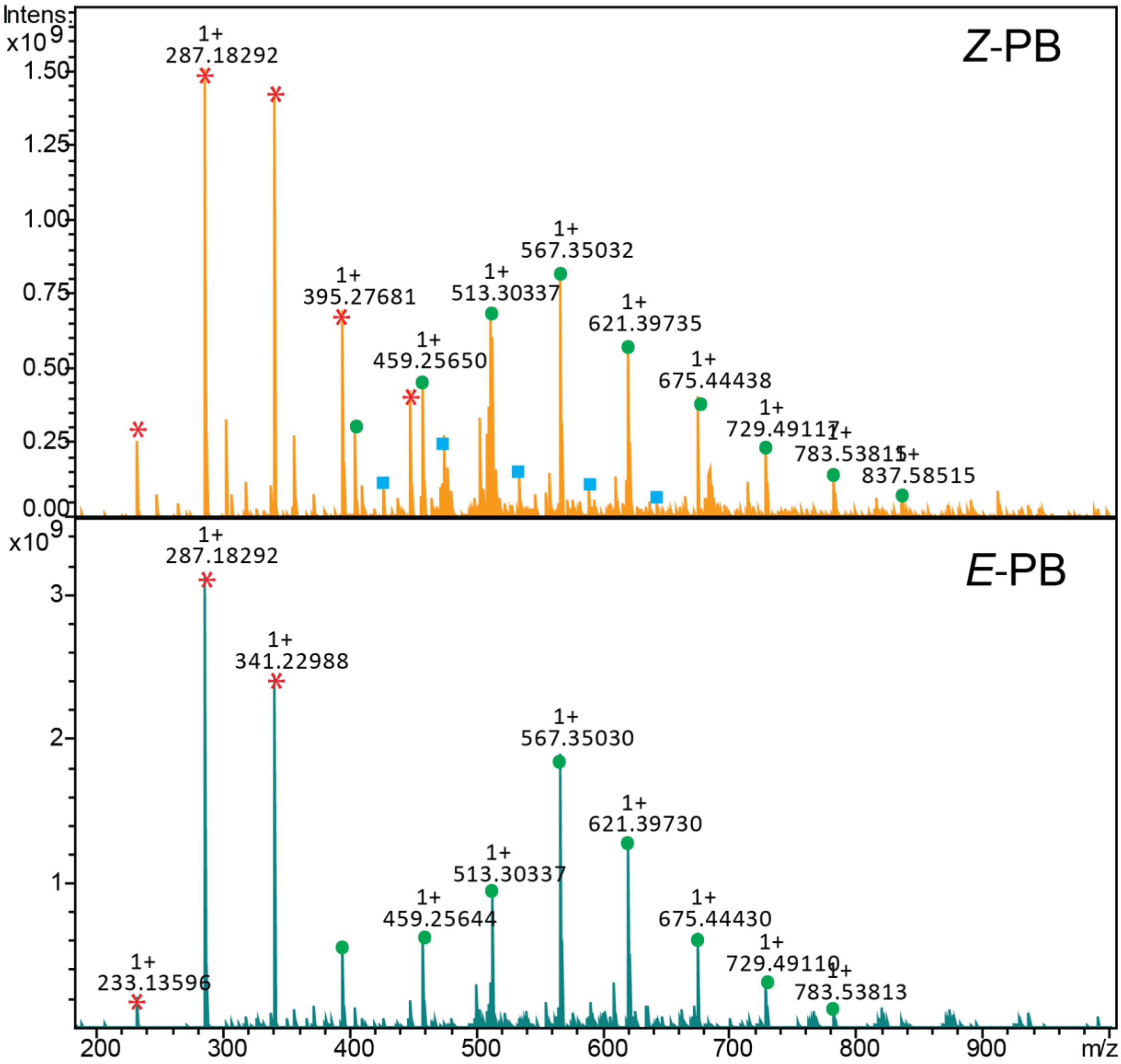

Figure 104. ESI (+) FT-ICR MS of depolymerized *E*- and *Z*-PB after UV irradiation

Three families of compounds were identified in the mass spectra of *E* and *Z*-PB. The first family (red) $[(C_6H_9)O_2]_2 + (C_4H_6)_n + {}^7Li^+$, represents a simple polymeric chain of PB depolymerized with acetoxy end chains. The second family (blue) $[(C_6H_9)O_2]_3 + C_2H_3 + (C_4H_6)_n + (C_4H_6)_m + {}^7Li^+$, consists of three chains of polybutadiene reticulated by a CH group. The third family (green) $[(C_6H_9)O_2]_4 + (C_4H_6)_n + {}^7Li^+]$, is the major family formed of three chains of polybutadiene and one saturated chain reticulated by a carbon atom.

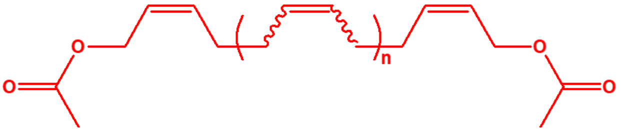

Theoretical ***m/z*** **[M+Li]$^+$**	**Experimental** ***m/z*** **[M+Li]$^+$**	**Error** **(ppm)**	**Monomers (n)**	**Formula**	**DBE**
233.135964	233.135955	-0.04	1	$C_{12}H_{18}O_4$	4
287.182914	287.182921	0.02	2	$C_{16}H_{24}O_4$	5
341.229864	341.229879	0.04	3	$C_{20}H_{30}O_4$	6
395.276814	395.276812	-0.005	4	$C_{24}H_{36}O_4$	7
449.323765	449.323799	0.07	5	$C_{28}H_{42}O_4$	8

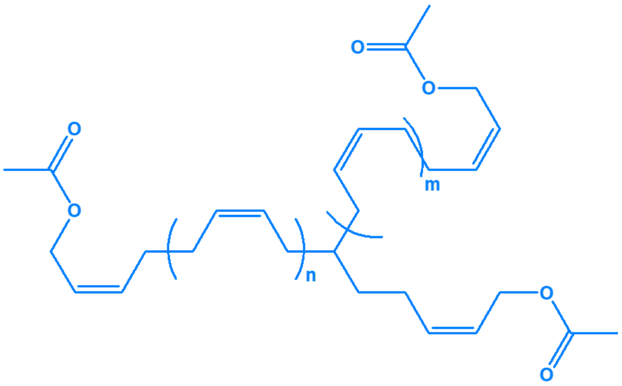

Theoretical ***m/z*** **[M+Li]$^+$**	**Experimental** ***m/z*** **[M+Li]$^+$**	**Error** **(ppm)**	**Monomers (n)**	**Formula**	**DBE**
427.266644	427.266628	-0.03	1	$C_{24}H_{36}O_6$	7
481.313594	481.313580	-0.03	2	$C_{28}H_{42}O_6$	8
535.360544	535.360496	-0.09	3	$C_{32}H_{48}O_6$	9
589.407494	589.407501	0.01	4	$C_{36}H_{54}O_6$	10
643.454445	643.454555	0.17	5	$C_{40}H_{60}O_6$	11

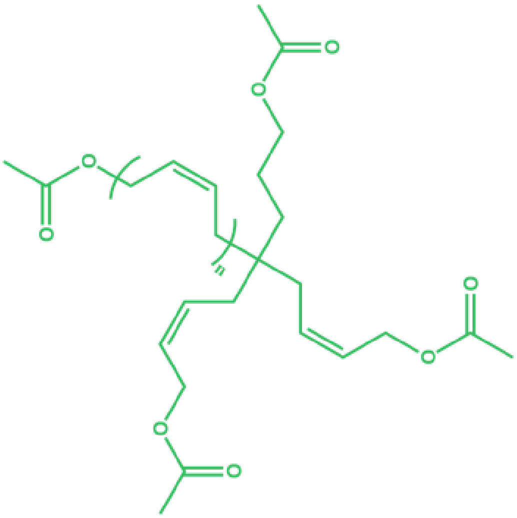

Theoretical ***m/z* [M+Li]$^+$**	**Experimental** ***m/z* [M+Li]$^+$**	**Error (ppm)**	**Monomers (n)**	**Formula**	**DBE**
405.209523	405.209558	0.08	0	$C_{20}H_{30}O_8$	6
459.256473	459.256504	0.07	1	$C_{24}H_{36}O_8$	7
513.303423	513.303389	-0.06	2	$C_{28}H_{42}O_8$	8
567.350373	567.350337	-0.06	3	$C_{32}H_{48}O_8$	9
621.397324	621.397374	0.08	4	$C_{36}H_{54}O_8$	10
675.444274	675.444413	0.2	5	$C_{40}H_{60}O_8$	11
729.491224	729.491210	-0.1	6	$C_{44}H_{66}O_8$	12
783.538174	783.538203	0.09	7	$C_{48}H_{72}O_8$	13
837.585124	837.585212	0.02	8	$C_{52}H_{78}O_8$	14
891.632075	891.632185	0.007	9	$C_{56}H_{84}O_8$	15
945.679025	945.679046	0.1	10	$C_{60}H_{90}O_8$	16

In a second stage, the stereochemistry of the cross-linked products was studied by ion mobility spectrometry mass spectrometry (IMS-MS). For this reason, different *m/z* were chosen form the major reticulated family and their drift times were recorded and compared. The *m/z* values are: 567.3503, 621.3973, 675.4443, 729.4911, 783.5381, 837.5851 and 891.6321. In all the cases, the same drift times were recorded for both *E* and *Z*-PB which proves that the double bond geometry is completely lost after UV irradiation (Figure 105, 106 and 107).

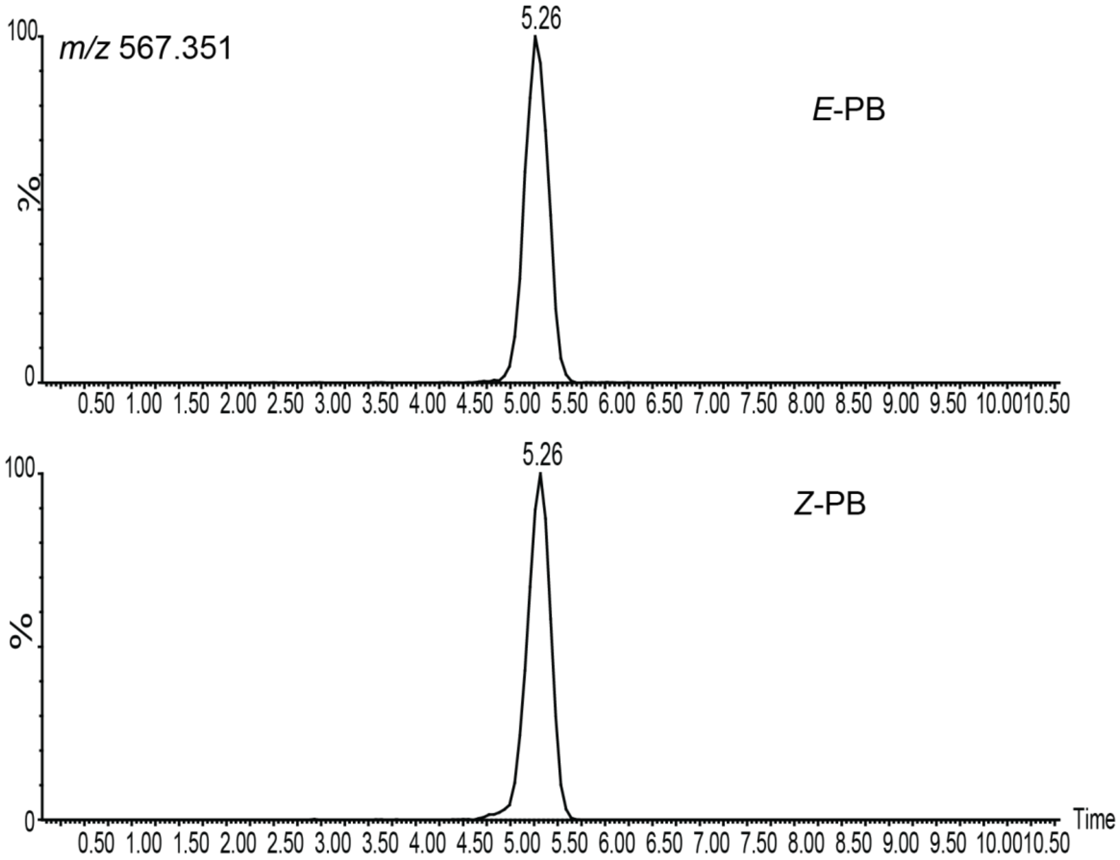

Figure 105. Ion mobility profiles of *m/z* 567.351 in the case of depolymerized *E*- and *Z*-PB after UV irradiation

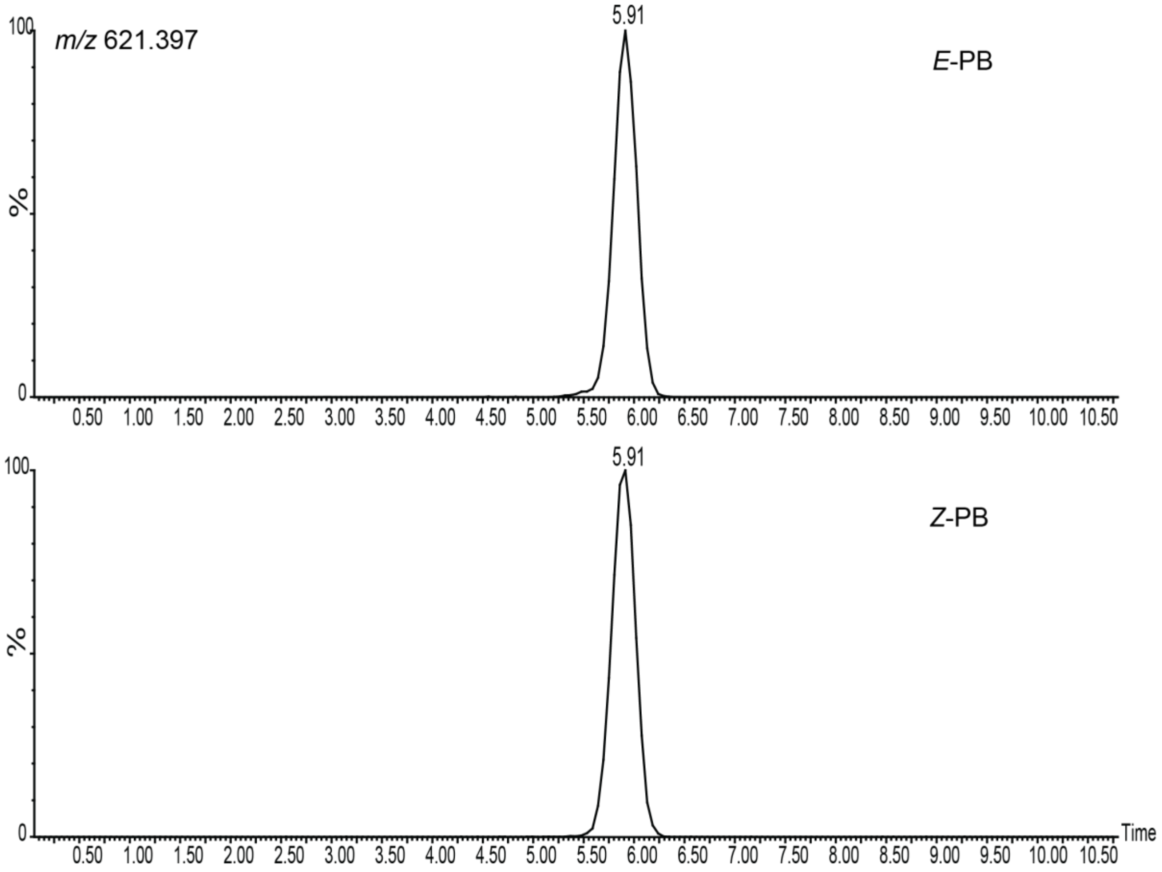

Figure 106. Ion mobility profiles of *m/z* 621.397 in the case of depolymerized *E*- and *Z*-PB after UV irradiation

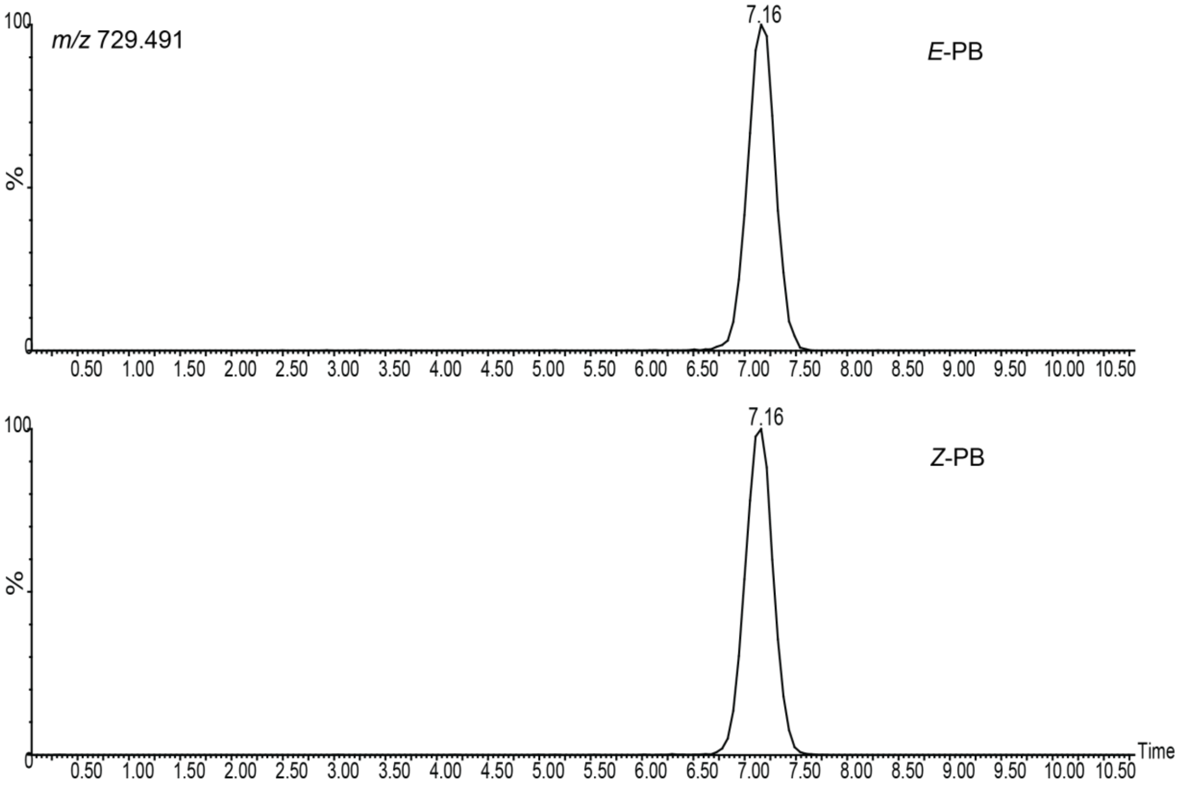

Figure 107. Ion mobility profiles of *m/z* 729.491 in the case of depolymerized *E*- and *Z*-PB after UV irradiation

Finally, PB in *E* and *Z* configurations were analyzed by atmospheric solid analysis probe coupled to ion mobility-mass spectrometry on a Q-TOF instrument (ASAP-MS). The initial analysis showed the presence of additives and stabilizers in both polymers (Figure 109) The highest *m/z* value at 514.4269 in *E*-PB corresponds to the molecular ion of an antioxidant, *Irganox 1076* ($C_{35}H_{62}O_3$) which was fragmented and lost a hydroxyl group. The peak at m/z 662.4729 could be assigned to oxidized *Irgafos 168*. The highest peak in *Z*-PB at *m/z* 530.4921 corresponds to the *Irganox 1076.* (figure 108). These additives are used to protect the polymer materials from degradation during processing or outdoor exposure to oxygen or UV light. As seen in the spectra of PB, several classes of additives can be used such as antioxidant or UV stabilizers.

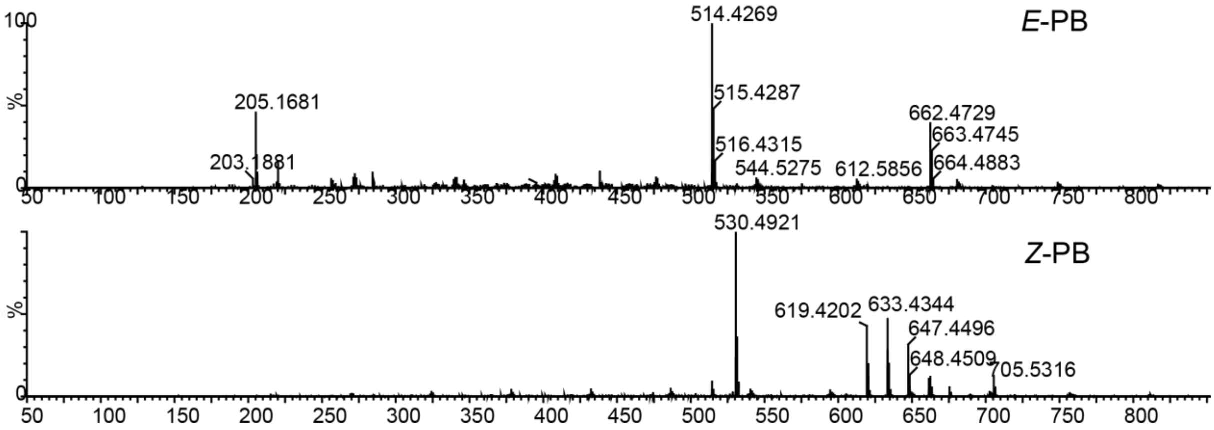

Figure 108. Additives and stabilizers found in *E*- and *Z*-PB after pyrolysis

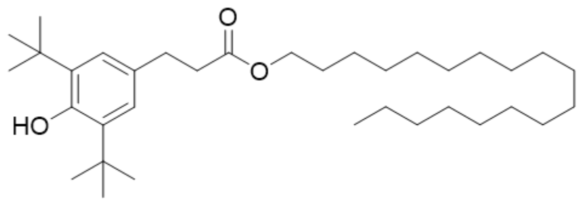

Figure 109. ***Irganox 1760***

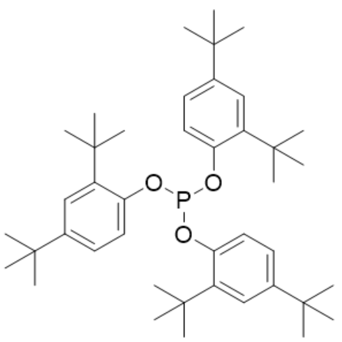

Figure 110. ***Irgafos 168***

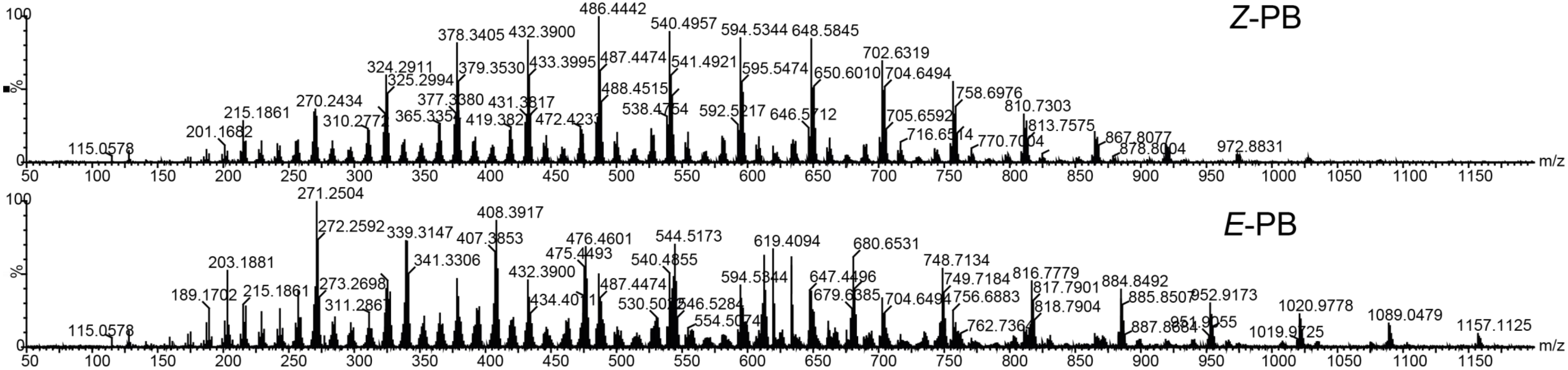

Figure 111. Full ASAP mass spectra of UV irradiated *E*- and *Z*-PB

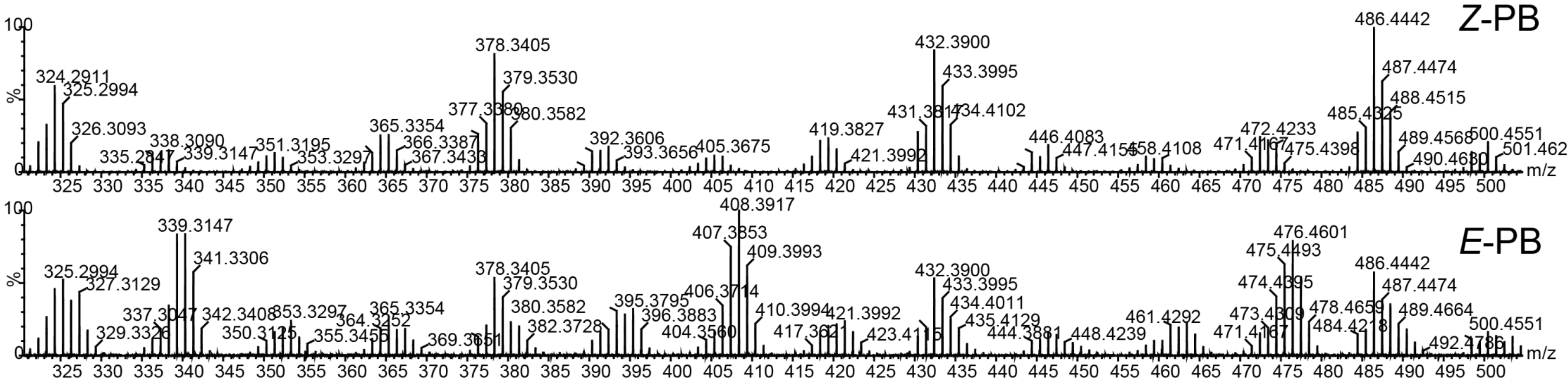

Figure 112. Expanded view of the ASAP mass spectra of UV irradiated *E*- and *Z*-PB

The full ASAP mass spectra showed radical cation series separated by 54.04 Da for *E*- and *Z*-PB which correspond to C_4H_6 repeating units (Figure 111). *E*- and *Z*-polymers yielded different mass spectra which was not the case before UV irradiation. An expanded view for *E*-PB and *Z*-PB (Figure 112) allowed the identification of different ion distributions: I: $M_w = 54.046n$; II: $M_w = 54.046n + 12.000$ (C); III: $M_w = 54.046n + 14.015$ (CH_2); IV: $M_w = 54.046n + 28.031$ (C_2H_4); V: $M_w = 54.046n + 40.031$ (C_3H_4); VI: $M_w = 54.046n + 42.046$ (C_3H_6); VII: $M_w = 54.046n + 15.994$ (O). Distribution I was detected as the most intense in the case of *Z*-PB, however, it was distribution III the most intense in the spectrum of *E*-PB. This proves that the microstructure of *E*-PB was altered following irradiation by UV by forming new bonds and that *Z*-PB is more resistant to degradation.

V.3. Case of irradiated commercial polyisoprene

After UV irradiation, (*E*- and *Z*-) PI were subjected to the cross-metathesis reaction using the second-generation Hoveyda-Grubbs catalyst and *Z*-1,4-acetoxy-2-butene as chain transfer agent and dichloromethane as solvent.

E-PI formed a very insoluble plastic-like film that was not depolymerized by cross-metathesis even after several tries. On the other hand, the reaction was successful with irradiated *Z*-PI.

FT-ICR ultra-high-resolution mass spectrum was recorded for *Z*-PI and is shown in Figure 113. A very complex spectrum was obtained in which multiple new compound families were present. Surprisingly, the major family of depolymerized products previously identified has completely disappeared and the masses in the spectrum shifted towards the cross-linked species. We should note that signals of newly appeared cross-linked products are also separated by 68.0620 Da corresponding to the monomer C_6H_8.

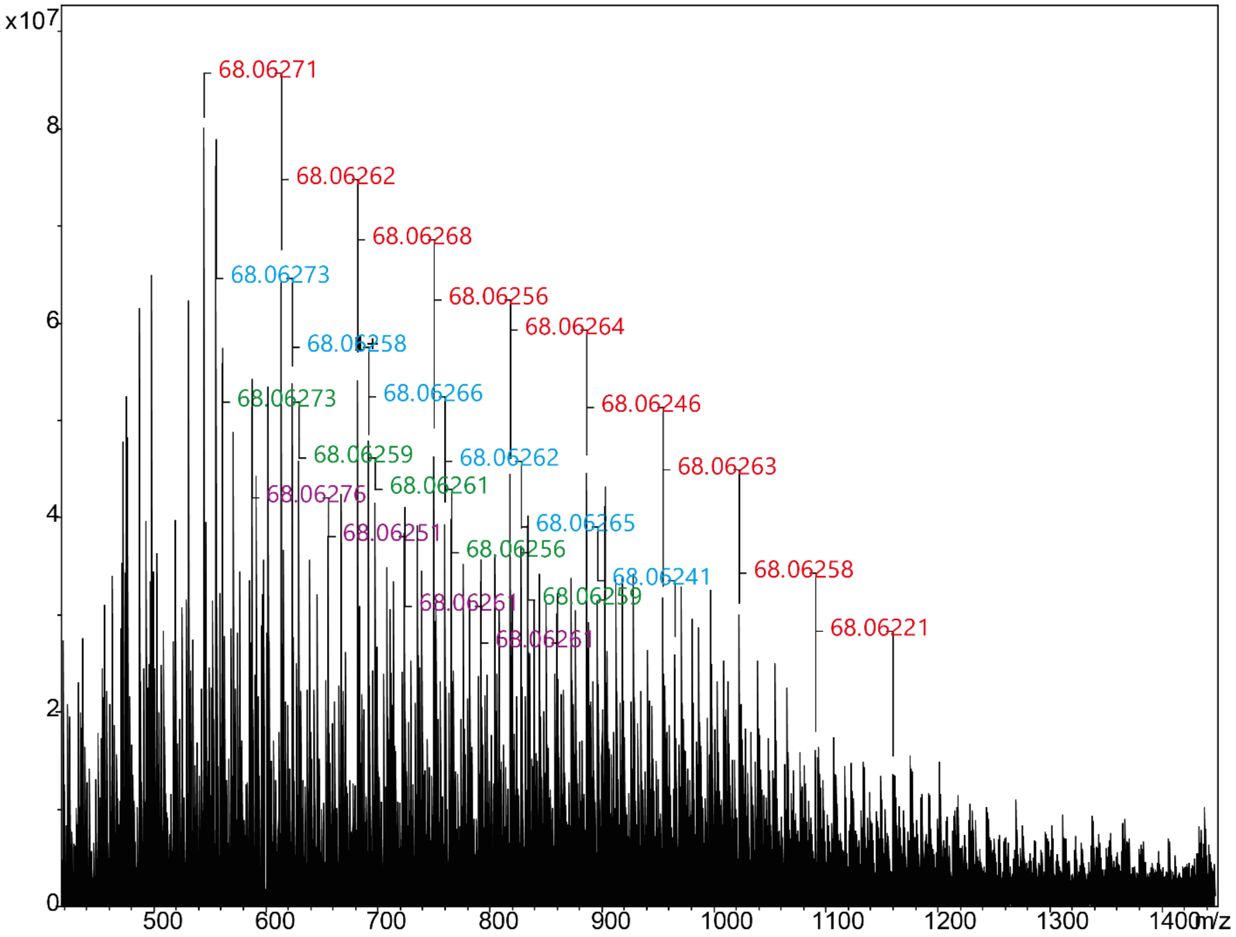

Figure 113. ESI (+) FT-ICR MS of depolymerized *Z*-PI after UV irradiation

A very high number of reticulated families of compounds were identified in the mass spectra of UV irradiated *Z*-PI. Here, we will show the four most intense groups. The first family (red) [$(C_8H_{12})\ O_4 + (C_5H_8)_n + C_2H_4 + {}^7Li^+$], represents a simple polymeric chain of PI depolymerized with acetoxy end chains and with an additional C_2H_4. The second family (blue) [$(C_7H_{12})O_3 + (C_5H_8)_n - H_2 + {}^7Li^+$, consists of one depolymerized polyisoprene chain with one acetoxy and one methoxy end chains and with an additional unsaturation. The third family (green) [$(C_8H_{12})\ O_4 + (C_5H_8)_n + C_2H_4O + {}^7Li^+$] is formed by the addition of a C_2H_4O molecule increasing the total number of oxygen in the molecule to five. The last family (violet) [$(C_8H_{12})\ O_4 + (C_5H_8)_n + C_4H_6O + {}^7Li^+$] corresponds to the previous family (green) with addition of a C_2H_2 molecule.

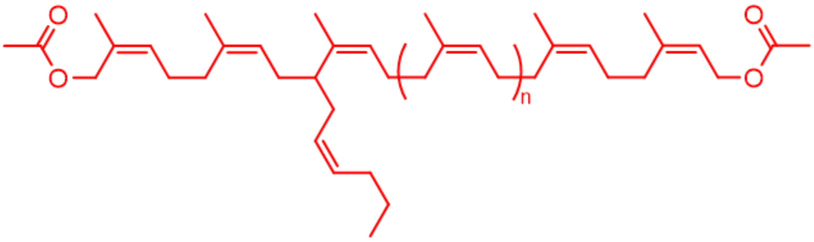

Theoretical m/z $[M+Li]^+$	Experimental m/z $[M+Li]^+$	Error (ppm)	Monomers (n)	Formula	DBE
275.182914	275.182881	-0.1	1	$C_{15}H_{24}O_4$	4
343.245514	343.245484	-0.09	2	$C_{20}H_{32}O_4$	5
411.308115	411.308028	-0.2	3	$C_{25}H_{40}O_4$	6
479.370715	479.370645	-0.1	4	$C_{30}H_{48}O_4$	7
547.433315	547.433191	-0.2	5	$C_{35}H_{56}O_4$	8
615.495915	615.495904	-0.02	6	$C_{40}H_{64}O_4$	9
683.558516	683.558522	0.01	7	$C_{45}H_{72}O_8$	10
751.621116	751.621200	-0.03	8	$C_{50}H_{80}O_4$	11
819.683716	819.683759	-0.08	9	$C_{55}H_{88}O_4$	12
887.746316	887.746399	-0.05	10	$C_{60}H_{96}O_4$	13
955.808917	955.808863	-0.2	11	$C_{65}H_{104}O_4$	14
1023.871517	1023.871498	-0.1	12	$C_{70}H_{112}O_4$	15
1091.934117	1091.934082	-0.1	13	$C_{75}H_{120}O_4$	16
1159.996717	1159.996291	-0.5	14	$C_{80}H_{128}O_4$	17

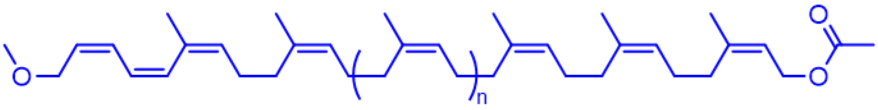

Theoretical m/z $[M+Li]^+$	Experimental m/z $[M+Li]^+$	Error (ppm)	Monomers (n)	Formula	DBE
557.454051	557.453959	-0.1	7	$C_{37}H_{58}O_3$	9
625.516651	625.516691	0.06	8	$C_{42}H_{66}O_3$	10
693.579251	693.579265	0.02	9	$C_{47}H_{74}O_3$	11
761.641851	761.641924	-0.05	10	$C_{52}H_{82}O_3$	12
829.704452	829.704543	-0.03	11	$C_{57}H_{90}O_3$	13
897.767052	897.767194	0.01	12	$C_{62}H_{98}O_3$	14
965.829652	965.829605	-0.2	13	$C_{67}H_{106}O_3$	15

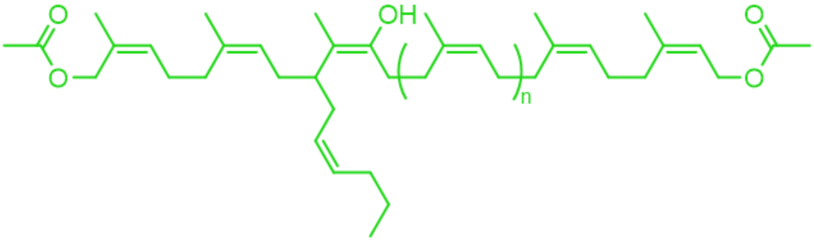

Theoretical *m/z* [M+Li]$^+$	Experimental *m/z* [M+Li]$^+$	Error (ppm)	Monomers (n)	Formula	DBE
359.240429	359.240368	-0.1	2	$C_{20}H_{32}O_5$	5
427.303029	427.303004	-0.06	3	$C_{25}H_{40}O_5$	6
495.365630	495.365588	-0.08	4	$C_{30}H_{48}O_5$	7
563.428230	563.428123	-0.2	5	$C_{35}H_{56}O_5$	8
631.490830	631.490852	0.03	6	$C_{40}H_{64}O_5$	9
699.553430	699.553440	-0.1	7	$C_{45}H_{72}O_5$	10
767.616031	767.616051	-0.1	8	$C_{50}H_{80}O_5$	11
835.678631	835.678614	-0.1	9	$C_{55}H_{88}O_5$	12
903.741231	903.741200	-0.1	10	$C_{60}H_{96}O_5$	13

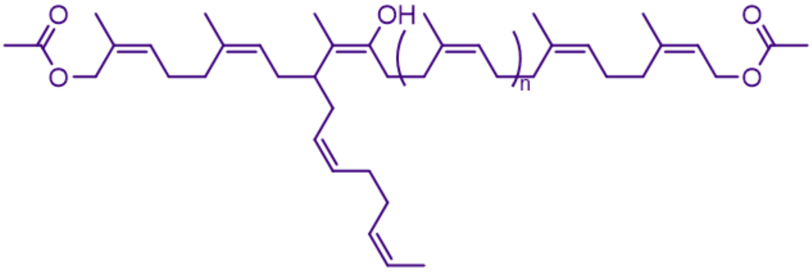

Theoretical *m/z* [M+Li]$^+$	Experimental *m/z* [M+Li]$^+$	Error (ppm)	Monomers (n)	Formula	DBE
589.443880	589.443823	-0.09	5	$C_{37}H_{58}O_5$	9
657.506480	657.506577	0.1	6	$C_{42}H_{66}O_5$	10
725.569080	725.569087	-0.1	7	$C_{47}H_{74}O_5$	11
793.631681	793.631701	-0.1	8	$C_{52}H_{82}O_5$	12
861.694281	861.694315	-0.09	9	$C_{57}H_{90}O_5$	13
929.756881	929.756928	-0.08	10	$C_{62}H_{98}O_5$	14

We investigated then the stereochemistry of the obtained cross-linked products by ion mobility spectrometry mass spectrometry (IMS-MS). Ions were chosen from the different families and their drift times were recorded and compared. The studied *m/z* are: 343.2483, 359.2403, 411.3114, 965.8296, 761.6419 and 427.3030. In all the cases, the same drift times were recorded for both *E* and *Z*-PI which proves that the double bond geometry is also completely lost after UV irradiation (Figure 114)

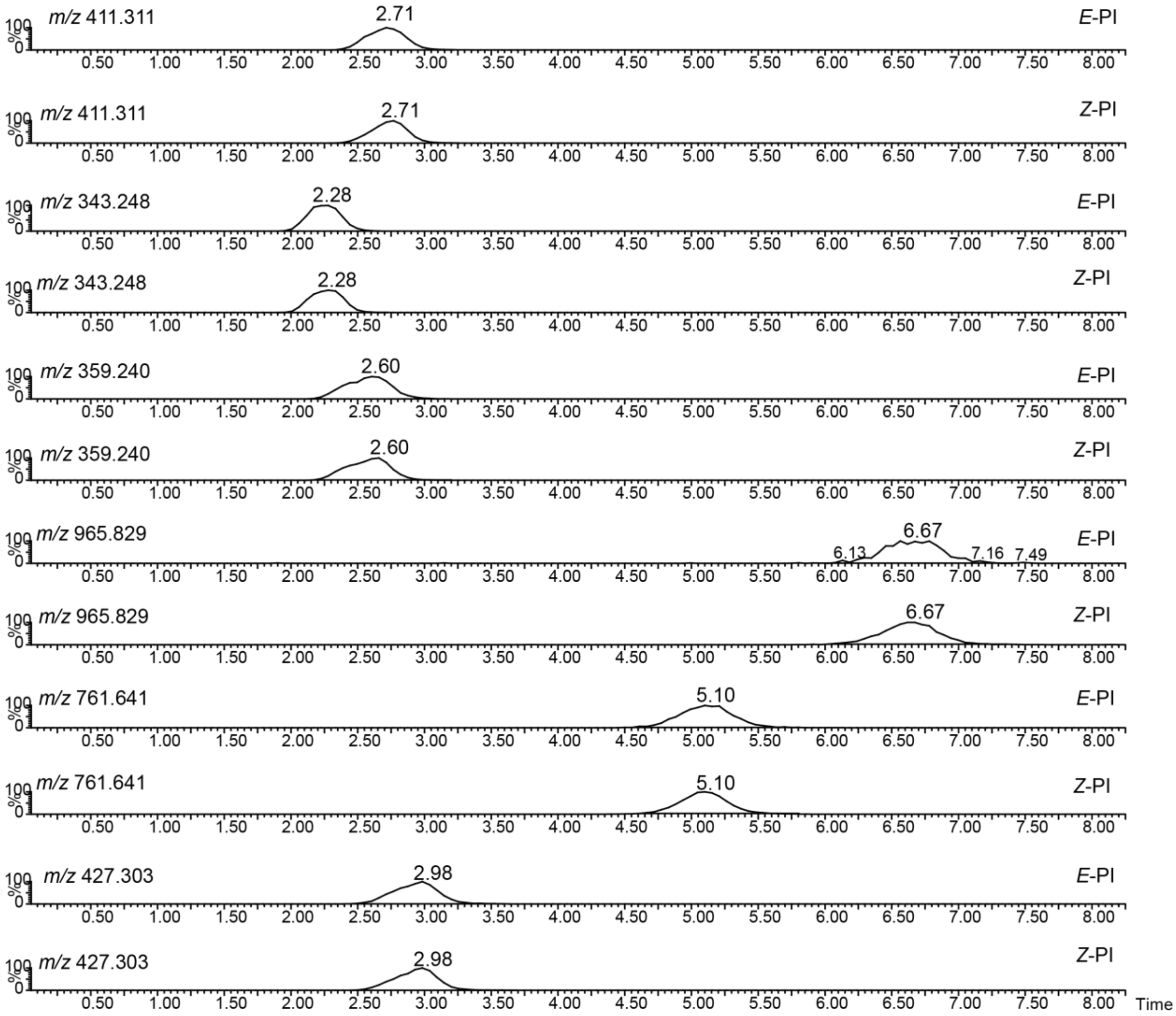

Figure 114. Ion mobility profile of multiple extracted ions from depolymerized *E*- and *Z*- PI following UV irradiation

Similar to PB, *E* and *Z*- PI were finally analyzed by atmospheric solid analysis probe coupled to ion mobility-mass spectrometry on a Q-TOF instrument (ASAP-MS). Only *E*-PI contained additives and stabilizers and this is due to the fact that *Z*-PI is a pure natural polymer. The highest peak in *E*-PI at *m/z* 530.4921 also corresponds to the *Irganox 1076.* (figure 115).

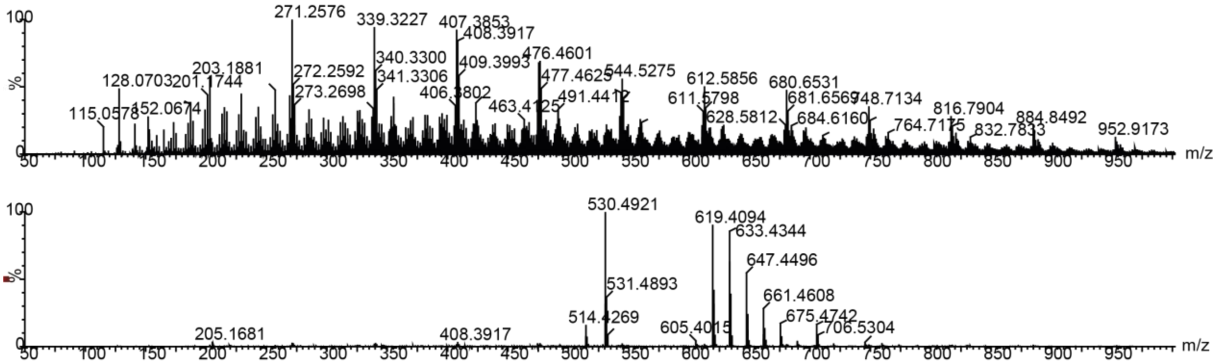

Figure 115. Additives and stabilizers found in *E*- and *Z*-PI after pyrolysis

In the case of *E*-PI and *Z*-PI, both configurations produced the same mass spectrum, however, *Z*-PI spectrum was much more complex (Figure 116). The expanded view allowed the identification of the following distributions: I: $M_w = 68.062n$; II: $M_w = 68.062n + 12.000$ (C); III: $M_w = 68.062n + 14.015$ (CH_2); IV: $M_w = 68.062n + 28.031$ (C_2H_4); V: $M_w = 68.062n + 40.031$ (C_3H_4); VI: $M_w = 68.062n + 42.046$ (C_3H_6); VII: $M_w = 68.062n + 56.062$ (C_4H_8); VIII: $M_w = 68.062n + 15.994$ (O). Distribution I was detected with the highest intensity and extended on the entire mass range (Figure 117). The complexity of the mass spectrum of *Z*-PI proves the variety of products produced from the degradation of natural rubber. On the other, synthetic polyisoprene is very resistant to environmental conditions as the spectrum obtained of *E*-PI after irradiation is very similar to that before irradiation.

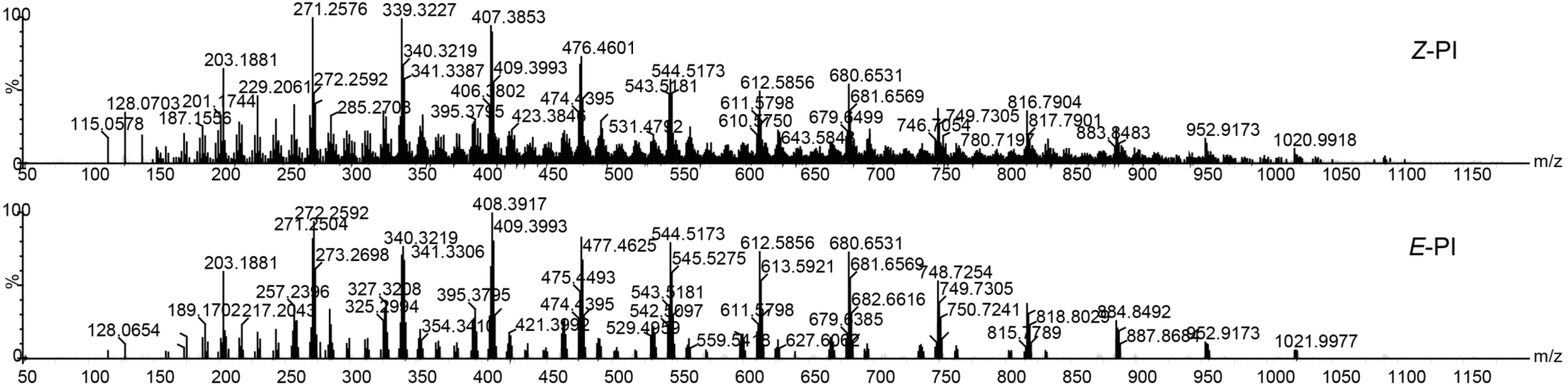

Figure 116. Full ASAP mass spectra of UV irradiated *E*- and *Z*-PB

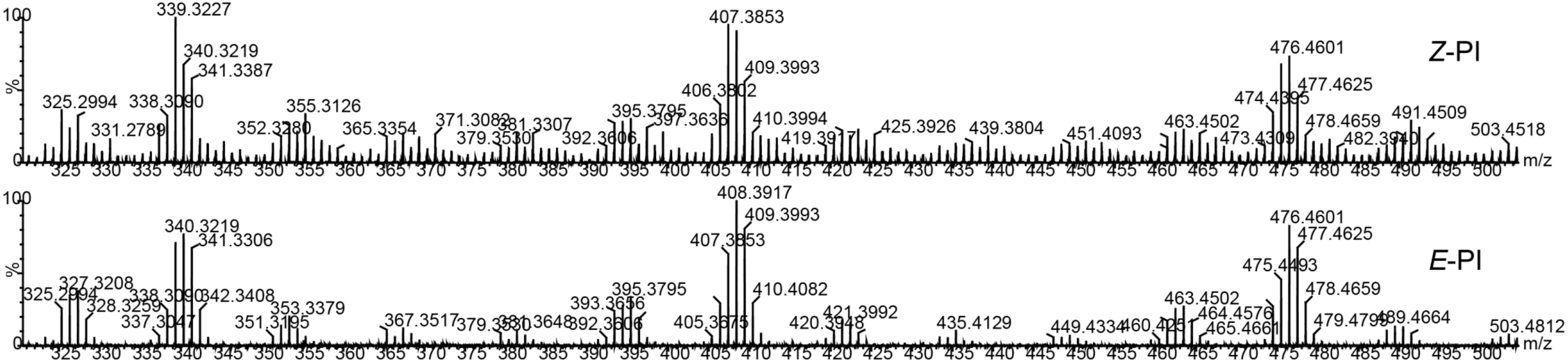

Figure 117. Expanded view of the ASAP mass spectra of UV irradiated *E*- and *Z*-PI

VI. Application on real-world samples

Synthetic polyisoprene films are found for example in medical examination gloves and in condoms. Due to covid-19 pandemic only the latter were available for this test. Two types of polyisoprene condoms were studied. The first type is based on non-lubricated natural polyisoprene. The second type is based on synthetic polyisoprene to which lubricants were added. The optimized depolymerization reaction was carried out on these types of condoms in native form after lubricant removal and after photo-weathering. We must point out that additives were freed by depolymerization and that they were consumed during photo-weathering.

VI.1. Non-lubricated natural polyisoprene condoms

In the case of this type of condoms, no washing step was needed and the depolymerization reaction could be directly applied before and after UV irradiation. The obtained products were analyzed by FT-ICR MS (Figure 118). We can notice that in his native form, natural polyisoprene condom was successfully depolymerized giving a family of polyisoprene chains with acetoxy chain ends. This family can be represented by $[(C_8H_{12})\ O_4 + (C_5H_8)_n + {}^7Li^+]$. However, after applying weathering conditions, the original compounds family completely disappeared and a new group of molecules formed from reticulated polyisoprene chains appeared. This new group can be represented by $[((C_8H_{12})\ O_4)_2 + (C_5H_8)_n + {}^7Li^+]$.

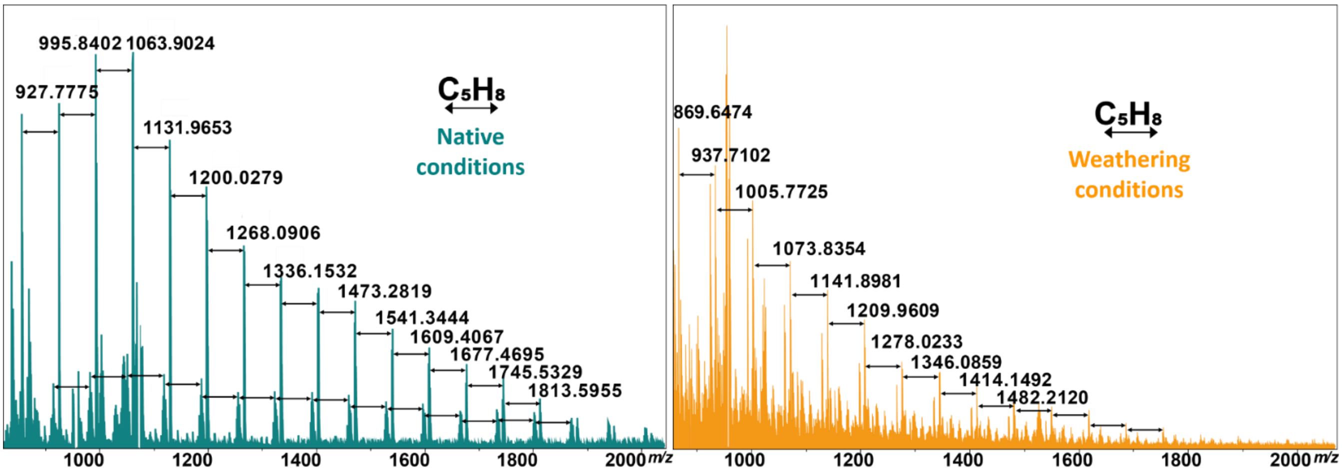

Figure 118. ESI (+) FT-ICR MS of depolymerized natural polyisoprene condoms in native and weathering conditions

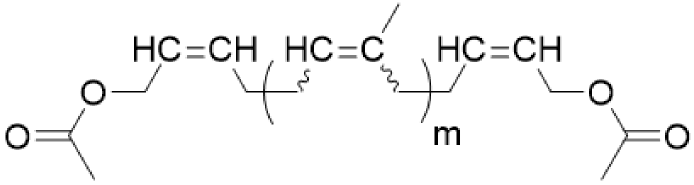

Table 14: Identified family of depolymerized natural PI condoms under native conditions

Theoretical *m/z* **[M+Li]$^+$**	**Experimental** *m/z* **[M+Li]$^+$**	**Error (ppm)**	**Monomers (m)**	**Formula**	**DBE**
927.777617	927.777478	-0.3	11	$C_{63}H_{100}O_4$	14
995.840217	995.840297	-0.06	12	$C_{68}H_{108}O_4$	15
1063.902817	1063.902669	-0.3	13	$C_{73}H_{116}O_4$	16
1131.965417	1131.965495	-0.08	14	$C_{78}H_{124}O_4$	17
1200.028018	1200.028119	-0.06	15	$C_{83}H_{132}O_4$	18
1268.090618	1268.091180	0.3	16	$C_{88}H_{140}O_4$	19
1336.153218	1336.153861	0.3	17	$C_{93}H_{148}O_4$	20
1404.215818	1404.216847	0.5	18	$C_{98}H_{156}O_4$	21
1472.278419	1472.279644	0.6	19	$C_{103}H_{164}O_4$	22
1540.341019	1540.342720	0.9	20	$C_{108}H_{172}O_4$	23
1608.403619	1608.405185	0.8	21	$C_{113}H_{180}O_4$	24
1676.466219	1676.467968	0.8	22	$C_{118}H_{188}O_4$	25
1744.528820	1744.531225	1	23	$C_{123}H_{196}O_4$	26
1812.591420	1812.593095	0.8	24	$C_{128}H_{204}O_4$	27

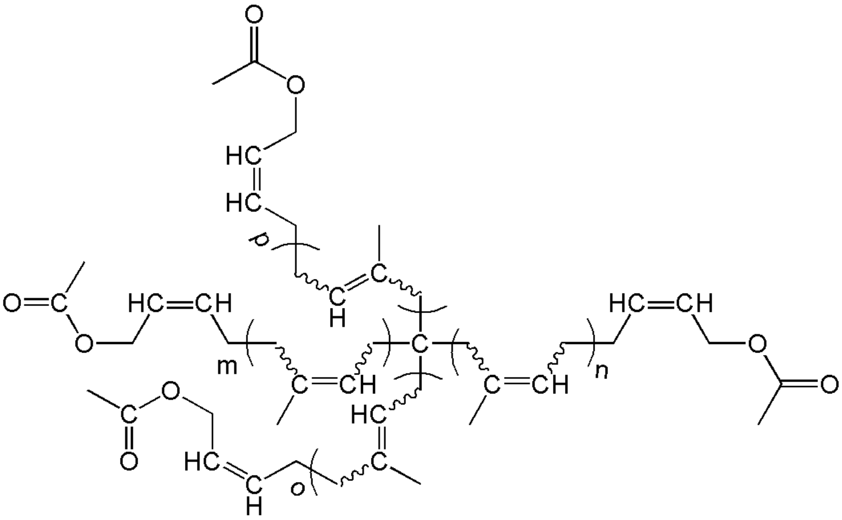

Table 15: Identified family of depolymerized natural PI condoms under weathering conditions

Theoretical ***m/z*** **[M+Li]$^+$**	**Experimental** ***m/z*** **[M+Li]$^+$**	**Error (ppm)**	**Monomers**	**Formula**
937.710325	937.709939	-0.5	10	$C_{59}H_{94}O_8$
1005.772925	1005.772680	-0.3	11	$C_{64}H_{102}O_8$
1073.835525	1073.535159	-0.4	12	$C_{69}H_{110}O_8$
1141.898126	1141.898224	-0.05	13	$C_{74}H_{118}O_8$
1209.960726	1209.960751	-0.1	14	$C_{79}H_{126}O_8$
1278.023326	1278.023539	0.03	15	$C_{84}H_{134}O_8$
1346.085926	1346.086314	0.1	16	$C_{89}H_{142}O_8$
1414.148527	1414.149480	0.5	17	$C_{94}H_{150}O_8$
1482.211127	1482.212006	0.4	18	$C_{99}H_{158}O_8$

VI.2. Lubricated synthetic polyisoprene condoms

This type of condoms requires a washing step before the depolymerization reaction could be directly applied. The presence of silicone-based lubricants will inhibit the activity of the organometallic catalyst and stop the cross-metathesis reaction. However, as much as these condoms were washed with a variety of solvents, lubricants could not be completely removed and the depolymerization reaction did not work. The mass spectrum recorded after depolymerization showed a series of peaks separated by 74.0182 which corresponds to one unit of polydimethylsiloxane (PDMS). On the other hand, by exposing the condoms to UV radiations, additives were consumed during photo-weathering and the depolymerization was successful.

Following analysis by FT-ICR MS, the major family obtained with the highest intensity was similar to that of natural PI condoms [$(C_8H_{12})\ O_4 + (C_5H_8)_n + {}^7Li^+$] (Figure 119). Other families such as the one formed from reticulated polyisoprene chains appeared with very low intensity. This proves that synthetic polyisoprene can resist more efficiently to weathering conditions than natural polyisoprene.

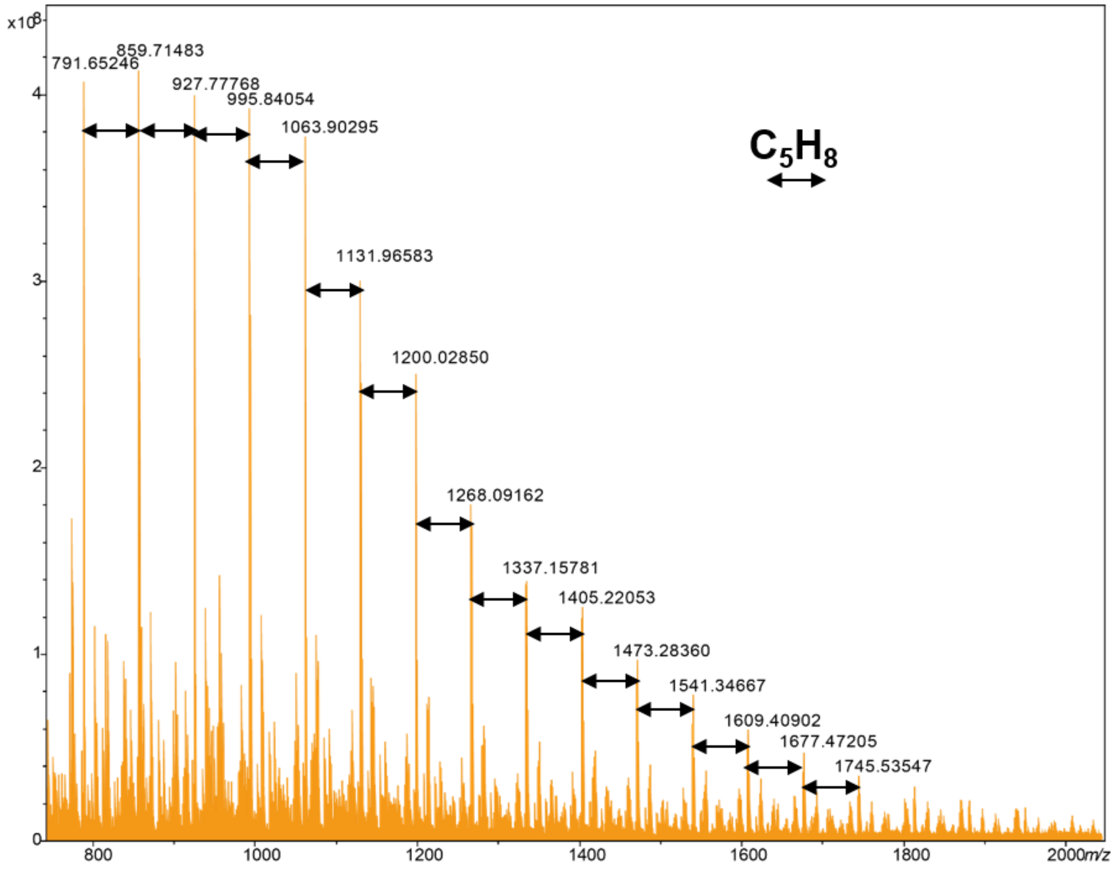

Figure 119. ESI (+) FT-ICR MS of depolymerized synthetic polyisoprene condoms under weathering conditions

VII. Application on industrial polydienes

Industrial samples of hydroxy terminated polydienes (HTPB) were supplied by Cray Valley company. Hydroxyl terminated polybutadiene are the most often modified at the end of their chains in order to add special properties to the polymer which can be used for example in propellers and explosives. These polydienes were studied before and after UV irradiation in order to understand the chemical behavior of the polymer during degradation when a hydroxyl group is added to its chain ends. The same depolymerization reaction was applied on these polymers followed by analysis by FT-ICR high resolution mass spectrometry. The obtained mass spectra showed the presence of over ten families of peaks that are separated by C_4H_8 butadiene unit (Figure 120).

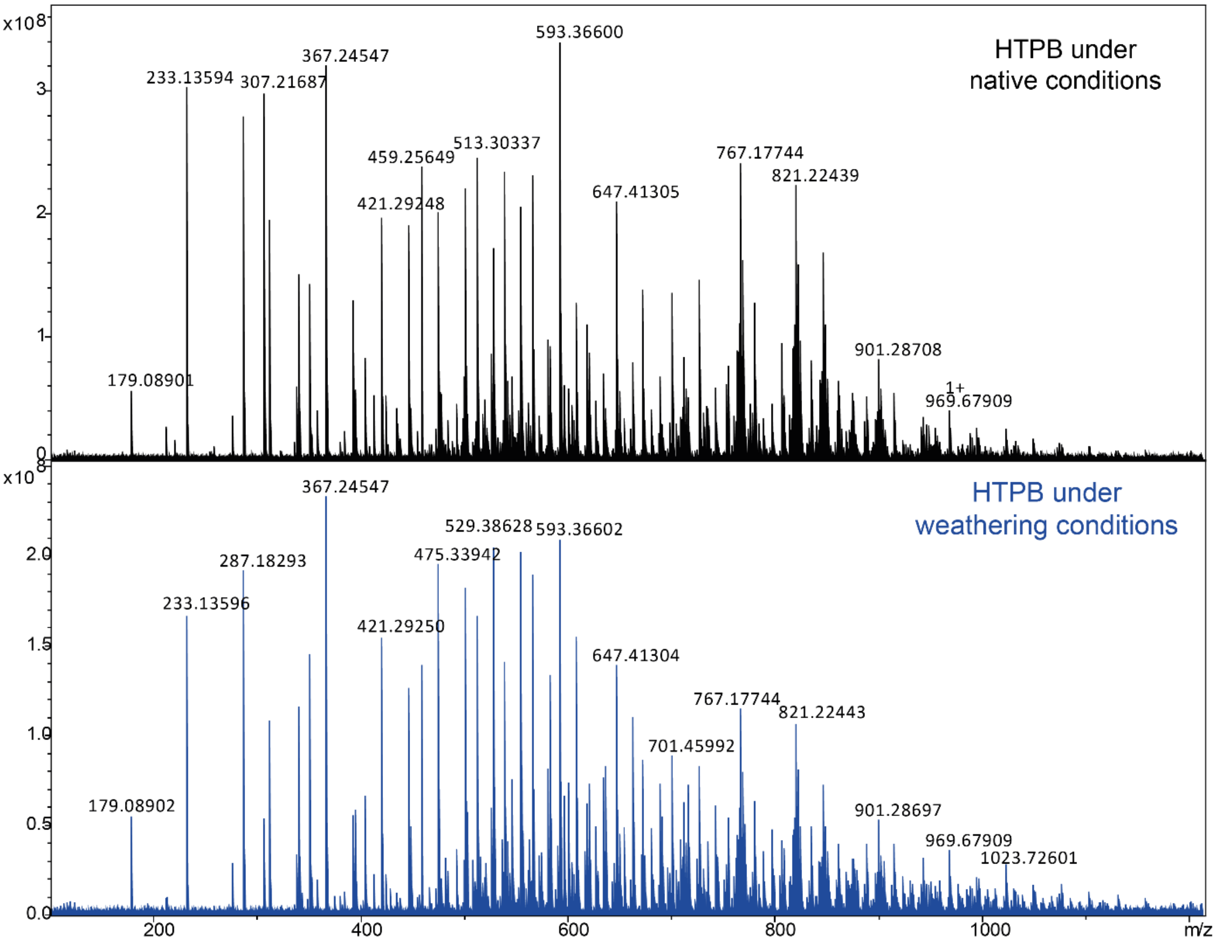

Figure 120. ESI (+) FT-ICR MS of depolymerized HTPB under native and weathering conditions

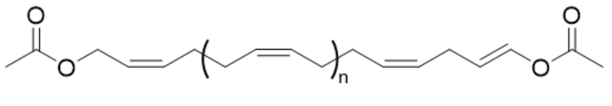			
***m/z* [M+Li]⁺**	**Monomers**	**Formula**	**DBE**
313.1985	3	$C_{18}H_{26}O_4$	6
367.2454	4	$C_{22}H_{32}O_4$	7
421.2924	5	$C_{26}H_{38}O_4$	8
475.3394	6	$C_{30}H_{44}O_4$	9
529.3863	7	$C_{34}H_{50}O_4$	10
583.4332	8	$C_{38}H_{56}O_4$	11
637.4803	9	$C_{42}H_{62}O_4$	12

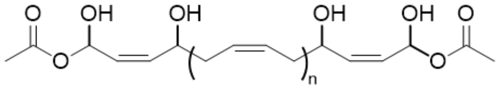			
***m/z* [M+Li]⁺**	**Monomers**	**Formula**	**DBE**
351.1625	3	$C_{16}H_{24}O_8$	5
405.2095	4	$C_{20}H_{30}O_8$	6
459.2564	5	$C_{24}H_{36}O_8$	7
513.3033	6	$C_{28}H_{42}O_8$	8
567.3503	7	$C_{32}H_{48}O_8$	9
621.3974	8	$C_{36}H_{54}O_8$	10
675.4444	9	$C_{40}H_{60}O_8$	11

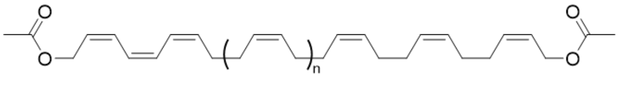			
***m/z* [M+Li]⁺**	**Monomers**	**Formula**	**DBE**
447.3080	6	$C_{28}H_{40}O_4$	9
501.3550	7	$C_{32}H_{46}O_4$	10
555.4019	8	$C_{36}H_{52}O_4$	11
609.4490	9	$C_{40}H_{58}O_4$	12
663.4960	10	$C_{44}H_{64}O_4$	13
717.5428	11	$C_{48}H_{70}O_4$	14

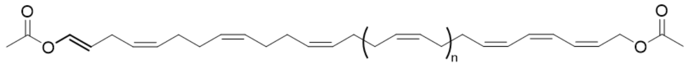			
***m/z* [M+Li]⁺**	**Monomers**	**Formula**	**DBE**
473.3238	5	$C_{30}H_{42}O_4$	10
527.3706	6	$C_{34}H_{48}O_4$	11
581.4176	7	$C_{38}H_{54}O_4$	12
635.4647	8	$C_{42}H_{60}O_4$	13
689.5116	9	$C_{46}H_{66}O_4$	14
743.5584	10	$C_{50}H_{72}O_4$	15

Material and methods

Chemicals

Two samples of PB and two samples of PI were used in this study. *Z*-PB (1,4-PB; 98% *Z*; Mw ~200,000− 300,000 g·mol−1), *E*-PB (1,4-PB; 36% *Z*; 55% E; Mw ~200,000 g·mol−1), *Z*-PI (1,4-PI; 98% *Z*; Mw ~38,000 g·mol−1), and *E*-PI (1,4-PI; 99% *E*; Mw ~35,000 g·mol−1) were purchased from Sigma-Aldrich and used as received. (*Z*)-1,4-Diacetoxy-2- butene (95%), 2,6-dichloro-1,4-benzoquinone (98%), and (1,3-bis-(2,4,6-trimethylphenyl)-2-imidazolidinylidene) dichloro(o-isopropoxyphenylmethylene) ruthenium (Hoveyda−Grubbs second-generation catalyst; 97%; Mw ~626.62 g· mol−1) were purchased from Sigma-Aldrich and used as received. Lithium-7 Li chloride, methanol, and dichloromethane (anhydrous; ≥ 99.8%) were also obtained from Sigma-Aldrich and used without further purification.

PB and PI Cross-Metathesis

All experiments were conducted in Schlenk tubes in an atmosphere of dry nitrogen. Either the *Z*- or the *E*-polymer (25 mg, Mw ~200,000 g·mol−1 , 0.125 μmol) was first introduced in a Schlenk tube. A prepared solution containing the chain transfer agent (*Z*)-1,4-diacetoxy2-butene (10 μL, [CTA]/[PB] = 500) and the Hoveyda− Grubbs second-generation catalyst (1.5 mg, [catalyst]/[PB] = 20) dissolved in 1 mL of dry dichloromethane was then injected in the tube under magnetic stirring at 40 °C in a nitrogen atmosphere. The reaction was quenched after 2 h by turning off the heating and adding methanol. The resulting solution was then concentrated under vacuum at room temperature, dissolved in acetonitrile, and prepared for analysis. The protocol was the same for *Z*- or *E*-PI with only modified ratios and temperature. For 25 mg of polymer (Mw ~38,000 g·mol^{-1}, 0.657 μmol), 10 μL of the chain transfer agent ([CTA]/[PI] = 100) and 1.5 mg of the catalyst ([catalyst]/[PB] = 5) were added and the mixture was heated at 50 °C.

Isomerization Suppression

The cross-metathesis of PB and PI in both *Z*- and *E*-configurations was performed under the same conditions as above with the addition of 10% (w/w of the polymer) of the 2,6-dichloro-1,4-benzoquinone as a suppressor for olefin isomerization.

^{1}H-NMR spectroscopy

Spectra were recorded for all individual polybutadiene and polyisoprene in both configurations (*Z* and *E*) and for the solutions obtained after depolymerizations. Acquisition was done on a Bruker AVANCE III HD spectrometer (Bruker Biospin, GmbH) operating at 300 MHz and equipped with a SampleXpress auto-sampler (Bruker Biospin, GmbH). The solvent used for all experiments was deuterated chloroform and 5 mm NMR tubes were used. Chemical shifts of hydrogen atoms on NMR spectra are given relative to the signal of $CDCl_3$ (7.27 ppm).

Atmospheric solid analysis probe (ASAP)

Data acquisitions were performed using a SYNAPT G2 HDMS fitted with an ASAP source (Waters Corp., Manchester, UK). This instrument is a hybrid quadrupole/time-of-flight mass spectrometer, which incorporates a traveling wave (T-Wave)-based mobility separation device. The samples were dissolved by heating in chloroform and ASAP capillary tube was dipped in the melt polymer before cooling at room temperature. ASAP was conditioned to experimental temperature during 1 h before experiments. Finally, the capillary tube was fixed to the ASAP probe holder and introduced in the ionization source. For all experiments, ASAP mass spectra were acquired in positive ion mode over the *m/z* 50-1200 range using the W reflectron mode. Note that a blank was recorded during 1 min before sample introduction. A nitrogen flow of 1200 L.h^{-1} heated at 650°C was used for thermal desorption. The corona discharge voltage was 4 kV, and sampling cone voltage was 40 V. Trap and transfer collision gas flow were set at 2.0 mL.min^{-1} (0.02 mbar for Ar cell pressure). Helium cell gas flow was set at 180 mL.min-1, and IMS gas flow (N_2) was set at 70 mL.min^{-1} of 3.0 mbar for IMS cell pressure. TWIM traveling wave height and velocity were set, respectively, at 40 V and 600 m.s^{-1}. Data acquisition and mass spectra treatment were provided by MassLynx (version 4.1). DriftScope (version 2.1) software was used for the treatment of *m/z* vs drift-time maps. Note that the peak at *m/z* 277.0777 observed on mass spectrum is a background ion of the ASAP source; it corresponds to a fragment ion (loss of H•) of triphenylphosphine oxide ($C_{18}H_{14}OP$), present in flame retardant. This background ion is used as internal standard for accurate mass measurement.

DIP-APCI-FTICR analysis

Experiments were carried out using a Bruker Solarix XR instrument equipped with a 12 T actively shielded superconducting magnet and a dynamically harmonized ICR cell. Spectra were acquired with 8 M data points resulting in a resolution of 1,000,000 at *m/z* 400 in the magnitude mode. The masses were recorded between *m/z* 147 and 1200. The bias of the cell was set to 0.5 V with front and back trapping potentials of 1.7 V. The skimmer 1 voltage was set to 15 V. The polyolefin samples were heated to their melting point in a glass vial. A glass capillary tube was dipped in the melted polymer before cooling at room temperature. This capillary was directly inserted into a direct introduction probe fitted on the APCI source. It allows direct analysis of polyolefin without sample preparation by using single-use glass tubes. The ionization principle is the same as the one of ASAP. Note that a blank was recorded during 1 min before sample introduction. Spectra were internally calibrated in the Data Analysis software ver. 5.0 (Bruker Daltonics, Bremen; Germany) with assigned signals yielding mass error below 100 ppb for the detected signals. At least 30 scans were accumulated. APCI settings were as follows: vaporizer temperature: 400°C, drying gas temperature: 200°C, drying gas flow: 2 L.min^{-1}, nebulizer pressure: 3.0 bar, capillary voltage: 1000 V, end plate voltage: -500 V and corona needle current: 3000 nA. Ions were accumulated in the hexapole during 0.02 s.

Py-GCxGC/MS analysis

Py-GCxGC/MS analyses were conducted with a Shimadzu QP 2010-Ultra mass spectrometer (Shimadzu, Champs-sur-Marne, France) equipped with a two-stage thermal modulator ZX 2 (Zoex, Houston, USA). Pyrolysis was performed using a vertical micro-furnace-type pyrolyzer PY-3030iD (Frontier Lab, Fukushima, Japan) directly connected to the injection port of the gas chromatograph. The sample was placed in a stainless-steel sample cup. Typical quantities of polymers used in this work ranged from 20 to 50 µg. The sample cup was placed on top of the pyrolyser at near ambient temperature. The sample cup was introduced into the furnace at 500°C, and then the temperature program of the gas chromatograph oven was started. The Py-GCxGC interface was held at 320°C. A OPTIMA-5HT column (30 m × 0.25 mm I.D., 0.25 µm film thickness, Macherey-Nagel, Hoerdt, France) was used as first dimension column and a Zebron ZB-50 (2.8 m× 0.1 mm I.D., 0.1 µm film thickness, Phenomenex, Le Pecq, France) was used as a second-dimension column and for the loop modulator system. The separation was carried out at an initial constant pressure of 300 kPa (which resulted in a flow rate varying from 1.3 mL/min to 0.4 mL/min during the acquisition), and using Helium Alphagaz 1 as carrier gas (Air Liquide, Bagneux, France). The ZX 2 two-stage thermal modulator employs a closed cycle refrigerator/heat exchanger to produce a −94°C cooled air jet regularly modulated with a pulsed hot air jet. The optimized modulation period was 6 to 9s with a programmed hot pulse of 0.350s. A two-step temperature program was used for the hot jet set at 200°C to 250°C for 30 min and subsequently raised to 280°C for 40 min in order to increase the modulation step efficiency in correlation with the volatility of pyrolysis products. The oven temperature was initially held 1 min at 70 C, and then ramped at 3°C min^{-1} to 300°C, where it was held for 15 min. The total duration of GC analysis was 99.3 min. The injector was held at 280°C and used in split mode (1:50 for E-polymers and 1:70 for *Z*-polymers of the total flow). The mass spectrometer was operated at 20,000 Da. s^{-1}, with a scan range from 45 to 600 Da, using electron ionization at 70 eV. The interface was kept at 320°C and the ion source at 200°C. Data processing of the Py-GCxGC/MS raw data was achieved using GC Image software, version 2.4 (Lincoln, Nebraska). Identification of polymers composition was performed by comparing the mass spectra of unknown components with the ones of the NIST mass spectra library, 2011 edition.

FT-ICR MS analysis

Analyses were performed on a SolariX XR instrument with a 9.4 T actively shielded superconducting magnet and a dynamically harmonized cell (Bruker Daltonics, Bremen, Germany). The mass spectrometer is equipped with a Varian Nano-electrospray online source (Varian Nano ESI ON, Bruker Daltonics, Bremen, Germany). For all experiments, FT-ICR mass spectra were acquired in positive ion mode. Depolymerized polybutadiene samples were diluted in acetonitrile (10 mg/mL) and depolymerized polyisoprene samples were diluted (10 mg/mL) in acetonitrile/dichloromethane (75/25 v/v). The obtained solutions were further diluted to 100 ng/µL in acetonitrile. Lithium-^{7}Li chloride (99% ^{7}Li) was dissolved in methanol to a concentration of 1 mg/mL Mixture solutions of sample and lithium chloride at a ratio of 10:1 (sample/LiCl, v/v) were introduced in the spectrometer by direct infusion using a Cole-Parmer single-syringe infusion pump (Cole-Parmer®, Vernon Hills, USA) at a rate of 10µL/min through a 250 µL Hamilton syringe (51 mm, Gastight). The syringe is connected to a capillary line (100 µm I.D., 360 µm O.D.) equipped with a SilicaTipTM needle (10±1 µm, PicoTipTM Emitter, New Objective, Woburn, MA, USA) to which a potential of 1.3 kV was applied. The front and back trapping potentials were set at 1.5 V with a skimmer 1 voltage at 20 V. Spectra were acquired using broadband detection, 8 M data points; 300 scans accumulation for a better signal-to-noise ratio with a mass range from *m/z* 144 to 1500. The transient time consisted of 4.20 s which resulted in a resolution of 1,000,000 at *m/z* 400 in the magnitude mode. Ions were accumulated in the hexapole during 0.05 s. Instrument calibration was achieved using an external calibrant (Sodium trifluoroacetate TFA, 0.01 mg/mL in H_2O/MeOH 50/50 v/v) with a linear calibration. Following acquisition, spectra were internally calibrated in the Data Analysis software version 5.0 (Bruker Daltonics, Bremen, Germany) using a calibration list of assigned signals limiting the mass error to under 100 ppb. Mass spectra treatment was done using a modified python script originating from the FTMS Visualisation software (also known as i-van Krevelen) in which masse to formula assignment is based on the Kendrick mass defect and z* approach to formulae assignment. The attributed compounds were classed according to the number of CH_2, unsaturation and oxygen atoms in the molecule.

MS/MS experiments

These experiments were conducted to study the fragmentation patterns of the different configurations of each polymer (*Z*- and *E*- configurations) in order to build their breakdown curves. All energy resolved mass spectrometry experiments were achieved on the SolariX XR instrument with a 9.4 T actively shielded superconducting magnet and a dynamically harmonized cell (Bruker Daltonics, Bremen, Germany) using collision-induced dissociation (CID). Spectra were acquired in the *m/z* range from 144 to 700 with Argon as collision gas and by a gradual increase of the collision energy from 0 to 25 eV. Fragmentation data of each polymer's configuration were collected by accumulating 16 scans for each collision energy. Breakdown curves were plotted using the data collected of each daughter spectra.

Ion-mobility spectrometry-mass spectrometry

IMS-MS analyses were carried out using a Synapt G2 HDMS (Waters, Manchester, United Kingdom). This instrument is a hybrid quadrupole/time-of-flight mass spectrometer, which has a traveling wave ion mobility (TWIM) feature. The experiments were performed by direct infusion of the samples at 10 μL.min^{-1} flow rates into the ESI source of the instrument, with the capillary and sampling cone voltage fixed between 2.8–3.2 kV and 10 V respectively under a nitrogen flow of 500 L h^{-1} at 250 °C. For all experiments, IMS-MS spectra were acquired in positive mode over a *m/z* 50–1200 range. The helium cell gas flow was set at 180 mL min^{-1}. The IMS gas flow (N_2) was set at 80 mL min^{-1} with an IMS cell pressure of 2.00 mbar. The traveling wave height and velocity in the IMS cell were set at 40 V and 500 m. s^{-1}, respectively. The data acquisition and mass spectra processing were carried out using the MassLynx v4.1 software (Waters, Manchester, United Kingdom). For all experiments, depolymerized polybutadiene samples were diluted in acetonitrile (10 mg/mL) and depolymerized polyisoprene samples were diluted (10 mg/mL) in acetonitrile/dichloromethane (75/25 v/v). The obtained solutions were further diluted to 100 ng/µL in acetonitrile. Lithium-^{7}Li chloride (99% ^{7}Li) was dissolved in methanol to a concentration of 1 mg/mL. Mixture solutions of sample and lithium chloride at a ratio of 10:1 (sample/LiCl, v/v) were introduced in the spectrometer by direct infusion. For the ion mobility spectra, a Gaussian fit of each peak was carried out using OriginPro software v9.0 (OriginLab Corporation). All of the masses and *m/z* reported in the manuscript correspond to monoisotopic values.

References

1. Schmidt, B., In situ conversion of a Ru metathesis catalyst to an isomerization catalyst. *Chemical Communications* **2004,** (6), 742-743.
2. Kotha, S.; Misra, S.; Sreevani, G.; V. Babu, B., Non-Metathetic Behaviour of Olefin Metathesis Catalysts. *Current Organic Chemistry* **2013,** *17* (22), 2776-2795.
3. Biswas, S., Mechanistic Understanding of Transition-Metal-Catalyzed Olefin Isomerization: Metal-Hydride Insertion-Elimination vs. π-Allyl Pathways. *Comments on Inorganic Chemistry* **2015,** *35* (6), 300-330.
4. Hong, S. H.; Day, M. W.; Grubbs, R. H., Decomposition of a Key Intermediate in Ruthenium-Catalyzed Olefin Metathesis Reactions. *Journal of the American Chemical Society* **2004,** *126* (24), 7414-7415.
5. Fürstner, A.; Ackermann, L.; Gabor, B.; Goddard, R.; Lehmann, C. W.; Mynott, R.; Stelzer, F.; Thiel, O. R., Comparative Investigation of Ruthenium-Based Metathesis Catalysts Bearing N-Heterocyclic Carbene (NHC) Ligands. *Chemistry – A European Journal* **2001,** *7* (15), 3236-3253.
6. Lehman Jr, S. E.; Schwendeman, J. E.; O'Donnell, P. M.; Wagener, K. B., Olefin isomerization promoted by olefin metathesis catalysts. *Inorganica chimica acta* **2003,** *345*, 190-198.
7. Higman, C. S.; Plais, L.; Fogg, D. E., Isomerization During Olefin Metathesis: An Assessment of Potential Catalyst Culprits. *ChemCatChem* **2013,** *5* (12), 3548-3551.
8. Chatterjee, A. K.; Choi, T.-L.; Sanders, D. P.; Grubbs, R. H., A general model for selectivity in olefin cross metathesis. *Journal of the American Chemical Society* **2003,** *125* (37), 11360-11370.
9. Pump, E.; Poater, A.; Bahri-Laleh, N.; Credendino, R.; Serra, L.; Scarano, V.; Cavallo, L., Regio, stereo and chemoselectivity of 2nd generation Grubbs ruthenium-catalyzed olefin metathesis. *Catalysis Today* **2020**.
10. Hong, S. H.; Sanders, D. P.; Lee, C. W.; Grubbs, R. H., Prevention of undesirable isomerization during olefin metathesis. *Journal of the American Chemical Society* **2005,** *127* (49), 17160-17161.
11. Gimeno, N.; Formentín, P.; Steinke, J. H. G.; Vilar, R., Phenylphosphoric Acid as a New Additive to Inhibit Olefin Isomerisation in Ruthenium-Catalysed Metathesis Reactions. *European Journal of Organic Chemistry* **2007,** *2007* (6), 918-924.
12. Timmer, B. J. J.; Ramström, O., Acid-Assisted Direct Olefin Metathesis of Unprotected Carbohydrates in Water. *Chemistry – A European Journal* **2019,** *25* (63), 14408-14413.
13. Csjernyik, G.; Éll, A. H.; Fadini, L.; Pugin, B.; Bäckvall, J.-E., Efficient Ruthenium-Catalyzed Aerobic Oxidation of Alcohols Using a Biomimetic Coupled Catalytic System. *The Journal of Organic Chemistry* **2002,** *67* (5), 1657-1662.
14. McLuckey, S. A.; Sallans, L.; Cody, R. B.; Burnier, R. C.; Verma, S.; Freiser, B. S.; Cooks, R. G., Energy-resolved tandem and fourier-transform mass spectrometry. *Int. J. Mass Spectrom. Ion Phys.* **1982,** *44* (3), 215 - 229.
15. Fetterolf, D. D.; Yost, R. A., Energy-resolved collision-induced dissociation in tandem mass spectrometry. *Int. J. Mass Spectrom. Ion Phys.* **1982,** *44* (1), 37 - 50.
16. Arisawa, H.; Brill, T. B., Flash pyrolysis of hydroxyl-terminated polybutadiene (HTPB) I: Analysis and implications of the gaseous products. *Combust. Flame* **1996,** *106* (1-2), 131-143.
17. Ganesh, K.; Sundarrajan, S.; Kishore, K.; Ninan, K. N.; George, B.; Surianarayanan, M., Primary pyrolysis products of hydroxy-terminated polybutadiene. *Macromolecules* **2000,** *33* (2), 326-330.
18. Radhakrishnan, T. S.; Rao, M. R., Thermal decomposition of polybutadienes by pyrolysis gas chromatography. *J. Polym. Sci., Polym. Chem. Ed.* **1981,** *19* (12), 3197-3208.
19. Barrère, C.; Maire, F.; Afonso, C.; Giusti, P., Atmospheric Solid Analysis Probe–Ion Mobility Mass Spectrometry of Polypropylene. *Anal. Chem.* **2012,** *84* (21), 9349-9354.
20. Trimpin, S.; Inutan, E. D.; Karki, S.; Elia, E. A.; Zhang, W.-J.; Weidner, S. M.; Marshall, D. D.; Hoang, K.; Lee, C.; Davis, E. T., Fundamental Studies of New Ionization Technologies and Insights from IMS-MS. *J. Am. Soc. Mass Spectrom.* **2019,** *30* (6), 1133-1147.
21. Smith, M. J. P.; Cameron, N. R.; Mosely, J. A., Evaluating Atmospheric pressure Solids Analysis Probe (ASAP) mass spectrometry for the analysis of low molecular weight synthetic polymers. *Analyst* **2012,** *137* (19), 4524-4530.

22. Golub, M. A.; Gargiulo, R. J., Thermal degradation of 1,4-polyisoprene and 1,4-polybutadiene. *Journal of Polymer Science Part B: Polymer Letters* **1972,** *10* (1), 41-49.
23. Chen, F.; Qian, J., Studies on the thermal degradation of polybutadiene. *Fuel Process. Technol.* **2000,** *67* (1), 53 - 60.
24. Chen, F.; Qian, J., Studies on the thermal degradation of cis-1, 4-polyisoprene. *Fuel* **2002,** *81* (16), 2071-2077.
25. Domján, A.; Bajdik, J.; Pintye-Hódi, K., Understanding of the Plasticizing Effects of Glycerol and PEG 400 on Chitosan Films Using Solid-State NMR Spectroscopy. *Macromolecules* **2009,** *42* (13), 4667-4673.
26. Wang, F. C.-Y., Polymer additive analysis by pyrolysis–gas chromatography: IV. Antioxidants. *J. Chromatogr. A* **2000,** *891* (2), 325 - 336.
27. Dlugogorski, B. Z.; Kennedy, E. M.; Mackie, J. C., Roles of peroxides and unsaturation in spontaneous heating of linseed oil. *Fire Safety Journal* **2013,** *61*, 108-115.
28. Young, R. J.; Lovell, P. A., *Introduction to polymers*. CRC press: 2011.

Polymers in cultural heritage

Chapter 5:

Introduction to oil paints

Chapter 5. Introduction to oil paints

I. Oil paints

Oil paints are typically composed of two major phases: organic and inorganic. The inorganic phase represents the group of pigments responsible for the color of the paint while the organic phase includes binders, adhesives and varnishes.

Several types of binders have been used in paintings and they are considered as the determining factor of painting techniques. Beeswax, for example, was used as binding medium for the preparation of Encaustic painting. The binder of Tempera painting is composed of proteinaceous emulsions such as eggs, gelatin, casein or their mixture. Polysaccharides such as Arabic gum are also used as binding media of aquarelle paints.

The technique of oil painting was introduced in the early fifteenth century by the Flemish painter Van Eyck, and this technique became very quickly used. Binders used in these historic paints were natural drying vegetable oils such as linseed oil, walnut oil or poppy oil also known as siccative oils. An oil is said to be drying or siccative if, exposed to air, is able to form a solid film. From a purely chemical point of view, oils are essentially made up of triglycerides (glycerol triesters) formed from saturated (5-15% by mass) and unsaturated (85-95%) fatty acids, a small amount of free fatty acids and impurities (mucilaginous substances, sterols, etc.) that the purification of the oil aims to eliminate. The main fatty acids composing the triglycerides of drying oils are palmitic acid, stearic acid, oleic acid, linoleic acid and linolenic acid. The average fatty acid composition for linseed, walnut and poppy oils is given in the following table

Table 16. Fatty acid compositions of some drying oils

Fatty acid	Palmitic acid	Stearic acid	Oleic acid	Linoleic acid	Linolenic acid
Number of C	16	18	18	18	18
Number of C=C	0	0	1	2	3
Notation	C16:0	C18:0	C18:1	C18:2	C18:3
% in linseed oil	4-10	2-8	10-24	12-29	**48-60**
% in walnut oil	9-11	1-2	11-18	**69-77**	3-5
% in poppy oil	3-8	0.5-3	9-30	**57-76**	2-16

The dryness of an oil depends on the number of double bonds (unconjugated in the case of linseed, walnut and poppy oils). Indeed, the oxidation mechanism that allows the "Drying" of oils relies on the crosslinking of double bonds present in fatty acids. Thus, the more double bonds an oil contains, the faster the film formation will be. An oil must contain at least 65% carboxylic acids polyunsaturated to be siccative.[1] The good siccativity of linseed oil is explained by its high percentage of linolenic acid (3 double bonds): 48 to 60%. In addition, heavy metals such as lead are initiators of oxidation, the addition of PbO therefore makes the oil more drying.[2-3]

II. Pigments and dyes

there are two types of coloring matter: pigments and dyes. Pigments can be defined as "fine white or colored powders, insoluble or poorly soluble in the dispersion medium” (Perego 2005). The number of pigments available to painters has increased considerably over the years mainly from the 19th century with the boom in chemistry and the arrival of synthetic pigments on the market.

Unlike pigments, dyes are soluble in the binder. They can be from natural or synthetic origin. To get a powder that can be dispersed in oil, most dyes must first be fixed on a substrate. The most used pigments in paintings are red lacquered from the anthraquinone family (carmine / cochineal, kermes, madder) and yellow lacquer pigments from the flavonoid family.

III. Additives

Different additives can also be added to modify the properties of paint, among which we can cite driers, fillers and thinners. The most common filler used in painting is chalk (calcium carbonate). The refractive index of calcium carbonate (1.51-1.65) is similar to that of oil (1.48 for fresh oil and about 1.55- 1.56 for an oil dating from the 17th century).[4-5] Therefore, crushed in oil, calcium carbonate will appear transparent and allow light to penetrate deeper into the pictorial layers, giving the impression of a layer slightly translucent.

The term diluent in paint designates a solvent, the addition of which makes it possible to thin the paint without modifying its composition. The main thinner used by painters is the essence of turpentine. Volatile, the diluent evaporates after application of the paint during drying. The evaporation of turpentine is however quite slow.

IV. Polymerization of drying oils

The drying, curing and ageing of linseed oil is an autoxidative process. A complex cascade of reactions between the triglycerides and oxygen from atmosphere lead to the polymerization of linseed oil and the formation of a highly cross-linked structure. Triglycerides are the major component of linseed oil and are composed mainly of polyunsaturated fatty acids. Linoleate and linolenate structures oxidize rapidly since they contain allylic hydrogen between double bonds. The allylic hydrogen will lead to formation of radical species. Subsequent reaction with oxygen generates hydroperoxide functions and lunch free radical-chain mechanisms.

IV.1. Mechanism

Drying oil autooxidation mechanism is composed of three steps: initiation, propagation and termination. This process is carried out in several stages:

1) Formation of hydroperoxides
2) Propagation of free radicals
3) Decomposition of hydroperoxides into free radicals
4) Free radical species react with each other to form crosslinked products

The organic material or substrate is represented by RH, where R is a hydrocarbon having a labile hydrogen atom H.

Initiation: $RH \rightarrow R^* + H$

Propagation: $R^* + O_2 \rightarrow ROO^*$

$ROO^* + RH \rightarrow ROOH + R^*$

Hydroperoxide decomposition: $ROOH \rightarrow RO^* + OH^*$

$ROOH \rightarrow ROO^* + H^*$

Termination: $2RO^* \rightarrow ROOR$

$2ROO^* \rightarrow ROOR + O_2$

$2R^* \rightarrow RR$

$RO^* + R^* \rightarrow ROR$

IV.1.1. Initiation

Drying oils are composed in majority from unsaturated fatty acids such Oleic, linoleic and linolenic acids. Allylic carbons are an attractive site to create radicals which are initiated by the presence of light and catalysts such as driers (e.g. cobalt salts) in the case of modern paints or pigments (e.g. lead white) in the case of art oil paintings.

Reaction 1:

$$RH + M^{(n+1)+} \longrightarrow R^* + M^{n+} + H^+$$

$M^{(n+1)+}$ is the higher oxidation state of the metal ions and M^{n+} is the lower oxidation state.

The primary class of driers catalyzes the oxidation step and includes Co^{2+}, Mn^{2+}, and Fe^{2+} metal salts. The second class of driers includes Pb^{2+}, Zr^{4+}, and Al^{3+} and catalyzes the polymerization step.[6] The oxidation states of iron, copper, manganese, nickel, lead and cobalt are known to change through the single electron transfer.[7-8] Auxiliary driers like calcium and zirconium are used in combination with other driers in order to improve stability through drying and hardness.

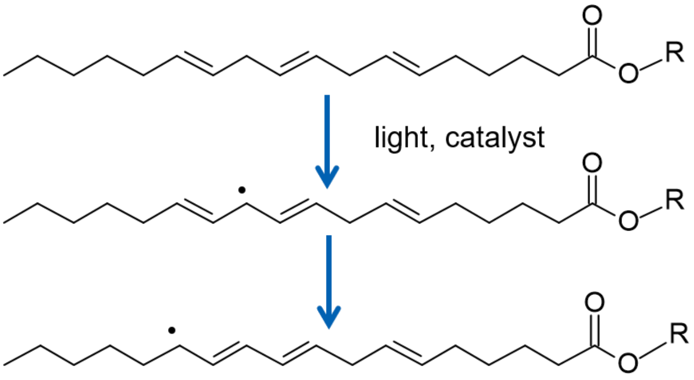

Figure 121. Initiation: radical formation on the allylic position

IV.1.2. Propagation

The free radicals produced in the previous step react easily with their environment. However, they have certain preferences. They react more easily with each other and this reactivity increases with the presence of oxygen atoms in their structure. At the beginning of the oxidation of lipids, the concentration of free radicals is too low for them to react with each other. The radicals then preferentially react with the oxygen of the air and optionally with the substrate, as shown in reaction R2 and R3 respectively. The hydroperoxide formed in reaction R3 can decompose into free radicals. Finally, these reactions generate new free radicals that will subsequently react with oxygen and between each other to create a cross-linked polymer.[9]

In reaction 2, the electrons of the double bond of the active methylene group form a complex with an oxygen molecule before generating the hydroperoxide. The resulting complex is relatively stable due to the creation of a hydrogen bridge. Once the labile hydrogen of the methylene moiety moves to the oxygen molecule, rearrangement of the double bonds occurs. The hydroperoxide thus formed is conjugated with a cis-trans structure. The double bonds of the conjugated hydroperoxides can react under severe conditions with oxygen. Once the hydroperoxides are formed, they can decompose free radicals by mono or bimolecular decomposition.[10]

Reaction 2 :

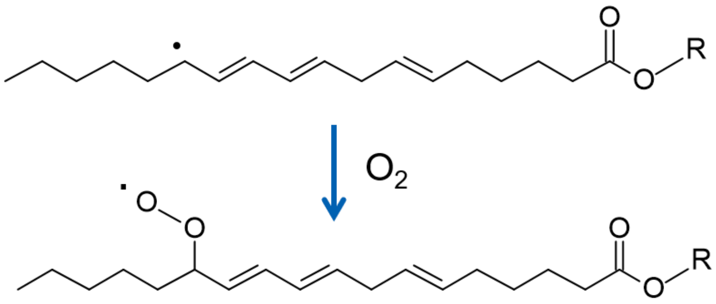

Figure 122. Hydroperoxides formation by reaction with oxygen

Reaction 3:

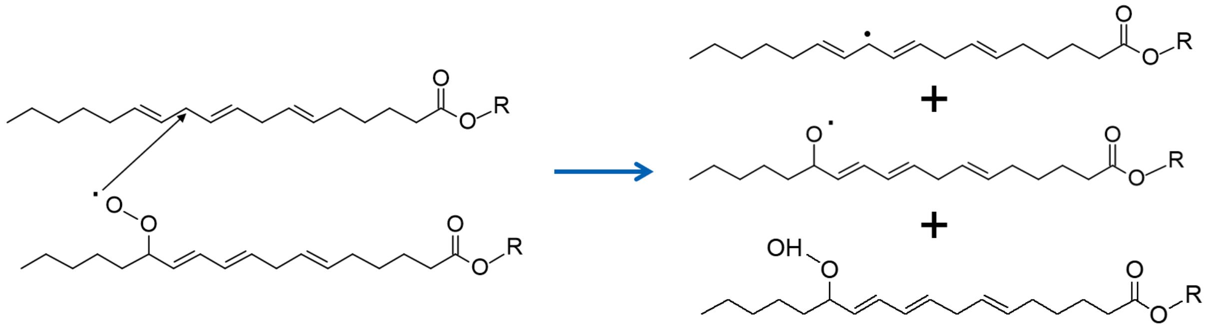

Figure 123. New radical formation

IV.1.3. Hydroperoxide decomposition

Hydroperoxide decomposition is initiated by the presence of driers such as Cobalt salts and lead to the generation of alkoxyl and peroxyl radicals which induce in their turn the propagation and the recombination steps. Hydrogen abstraction from the tertiary carbon with a hydroperoxide function leads to further product-formation, forming cross-linked (non-volatile) species and numerous other oxygen containing products such as alcohols, ketones, aldehydes and carboxylic acids.[11-13]

Reaction 4 :

$ROOH + M^{(n+1)+} \rightleftharpoons [(ROOH)M]^{(n+1)+}$

$[(ROOH)M]^{(n+1)+} \longrightarrow ROO^* + M^{n+} + H^+$

Reaction 5:

$ROOH + M^{n+} \rightleftharpoons [(ROOH)M]^{n+}$

$[(ROOH)M]^{n+} \longrightarrow RO^* + [M^{(n+1)+}(OH^-)]^{n+}$

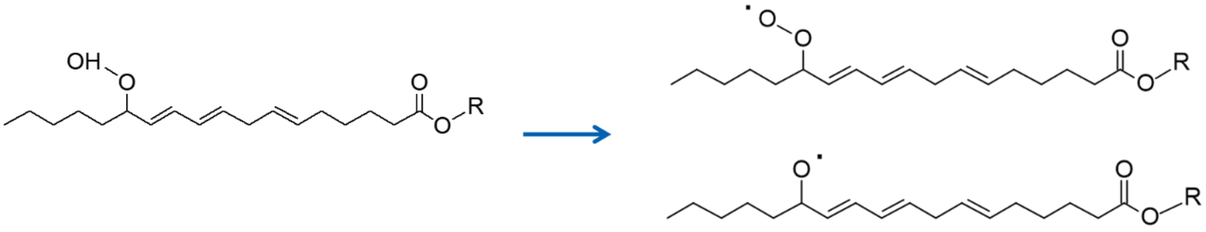

Figure 124. Hydroperoxide decomposition

IV.1.4. Termination

Once the free radicals are in appreciable quantity, they react with each other to form cross-linked products. The subsequent and successive reactions of cross-linked products with free radicals, gradually form a three-dimensional polymeric network, responsible for the solidification of the substrate, when the amount of the reactive sites is sufficiently high.

The bonds formed during this polymerization process may be carbon-carbon (-C-C-) (Figure 125), ether (-C-O-C-) (Figure 126) or peroxide (-C-O-O-C) (Figure 127). The nature of these bonds strongly influences the properties of the cross-linked products such as stability and strength. Generally, the best properties are found in polymers having a high carbon-carbon bond content. On the other hand, the flexibility of oxygen, ether and peroxide bonds generates polymers with low mechanical strengths.[14-15]

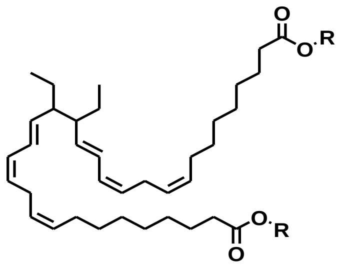

Figure 125. Dimer of two fatty acids with carbon-carbon bond

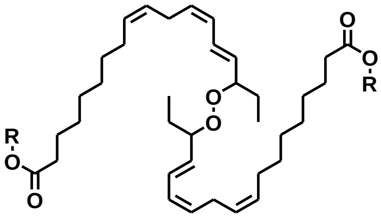

Figure 126. Dimer of two fatty acids with peroxide bond

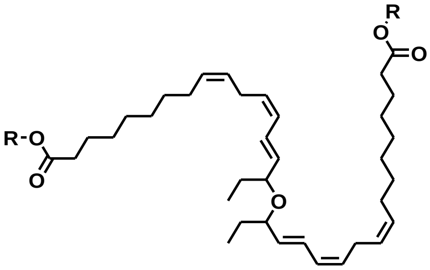

Figure 127. Dimer of two fatty acids with ether bond

The type of polymeric linkages is defined primarily by three factors: the nature of the hydrocarbon or lipids, the oxygen concentration and the temperature. Various studies have shown that oxygen uptake by the substrate is greatly increased by the level of unsaturation in the chain. Under the same conditions, the contribution of ether and peroxide bonds to the polymerization of unsaturated substrates (drying oils) is greater than that in saturated substrates (mineral oil). On the other hand, the contribution of carbon-carbon bonds is favored by relatively high temperatures and low oxygen concentrations. The polymerization process is often associated with a loss of unsaturation. During the formation and decomposition of hydroperoxides, double bonds are not usually consumed but rather restructured. This loss of unsaturation is therefore achieved during the polymerization step.

Reaction 6:

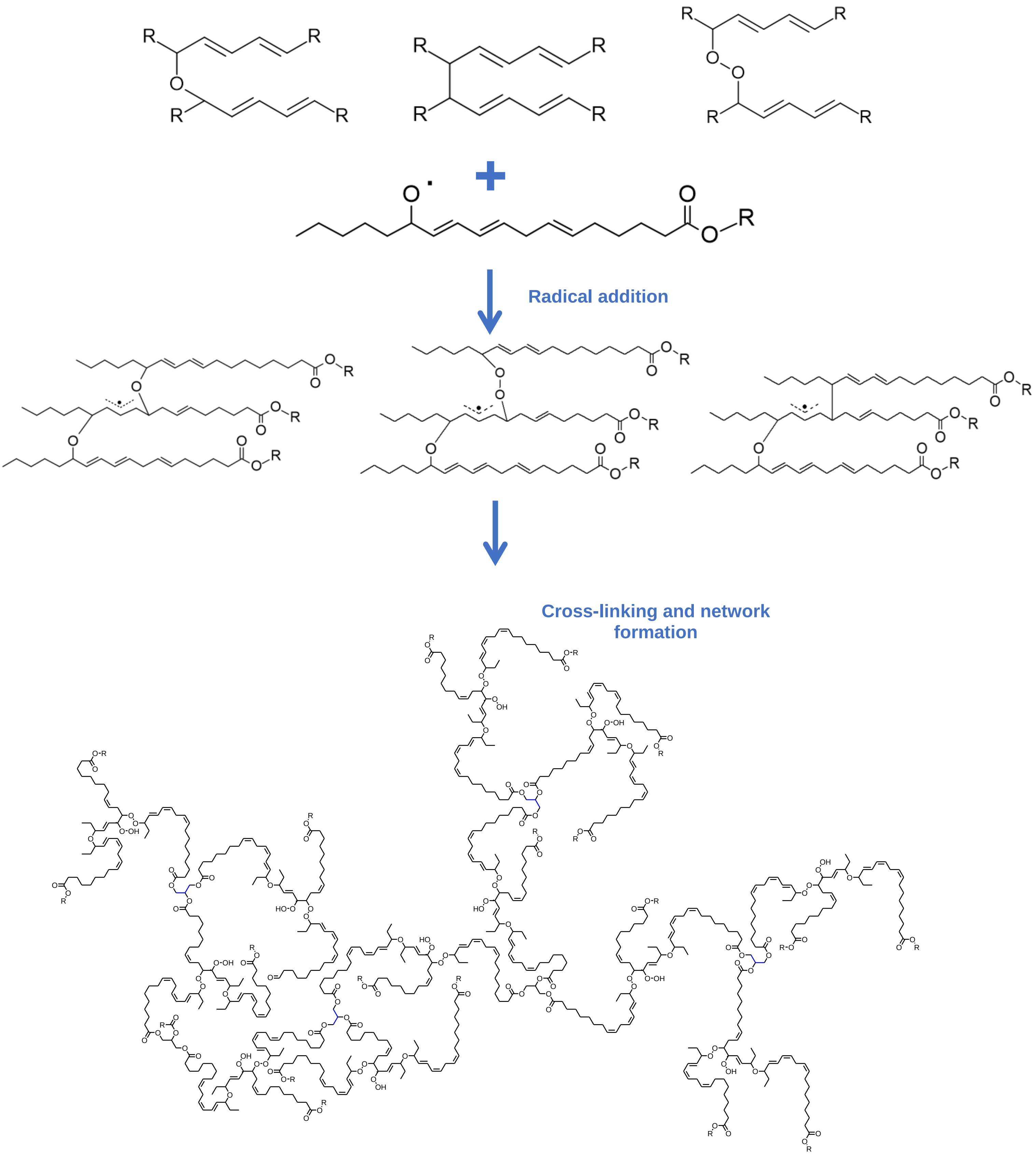

Figure 128. Cross-linking of triglycerides in siccative oils

V. Oil paint degradation

V.1. β-scission degradation

During oil paint autoxidation and the formation of cross-linked polymer, fatty acid chains can be degraded and release low molecular weight volatile compounds at the same time. Those volatile compounds produce the specific smell of an oil painting. Alkoxy radicals, RO, are formed due to the homolytic cleavage of the hydroperoxides. These evolve by fragmentation of adjacent C-C and C-H bonds to produce aldehydes, ketones, alkyl and vinyl radicals which in turn react with H« and OH», and produce aldehydes or (un)saturated hydrocarbons.

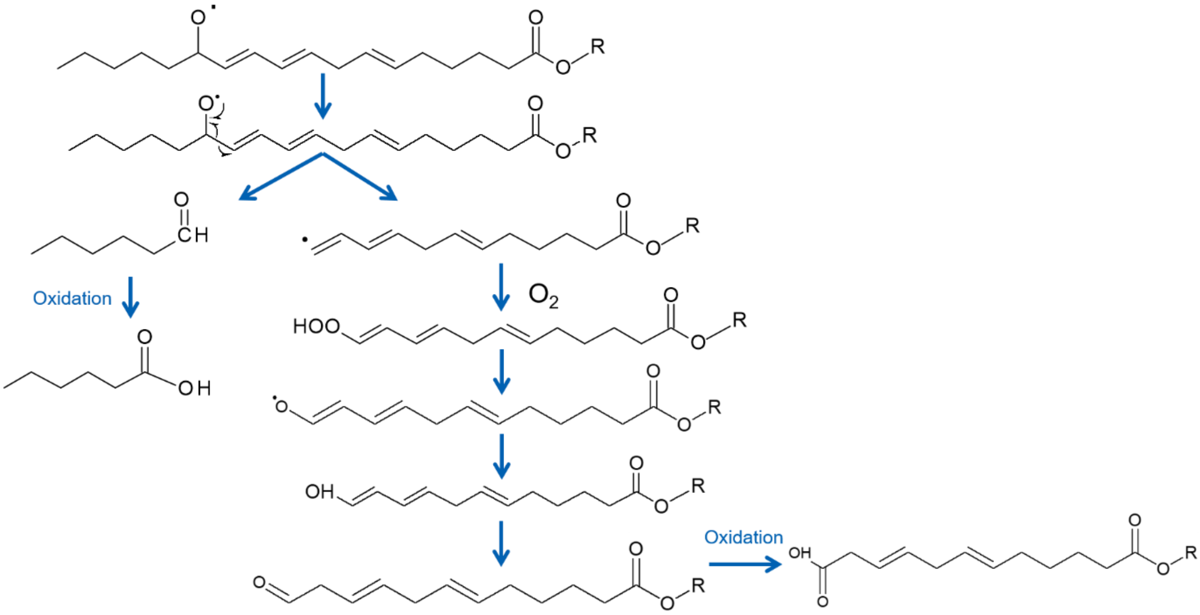

Figure 129. β-scission degradation of fatty acid chains

Chapter 6:
Analysis of oil paints

Chapter 6. Analysis of oil paints

Different components of an art painting may be can be identified by using various through analytical methods. These methods help unravel the history of the artwork. They can also provide conservators with the optimized conditions of restoration, storage and conservation. On the other, artworks such as famous paintings have usually very high values and should be carefully treated. As most analytical techniques require the availability of samples for a successful analysis, it is very important to perform micro-scale non-destructive analyses, leading to very limited quantities of materials. To overcome this problem, constant progress has been made in the field of analytical chemistry to propose techniques that are efficient and meet these criteria at the same time.

I. Fourier transform infrared spectroscopy (FT-IR)

Fourier transform infrared spectroscopy (FTIR) is an analytical technique capable of characterizing chemical functions in organic, inorganic, crystalline and amorphous compounds.

The principle of this method is to expose the sample to infrared radiation of different wavelengths. Molecules absorb some of these radiations at wavelengths corresponding to the vibration frequencies of their chemical classes.

When the intensity of light absorbed at each wavelength is measured, a specific spectrum is generated for the various present chemical groups. The advantage of this technique in the field of art paint is its ability to obtain information on the type of the organic constituents (oil, wax, resin, proteins).

Derrick et al (1999), described the characteristics of the infrared spectra of various compounds found in paint materials[16]. The FTIR analysis also makes it possible to trace the evolution of certain chemical modifications in oil paintings during time or to study the influence of different conditions as thermal exposure, ageing and degradation.

FT-IR technique was also applied in order to understand the mechanism of autoxidation of siccative oils. Mallégol et al.[10, 17-19] studied the long-term behavior of oil-based varnishes and paint as linseed and poppy-seed oil. They focused on the formation of hydroperoxide groups by observing the broad vibration band centered around 3425 cm^{-1}, the cis-double bond disappearance at 3010 cm^{-1} and 716 cm^{-1} as well as the appearance of trans–trans conjugated double bonds at 987 cm^{-1} and trans–cis conjugated double bonds at 950 cm^{-1}. They also detected the formation of alcohols (nitrite band at 779 cm^{-1} after nitrogen monoxide treatment), aldehydes (bands at 2810 and 2717 cm^{-1} in gas phase), ketones (saturated and unsaturated at 1720 and 1698 cm^{-1}, respectively), carboxylic acids (saturated and unsaturated acid fluorides identified at 1843 and 1810 cm^{-1} after SF4 treatment), and peresters or γ-lactones (near 1770 cm^{-1}).

The same group presented the role of transition metals such as cobalt in accelerating the polymerization of linseed oil.[18] Lazzari et al. investigated the polymerization process and the degradation of linseed oil films, under both natural and accelerated weathering conditions.[20] In their study, they remarked the decrease in the intensity of peaks at 2928 cm^{-1}, 2856 cm^{-1} and 727 cm^{-1}, attributed to unconjugated double bonds. At the same time, they observed the appearance of a broadband centered at 3430 cm^{-1}, due to hydroxyl groups, and of a weak absorption at 1633 cm^{-1} related to the formation of a conjugated double bond.

FT-IR also helped understand the effect of lead oxide on the polymerization of linseed oil and proved that lead oxide accelerates the drying process and reduces the induction time, without major changes in the mechanisms involved and in the final composition.[21] Metal stearate was also detected by FT-IR in oil paints. Metal soaps formation is characterized by the appearance of bands with COO^- antisymmetric and symmetric stretch at ~1550 cm^{-1} and 1400 cm^{-1} reflecting the ionized structure of the COO–metal bond.[22] FT-IR was applied to identify degradation products formed due to ageing or deterioration of works of art.[23]

II. RAMAN spectroscopy

Raman spectroscopy is a non-destructive analytical technique, based on the physical phenomenon of Raman scattering. This phenomenon, highlighted by the Indian physicist Raman in 1928, is the inelastic diffusion of a monochromatic radiation (usually generated today by a laser) by a given material, generated by the coupling between the incident electromagnetic field and the vibration of molecules. This generates the emission of Stokes and anti-Stokes radiations, which are symmetrically offset with respect to the excitation wavelength. This offset corresponds to the vibration wavelength of the molecules. The Raman spectrum, obtained from the measurement of scattered intensity, constitutes a structural imprint of the studied material and gives information on the chemical composition, the structure and the molecular interactions of the material.

Raman spectroscopy is a very useful tool for the study of paints. It does not require any contact with the sample. An important asset of this analytical technique, especially in the case of hybrid materials such as paint, is that it can be used to characterize both amorphous and crystalline materials,[24] organic[25] and mineral materials. The identification of the binder is thus possible with Raman spectroscopy, but often difficult because of the changes caused by the aging of the paint. Raman spectroscopy proved its capability in monitoring the polymerization mechanism of linseed oil by following the formation and the disappearance of peroxide species and the evolution of unsaturation [26]. The comparison between obtained spectra of linseed oil before and after treatment by at 80 °C for 8 hours shows the disappearance of peaks at 3010 and 1654 cm^{-1} corresponding for cis =C–H stretch and cis C=C stretch. The appearance of a broad band centered at 3472 cm^{-1} is also remarkable due to the presence of hydroxyl groups and the formation of the 987 and 971 cm^{-1} peaks, which belong to trans-conjugated double bond and trans-out-of-plane C–H bend. Raman was used as well to study the difference in the oxidation reactions of fatty acids containing non-conjugated and conjugated double bonds in the presence of cobalt catalyst. The study shows that the presence of allylic hydrogen contributes in the radical formation and the autoxidation mechanisms.[27]

III. X-ray fluorescence (XRF)

XRF is a non-destructive elemental analytical technique based on the interaction between an X-ray beam and the electronic procession of the atoms constituting the studied material. Under certain conditions, the interaction with an X-ray beam can cause the ejection of an E1 energy electron in a deep layer of the target atom, creating a gap in the atomic electron cortege. This generates an electronic reorganization allowing the return to equilibrium: the electronic gap is filled by an energy electron E2 originating from a more external layer. It is an electronic transition, accompanied by the release of excess energy, resulting in the emission of an X-ray energy E2 - E1, characteristic of the target atom. Depending on the electronic level to which the ejected electron belongs, different emission lines will be detected. The XRF analysis does not require any contact with the sample and therefore provides a knowledge of the elemental composition of the material by short-term analysis (of the order of a few minutes per tip).

This concept helps obtain an idea on the pigments constituting the material, especially when the characteristic chemical elements of certain pigments are detected.

In several studies, XRF was combined with other techniques such as Raman spectroscopy, in order to determine the composition of some cultural heritage objects. For example, the analysis of a precious illuminated manuscript belonging to the Trivulziana library collection led to the identification of the original pigments and the overpainting layers.[28] The XRF mapping allows pigments identification as well as their spatial distribution in the painting. Moreover, X-rays penetration inside the paintings allows the identification of elements from different layers of the painting. More recently, XRF spectroscopy alongside other techniques were applied to the analysis of paintings present on an old Egyptian coffin. XRF analysis were done with a portable spectrometer. The analysis revealed the elemental composition of different pigments.[29]

IV. ^{1}H Nuclear magnetic resonance spectroscopy (NMR)

Nuclear magnetic resonance spectroscopy was also applied to the study of oil paintings dating to the late 17th and early 20th and centuries in order to investigate the hydrolysis and oxidation processes of oil paint.[30] Proton NMR only allows the analysis of the “Mobile phase” of oil paintings. “Mobile phase” of an oil paint sample is easily separated by solvent extraction from the insoluble part. It provides information about the change in oxidation levels that have occurred during aging of an oil painting. The comparison between fresh and aged linseed oil (Figure 130) reveals that the number of unsaturation in the alkyl chain of fatty acid decreased in the aged oil.

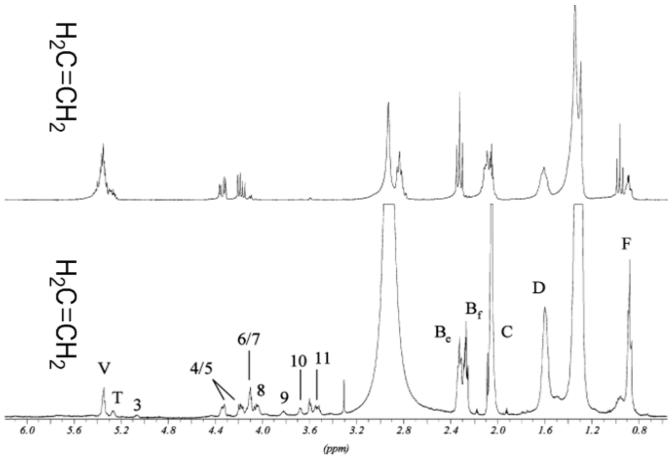

Figure 130. ^{1}H NMR spectra of fresh (top) and five-year-old (bottom) oil paint in acetone-d[30]

V. Solid-state NMR spectroscopy (ssNMR).

Solid-state NMR can be used as a non-destructive technique for the analysis of solid paint films. This technique is suitable for the analysis of both organic and inorganic components of paintings. However, low sensitivity is a main disadvantage which kept this technique limited to the analysis and detection of organic and metallic complexes known as metallic soaps.

Catalano et al. synthesized and analyzed different types of lead carboxylates metallic soaps such as lead stearate, lead palmitate, lead azelate, lead oleate and lead heptanoate. Based on the ^{207}Pb chemical-shift tensor, they succeeded to distinguish between lead azelate which has a span around 2640 ppm and an isotropic chemical shift at 1188 ppm and both lead stearate and lead palmitate that have similar NMR parameters (spans of 700 ppm, skews of 0.5, and isotropic chemical shifts near 2130 ppm). Lead heptanoate has similar span and skew values as lead azelate but a difference of 100 ppm in the isotropic chemical shift. These data indicate that ^{207}Pb NMR results depend on the length of the carboxylate chain.

The sensitivity of these experiments was further enhanced by Dynamic Nuclear Polarization DNP, in which the proton polarization is increased by a microwave-driven transfer of polarization between unpaired electrons and protons. Recently, Kobayashi et al. demonstrated that DNP could be used to record the ^{207}Pb spectrum of lead carbonate phase in white lead pigment. A mixture of TEKPoL biradical and 1,1,2,2 tetrachloroethane:methanol-d4 (96/4) was added to the sample and play the role of polarization source and enhancing the signal by a factor of eight.

Kehlet el al. applied ultrafast spinning solid-state NMR spectroscopy, which offers higher resolution in comparison to the conventional solid-state NMR. This technique requires only few milligrams of sample making it a suitable method for the analysis of art paint. ^{13}C showed a shift in the carbonyl signal from 173 ppm in the linseed oil reference sample to 182 ppm in oil paint sample, which corresponds more to a carboxylate rather than an ester bond. Those results indicate that triglycerides ester bonds were hydrolyzed during polymerization and aging process.

VI. Gas chromatography mass spectrometry pyrolysis

GC-MS provides information on the organic compounds present in paint. It consists on the coupling of gas chromatography (GC) and a mass spectrometer (MS). GC-MS separates the constituents of a sample by chromatography and collects their mass spectrum in order to identify them. The presence of oil, waxes, resins, polysaccharide gums and animal glues can thus be demonstrated in paint samples.[31] However, this technique does not allow the analysis of non-volatile products, which often make up the majority of old paintings.

Gas chromatography techniques are used and applied for the analysis of non-cross-linked linseed oil paint films. Methanolic extracts of the soluble part of a linseed oil film were investigated by GC-MS following an offline or online derivatization. The two strategies gave reproducible and comparable results, online method is faster however the offline one is more suitable for a mixture of binding media.[32] The offline methylation was done by methylation or trimethylsilyl derivatization.[33] Both modes of derivatization allowed the detection by GC-MS of a series of short-chain fatty (di)acids and C_{16} and (oxidized) C_{18} fatty acids.

In another study, GC-MS was applied to investigate lipids based paint film degradation after irradiation with UV light and exposition to NO_x and SO_2 gases.[34] The obtained results showed the cleavage of fatty acids chains and the formation of oxalic acid. The developed method was later applied on Cimabue, Raffaello and Boucher paintings, and analysis by GC-MS indicates the presence of oxalic acid and oxidized carboxylic acids. This study focused on the understanding of oil paint ageing, highlighting on the fatty acid chains degradation and the formation of free carboxylic acids. GC-MS allows as well the identification of lipid binders used in oil paintings by calculating the ratio between the areas of stearic and palmitic acid peaks (S/P). Saturated fatty acids as palmitic and stearic acids, in contrary to the unsaturated fatty acids, are more stable during ageing of oil paints, do not participate in the polymerization and are less influenced by the present pigments in the sample process.[35,36] The effect of pigments on the cross-linking mechanism of siccative oils was also under investigation using GC-MS.[37]

VII. Mass spectrometry

Mass spectrometry is an accurate and robust technique for the identification of siccative oil composition such as linseed oil.[38] *Van den Berg et al.*[39] applied MALDI-TOF MS and FT-ICR techniques to study the effect of linseed oil processing on its triglycerides composition. Results showed that the degree of oxidation increases after oil heating, and is enhanced by the presence of lead pigment. They also succeeded to identify triglycerides oligomers.

MALDI-TOF MS approach was used for the discrimination of egg and oil binders in painted artworks by fingerprinting. The identification of specific markers belonging to various lipid classes, such as triacylglycerols (TAGs) and phospholipids (PLs), and their oxidation by-products allows the differentiation between egg and oil binders.[40-41]

However, the analysis of dried siccative oil is more challenging, since siccative oils transform into a highly cross-linked and insoluble polymer upon autoxidation. *Muizebelt et al.* worked on the identification of cross-linked fatty acids by ESI-MS techniques.[42] In their studies, they prepared layers of ethyl ester of linoleic acid and methyl ester of ricinoic acid (MR) mixed with Co/Ca/Zr drier, which were allowed to react with air. The recovered oligomer from the polymerization mechanism of unsaturated fatty acids was analyzed with ESI-MS equipped with a quadrupole analyzer. The mass spectrum (Figure 131) shows the presence of dimers, trimers and tetramers of linoleic acid. The identified compounds indicate the formation of C-C, ether and peroxide crosslinks. *Zovi et al.*[43] investigated stand oil reactions by identifying the resulting products using NMR and mass spectrometry. In their work, they heated linseed oil at 270 to 360 °C under nitrogen flux, and then they cleaved the bonds between the glycerol and the fatty acids by saponification in order to recover only the cross-linked fatty acids. The NMR and MS analysis confirmed the formation of monounsaturated ring of six carbon atoms resulting from a Dials-alders addition. Furthermore, the MS analysis, signals the addition of an allylic radical on double bonds, followed by combination or elimination reactions. HPLC-ESI-Q-ToF allows the acquisition of triglycerides profile and the characterization of lipids present in oil paints unlike the GC-MS which is limited by the identification of the composition of fatty acids only.[44]

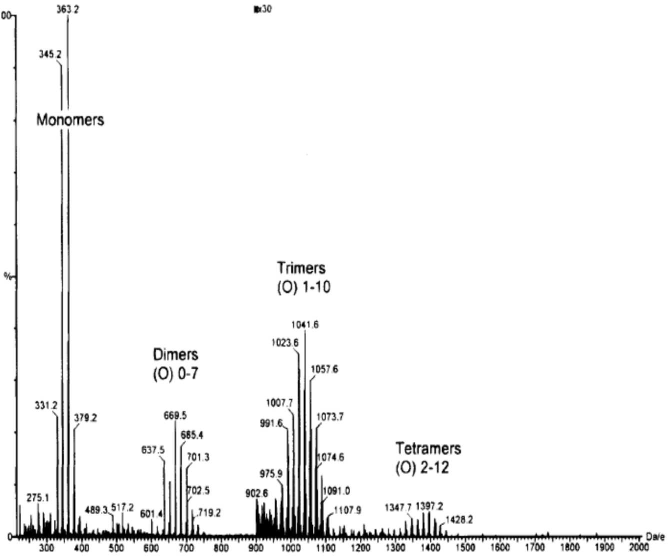

Figure 131. ESI-MS spectrum of cross-linked linoleic acid[42]

Van Loon et al.[45] proposed direct temperature-resolved TOF-MS techniques as a fingerprinting strategy for the identification of oils, resins, waxes and other compounds present in complex samples in paintings. Modern time-of-flight mass spectrometers can offer high resolution and sensitivity. The acquisition of accurate mass permits to calculate the Kendrick mass defect which can be graphically represented by Kendrick plot (Figure 132).

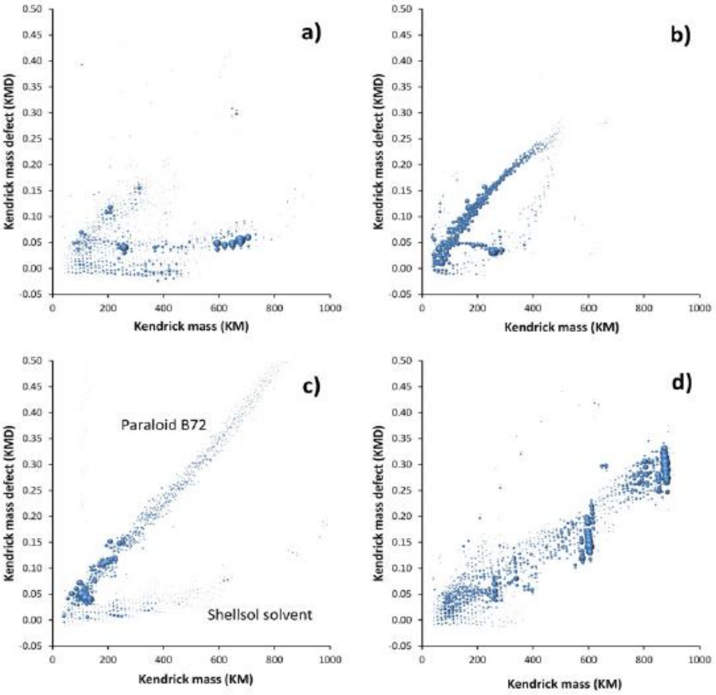

Figure 132. Kendrick plots of paintings and conservation reference materials, beeswax (a), rabbit skin glue (b), Paraloid B72 in Shellsol A (c), fresh linseed oil (d).[45]

References

1. Js, M.; White, R., The organic chemistry of museum objects. *Buttersworth: London, UK* **1994**.
2. Maroger, J., The secret formulas and techniques of the masters. **1948**.
3. Perego, F., *Dictionnaire des matériaux du peintre*. Belin Paris: 2005; Vol. 895.
4. Laurie, A., The refractive index of a solid film of linseed oil rise in refractive index with age. *Proceedings of the Royal Society of London. Series A-Mathematical and Physical Sciences* **1937,** *159* (896), 123-133.
5. Gavrilov, D.; Maev, R. G.; Almond, D., A review of imaging methods in analysis of works of art: Thermographic imaging method in art analysis. *Canadian Journal of Physics* **2014,** *92* (4), 341-364.
6. Meneghetti, S. M.; de Souza, R. F.; Monteiro, A. L.; de Souza, M. O., Substitution of lead catalysts by zirconium in the oxidative polymerization of linseed oil. *Progress in organic coatings* **1998,** *33* (3-4), 219-224.
7. Schaich, K., Metals and lipid oxidation. Contemporary issues. *Lipids* **1992,** *27* (3), 209-218.
8. Tumosa, C. S.; Mecklenburg, M. F., The influence of lead ions on the drying of oils. *Studies in Conservation* **2005,** *50* (sup1), 39-47.
9. Zhang, Q.; Saleh, A. S. M.; Chen, J.; Shen, Q., Chemical alterations taken place during deep-fat frying based on certain reaction products : A review. *Chemistry and Physics of Lipids* **2012,** *165*, 662-681.
10. Mallégol, J.; Gonon, L.; Commereuc, S.; Verney, V., Thermal (DSC) and chemical (iodometric titration) methods for peroxides measurements in order to monitor drying extent of alkyd resins. **2001,** *41*, 171-176.
11. Tanase, S.; Bouwman, E.; Reedijk, J., Role of additives in cobalt-mediated oxidative crosslinking of alkyd resins. **2004,** *259*, 101-107.
12. Muizebelt, W. J.; Hubertb, J. C.; Venderboschb, R. A. M., Mechanistic study of drying of alkyd resins using ethyl linoleate as a model substance. **1994,** *24*, 263-279.
13. Black, J., Metal-catalyzed autoxidation. The unrecognized consequences of metal-hydroperoxide complex formation. *Journal of the American Chemical Society* **1978,** *100* (2), 527-535.
14. Reviews, C.; Science, F., Chemistry of Deep-Fat Frying Oils. **2015,** *72*.
15. Boer, J. W. D.; Wesenhagen, P. V.; Wenker, E. C. M.; Maaijen, K.; Gol, F.; Gibbs, H.; Hage, R., The Quest for Cobalt-Free Alkyd Paint Driers. **2013**, 3581-3591.
16. Derrick, M. R.; Stulik, D.; Landry, J. M., *Infrared spectroscopy in conservation science*. Getty Publications: 2000.
17. Mallégol, J.; Gardette, J.-l.; Lemaire, J., Long-Term Behavior of Oil-Based Varnishes and Paints I . Spectroscopic Analysis of Curing Drying Oils. **1999,** *76*, 967-976.
18. Mallégol, J.; Lemaire, J.; Gardette, J.-l., Drier influence on the curing of linseed oil. **2000,** *39*, 107-113.
19. Mallégol, J.; Gardette, J.-l.; Lemaire, J., Long-Term Behavior of Oil-Based Varnishes and Paints . Photo- and Thermooxidation of Cured Linseed Oil. **2000,** *77*, 257-263.
20. Lazzari, M.; Chiantore, O., Drying and oxidative degradation of linseed oil. **1999,** *65*, 303-313.
21. De Viguerie, L.; Payard, P.; Portero, E.; Walter, P.; Cotte, M., The drying of linseed oil investigated by Fourier transform infrared spectroscopy: historical recipes and influence of lead compounds. *Progress in Organic Coatings* **2016,** *93*, 46-60.
22. Osmond, G.; Boon, J. J.; Puskar, L., Metal Stearate Distributions in Modern Artists ’ Oil Paints : Surface and Cross-Sectional Investigation of Reference Paint Films Using Conventional and Synchrotron Infrared Microspectroscopy. **2012,** *66*, 1136-1144.
23. Kaszowska, Z.; Malek, K.; Pa, M.; Mikołajska, A., Vibrational Spectroscopy A joint application of ATR-FTIR and SEM imaging with high spatial resolution : Identification and distribution of painting materials and their degradation products in paint cross sections. **2013,** *65*, 1-11.
24. Ko, V.; Hradil, D.; Hradilová, J.; Ivan, N.; Schreiner, M., Spectrochimica Acta Part A : Molecular and Biomolecular Spectroscopy The ef fi ciency of micro-Raman spectroscopy in the analysis of complicated mixtures in modern paints : Munch ' s and Kupka ' s paintings under study. **2016,** *156*, 36-46.

25. Daher, C.; Paris, C.; Le Hô, A. S.; Bellot-Gurlet, L.; Échard, J. P., A joint use of Raman and infrared spectroscopies for the identification of natural organic media used in ancient varnishes. *Journal of Raman Spectroscopy* **2010,** *41* (11), 1494-1499.

26. Dlugogorski, B. Z.; Kennedy, E. M.; Mackie, J. C., Roles of peroxides and unsaturation in spontaneous heating of linseed oil. *Fire Safety Journal* **2013,** *61*, 108-115.

27. Oyman, Z. O.; Ming, W.; Linde, R. V. D., Oxidation of 13 C-labeled ethyl linoleate monitored and quantitatively analyzed by 13 C NMR. **2006,** *42*, 1342-1348.

28. Mosca, S.; Frizzi, T.; Pontone, M.; Alberti, R.; Bombelli, L.; Capogrosso, V.; Nevin, A.; Valentini, G.; Comelli, D., Identification of pigments in different layers of illuminated manuscripts by X-ray fluorescence mapping and Raman spectroscopy. *Microchemical Journal* **2016,** *124*, 775-784.

29. Zidan, E. H.; Mosca, S.; Bellei, S.; Frizzi, T.; Gironda, M.; El-Rifai, I.; Mahgoub, H.; Sadik, S.; Rashed, M. G.; Osticioli, I., In situ imaging, elemental and molecular spectroscopy for the analysis of the construction and painting of a Late Period coffin at the Egyptian Museum of Cairo. *Measurement* **2018,** *118*, 379-386.

30. Spyros, A.; Anglos, D., Study of Aging in Oil Paintings by 1D and 2D NMR. **2004,** *76*, 4929-4936.

31. Colombini, M. P.; Andreotti, A.; Bonaduce, I.; Modugno, F.; Ribechini, E., Analytical Strategies for Characterizing Organic Paint Media Using Gas Chromatography / Mass. **2010,** *43*, 715-727.

32. Piccirillo, A.; Scalarone, D.; Chiantore, O., Comparison between off-line and on-line derivatisation methods in the characterisation of siccative oils in paint media. **2005,** *74*, 33-38.

33. Berg, J. D. J. V. D.; Berg, K. J. V. D.; Boon, J. J., Identification of non-cross-linked compounds in methanolic extracts of cured and aged linseed oil-based paint films using gas chromatography – mass spectrometry. **2002,** *950*, 195-211.

34. Colombini, M. P.; Modugno, F.; Fuoco, R.; Tognazzi, A., A GC-MS study on the deterioration of lipidic paint binders. **2002,** *73*, 175-185.

35. Manzano, E.; Rodriguez-simón, L. R.; Navas, N.; Checa-moreno, R., Talanta Study of the GC – MS determination of the palmitic – stearic acid ratio for the characterisation of drying oil in painting : La Encarnación by Alonso Cano as a case study. *Talanta* **2011,** *84*, 1148-1154.

36. Identification of lipid binders in paintings by gas chromatography. **2001,** *922*, 385-390.

37. Chiavari, G.; Fabbri, D.; Prati, S., Effect of pigments on the analysis of fatty acids in siccative oils by pyrolysis methylation and silylation §. **2005,** *74*, 39-44.

38. Loutelier-bourhis, C.; Zovi, O.; Lecamp, L.; Bunel, C.; Lange, C. M., Contribution of two approaches using electrospray ionization with multi-stage mass spectrometry for the characterization of linseed oil. **2009**, 3743-3752.

39. Van Den Berg, J. D.; Vermist, N. D.; Carlyle, L.; Holčapek, M.; Boon, J. J., Effects of traditional processing methods of linseed oil on the composition of its triacylglycerols. *Journal of separation science* **2004,** *27* (3), 181-199.

40. Calvano, C. D.; Werf, I. D. V. D.; Palmisano, F., Fingerprinting of egg and oil binders in painted artworks by matrix-assisted laser desorption ionization time-of-flight mass spectrometry analysis of lipid oxidation by-products. **2011**, 2229-2240.

41. Werf, I. D. V. D.; Calvano, C. D.; Palmisano, F.; Sabbatini, L., Analytica Chimica Acta A simple protocol for Matrix Assisted Laser Desorption Ionization- time of flight-mass spectrometry (MALDI-TOF-MS) analysis of lipids and proteins in single microsamples of paintings. *Analytica Chimica Acta* **2012,** *718*, 1-10.

42. Muizebelt, W. J.; Nielen, M. W. F., Oxidative Crosslinking of Unsaturated Fatty Acids Studied with Mass Spec t rornet r y. **1996,** *31*, 545-554.

43. Zovi, O.; Lecamp, L.; Loutelier-bourhis, C.; Lange, C. M.; Bunel, C., Stand reaction of linseed oil. **2011**, 616-626.

44. La, J.; Zanaboni, M.; Uldanck, D.; Degano, I.; Modugno, F.; Kutzke, H.; Storevik, E.; Topalova-casadiego, B.; Perla, M., Analytica Chimica Acta Novel application of liquid chromatography / mass spectrometry for the characterization of drying oils in art : Elucidation on the composition of original paint materials used by Edvard Munch (1863 e 1944). **2015,** *896*, 177-189.

45. Loon, A. V.; Genuit, W.; Pottasch, C.; Smelt, S.; Noble, P., Analysis of old master paintings by direct temperature-resolved time-of- fl ight mass spectrometry : Some recent developments ☆. *Microchemical Journal* **2016,** *126*, 406-414.

46. Johnson, D. W., Alkyldimethylaminoethyl ester iodides for improved analysis of fatty acids by electrospray ionization tandem mass spectrometry. *Rapid Communications in Mass Spectrometry* **2000,** *14* (21), 2019-2024.

Chapter 7:

Results and Discussion

Chapter 7. Results and discussion

The characterization of the cross-linked structure formed during the drying of oil paint and its degradation is still a major challenge in analytical chemistry. The characterization of the structure as well as the knowledge of all the reactions that occur during the ageing of the painting will allow us to evolve the techniques of conservations and restorations. Polymerized drying oils form a very complex and insoluble solid network which makes their analysis very difficult. In addition, these complex materials are generally available only in very small quantities due to strict limits imposed on the sampling of works of art. Despite all these difficulties, several studies were carried out for the characterization of these structures "crosslinked" and several analytical techniques were proposed, however, they only provided general information on the polymerization process without succeeding to unveil the structure of the formed network. High resolution mass spectrometry is the only technique that can give us the opportunity from very low quantity of sample to identify the cross-linked structure formed between different unsaturated fatty acids as well as the different modifications that may occur at the level of this structure. However, limitations still exist. The film of polymerized oil is insoluble and the free fatty acids are difficult to ionize, which makes the analysis more complex and their detections less sensitive.

To overcome these problems, the development of a specific strategy is required (Fig.133). This strategy is based on a soft depolymerization and the correlation between analyses by nuclear magnetic resonance and ultra-high-resolution mass spectrometry and consists of the following steps:

- Analysis of fresh drying oils: This step consists on performing a survey on pure siccative oils using NMR and HRMS to identify their composition in triglycerides.
- Classification of present-day oil paint tubes: the majority of oil paint suppliers still exist until these days and manufacture a wide variety of paint tubes. In this step, oils containing in oil paint tubes from several supplier were extracted and identified.
- Classification of old oil paint tubes: This step is very similar to the previous one, however, the oil paint tubes originated from different past periods.
- Development of a soft depolymerization technique that can be applied on both fresh and dried siccative oils.

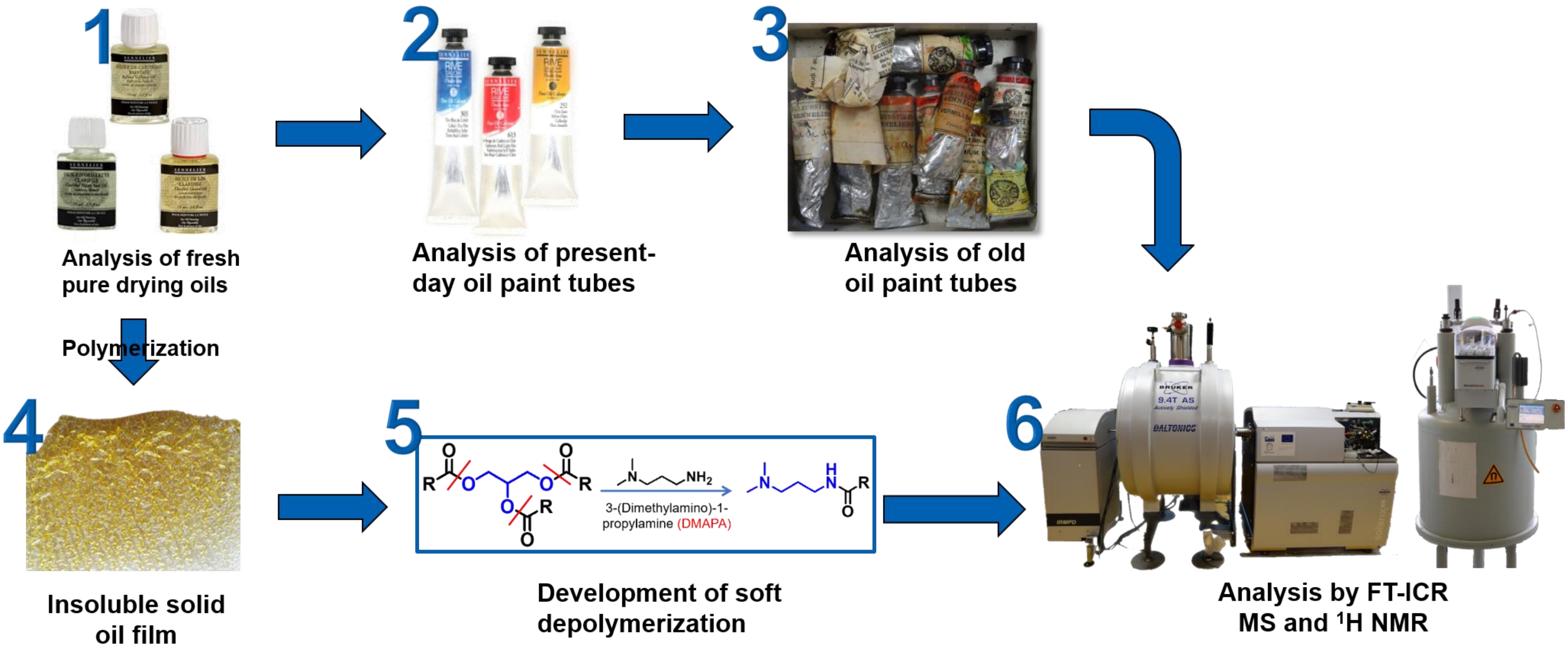

Figure 133. Developed strategy for the analysis of art oil painting

I. Analysis of fresh drying oils

First, we studied the composition of fresh pure drying oils before the drying process. Five different oils used in oil paints were analyzed using ^{1}H NMR and direct infusion on the FT-ICR ultra-high-resolution mass spectrometer:

Linseed oil: linseed oil, also called flaxseed oil can be extracted from the dried and ripened seeds of the flax plant. It is colorless to yellowish and has a very high drying effect due to its high content in polyunsaturated fatty acids.

Safflower oil: it comes from the seeds of the safflower plant. It can be used in cosmetics and as a paint solvent. It has a moderate drying effect.

Walnut oil: walnut oil is extracted from walnuts. It is composed mainly of linolenic acid (58%). It is considered one of the most important oils used by Renaissance painters due to its short drying time and resistance to yellowing.

Soya oil: Also known as soybean oil, it is extracted from the seeds of soybean. As a drying oil, it is used as a base for printing inks and oil paints.

Poppy oil: It is an edible oil from poppy seeds. It is used as drying oil in oil painting and especially in white paints as it does not leave an unwanted yellow tint.

Triglycerides are the major components of drying oils. They are formed by a backbone of glycerol and three chains of fatty acids. The chains can be combinations of five different fatty acids: saturated acids (palmitic (C16:0) and stearic (C18:0)) monounsaturated acid (oleic (C18:1)) and polyunsaturated acids such as linoleic (C18:2) and linolenic (C18:3) (Fig. 134).

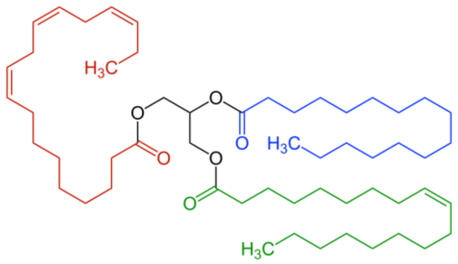

Figure 134. Triglyceride molecule formed of glycerol (in black), palmitic acid (blue), oleic acid (green) and linolenic acid (red)

I.1. ^{1}H NMR analysis

In a first stage, ^{1}H-NMR was employed for qualitatively screening the various drying oils.

I.1.1. Linseed oil

Linseed oil was first analyzed by ^{1}H NMR and used as reference for all other oils. Signals for protons of triglycerides were identified (Figure 135).

On the spectrum we observe that signal **A** corresponds to the triplet arising from the terminal methyl group in the fatty acid chains with no unsaturation at their end. The proton "**B**" is a triplet corresponding to the terminal methyl of linolenic acid. This proton can be used as a marker for the presence of unsaturation at the end of the chain specific for linoleic acids. Signal **C** and **D** represent CH_2 groups constituting the fatty acid chain backbone and β-CH_2 respectively. The signal **E** around 2.04 ppm corresponds to methylene protons in β-position with respect to the carbonyl group. Signal **F** and **G** correspond to allylic protons and α-hydrogens of triglycerides respectively. Signal **H** constituted of two doublets of doublets at around 4.14 and 4.29 ppm, corresponds to the CH_2 protons of the glycerol while the signal corresponding to the CH proton of glycerol may be identified as peak **I**. Finally, signal **J** can be attributed to the olefinic protons of unsaturation in the fatty acid chains.

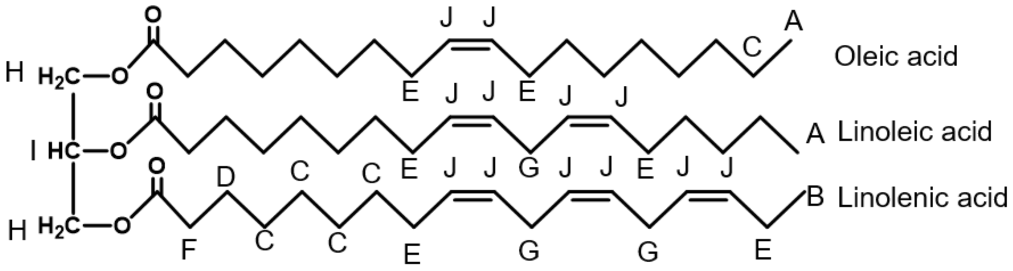

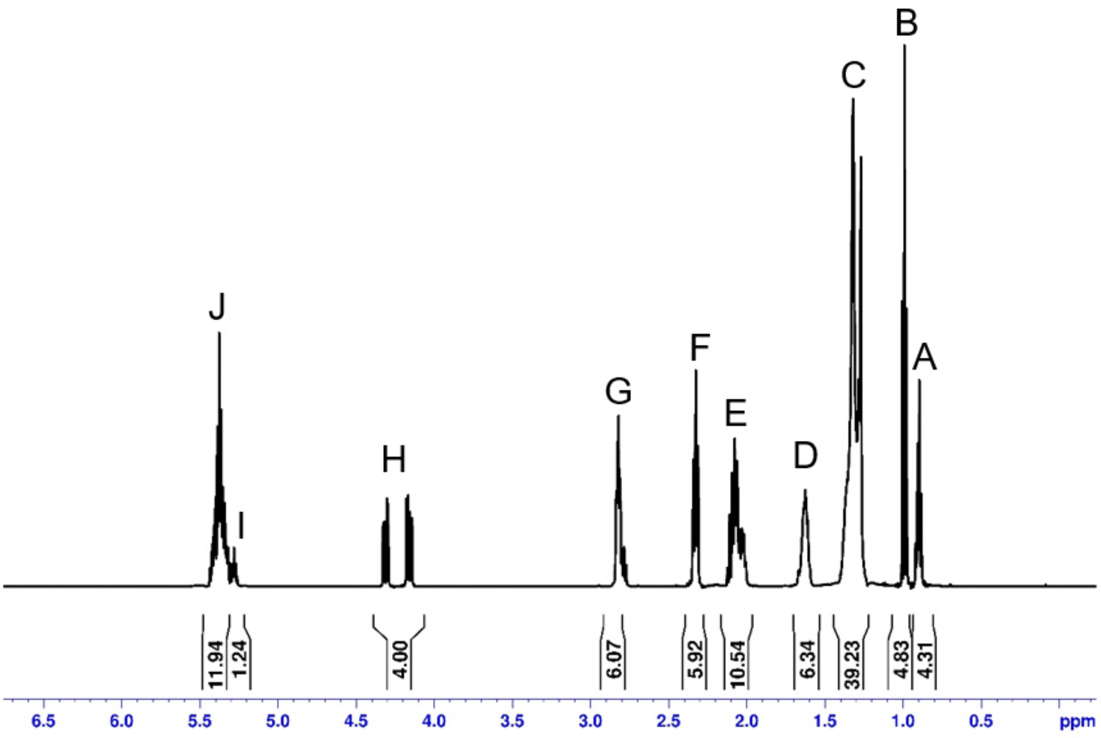

Figure 135. ^{1}H NMR spectrum of fresh linseed oil

Proton	Attribution	Chemical shift	Integration
J	CH=CH	5.4 - 5.28 ppm	11.94
I	O-$\underline{CH}$-CH_2	5.26 ppm	1.24
H	O-$\underline{CH_2}$-CH	4.29 and 4.14 ppm	4.00
G	=CH-$\underline{CH_2}$-CH=	2.76 ppm	6.07
F	CO-$\underline{CH_2}$	2.30 ppm	5.92
E	=CH-$\underline{CH_2}$-$\underline{CH_2}$	2.04 ppm	10.54
D	CO-CH_2-$\underline{CH_2}$	1.6 ppm	6.34
C	CH_2-$\underline{CH_2}$-CH_2	1.3 ppm	39.23
B	CH_3	1.02 - 0.95 ppm	4.83
A	CH_3	0.88 ppm	4.31

By estimating the number of unsaturation in the triglyceride's molecules of linseed oil, we notice that we have around 6 unsaturation by triglyceride and around 3 CH_2 in alpha position between two unsaturation.

The next step is to calculate the average length of the fatty acid's chains:

Average composition	Number of protons	Number of carbon
CH	~12	12
CH_2	72	36
CH_3	9	3
Total	**93**	**51**

The total number of carbons in the three chains of fatty acids is 51 carbons. In average we have 51/3 = 17 carbon atoms in each chain without including the carboxyl. This gives an average of 18 carbon chains in the triglyceride molecules of linseed oil.

By combining all the calculated values:

Total number of unsaturation = 6 unsaturation

Number of CH_2 in alpha position = 3 CH_2

Number of carbon atoms in each fatty acid chain = 18 carbons

In addition to the presence of a very high intensity signal of proton B specific to linolenic acid

We can conclude that the average major triglycerides in linseed oil are formed of the three unsaturated fatty acids oleic (C18:1), linoleic (C18:2) and linolenic (C18:3) giving the following representation:

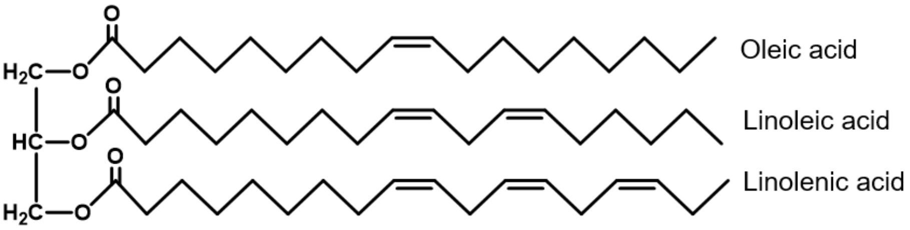

I.1.2. Walnut oil

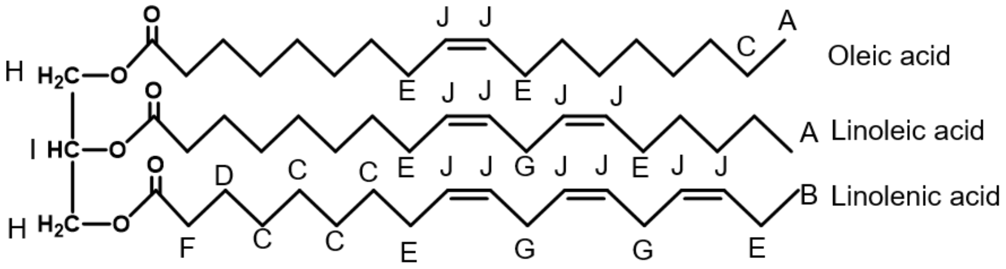

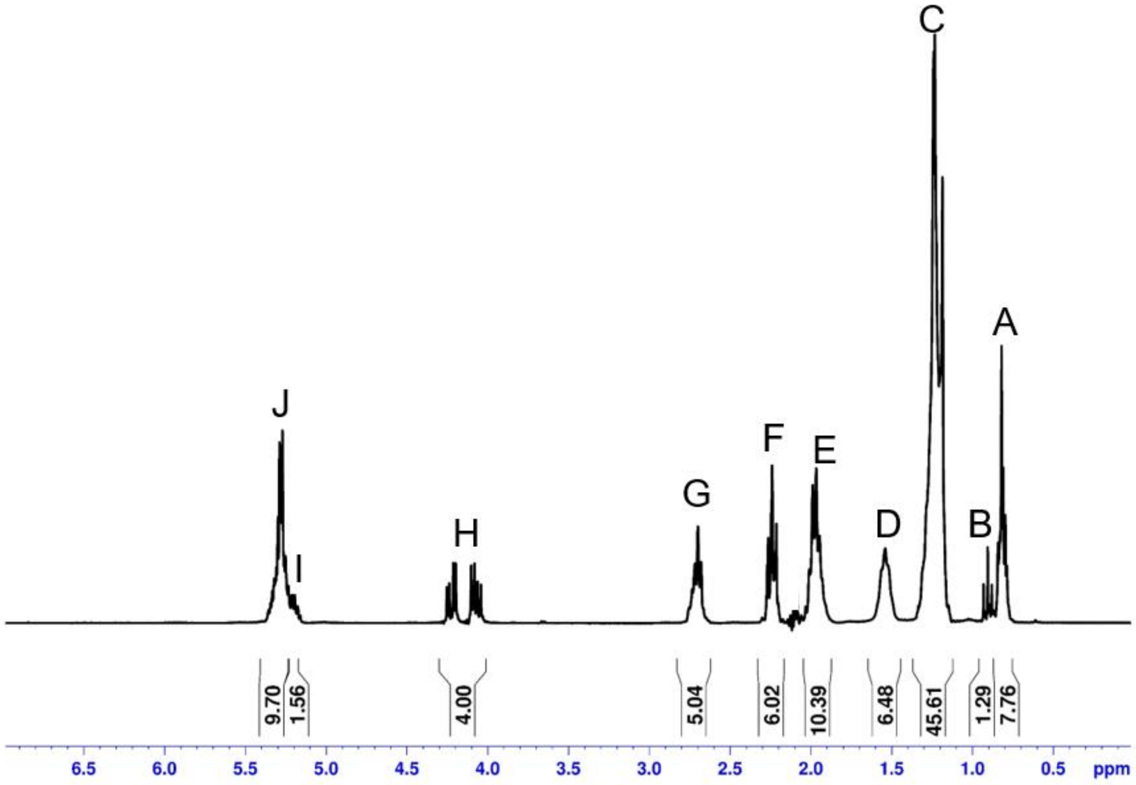

Figure 136. ^{1}H NMR spectrum of fresh walnut oil

Proton	Attribution	Chemical shift	Integration
J	CH=CH	5.4 - 5.28 ppm	9.70
I	$O\text{-}\underline{CH}\text{-}CH_2$	5.26 ppm	1.56
H	$O\text{-}\underline{CH_2}\text{-}CH$	4.29 and 4.14 ppm	4.00
G	$=CH\text{-}\underline{CH_2}\text{-}CH=$	2.76 ppm	5.04
F	$CO\text{-}\underline{CH_2}$	2.30 ppm	6.02
E	$=CH\text{-}\underline{CH_2\text{-}CH_2}$	2.04 ppm	10.39
D	$CO\text{-}CH_2\text{-}\underline{CH_2}$	1.6 ppm	6.48
C	$CH_2\text{-}\underline{CH_2}\text{-}CH_2$	1.3 ppm	45.61
B	CH_3	1.02 - 0.95 ppm	1.29
A	CH_3	0.88 ppm	7.76

By estimating the number of unsaturation in the triglyceride's molecules of walnut oil, we notice that we have around 5 unsaturation by triglyceride and around 2.5 CH_2 in alpha position between two unsaturation.

The next step is to calculate the average length of the fatty acid's chains:

Average composition	Number of protons	Number of carbon
CH	~10	10
CH_2	77	38.5
CH_3	9	3
Total	**96**	**51.5**

The total number of carbons in the three chains of fatty acids is 51.5 carbons. In average we have 51.5/3 = 17 carbon atoms in each chain without including the carboxyl.

We can conclude that in the triglyceride molecules of walnut oil, there are chains with an average of 18 carbon atoms.

By combining all the calculated values:

Total number of unsaturation = 5 unsaturation

Number of CH_2 in alpha position = 2.5 CH_2

Number of carbon atoms in each fatty acid chain = 18 carbons

In addition to the presence of a low intensity signal of proton B specific to linolenic acid

We can conclude that the average major triglycerides in walnut oil are formed of two unsaturated fatty acids oleic (C18:1) and linolenic (C18:3) giving the following representation:

I.1.3. Soybean oil

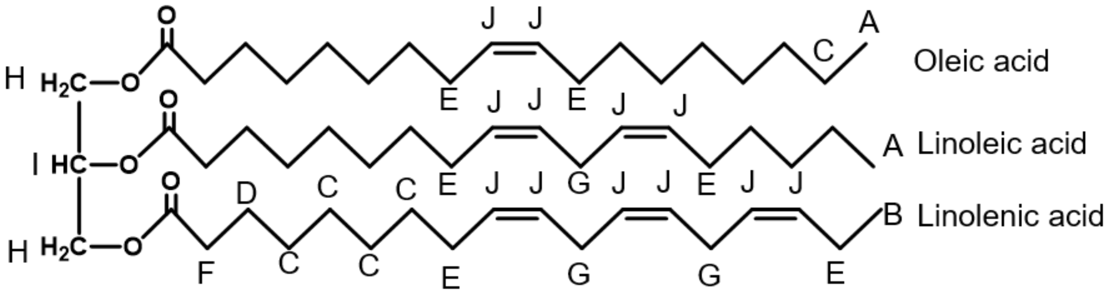

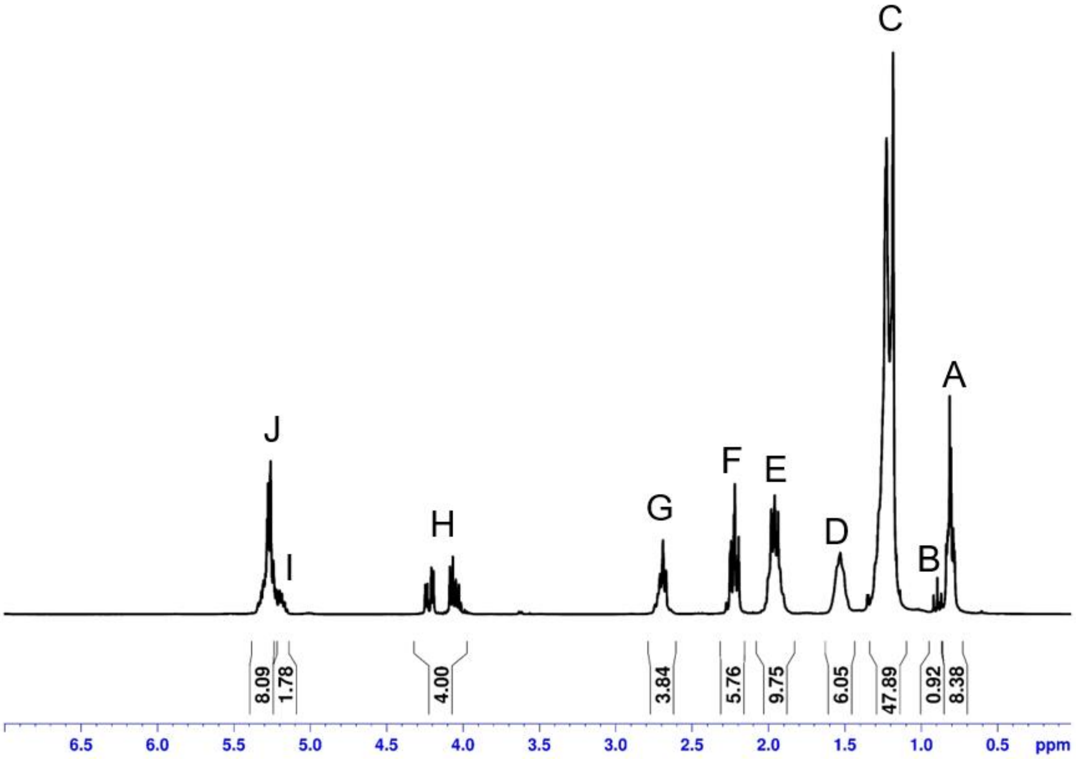

Figure 137. ^{1}H NMR spectrum of fresh soybean oil

Proton	Attribution	Chemical shift	Integration
J	CH=CH	5.4 - 5.28 ppm	8.09
I	O-$\underline{CH}$-CH_2	5.26 ppm	1.78
H	O-$\underline{CH_2}$-CH	4.29 and 4.14 ppm	4.00
G	=CH-$\underline{CH_2}$-CH=	2.76 ppm	3.84
F	CO-$\underline{CH_2}$	2.30 ppm	5.76
E	=CH-$\underline{CH_2}$-$\underline{CH_2}$	2.04 ppm	9.75
D	CO-CH_2-$\underline{CH_2}$	1.6 ppm	6.05
C	CH_2-$\underline{CH_2}$-CH_2	1.3 ppm	47.89
B	CH_3	1.02 - 0.95 ppm	0.92
A	CH_3	0.88 ppm	8.38

By estimating the number of unsaturation in the triglyceride's molecules of soybean oil, we notice that we have around 4 unsaturation by triglyceride and around 2 CH_2 in alpha position between two unsaturation.

The next step is to calculate the average length of the fatty acid's chains:

Average composition	Number of protons	Number of carbon
CH	~8	8
CH_2	77	38.5
CH_3	9	3
Total	**94**	**49.5**

The total number of carbons in the three chains of fatty acids is 49.5 carbons. In average we have 49.5/3 = 16.5 carbon atoms in each chain without including the carboxyl.

We can conclude that in the triglyceride molecules of soybean oil, there are chains with an average of 17.5 carbon atoms.

By combining all the calculated values:

Total number of unsaturation = 4 unsaturation

Number of CH_2 in alpha position = 2 CH_2

Number of carbon atoms in each fatty acid chain = 17.5 carbons

In addition to the presence of very low intensity signal of proton B specific to linolenic acid

We can conclude that average triglycerides in soybean oil can be formed of two unsaturated fatty acids oleic (C18:1) and linolenic (C18:3) and one saturated fatty acid, palmitic (C16:0), or two unsaturated linoleic acids (C18:2) and one palmitic acid giving the following representations:

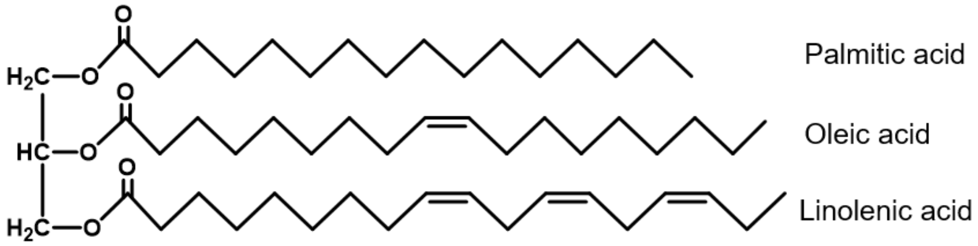

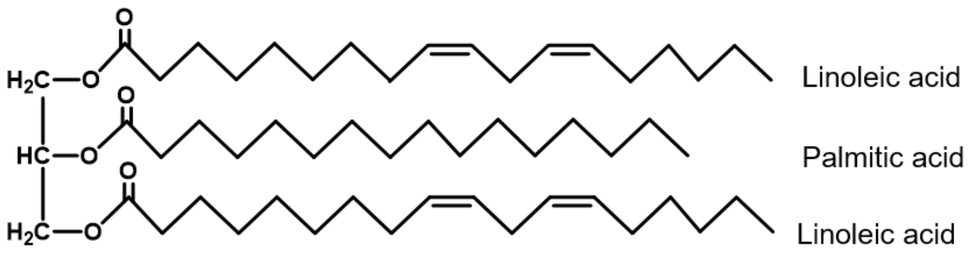

I.1.4. Safflower oil

The proton "B" which is used as a marker for linolenic acid does not appear on the spectrum of safflower oil meaning that this oil does not contain linolenic acid chains with three unsaturation.

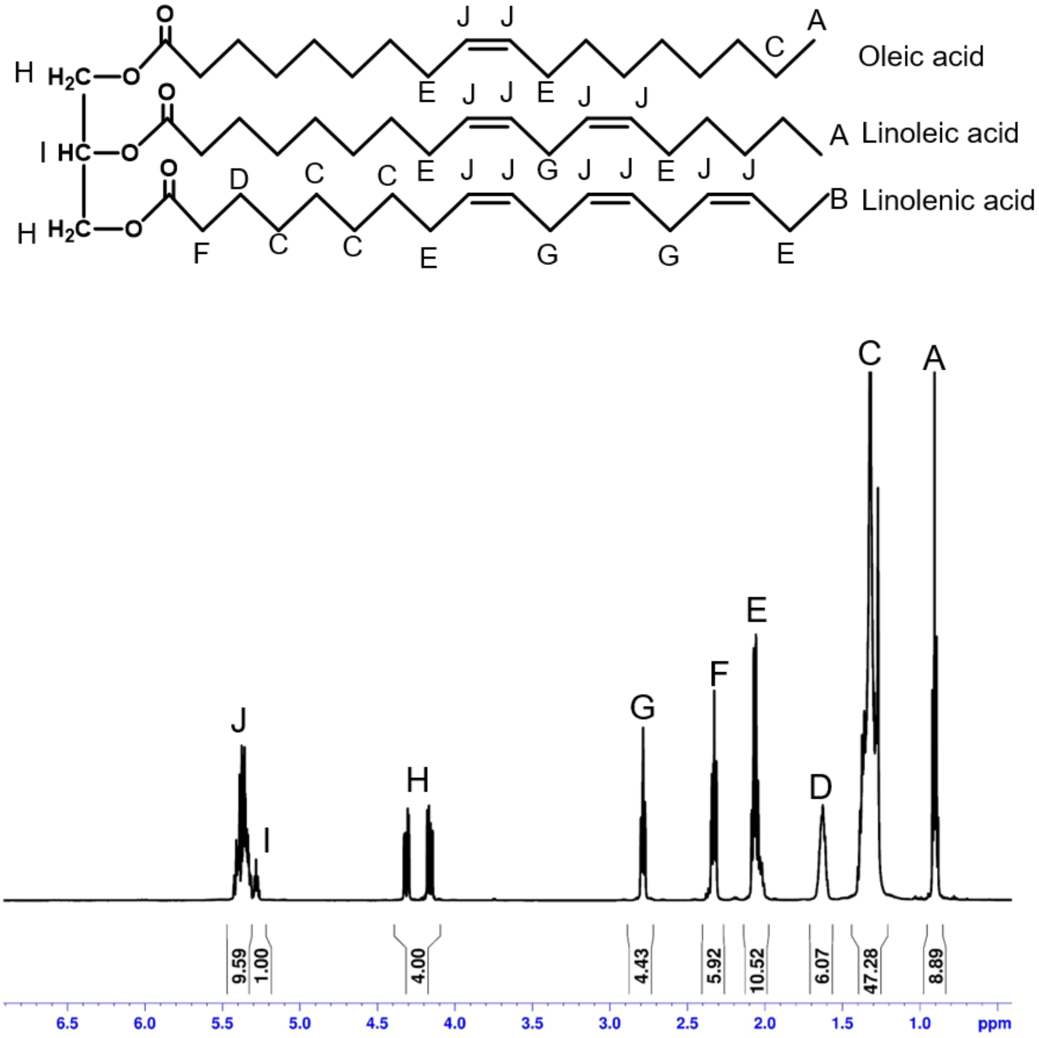

Figure 138. ^{1}H NMR spectrum of fresh safflower oil

Proton	Attribution	Chemical shift	Integration
J	CH=CH	5.4 - 5.28 ppm	9.59
I	$\mathrm{O{-}\underline{CH}{-}CH_2}$	5.26 ppm	1.00
H	$\mathrm{O{-}\underline{CH_2}{-}CH}$	4.29 and 4.14 ppm	4.00
G	$\mathrm{{=}CH{-}\underline{CH_2}{-}CH{=}}$	2.76 ppm	4.43
F	$\mathrm{CO{-}\underline{CH_2}}$	2.30 ppm	5.92
E	$\mathrm{{=}CH{-}\underline{CH_2{-}CH_2}}$	2.04 ppm	10.52
D	$\mathrm{CO{-}CH_2{-}\underline{CH_2}}$	1.6 ppm	6.07
C	$\mathrm{CH_2{-}\underline{CH_2}{-}CH_2}$	1.3 ppm	47.28
B	$\mathrm{CH_3}$	-	-
A	$\mathrm{CH_3}$	0.88 ppm	8.89

By estimating the number of unsaturation in the triglyceride's molecules of safflower oil, we notice that we have around 5 unsaturation by triglyceride and around 2.2 CH_2 in alpha position between two unsaturation.

The next step is to calculate the average length of the fatty acid's chains:

Average composition	Number of protons	Number of carbon
CH	~10	10
CH_2	78	39
CH_3	9	3
Total	**97**	**52**

The total number of carbons in the three chains of fatty acids is 52 carbons. In average we have 52/3 = 17.3 carbon atoms in each chain without including the carboxyl.

We can conclude that in the triglyceride molecules of safflower oil, there are chains with an average of 18 carbon atoms.

By combining all the calculated values:

Total number of unsaturation = 5 unsaturation

Number of CH_2 in alpha position = 2.2 CH_2

Number of carbon atoms in each fatty acid chain = 18 carbons

In addition to the absence of proton B specific to linolenic acid

We can conclude that the average major triglycerides in safflower oil are formed of two unsaturated fatty acids oleic (C18:1) and linoleic (C18:2) giving the following representation:

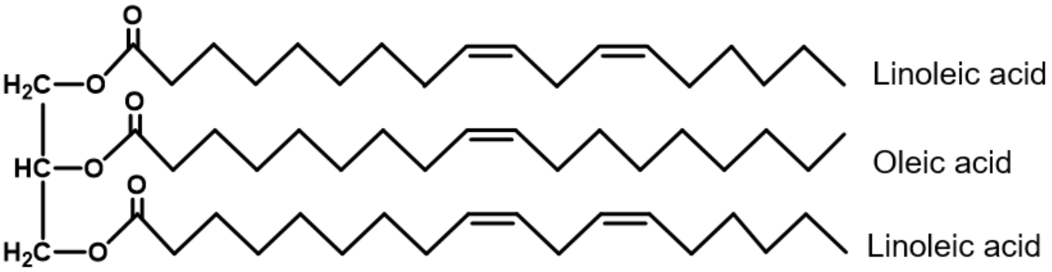

I.1.5. Poppy oil

As in the case of safflower oil, the proton "B" does not appear on the spectrum of poppy oil meaning that this oil also does not contain linolenic acid chains with three unsaturation.

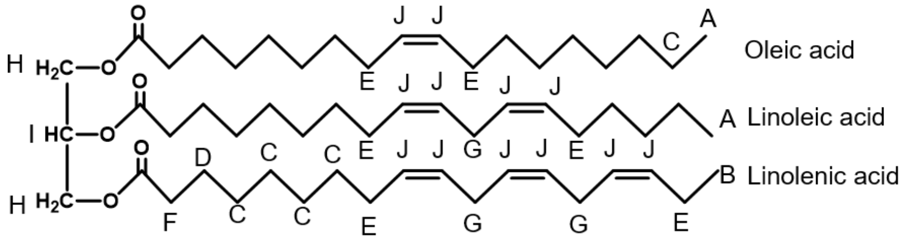

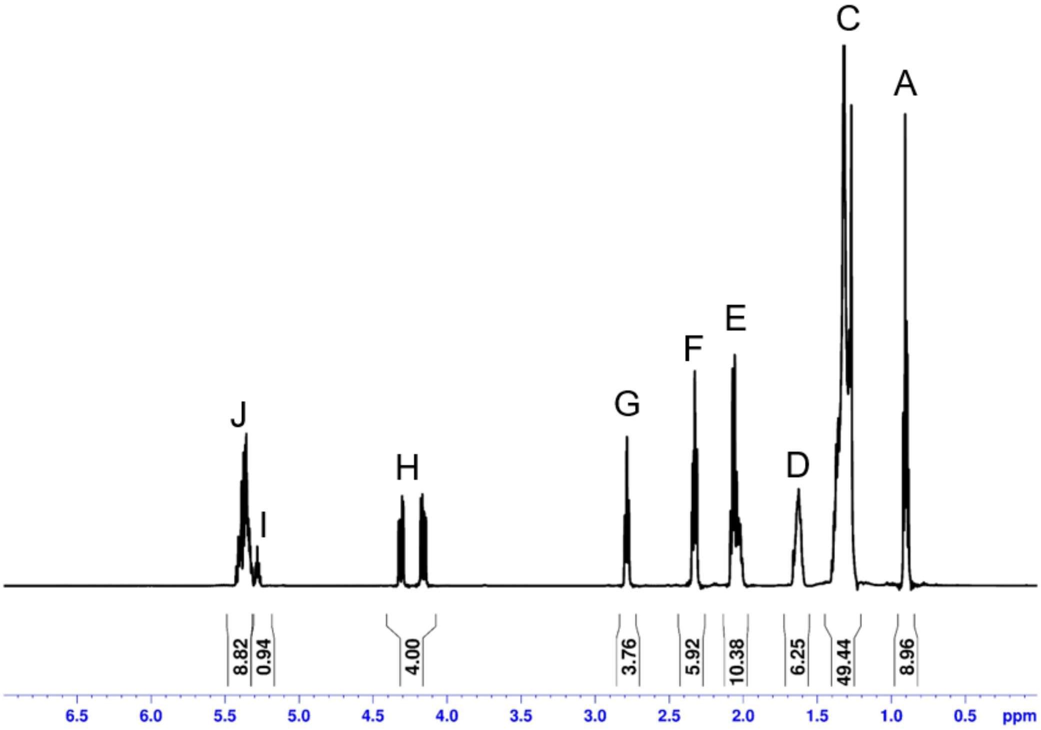

Figure 139. ^{1}H NMR spectrum of fresh poppy oil

Proton	Attribution	Chemical shift	Integration
J	CH=CH	5.4 - 5.28 ppm	8.82
I	O-$\underline{CH}$-CH_2	5.26 ppm	0.94
H	O-$\underline{CH_2}$-CH	4.29 and 4.14 ppm	4.00
G	=CH-$\underline{CH_2}$-CH=	2.76 ppm	3.76
F	CO-$\underline{CH_2}$	2.30 ppm	5.92
E	=CH-$\underline{CH_2}$-$\underline{CH_2}$	2.04 ppm	10.38
D	CO-CH_2-$\underline{CH_2}$	1.6 ppm	6.25
C	CH_2-$\underline{CH_2}$-CH_2	1.3 ppm	49.94
B	CH_3	-	-
A	CH_3	0.88 ppm	8.95

By estimating the number of unsaturation in the triglyceride's molecules of poppy oil, we notice that we have around 5 unsaturation by triglyceride and around 2 CH_2 in alpha position between two unsaturation.

The next step is to calculate the average length of the fatty acid's chains:

Average composition	Number of protons	Number of carbon
CH	~9	9
CH_2	80	40
CH_3	9	3
Total	**98**	**52**

The total number of carbons in the three chains of fatty acids is 52 carbons. In average we have 52/3 = 17.3 carbon atoms in each chain without including the carboxyl.

We can conclude that in the triglyceride molecules of soybean oil, there are chains with an average of 18 carbon atoms.

By combining all the calculated values:

Total number of unsaturation = 5 unsaturation

Number of CH_2 in alpha position = 2 CH_2

Number of carbon atoms in each fatty acid chain = 18 carbons

In addition to the absence of proton B specific to linolenic acid

We can conclude that the average major triglycerides in poppy oil are formed of two unsaturated fatty acids oleic (C18:1) and linoleic (C18:2) giving the following representation:

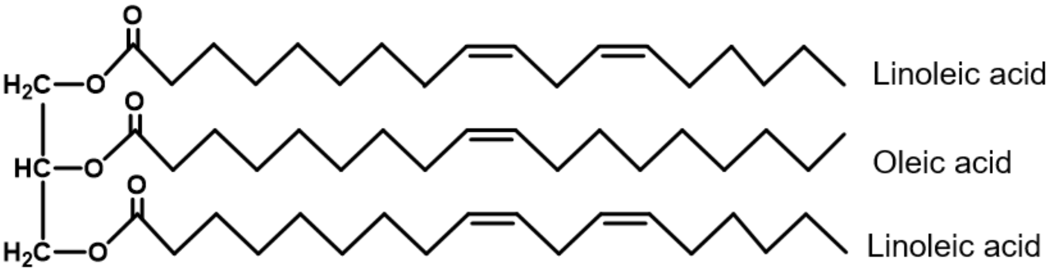

I.2. FT-ICR MS analysis

^{1}H NMR analysis afforded very important information about the triglyceride's composition of the different analyzed oils. However, several limitations still exist. For example, only one triglyceride molecule with one specific combination of fatty acid chains can be identified while other different combinations also exist. In addition, it is relatively easy to distinguish between linseed, walnut and soybean oil from the ^{1}H NMR spectra by looking at the intensity of the signal of the terminal B proton specific to linolenic acid. In fact, the intensity of this signal is the highest in linseed oil followed by walnut and finally soybean oil. On the other hand, safflower and poppy oils do not contain linolenic acids in their composition, thus the signal of the B proton does not appear on their spectra. These two oils are also formed of the same triglyceride molecule meaning that separating them based only on their ^{1}H NMR spectra is almost impossible.

For these reasons, the use of a more accurate and robust technique such as FT-ICR MS is required. This technique allows the identification of all possible combinations of triglycerides forming each oil.

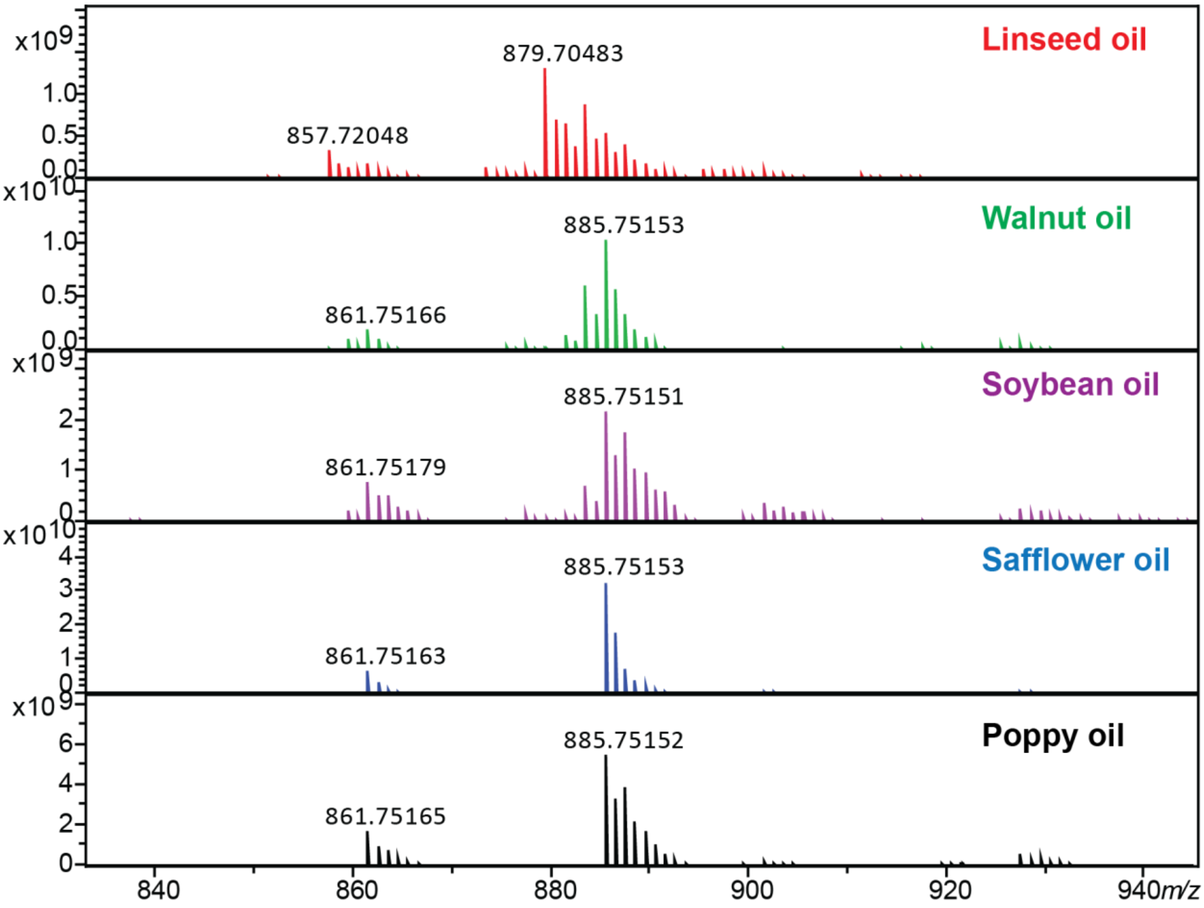

Figure 140. ESI (+) FT-ICR MS of the five most common siccative oils

I.2.1. Linseed oil

Commercial fresh linseed oil sample was directly injected in the FT-ICR mass spectrometer. The mass spectrum (Figure 141) shows the complexity of the fresh linseed oil. Different combinations of 5 different fatty acids were identified containing: saturated acids (palmitic acid (C16:0) and stearic acid (C18:0)), mono-saturated acid (oleic acid (C18:1)) and polyunsaturated acids such as linoleic acid (C18:2) and linolenic acid (C18:3). In addition, some identified triglycerides were oxidized by one or more oxygen atoms. According to the mass spectrum of linseed oil, the triglyceride molecule which has nine unsaturation is the major triglyceride present in the linseed oil (Table 17). This analysis shows the heterogenic and the complex composition of a linseed oil.

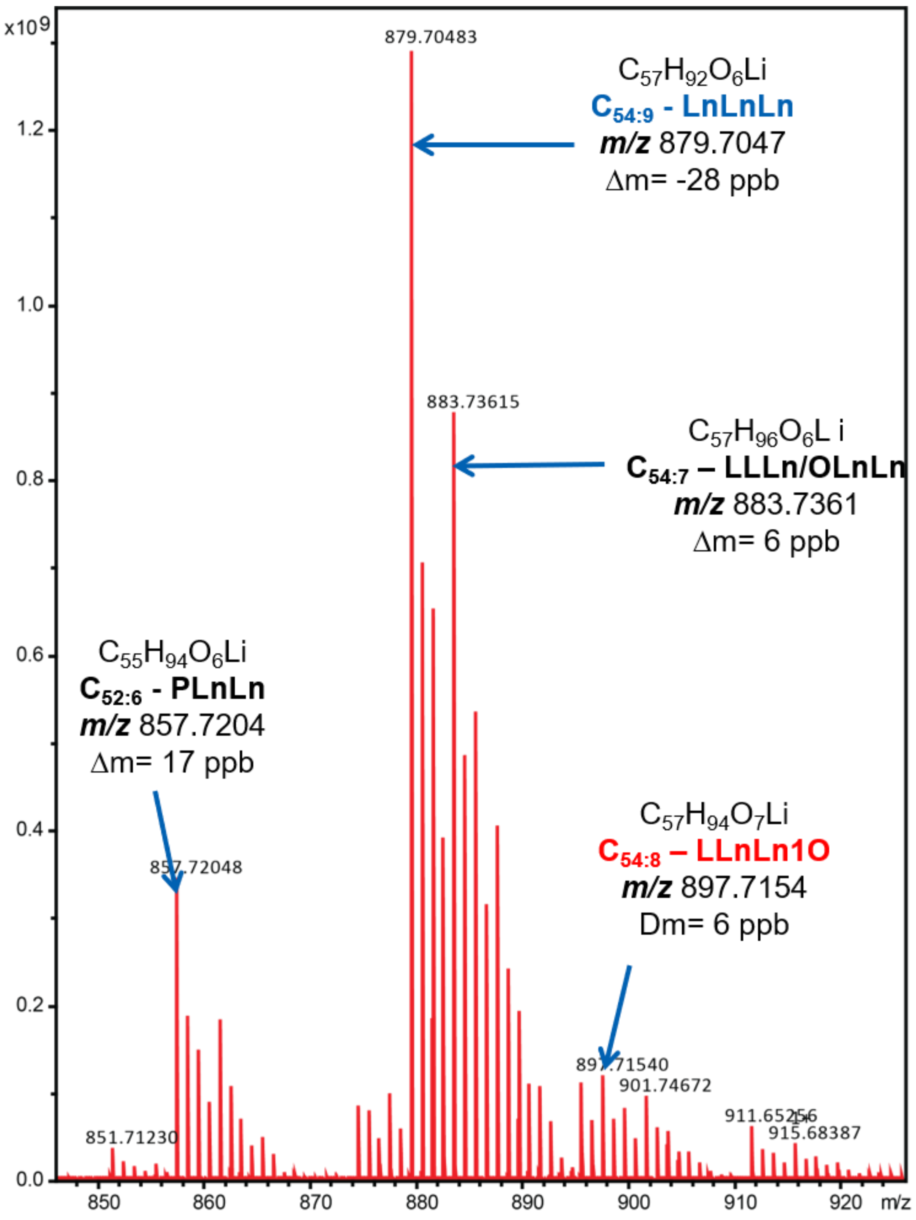

Figure 141. ESI (+) FT-ICR MS of fresh linseed oil

Table 17: Identified combinations of triglycerides in fresh linseed oil

TAG	**$C_xH_yO_zLi$**	**Theoretical *m/z* [M+Li]$^+$**	**Experimental *m/z* [M+Li]$^+$**	**Error (ppm)**	**CN : DB**	**Rel. Int. %**
PLnLn	$C_{55}H_{94}O_6Li$	857.720496	857.720479	-0.02	52 : 6	6.44
PLLn	$C_{55}H_{96}O_6Li$	859.736146	859.736166	0.02	52 : 5	2.78
PLL/POLn	$C_{55}H_{98}O_6Li$	861.751796	861.751799	-0.004	52 : 4	3.44
POL/PSLn	$C_{55}H_{100}O_6Li$	863.767446	863.767437	-0.01	52 : 3	1.30
PSL/POO	$C_{55}H_{102}O_6Li$	865.783096	865.783094	-0.002	52 : 2	0.94
PSO	$C_{55}H_{104}O_6Li$	867.798746	867.798817	0.08	52 : 1	0.18
PSS	$C_{55}H_{106}O_6Li$	869.814396	869.813946	-0.5	52 : 0	0.07
LnLnLn	$C_{57}H_{92}O_6Li$	879.704846	879.704827	-0.02	54 : 9	24.10
LLnLn	$C_{57}H_{94}O_6Li$	881.720496	881.720512	0.02	54 : 8	12.11
LLnLn/OLnLn	$C_{57}H_{96}O_6Li$	883.736146	883.736150	0.005	54 : 7	16.60
OLLn/SLnLn/LLL	$C_{57}H_{98}O_6Li$	885.751796	885.751799	0.003	54 : 6	9.93
OOLn/SLLn/OLL	$C_{57}H_{100}O_6Li$	887.767446	887.767470	0.03	54 : 5	7.57
SLL/SOLn/OOL	$C_{57}H_{102}O_6Li$	889.783096	889.783100	0.004	54 : 4	3.65
SOL/SSLn/OOO	$C_{57}H_{104}O_6Li$	891.798746	891.798775	0.03	54 : 3	2.03
SSL/SOO	$C_{57}H_{106}O_6Li$	893.814396	893.814431	0.04	54 : 2	0.50
SSO	$C_{57}H_{108}O_6Li$	895.830046	895.830038	-0.01	54 : 1	0.07
SSS	$C_{57}H_{110}O_6Li$	897.845696	897.846530	0.9	54 : 0	0.08
LnLnLn1O	$C_{57}H_{92}O_7Li$	895.699760	895.699742	-0.02	54 : 9	0.60
LLnLn1O	$C_{57}H_{94}O_7Li$	897.715410	897.715407	-0.003	54 : 8	2.27
OLnLn1O	$C_{57}H_{96}O_7Li$	899.731060	899.731062	0.002	54 : 7	1.56
OLLn1O/LLL1O	$C_{57}H_{98}O_7Li$	901.746710	901.746722	0.01	54 : 6	1.83
OLLn1O/OLL1O	$C_{57}H_{100}O_7Li$	903.762360	903.762335	-0.03	54 : 5	1.05
LnLnLn2O	$C_{57}H_{92}O_8Li$	911.694675	911.694728	0.06	54 : 9	0.18
LLnLn2O	$C_{57}H_{94}O_8Li$	913.710325	913.710331	0.007	54 : 8	0.35
OLnLn2O/LLLn2O	$C_{57}H_{94}O_8Li$	915.725975	915.725950	-0.03	54 : 7	0.26

I.2.2. Walnut oil vs Soybean oil

The same triglycerides molecules found in linseed oil can also be found in walnut and soybean oil (Table 17). According to the ^{1}H NMR analysis, both walnut and soybean oils contain linolenic acid. However, its intensity is higher in walnut oil. In the case of mass spectrometry, the major triglyceride molecule at *m/z* 885.7516 in walnut and soybean oils is composed of three chains of linoleic acid (LLL). Soybean oil contains more palmitic acid than walnut oil as its intensity is almost ten times higher. We can also notice that the abundance of monosaturated and saturated fatty acids is higher in soybean oil as triglycerides such as OOLn and OOL at *m/z* 887.7674 and *m/z* 889.7831 respectively are more intense in its spectrum while unsaturated triglycerides such as LLnLn at *m/z* 883.7361 is more intense in the spectrum of walnut oil.

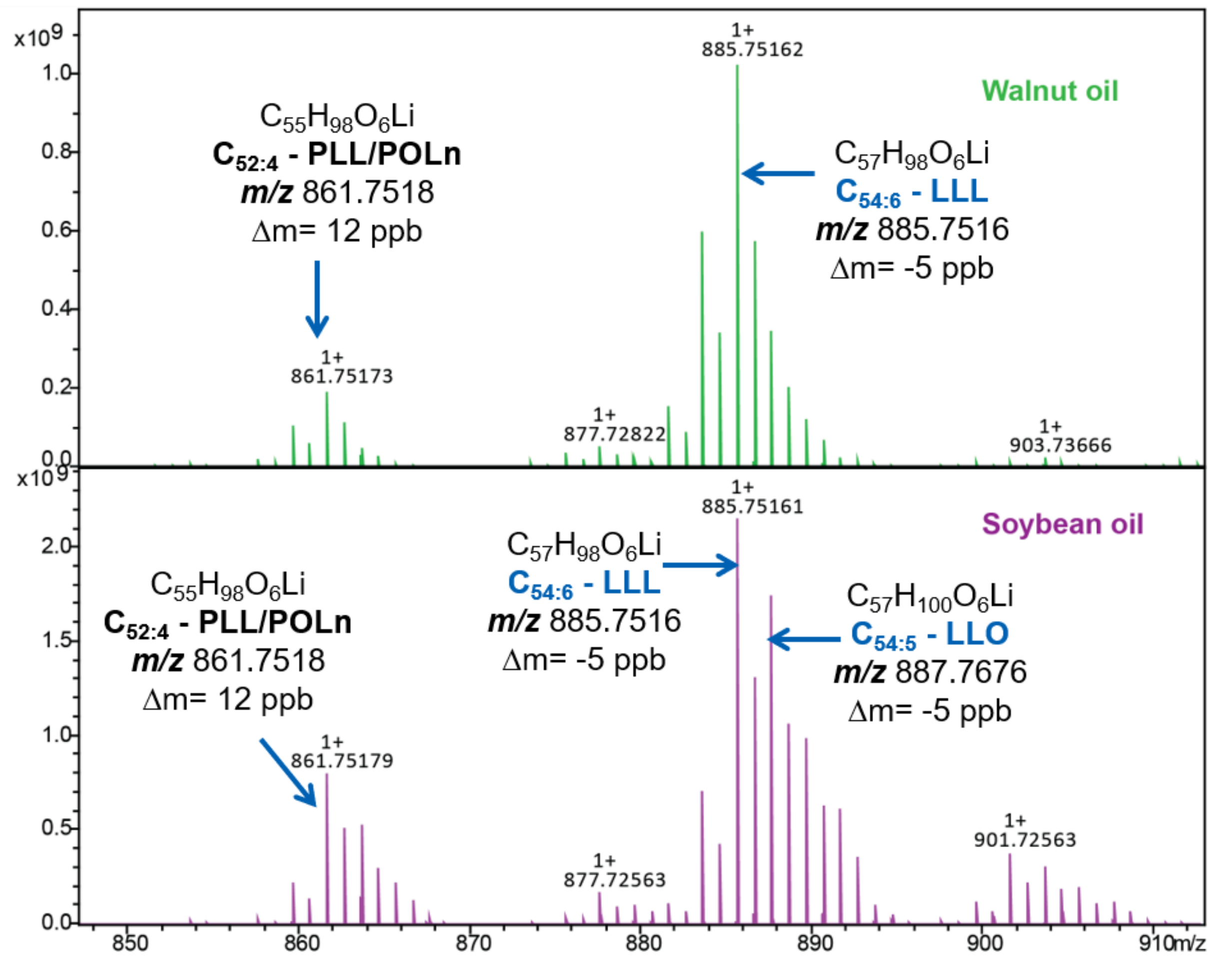

Figure 142. ESI (+) FT-ICR MS of fresh walnut and soybean oils

I.2.3. Safflower oil vs Poppy oil

Safflower and poppy oils do not contain linolenic acid in their fatty acid chains. Their separation in ^{1}H NMR is very difficult as both are based on the same triglyceride molecules with a majority of linoleic acid. Similar to walnut and soybean oils, the major triglyceride at *m/z* 885.7516 in safflower and poppy oils is composed of three chains of linoleic acid (LLL).

FT-ICR MS allowed to distinguish between these two oils as poppy oil contains a higher composition of monosaturated and saturated fatty acids. It can be observed on the spectra that triglyceride molecules with high composition of monosaturated oleic acid such as OOLn, OOL and OOO at *m/z* 887.7674, *m/z* 889.7831 and *m/z* 891.7987 are significantly more intense in the case of poppy oil.

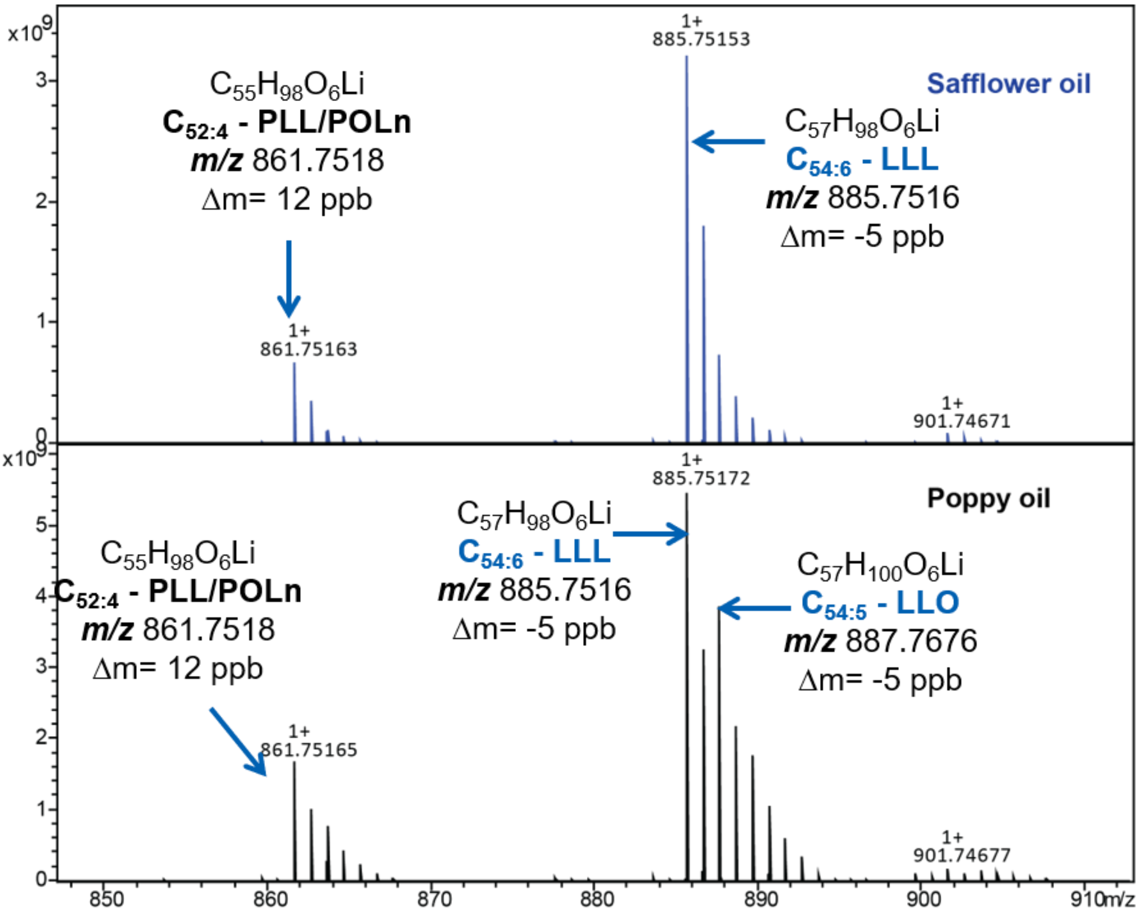

Figure 143. ESI (+) FT-ICR MS of fresh safflower and poppy oils

I.2.4. Conclusion

After all analyses, we can say that 1H NMR provides valuable information on the composition of siccative oils, however, it presents some limitations. On the other hand, FT-ICR MS affords detailed and accurate identification of triglycerides present in these oils. The combination of both techniques allows a full and complete characterization of fresh siccative oils.

II. Survey of present-day oil paint tubes

Present day oil paint tubes with different pigments from the following eight suppliers were studied: **Winsor & Newton, Sennelier, Gamblin, Micheal Harding, Old Holland, Talens, Daler-Rowney and Lefranc- Bourgeois.** Oil was extracted using organic liquid-liquid extraction and analyzed by ^{1}H NMR and direct infusion FT-ICR mass spectrometry.

After ^{1}H NMR analysis, we noticed the presence of the signal corresponding to the triplet at 0.95 ppm of the terminal methyl of linolenic acid used as marker for linseed oil in most spectra. The majority of the suppliers tend to use linseed oil as drying oil in their paints as it has a very high drying effect. However, some exceptions exist such as Sennelier® who uses safflower oil in all his paints (Table 18 and figure 144).

Table 18: Types of siccative oil identified in ivory black, cobalt blue, chromium oxide, cadmium red and yellow ochre colors of eight different paint tubes suppliers.

Color/Supplier	**Winsor &Newton**	**Sennelier**	**Gamblin**	**Micheal Harding**	**Old Holland**	**Talens**	**Daler-Rowney**	**Lefranc-Bourgeois**
Ivory black	Linseed oil	Safflower oil	Linseed oil	Linseed oil	Linseed oil	Linseed oil	Linseed oil	Linseed oil
Cobalt blue	Linseed oil	Safflower oil	Linseed oil	Linseed oil	Linseed oil	Linseed oil	Linseed oil	Linseed oil
Chromium oxide	Linseed oil	Safflower oil	Linseed oil	Linseed oil	Linseed oil	Linseed oil	Linseed oil	Linseed oil
Cadmium red	Linseed oil	Safflower oil	Linseed oil	Linseed oil	Linseed oil	Linseed oil	Linseed oil	Linseed oil
Yellow ochre	Linseed oil	Safflower oil	Linseed oil	Linseed oil	Linseed oil	Linseed oil	Linseed oil	Linseed oil

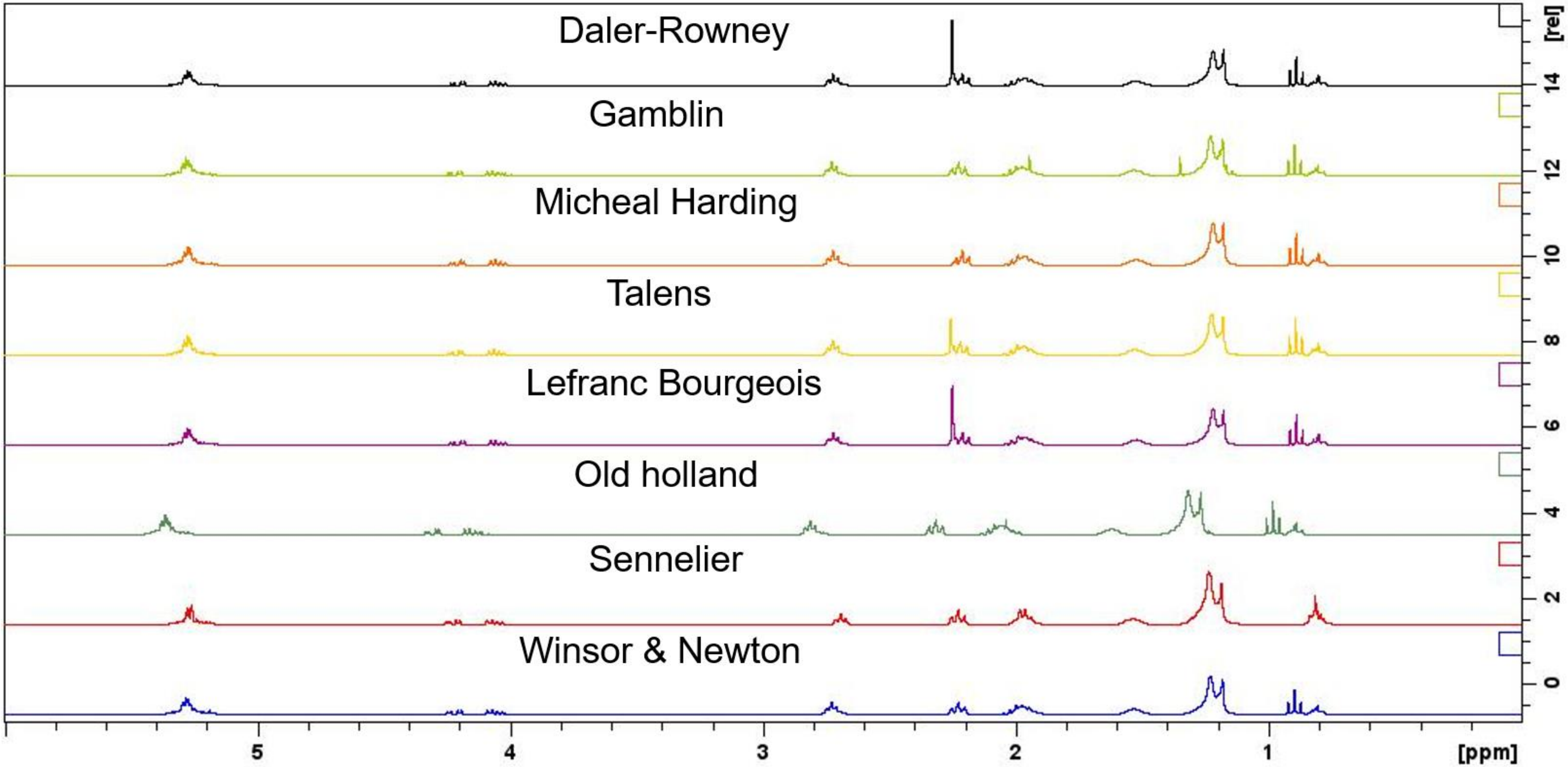

Figure 144. ^{1}**H NMR spectra of extracted oils from paint tubes of different paint suppliers**

Analysis by ESI FT-ICR MS of the same samples of extracted oils from Sennelier and Winsor & Newton confirmed the attribution of the oil types. In the case of Sennelier, the extracted oil presented a very intense peak at m/z 885.7517 corresponding to a LLL triglyceride while Winsor & Newton extracted oil was majorly formed of a LnLnLn triglyceride.

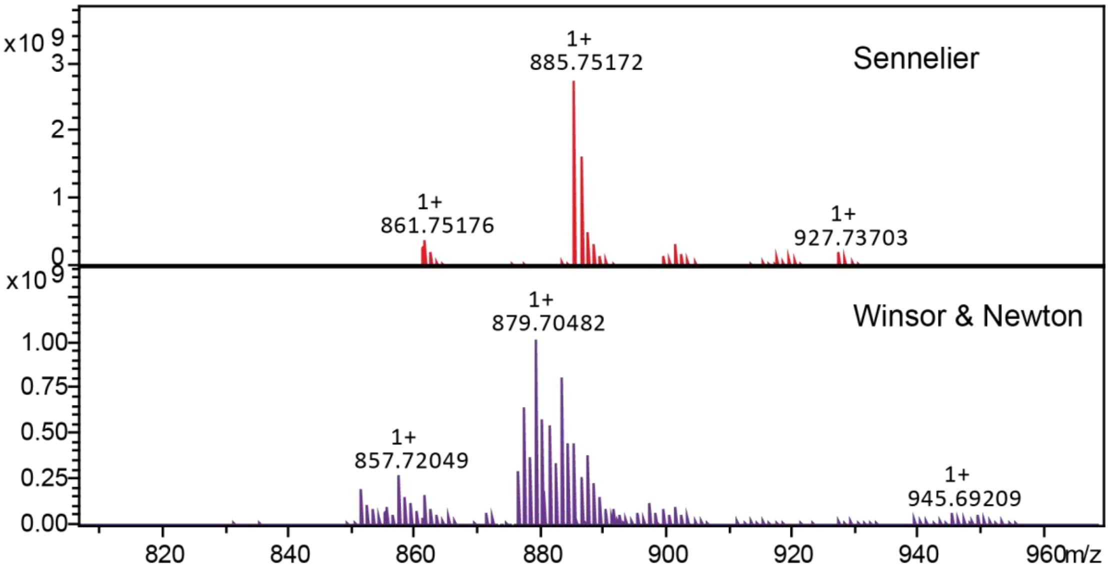

Figure 145. ESI (+) FTICR mass spectra of extracted oil from paint tubes of Sennelier and Winsor & Newton Cobalt blue

On the other hand, when oil was extracted from paint tubes with white pigments and analyzed by FT-ICR MS, we were able to identify that the totality of the suppliers prefers using safflower oil as a binder for white pigments as seen in figure 146. The reason for this change is that safflower oil preserves its white color for a very long time and resists to yellowing.

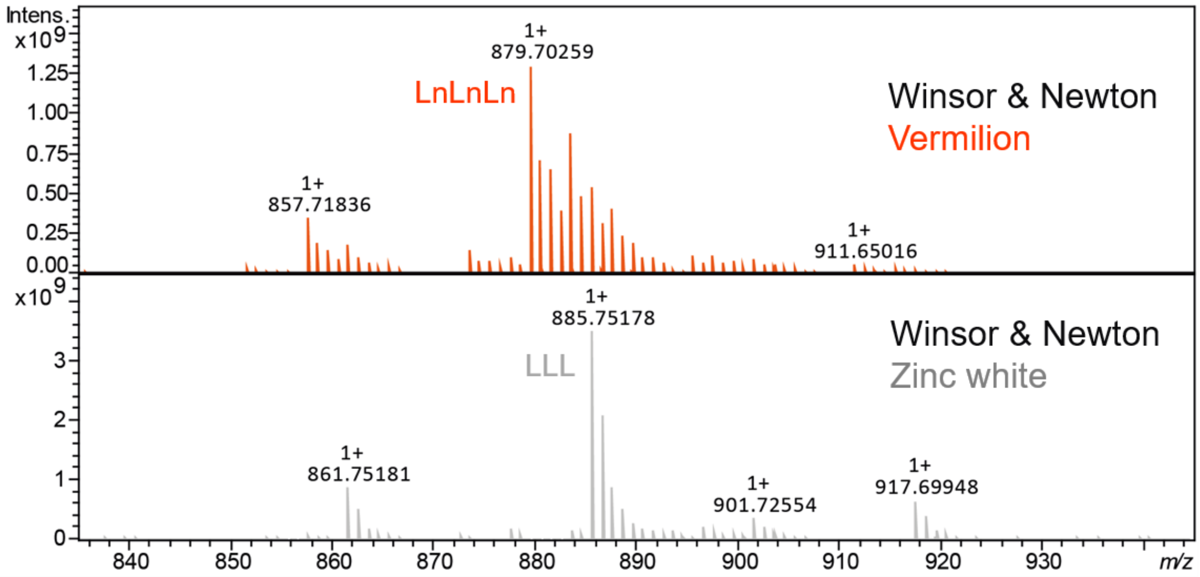

Figure 146. ESI (+) FTICR mass spectra of drying oil extracted from oil paint tubes from Winsor & Newton Vermilion and Zinc white.

III. Survey of old oil paint tubes

In the third step, drying oils were extracted from old paint tubes and analyzed by direct infusion FT-ICR mass spectrometry. Two historical paint suppliers were chosen for this study: Sennelier® and Artista.

Mass spectra showed that analyzed oil from old Sennelier paint tubes is composed in majority of the triglyceride LLL with *m/z* 885.7517 in the case of yellow ochre and burnt sienna and *m/z* 879.7048 for the black paint. Further interpretation proved that the used oil in these tubes is poppy oil (Figure 147). By comparison with present-day tubes, we noticed that the supplier substituted safflower oil by poppy oil.

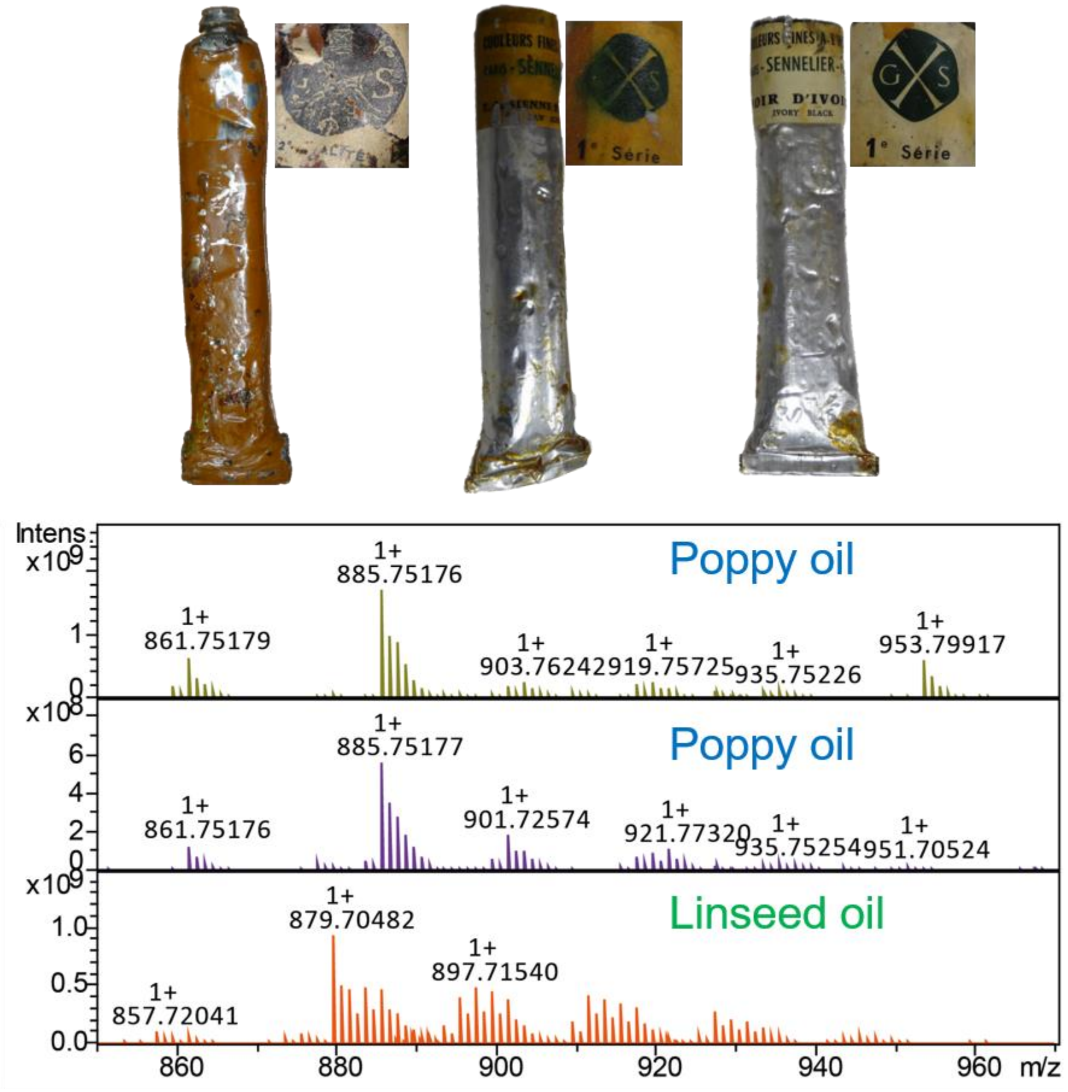

Figure 147. ESI (+) FTICR MS of oils extracted from old tubes from Sennelier

Concerning the supplier Artista, a completely opposite strategy was adopted to manufacture their paint tubes as poppy oil is mixed with the black pigment and linseed oil is detected in green paints tubes (Figure 148).

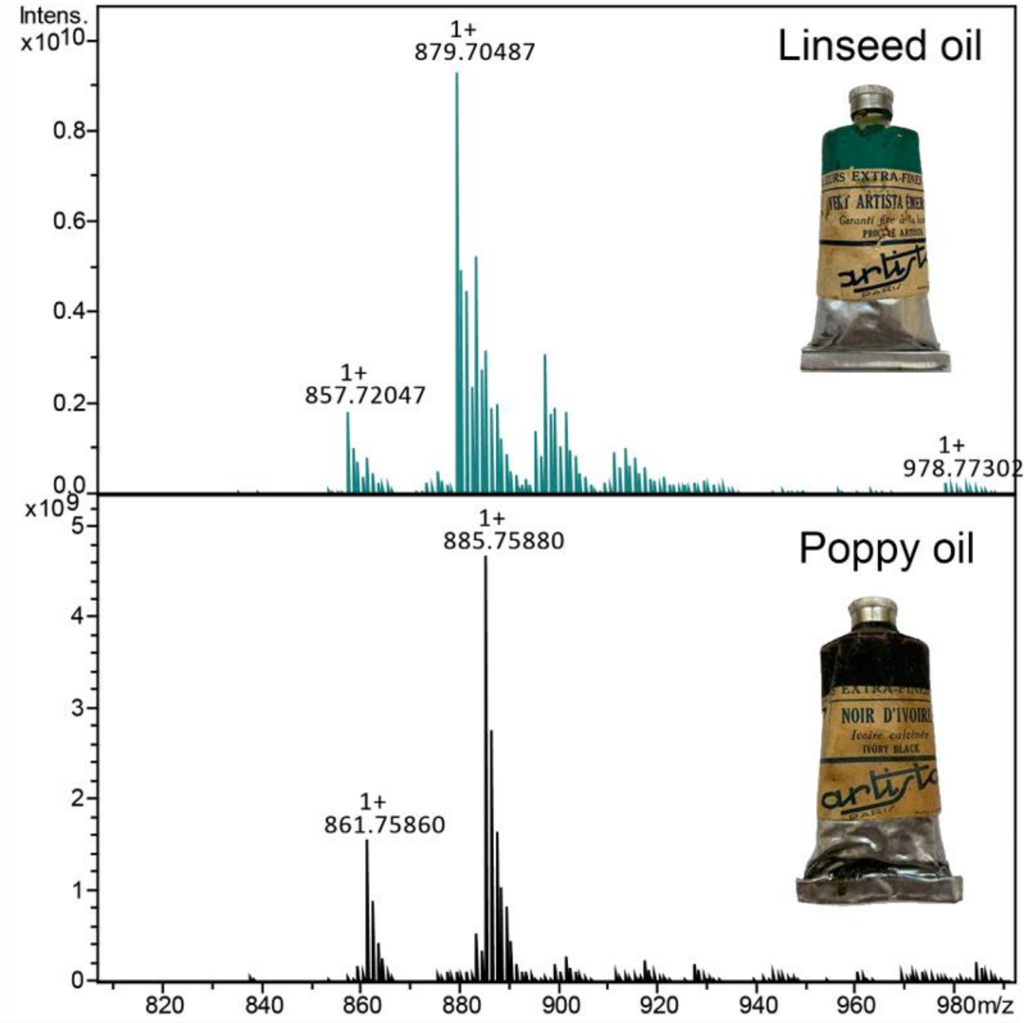

Figure 148. ESI (+) FTICR MS of oils extracted from old tubes from Artista

IV. Creation and analysis of model aged oil films

Fresh drying oils and were spread on a canvas to simulate the ageing of real art painting. Under the effect of natural light and in the presence of oxygen, the oil films became dry and very solid. They are polymerized and became insoluble. To solubilize and analyze these cross-linked polymers, we developed a soft depolymerization technique.

IV.1. Development of depolymerization method

Johnson et al. already proposed a mechanism for derivation of fatty acids by forming Alkyldimethylaminoethyl[46] ester. An amine function ionizes well in positive mode and improves the analysis of acids in mass spectrometry. The first step is to convert the free fatty acids to acyl chloride by reacting with an oxalyl chloride, then a nucleophilic addition/elimination reaction with dimethylaminoethanol lead to the esterification of the fatty acid. In our case, the fatty acids are linked to glycerol, and it is preferred to avoid hydrolyzing the triglyceride ester linkages, which causes side reactions able to bring changes in our fatty acid chains. For these reasons, we have chosen to carry out a trans-esterification of our triglycerides, this reaction is well known in the field of biodiesel production, used to obtain methyl esters of fatty acids from triglycerides. Starting from this notion, we replaced the methanol used in the production of biodiesel by an excess of amine containing molecule, the 3-(dimethylamino) -1-propylamine) (Figure 149) in the presence of sodium hydride which plays the role of a base. The base will deprotonate the amine which in turn will cleave the ester bond between fatty acids and glycerol, and reform an amide bond with the fatty acid.

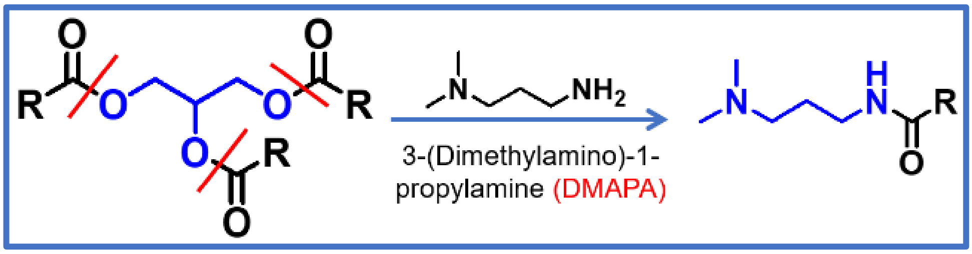

Figure 149. Transamidation reaction of triglycerides

The transamidation reaction was first carried out on linseed oil mainly composed of a triglyceride molecule with three linolenic acid chains in order to optimize the reaction conditions which can be applied later on all other oils and oil paints.

Analysis by ^{1}H NMR of the resulting products from the reaction with 3-(dimethylamino)-1-Propylamine and linseed oil showed a dramatic decrease in the intensity of glycerol characteristic peaks at 4 ppm, and the absence of carboxylic acid peaks with the presence of peaks corresponding to an amide proton (Figure 150).

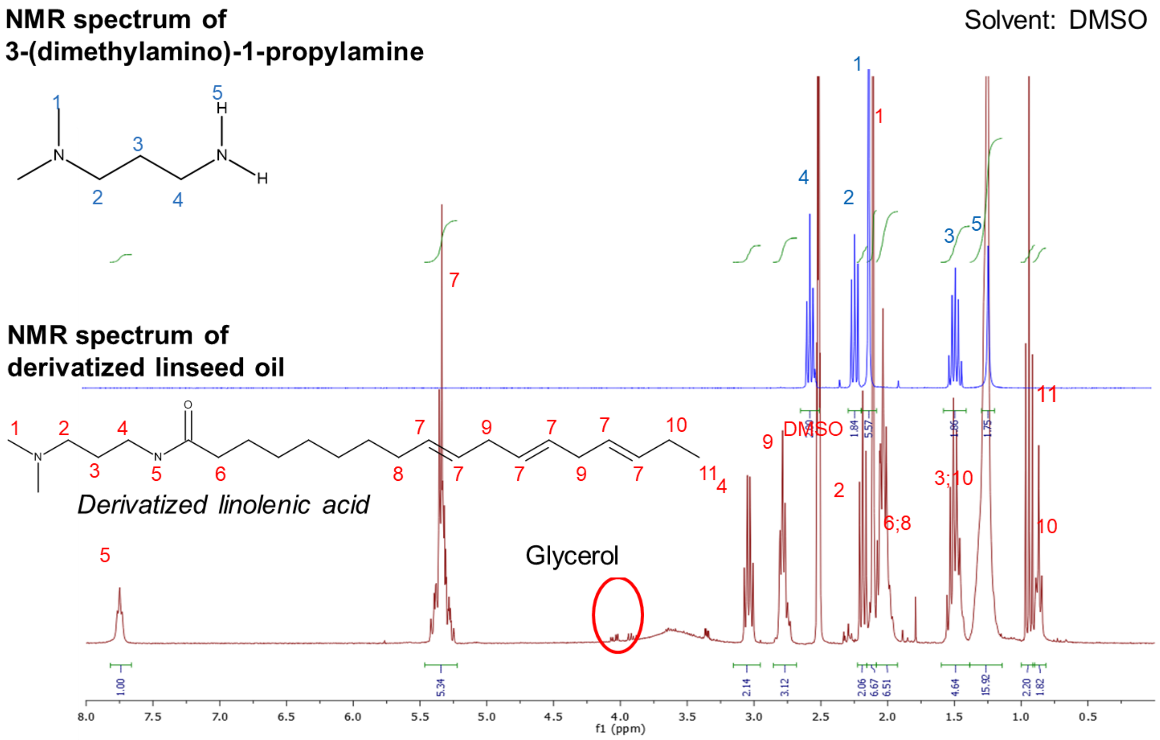

Figure 150. **^{1}H NMR spectrum in DMSO of 3-(dimethylamino)-1-propylamine (Upper panel) and ^{1}H NMR spectrum in DMSO of products obtained after 12 hours of reaction between linseed oil and 3-(dimethylamino)-1-propylamine (Lower panel).**

3-(dimethylamino)-1-propylamine produced a very good yield since the amide bond is more resistible to the hydrolysis reactions that can pass through the release of 2 H_2O by a glycerol molecule during its conversion to acrolein. This derivatization strategy will allow for the first time to analyze and identify the network structure formed between unsaturated fatty acids.

The obtained products from linseed oil transamidation were also analyzed by FT-ICR MS. The mass spectrum (Figure 151) shows that triglycerides were completely converted to derivatized fatty acids. The spectrum also indicates that linolenic acid is the main fatty acid in linseed oil. Moreover, MS spectrum confirms that the fatty acids carbon chain is intact and the trans-amidation reaction does not generate any alteration on their carbon chain.

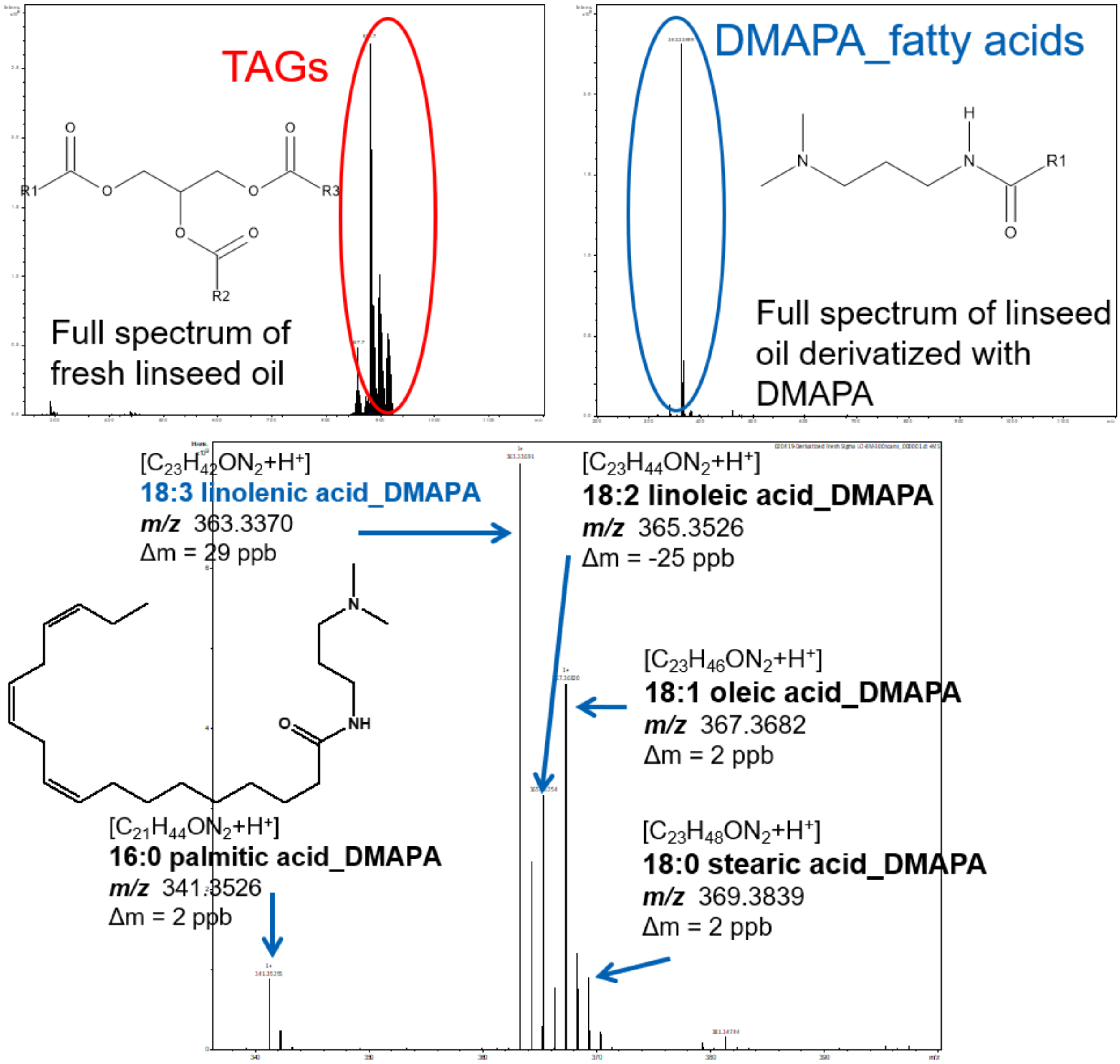

Figure 151. Drying oil FT-ICR MS spectrum after transamidation

IV.2. Application on fresh siccative oils

The reaction was used to depolymerize the three most used siccative oils in oil paintings: linseed oil, safflower oil and poppy oil. Triglycerides were completely converted to derivatized fatty acids. The spectrum also indicates that linolenic acid is the main fatty acid in linseed oil, while linoleic acid is the major acid in safflower and poppy oils (Figure 152).

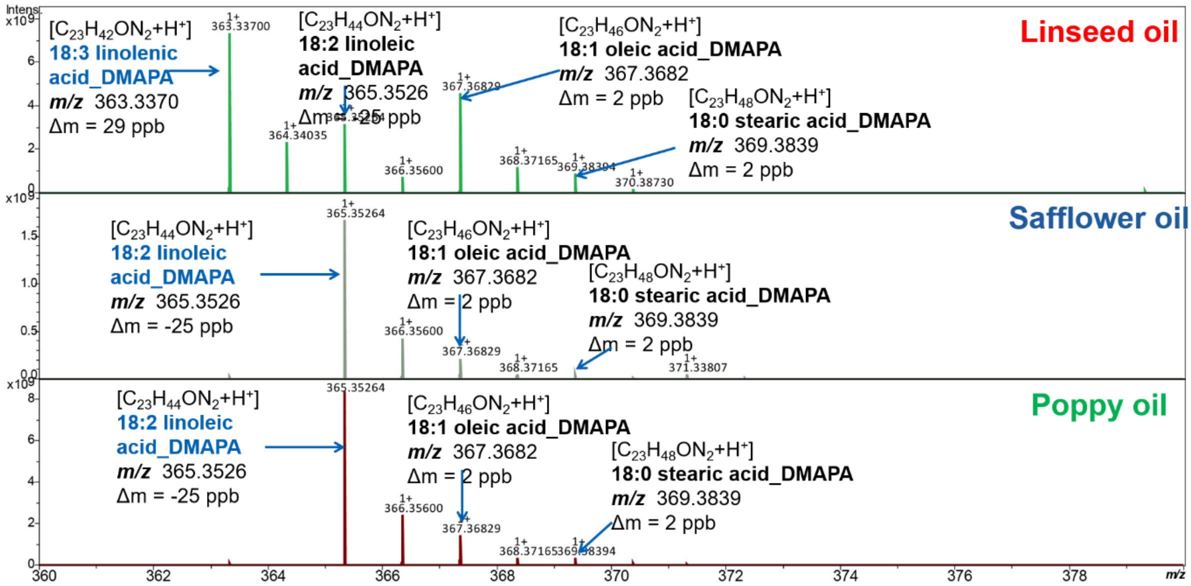

Figure 152. Application of the transamidation reaction on fresh linseed, safflower and poppy oils

Table 19: Composition of oils in fatty acids before and after transamidation

Composition of oils in fatty acids before transamidation					
	Palmitic	**Stearic**	**Oleic**	**Linoleic**	**Linolenic**
Linseed oil	**4%**	**9%**	**17%**	**24%**	**46%**
Safflower oil	**5%**	**5%**	**12%**	**76%**	**2%**
Poppy oil	**4%**	**9%**	**18%**	**65%**	**4%**
Composition of oils in fatty acids after transamidation					
	Palmitic	**Stearic**	**Oleic**	**Linoleic**	**Linolenic**
Linseed oil	**5%**	**5%**	**18%**	**27%**	**45%**
Safflower oil	**5%**	**4%**	**11%**	**79%**	**1%**
Poppy oil	**6%**	**5%**	**18%**	**68%**	**3%**

The percentage in fatty acids of the three transamidated oils before and after transamidation confirms that the fatty acids carbon chain is intact and the transamidation reaction does not generate any alteration on their carbon chain.

IV.2. Depolymerization of solid model siccative oil film

The developed and optimized strategy on fresh linseed oil was applied on dry oil and oil paint films. The obtained products from transamidation were analyzed by FT-ICR. Mass spectra revealed thousands of peaks corresponding to the products of polymerization and degradation process (Figure 153). The obtained MS spectrum can be divided into one zone corresponding to the fatty acid monomers with their different degree of oxidation and another more complex zone containing all the cross-linking products.

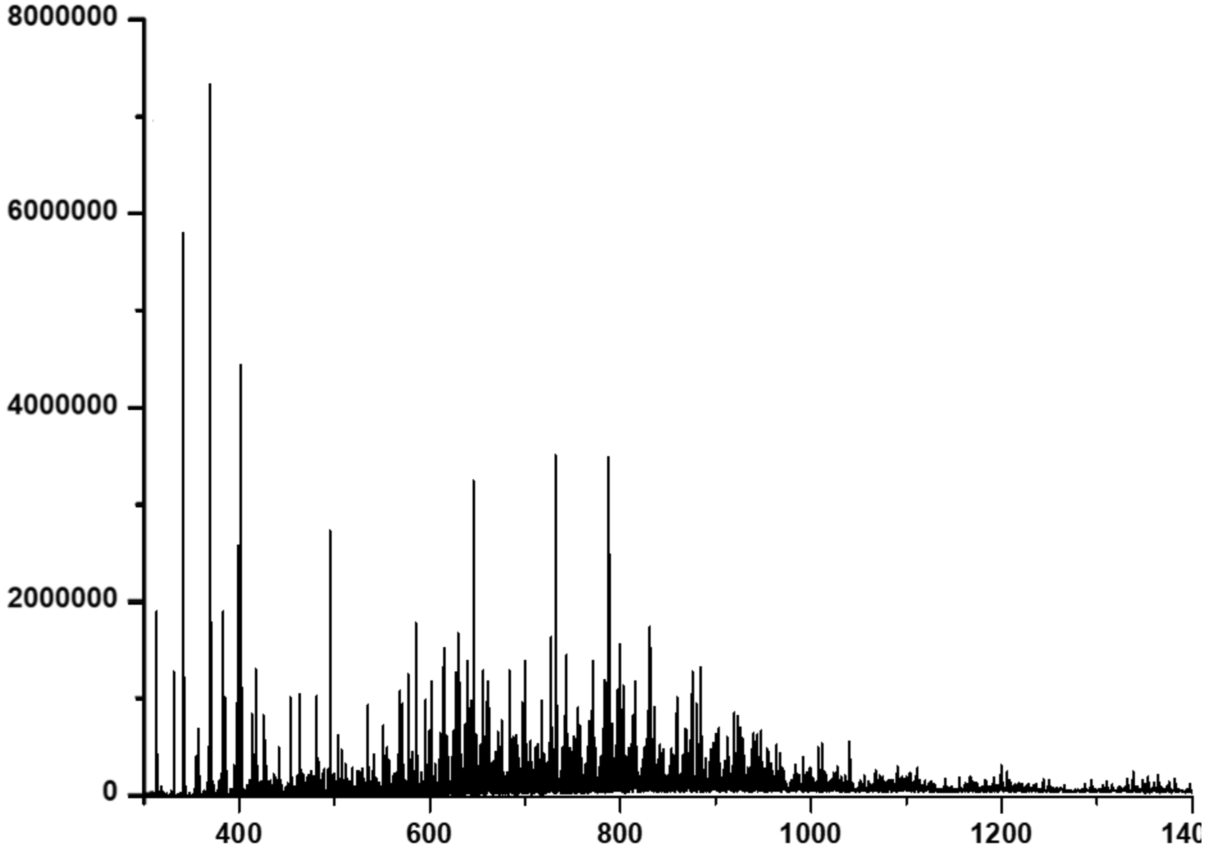

Figure 153. FT-ICR MS spectrum of derivatized siccative oil film

IV.2.1. Interpretation of the monomers zone

The mass spectrum represents the chemical complexity of the sample. The spectrum was linearly calibrated based on a mass reference list. This list is composed of five known masses *m/z*: 341.3526; $C_{21}H_{45}ON_2$ (DMAPA-palmitic acid)/ *m/z*: 363.3370; $C_{23}H_{43}ON_2$ (DMAPA-linolenic acid)/ *m/z*: 365.3521; $C_{23}H_{45}ON_2$ (DMAPA-linoleic acid)/ *m/z*: 367.3683; $C_{23}H_{49}ON_2$ (DMAPA-oleic acid)/ *m/z*: 369.3839; $C_{23}H_{47}ON_2$ (DMAPA-stearic acid).

The doubly and triply unsaturated fatty acids do not appear on the mass spectrum which means that they are completely polymerized. Only saturated fatty acids such as palmitic and stearic acid and monosaturated acids such as oleic acid can be identified. These acids can successfully resist to the polymerization and autooxidation of siccative oils as they do not have a proton in an allylic position so technically they do not participate during the reaction. However, we noticed that most of the remaining fatty acids became oxidized with one or more oxygen, and these compounds can be easily identified on the spectrum (Figure 154). These results confirm the important role of polyunsaturated fatty acids in the oil polymerization process.

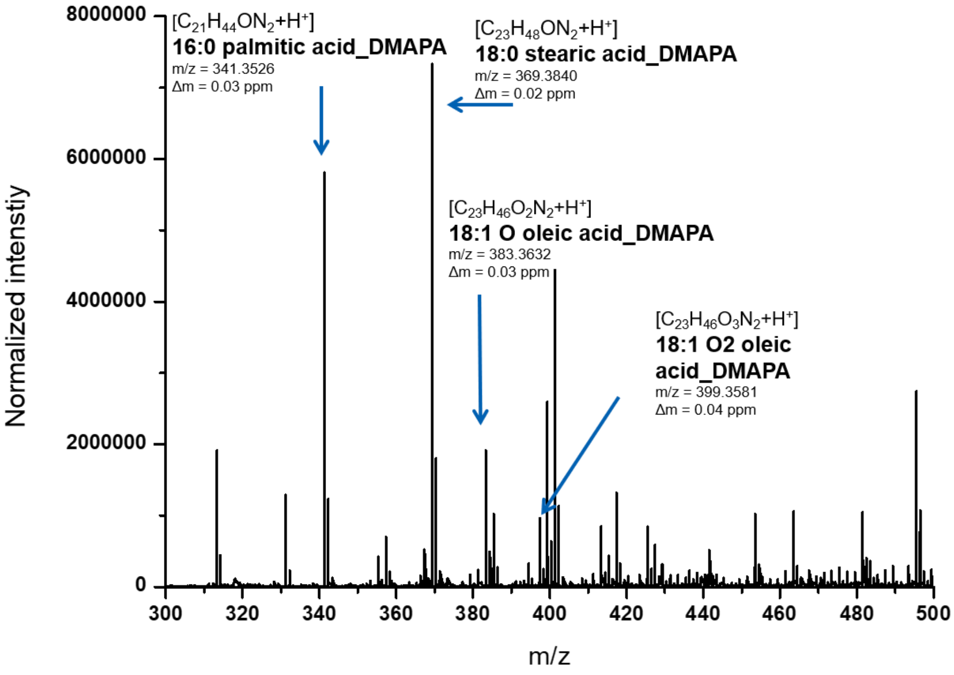

Figure 154. ESI (+) FT-ICR MS spectrum of derivatized paint film, zoom in on the monomers zone

Table 20. Identified derivated fatty acids after paint film transamidation

F.A._DMAPA	**$C_xH_yO_zN_2$**	**Theoretical** *m/z* **$[M+H]^+$**	**Experimental** *m/z* **$[M+H]^+$**	**Error (ppm)**	**CN:DB**
Plamitic acid_DMAPA	$C_{21}H_{45}ON_2$	341.352640	341.352640	-0.001	16 : 0
Oleic acid_DMAPA	$C_{23}H_{47}ON_2$	367.368291	367.368289	-0.004	18 : 1
Stearic acid_DMAPA	$C_{23}H_{49}ON_2$	369.383941	369.383940	-0.001	18 : 0
Oleic acid 1O_DMAPA	$C_{23}H_{47}O_2N_2$	383.363205	383.363197	-0.02	18 : 0
Oleic acid 2O_DMAPA	$C_{23}H_{47}O_3N_2$	399.358120	399.358118	-0.006	18 : 0
Oleic acid 3O_DMAPA	$C_{23}H_{47}O_4N_2$	415.353034	415.353026	-0.02	18 : 0

IV.2.2. Interpretation of the cross-linking products zone

When we zoomed in on the cross-linking products zone, a much more complex spectrum appeared (Figure 155). We were able to identify different classes of reticulated molecules separated by the number of carbons, oxygen, nitrogen or hydrogen atoms and considered as proof for the cross-linking and degradation phenomena that occurred during oil drying.

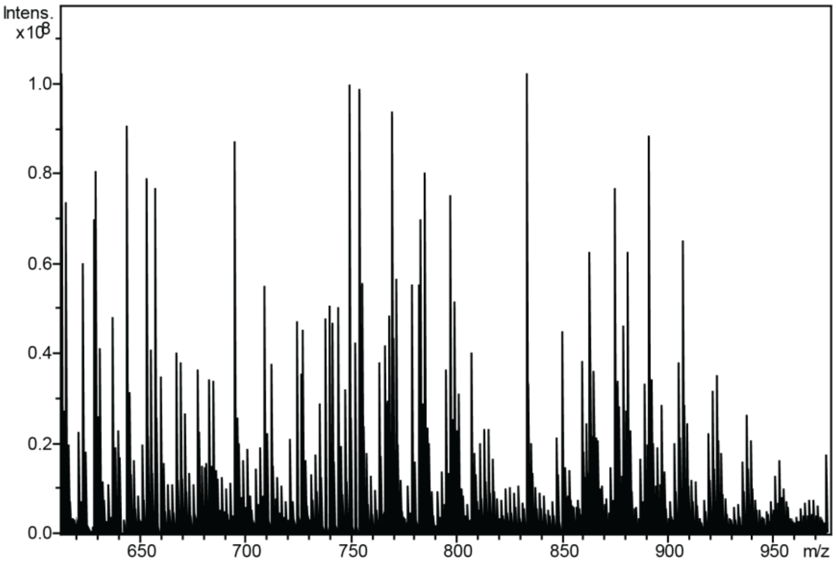

Figure 155. ESI (+) FT-ICR MS spectrum of derivatized paint film, zoom in on the cross-linking products zone

In the first compounds family, we notice a difference of two hydrogen atoms between the peaks (Figure 156). A same class of molecules that have the same number of carbons, oxygen and nitrogen but different hydrogen number. This hydrogen difference is illustrated in the variation of DBE. In our case, the DBE which indicate the number of unsaturation within the molecules represent an indication of the degree of polymerization and give an inside look on the cross-linked structure of oil paint film. Double bonds are involved in the polymerization process of siccative oils, the abstraction of allylic hydrogen located between the two double bonds lead to a radical addition combination or radical addition elimination. The two ways of radical addition generates dimers, trimers and tetramers but with different number of unsaturation.

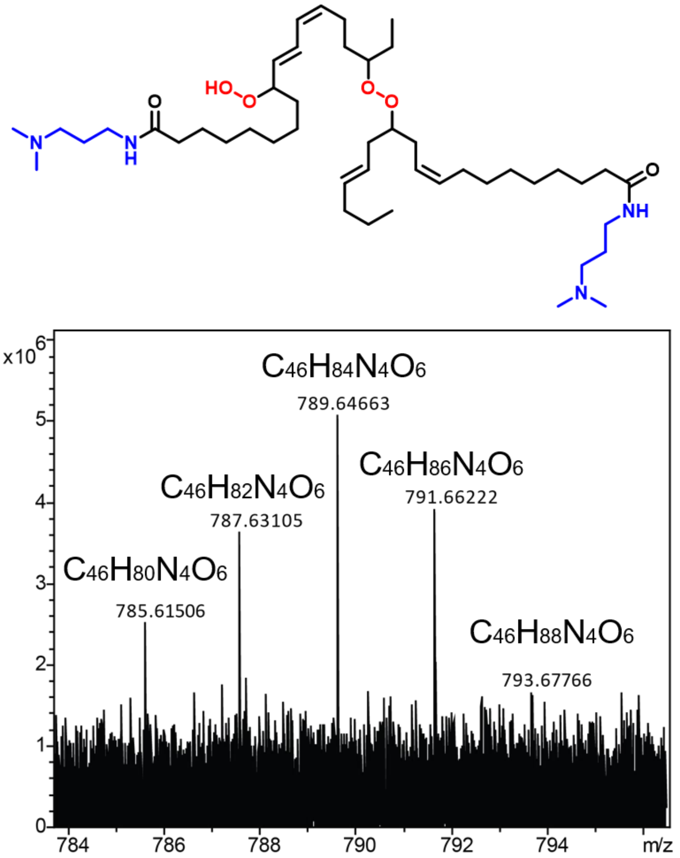

Figure 156. ESI (+) FT-ICR MS spectrum of derivatized family with a difference of two hydrogen atoms

Table 21. Identified family with a difference of two hydrogen atoms

Theoretical *m/z* [M+H]$^+$	**Experimental *m/z* [M+H]$^+$**	**Error (ppm)**	**DBE**	**Formula**
785.615063	785.614671	-0.5	9	$C_{46}H_{81}N_4O_6$
787.630713	787.631050	0.4	8	$C_{46}H_{83}N_4O_6$
789.646363	789.646631	0.3	7	$C_{46}H_{85}N_4O_6$
791.662013	791.662220	0.2	6	$C_{46}H_{87}N_4O_6$
793.677663	793.677668	0.007	5	$C_{46}H_{88}N_4O_6$

On the other hand, we found that some peaks in the spectra are correlated between each other with the difference of on oxygen atom (Figure 157 and 158). Table 21 represents an example of the identified derivatized fatty acids dimers, which shows that those dimers can have a degree of oxidation that vary from 0 to 5. Oxygen number is an important parameter that offers information about the degree of oxidation and the cross-linked structure of the polymer. For example, the identified molecule $C_{46}H_{84}N_4O_2$ (*m/z* 725.6667) have no additional oxygen atoms which leads us to believe that this dimer is linked by a carbon-carbon bond. Linseed oil drying is a chemical process that incorporate oxygen in the polymer structure in form of peroxide, alcohol, carbonyl and carboxylic acid. Additional oxygen atoms can indicate the presence of a peroxide function.

Table 22. Identified derivatized fatty acids dimers

Theoretical ***m/z*** **[M+H]$^+$**	**Experimental** ***m/z*** **[M+H]$^+$**	**Error (ppm)**	**DBE**	**Formula**
725.666704	725.666587	-0.1	4	$C_{46}H_{85}N_4O_2$
741.661619	741.661387	-0.3	5	$C_{46}H_{85}N_4O_3$
757.656534	757.656406	-0.1	3	$C_{46}H_{85}N_4O_4$
773.651448	773.651378	-0.09	4	$C_{46}H_{85}N_4O_5$
789.646363	789.646631	0.3	8	$C_{46}H_{85}N_4O_6$

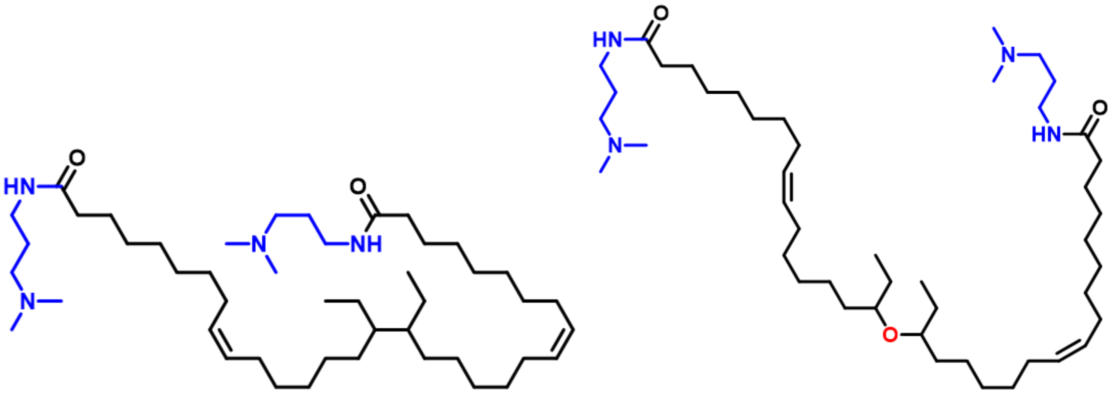

Figure 157. Structures of identified derivatized fatty acids dimers

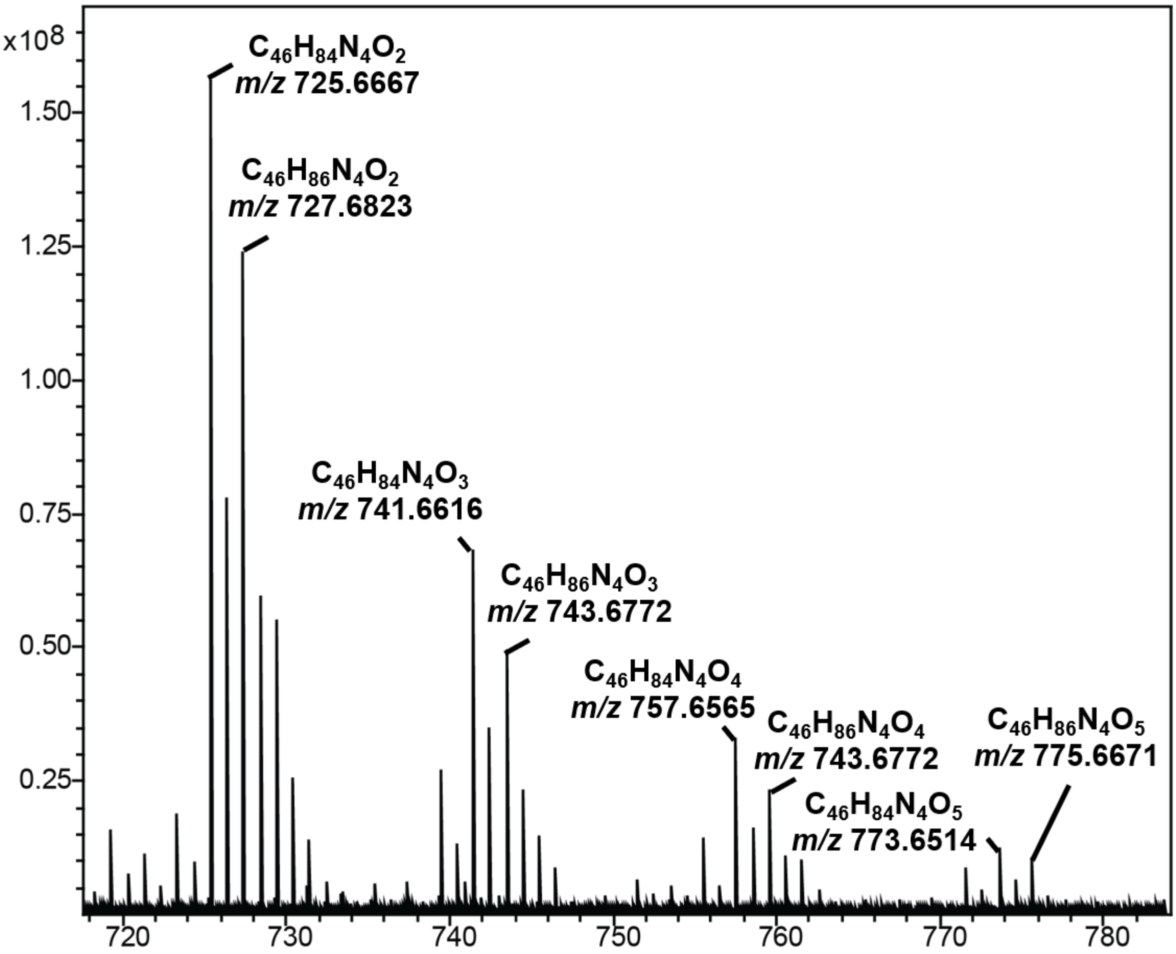

Figure 158. ESI (+) FT-ICR MS spectrum of derivatized family with a difference of oxygen atoms

Finally, the last group of identified compounds is composed of dimers or trimers of fatty acids however, with only two nitrogen atoms (Figure 159 and 160). In fact, each 3-dimethylaminopropylamine contains two nitrogen atoms, and it is used to cleave the ester bond between the fatty acid and the glycerol and form an amide bond with the acid functions. The number of nitrogen present in the molecule determine the number of cross-linked fatty acids. For example, 2 N is a monomer, 4 N is a dimer, 6 N is a trimer and 8 N is a tetramer. The transamidation reaction occur between DMAPA and the ester bond between the fatty acid and the glycerol, and the presence of free fatty acids in the final product present a proof of the ester bond hydrolysis before the transamidation reaction. This hydrolysis is responsible for the release of saturated fatty acids and the formation of metallic soaps leading to the degradation of oil paintings.

Table 23. Group of identified compounds composed of dimers or trimers of fatty acids

Theoretical *m/z* **[M+H]$^+$**	**Experimental** *m/z* **[M+H]$^+$**	**Error (ppm)**	**DBE**	**Formula**
641.561571	641.561518	-0.08	7	$C_{41}H_{73}N_2O_3$
657.556485	657.556463	-0.03	7	$C_{41}H_{73}N_2O_4$
673.551400	673.551391	-0.01	7	$C_{41}H_{73}N_2O_5$
689.546314	689.546297	-0.02	7	$C_{41}H_{73}N_2O_6$
655.540835	655.540789	-0.07	8	$C_{41}H_{71}N_2O_4$
671.535750	671.535698	-0.08	8	$C_{41}H_{70}N_2O_5$
687.530664	687.530620	-0.06	8	$C_{41}H_{70}N_2O_6$

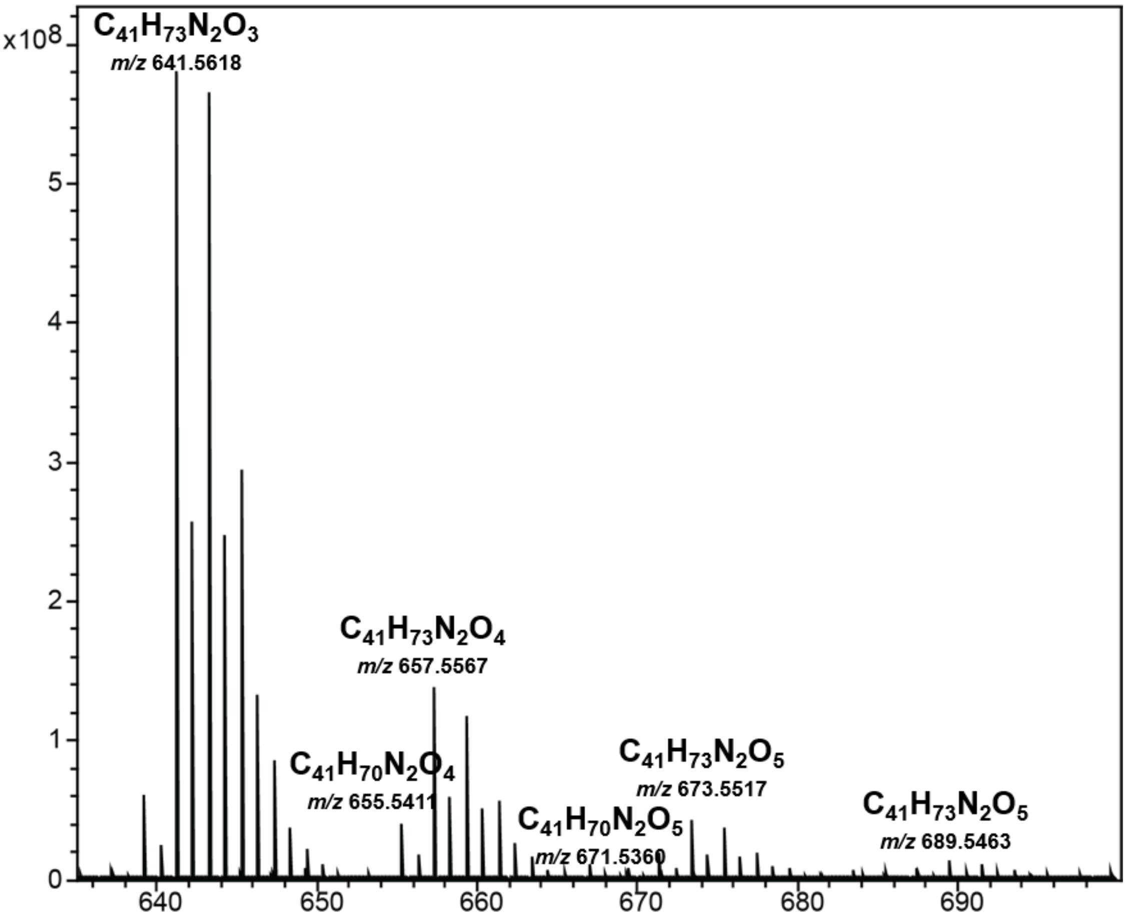

Figure 159. ESI (+) FT-ICR MS spectrum of derivatized family with a difference of oxygen atoms

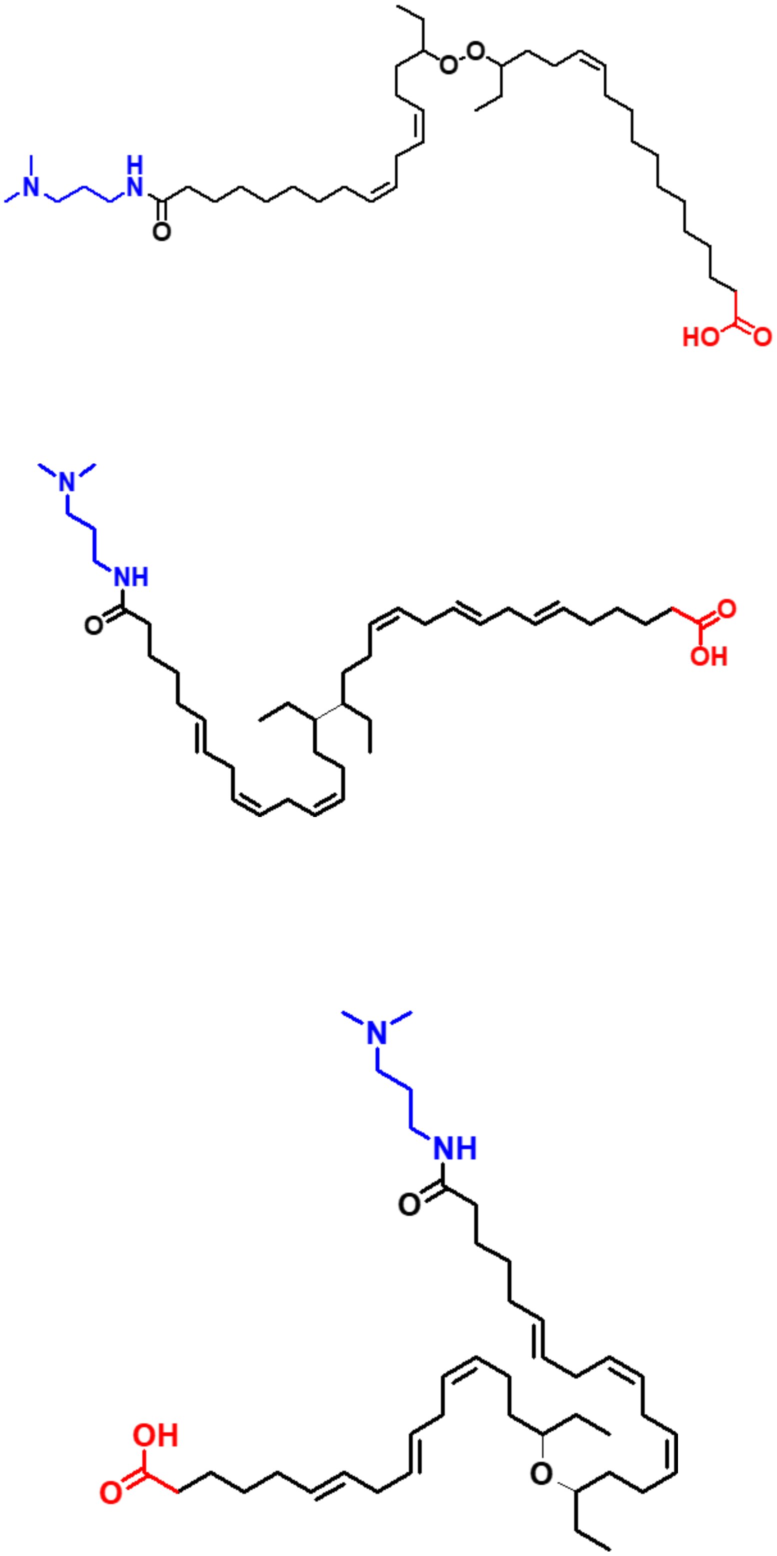

Figure 160. Identified compounds composed of dimers of fatty acids with only two nitrogen atoms

Material and methods

Chemicals and fresh oils

All fresh oils used in this study were commercially available and obtained from their respective suppliers. Linseed, Safflower and Poppy were purchased directly from Winsor&Newton while Walnut and Soybean oils were purchased from Kremer.

3- (Dimethylamino)-1-propylamine ($C_5H_{14}N_2$, 99.0%) (DMAPA), and Cobalt 2-ethylhexanoate (65% in white spirit),. Ethyl acetate (anhydrous, 99.8%), benzene (suitable for HPLC, ≥99.9%), acetonitrile (suitable for HPLC, gradient grade, ≥99.9%), sodium sulfate (ReagentPlus®, ≥99.0%) and sodium hydride (40% in mineral oil) were supplied by Sigma Aldrich and used without any further purification.

Preparation of model dry oil film

- A mixture of 1 g of linseed oil with 0.1% Cobalt 2-ethylhexanoate (65% in white spirit) (Sigma Aldrich) which acts as a catalyst for the oxidation reaction of linseed oil and 200 µl of toluene. The mixture is spread over a glass surface and left to polymerize at ambient temperature.
- 1 g of linseed oil is spread over a glass surface without any additives and left to polymerize at ambient temperature

Transamidation of linseed oil film

The paint film was swelled with THF for 1 night and the solvent (mobile phase) is separated from the film (solid phase). In a 100ml flask, 272.23mg (6.8mmol) of sodium hydride (NaH, 60% dispersed in mineral oil) are added and allowed to react for 15 minutes with stirring at room temperature with an excess of derivatization reagent (9ml). 1g of linseed oil film is added to the reaction medium and the mixture is left to react overnight (16 h) with continuous stirring and under inert atmosphere. Then the reaction is quenched by adding 2 ml of acetic acid followed by an ammonium solution until we reach pH 9. In the next step, the cross-linking products are extracted with ethyl acetate and brine solution. Products present in the organic phase are recovered, evaporated, resolubilized in acetonitrile with 0.1% formic acid and analyzed by FT-ICR high-resolution mass spectrometry.

Oil extraction and sample preparation.

For each paint tube, 1 mg oil paint was weighted and was transferred into a 15 mL conical centrifuge tube together with 10 mL ethyl acetate. The mixture was centrifuged (brand, City, Country) at 5000 rpm for 10 minutes for allowing the separation of the pigment from the binder. This step was repeated twice. After centrifugation the organic phases (ethyl acetate) were collected and evaporated at the rotary evaporator (room temperature at 10 mbar). The dried samples were then reconstituted in 10 mL benzene and 5 mL saturated Brine solution. The biphasic solution was transferred into a separating funnel. The organic phase was collected and the remaining aqueous solution was extracted again with 5 mL of benzene. The whole collected organic phase was dried with sodium sulfate for 2 hours to eliminate any possible trace of remaining water. Benzene was then evaporated at the rotary evaporator (room temperature at 10 mbar). The extracted paint binder was reconstituted in acetonitrile (1mg/mL) or $CDCl_3$ (50mg/ml) prior to FT-ICR MS and NMR analyses respectively.

^{1}H-NMR

Spectra were recorded for all the extracted oil paint tubes. Acquisition of ^{1}H spectra was performed on a Bruker AVANCE III HD spectrometer (Bruker Biospin, GmbH) operating at 300 MHz and equipped with a SampleXpress auto-sampler (Bruker Biospin, GmbH). 0.6 mL deuterated chloroform were employed as solvent for all the experiments and 5 mm NMR tubes were used. Spectra calibration on hydrogen atoms signals was performed using the chemical shift of $CDCl_3$ (7.27 ppm).

FT-ICR MS analysis

Analyses were performed on a SolariX XR instrument with a 9.4 T actively shielded superconducting magnet and a dynamically harmonized cell (Bruker Daltonics, Bremen, Germany). The mass spectrometer is equipped with a Varian Nano-electrospray online source (Varian Nano ESI ON, Bruker Daltonics, Bremen, Germany). For all experiments, FT-ICR mass spectra were acquired in positive ion mode. Fresh pure siccative and extracted oils were diluted in acetonitrile (1 mg/mL)). The obtained solutions were further diluted to 100 ng/µL in acetonitrile. Lithium-^{7}Li chloride (99% ^{7}Li) was dissolved in methanol to a concentration of 1 mg/mL Mixture solutions of sample and lithium chloride at a ratio of 10:1 (sample/LiCl, v/v) were introduced in the spectrometer by direct infusion using a Cole-Parmer single-syringe infusion pump (Cole-Parmer®, Vernon Hills, USA) at a rate of 10µL/min through a 250 µL Hamilton syringe (51 mm, Gastight). The syringe is connected to a capillary line (100 µm I.D., 360 µm O.D.) equipped with a SilicaTipTM needle (10±1 µm, PicoTipTM Emitter, New Objective, Woburn, MA, USA) to which a potential of 1.3 kV was applied. The front and back trapping potentials were set at 1.5 V with a skimmer 1 voltage at 20 V. Spectra were acquired using broadband detection, 8 M data points; 300 scans accumulation for a better signal-to-noise ratio with a mass range from *m/z* 144 to 1500. The transient time consisted of 4.20 s which resulted in a resolution of 1,000,000 at *m/z* 400 in the magnitude mode. Ions were accumulated in the hexapole during 0.05 s. Instrument calibration was achieved using an external calibrant (Sodium trifluoroacetate TFA, 0.01 mg/mL in H_2O/MeOH 50/50 v/v) with a linear calibration. Following acquisition, spectra were internally calibrated in the Data Analysis software version 5.0 (Bruker Daltonics, Bremen, Germany) using a calibration list of assigned signals limiting the mass error to under 100 ppb.

Conclusion

General conclusion

The objectives of this thesis were to develop new analytical approaches for the depolymerization and characterization of natural and synthetic polymers found in several fields such as polymer industry and cultural heritage using both high-resolution mass spectrometry and nuclear magnetic resonance). FT-ICR ultra-high-resolution mass spectrometry allowed the identification of a very wide range of products and the addition of ion mobility also allowed for an understanding of isomeric diversity.

The first part of this thesis was devoted for natural and synthetic polymers. It presented the first detailed investigation of polybutadiene and polyisoprene in *E* and *Z* configurations, by a new approach based on a metathesis reaction for obtaining end-functionalized oligomers easily ionizable by ESI. IMS showed that oligomers isomerize during the reaction affording mixtures of similar products for *E* and *Z* isomers. Improved catalytic conditions led to suppressing the isomerization. IMS demonstrated that the stereochemistry is well preserved. Additional experiments using ERMS proved differences in the fragmentation patterns of isomers and the success of preventing isomerization. Slow pyrolysis by ASAP or DIP-APCI coupled to respectively IMS-MS or FTICR-MS gave species with identical *m/z* values in the case of PB and PI. The existence of several ionization processes leading to protonated species or radical cation was proved by high resolution FTICR MS. On the other hand, analysis by GC×GC-MS of the PB and PI samples gave clearly visible peaks specific to *E* and *Z*. The previous polymers were then irradiated as thin films under UV at 365 nm in conditions of microplastic ageing. They were also successfully depolymerized by pyrolysis and the Grubbs cross-metathesis reaction revealing that the cross-linked species became in majority and additional analysis by ion mobility proved that the double bond geometry was lost. The same reaction was applied next on polyisoprene-based condoms in the form of synthetic and natural polyisoprene films. Both films were completely depolymerized and the analysis showed the disappearance of the initial family of oligomers separated by an isoprene unit and found under native conditions to give a newly formed family of reticulated polymeric chains under weathering conditions. Finally, industrial samples of hydroxy terminated polybutadiene (HTPB) were afforded by CRAY Valley company. These were also depolymerized by pyrolysis and by Grubbs cross-metathesis reaction. The obtained spectra showed over ten families of peaks that are separated by a C_4H_8 unit which were identified.

This successful and optimized depolymerization reaction can be extended on more complex natural and synthetic polymers with isoprene or butadiene units.

The second contribution focused on the development of a strategy for the characterization and identification of siccative or drying oils found in oil paints as well as the cross-linked structure formed following the polymerization of these oils. This strategy was based on multiple steps starting with a detailed analytical survey on fresh pure oils and extracted oils from present-day and old paint tubes, and ending with the development of a soft depolymerization reaction capable of solubilizing the highly insoluble polymerized structure. This technique is based on a specific chemical treatment which cleaves the polymer at the ester bond between the glycerol and fatty acids without altering their structure or composition. At the same time, it led to the derivatization of the fatty acids by a tertiary amine group which helped improve their detection in positive mode. The obtained products from transamidation were analyzed by FT-ICR ultra-high-resolution mass spectrometry and the obtained spectra showed thousands of peaks corresponding to the resulting products from the polymerization and degradation process. The different classes of products were identified and their structures revealed. This strategy allows for the first time to analyze and identify the network structure formed between the unsaturated fatty following the polymerization of drying oils. The next step consists on applying this new analytical methodology on real oil paints and precious artworks in order to find solutions for a better storage conditions and restorations.